NOTE TO USERS

Synthesis and Characterization of Annelated Nitronyl Nitroxides

Steven E. Bowles

A dissertation submitted in partial fulfillment of the requirements for the degree of:

Doctor of Philosophy

University of Washington

2005

Program Authorized to Offer Degree: Department of Chemistry

University of Washington
Graduate School

This is to certify that I have examined this copy of a doctoral dissertation by

Steven E. Bowles

and have found that it is complete and satisfactory in all respects,
and that any and all revisions required by the final
examining committee have been made.

Chair of Supervisory Committee:

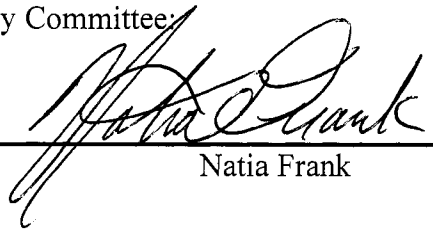

Natia Frank

Reading Committee:

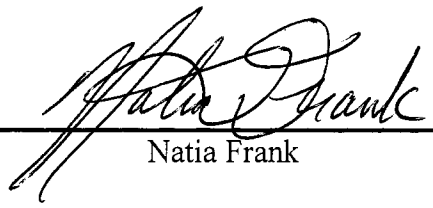

Natia Frank

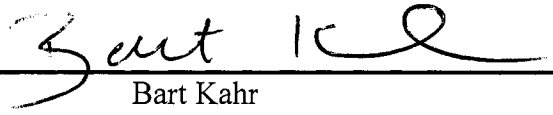

Bart Kahr

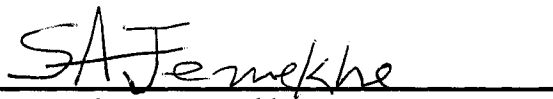

Samson Jenekhe

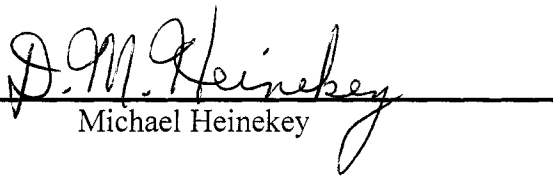

Michael Heinekey

Date: July 22, 2005

In presenting this dissertation in partial fulfillment of the requirements for the doctoral degree at the University of Washington, I agree that the Library shall make its copies freely available for inspection. I further agree that extensive copying of the dissertation is allowable only for scholarly purposes, consistent with "fair use" as prescribed in the U.S. Copyright Law. Requests for copying or reproduction of this dissertation may be referred to Proquest Information and Learning, 300 North Zeeb Road, Ann Arbor, MI 48106-1346, to whom the author has granted "the right to reproduce and sell (a) copies of the manuscript in microform and/or (b) printed copies of the manuscript made from microform."

Signature 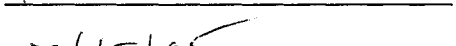

Date 7/15/05

University of Washington

Abstract

Synthesis and Characterization of Annelated Nitronyl Nitroxides

Steven E. Bowles

Chairperson of the Supervisory Committee:
Professor Natia Frank
Department of Chemistry

The heteroaromatic 2'-phenylbenzimidazole 1-nitronyl nitroxide (**PBNN**), 2'-pyridylbenzimidazole nitronyl nitroxide (**2PBNN**), 4'-pyridylbenzimidazole nitronyl nitroxide (**4PBNN**), 2'-thienylbenzimidazole nitronyl nitroxide (**2TBNN**), and 3'-thienylbenzimidazole nitronyl nitroxide (**3TBNN**) radicals were synthesized, and the 2-position heterocyclic group was found to have little effect on electronic structure. The structural change from tetramethyl to benzimidazole shifted the reductive potential to -0.300 V and raised the oxidation potential to 1.1 V. The band gap for BNN radical was found to be 1.5 eV, consistent with both electrochemical and UV-Vis spectroscopy techniques. Analysis of the EPR and calculations showed that the radical had a delocalized SOMO on the benzimidazole, with predictable high spin density on the annelated benzene ring. The X-ray structures for **2TBNN** and **3TBNN** were determined and showed the formation of slipped stacks. The magnetic susceptibility for **2TBNN** was found to be antiferromagnetic and weak, and **3TBNN** was found to be have long range

antiferromagnetic exchange of J = - 42.2 cm^{-1} and Θ = 3.23 K using an infinite chain model.

Three new radicals, 2-phenyl-5-azabenzimidazole nitronyl nitroxide (**P3PNN**), 2-phenyl-4-azabenzimidazole nitronyl nitroxide (**P2PNN**), and 2-phenylimidazo[4,5-b]quinoxaline nitronyl nitroxide (**PQNN**), were synthesized and characterized using EPR and DFT calculations. The substitution of nitrogen in the benzimidazole ring decreased the chemical stability of these radicals in solution. **PQNN** was determined to be the first example of an extended stable annelated nitronyl nitroxide.

A series of new brominated 2-phenylbenzimidazole 1-oxyl-3-oxides, 2-4'-hexylphenyl-5-bromobenzimidazole 1-oxyl-3-oxide, 2-phenyl-5-bromobenzimidazole 1-oxyl-3-oxide, 2-ethyl-5-bromobenzimidazole 1-oxyl-3-oxide, and 2-4'-*t*-butylphenyl-5-bromobenzimidazole 1-oxyl-3-oxide, were synthesized using methods developed and optimized in the synthesis of 2-phenylbenzimidazole 1-oxyl-3-oxides. Solubility was found to be a major problem with the 5-bromo-2-phenylbenzimidazole 1-oxyl-3-oxide class of molecules. The reactivity of benzofuroxan with functional groups on the 3- and 6-positions was investigated and it was found that their reactivity is drastically different, with the functional groups interfering with standard reaction conditions for the parent class.

Table of Contents

List of Figures

List of Schemes

List of Tables

List of Compounds

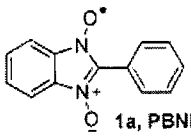
1a, PBNN

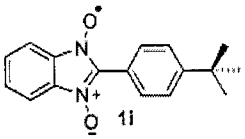
1i

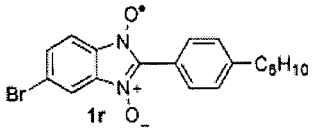
1r

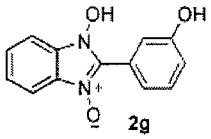
2g

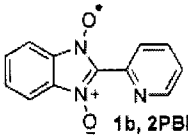
1b, 2PBNN

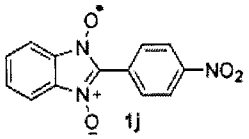
1j

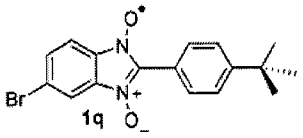
1q

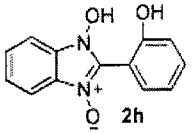
2h

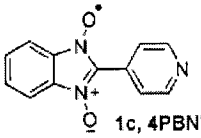
1c, 4PBNN

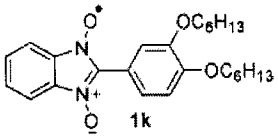
1k

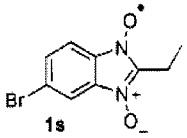
1s

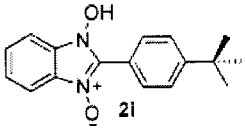
2i

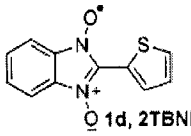
1d, 2TBNN

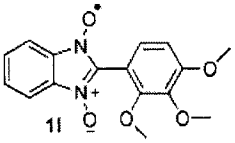
1l

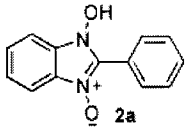
2a

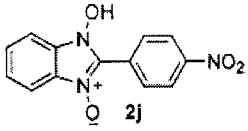
2j

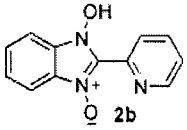
2b

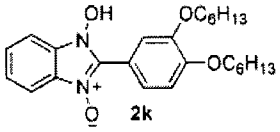
2k

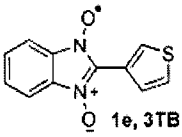
1e, 3TBNN

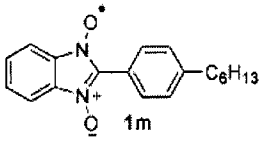
1m

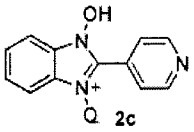
2c

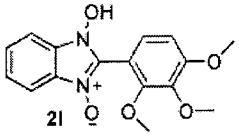
2l

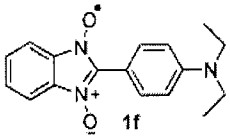
1f

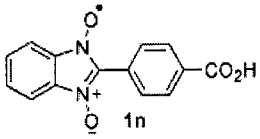
1n

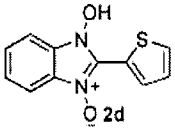
2d

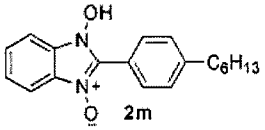
2m

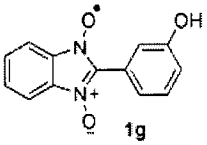
1g

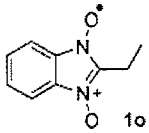
1o

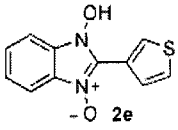
2e

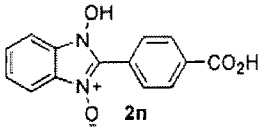
2n

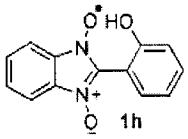
1h

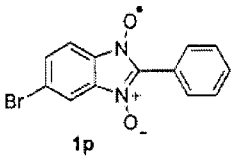
1p

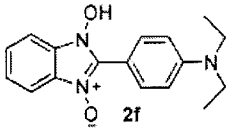
2f

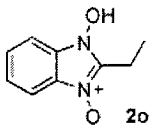
2o

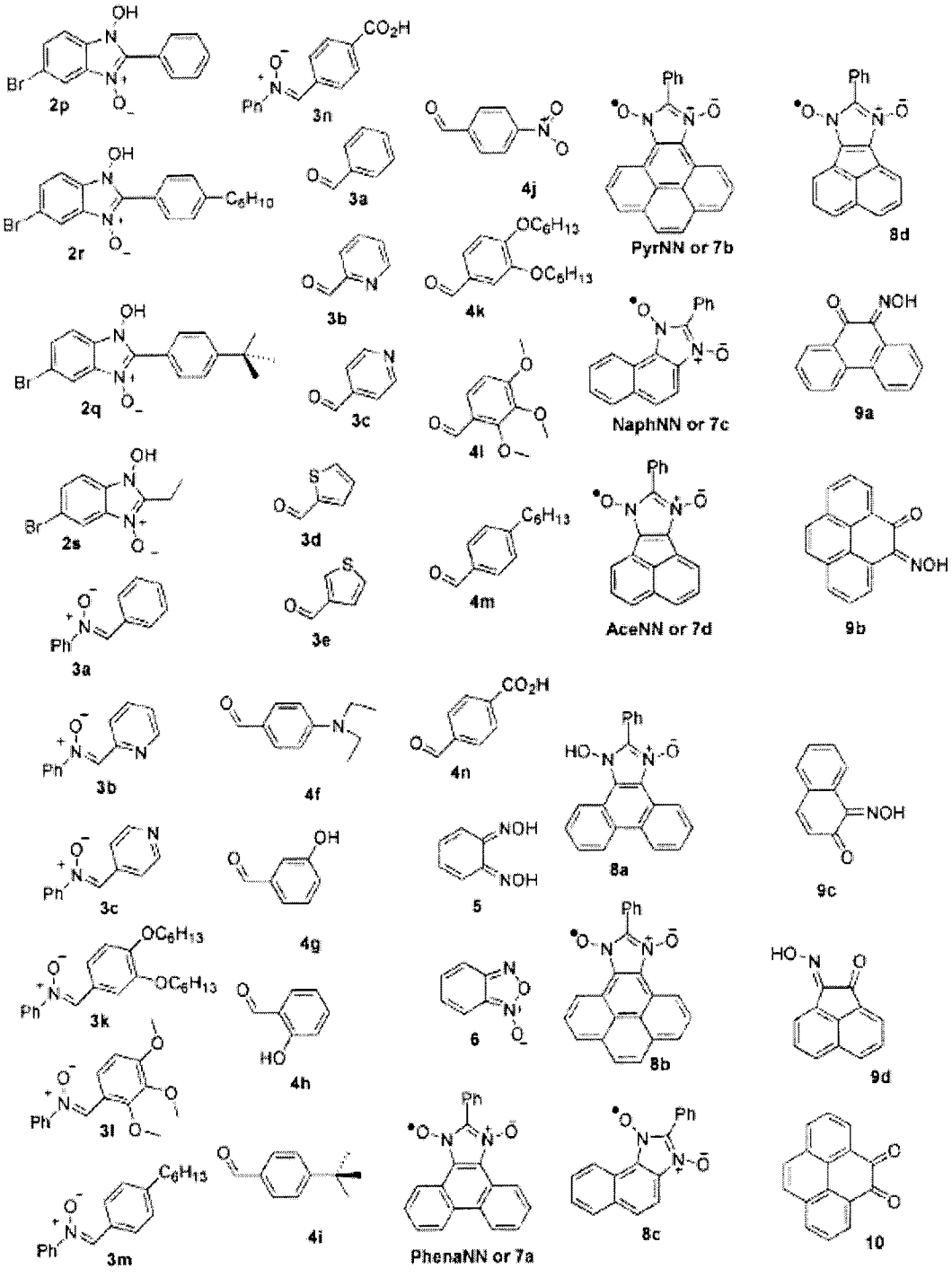
2p
3n
4j
PyrNN or 7b
8d
2r
3a
4k
3b
2q
3c
4l
NaphNN or 7c
9a
2s
3d
4m
AceNN or 7d
9b
3a
3e
3b
4f
4n
8a
9c
3c
4g
5
3k
6
8b
9d
4h
3l
3m
4i
PhenaNN or 7a
8c
10

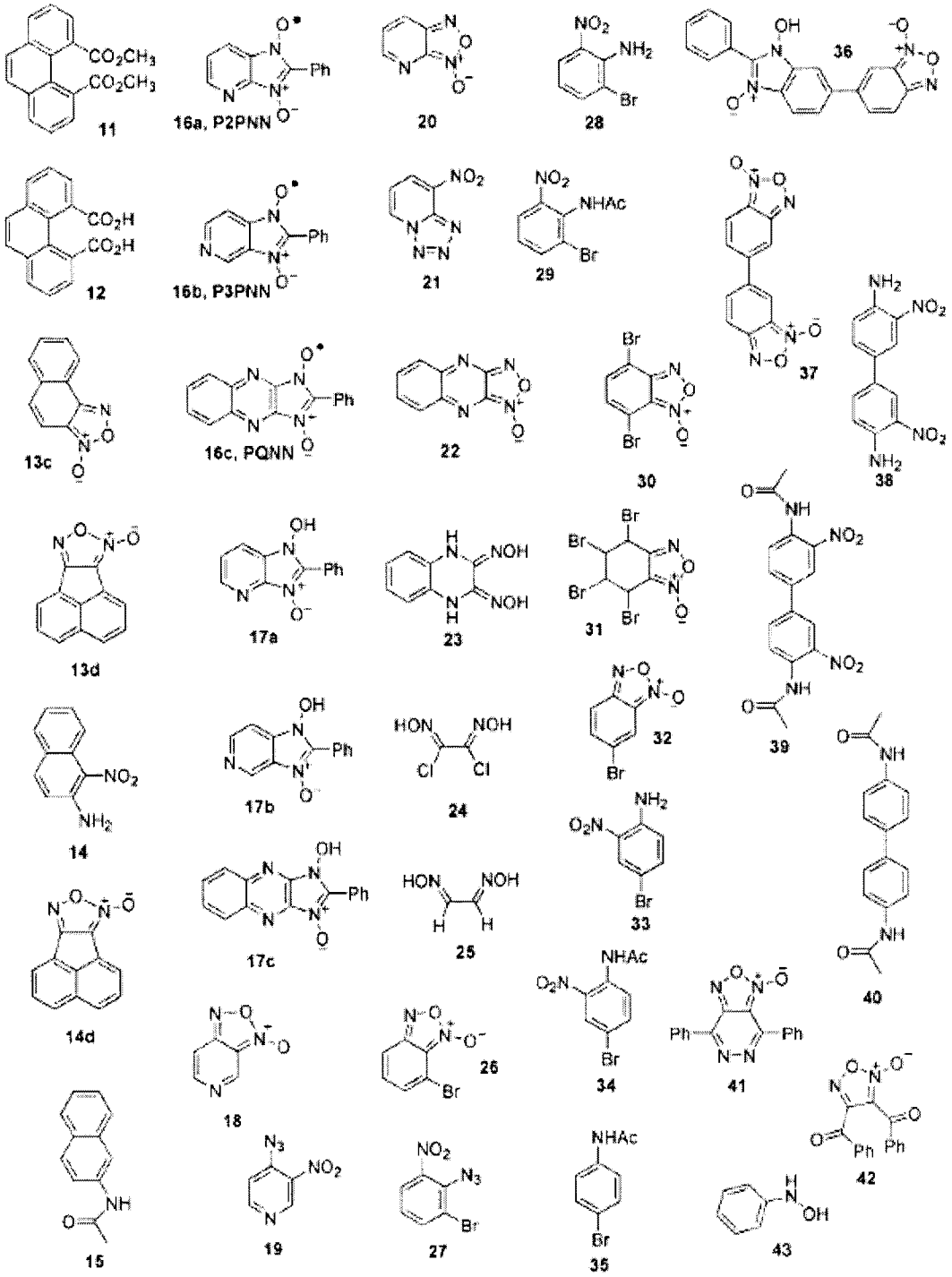
11
16a, P2PNN
20
28
36
12
16b, P3PNN
21
29
37
13c
16c, PQNN
22
30
38
13d
17a
23
31
39
14
17b
24
32
14d
17c
25
33
40
18
26
34
41
15
19
27
35
42
43

Abbreviations and Symbols

2PBNN 2-2'-pyridylbenzimidazole nitronyl nitroxide

4PBNN 2-4'-pyridylbenzimidazole nitronyl nitroxide

2TBNN 2-2'-thienylbenzimidazole nitronyl nitroxide

3TBNN 2-3'-thienylbenzimidazole nitronyl nitroxide

a_N hyperfine coupling constant to nitrogen

ACN Acetonitrile

ACS American chemical society

Anal. analysis

aq aqueous

Ar aromatic

BNN Benzimidazole nitronyl nitroxide

c concentration

C Celsius

c_1, c_2... constant

Calcd calculated

^{13}C-NMR carbon-13 nuclear magnetic resonance

cm^{-1} inverse centimeters

Δ heat

d doublet

dd doublet of doublet

DCM Dichloromethane

DFT density functional theory

DMF dimethylforamidine

DMSO dimethylsulfoxide

ε extinction coefficient

E_2 bimolecular elimination reaction

EA ethyl acetate, electron affinity

EI electron impact

EPR Electron paramagnetic resonance

Et_2O diethyl ether

EtOH Ethanol

ESI electrospray injections

eV electron volt

FTIR fourier transformation infared

g g-value, Zeeman splitting, grams

G Gauss

GHz gigahertz

HCl hydrochloric acid

Hfcc hyperfine coupling constant

HMO Huckel molecular orbital

^{1}H-NMR proton nuclear magnetic resonance

HOMO Highest occupied molecular orbital

HRMS High resolution mass spectroscopy

Hz Hertz

IR Infared

J coupling constant

L liters

LC liquid chromatography

λ_{max} absorbance maximum

lit. literature

LUMO Lowest occupied molecular orbital

k constant

k_B Boltzman's constant

K Kelvin

KOH potassium hydroxide

m multiplet

M molarity, parent mass

m/z mass divided by charge

MeOH methanol

mg milligrams

MHz megahertz

mL milliliter

mmol millimole

MO Molecular orbital

Mol mole

mp melting point

MS Mass spectroscopy

NaOH sodium hydroxide

NCS N-chlorosuccinimide

nm nanometers

ρ_r spin density

P2PNN 2-phenyl-4-azabenzimidazole nitronyl nitroxide

P3PNN 2-phenyl-5-azabenzimidazole nitronyl nitroxide

PQNN 2-phenylimidazo[4,5-b]quinoxaline nitronyl nitroxide

PBNN 2-phenylbenzimidazole nitronyl nitroxide

Q McConnell constant

R_f Distance traveled by compound on thin layer chromatography

RT room temperature

s seconds, singlet, spin

δ chemical shift

S_n2 bimolucular nucleophilic substitution

SOMO single occupied molecular orbital

t time, triplet

T Telsa

TCNQ tetracyanoquinone

TBAHFP Tetrabultylammonium hexafluorophosphate

THF tetrahydrofuran

TLC thin layer chromatography

UV-Vis Ultraviolet – Visible

V volts

Acknowledgements

When I first came to University of Washington, I was unsure what I wanted to do with my life. I enjoyed science and my undergraduate research experiences at Carnegie Mellon, but the five year plus time requirement for a Ph.D. just seemed too much for my notoriously short attention span. However, the first day of orientation I met this excited and energetic assistant professor by the name of Natia Frank. I loved the conversations I had with her. The long hours over the last 5 years of study were worth it. I am glad I stayed around.

In addition, I found a wonderful department full of people who were supportive, fun, stimulating, and personable. I would especially like to thank my fellow Frank Lab starting graduate students, Carla McDowell and Roni Kopelman, and the later additions, Dan Patel, Scott Gable, Tim Storr, and Jeremiah Miller. From the academic discussions to the depressing conversations about "why didn't this reaction work" over beers, you were the people who made graduate school much more bearable and entertaining. To my friends Paul M., Jill F., Jason B., Tyan C., Shawn D., Jasper L., Emily G., Brian S., Scott-Phil-Drew-Dan of the Dalton Lab, Mike M., Scott J., and Emily J. in the department, and outside, for your companionship and advice over the years. To Prof. Bart Kahr and Prof. Mike Heinekey for your help and guidance with the writing of my thesis. To Prof. Stuart Staley for your encouragement in getting into graduate school and for your patience in developing a young college student into a scientist.

Lastly, I would like to dedicate this to my parents, Anne and Gene Bowles, and sister, Kelly, for making sure I survived to this point in life and for all their support and advice through the years.

Chapter 1. Introduction

Section 1.1 - Molecular Magnetism.

Magnetism, and the application of magnetism, is a fundamental part of modern technology and society. From high capacity data storage to simple compasses, magnetism has a wide range of applications. The phenomenon of magnetism fascinated the ancient Greeks, and remains a subject of interest and research even after thousands of years, leading to changes in the theory and understanding of magnetism as a quantum mechanical phenomenon.[1]

The concept of using synthetically accessible spin carrying building blocks to construct magnetic materials, as opposed to the high temperature synthesis of metallic oxide or alloy magnetic materials, has led to a new focus in magnetochemistry. Magnetochemists have sought a better understanding of how a change in structure at the molecular and nanoscale levels affects the bulk magnetic properties of materials with unpaired electrons.[2,3,4,5] This represents a shift in focus, based on the assumption that design changes on the molecular level can affect bulk properties. Using persistent organic radicals[6] as building blocks for molecular magnetic materials has attracted particular attention due to the stability, synthetic flexibility, and tunable properties of organic systems.[7,8]

The bulk magnetic behavior of a system depends on both molecular electronic structure and intermolecular interactions. The molecular features that can affect the overall magnetic behavior are spin orbit coupling, zero field

splitting, and g-anisotropy. In organic molecules, the orbital angular momenta are effectively quenched and give rise to slight variations in the g-factor (g-anisotropy). The paramagnetism of organic molecules therefore arises almost entirely from electron spin. Magnetic behavior is dominated by spin-spin interactions. Intermolecular interactions (H) arise from exchange coupling between spin carrying units (s_i and s_j) and can be antiferromagnetic or ferromagnetic, depending on the relative energies of the potential and kinetic energy terms of the magnetic exchange integral (J_{ij}).[9]

$$H = -\Sigma_{i,j} J_{ij}\, s_i * s_j$$

$$\text{where } J_{ij} = J_{ij}^{0} - 2S_{ij}V_{ij}$$

For this exchange Hamiltonian, a negative J_{ij} indicates antiferromagnetic exchange (paired electrons) and a positive J_{ij} denotes ferromagnetic (parallel) exchange. J_{ij}^{0} represents the true exchange integral, S_{ij} the overlap between electrons, and V_{ij} the cross-matrix element of the attractive potential or Coulombic energy. In most cases, the second term dominates since the attractive potential is strong, and the exchange J_{ij} becomes large and negative. However, there are conditions in which ferromagnetic exchange is possible. The orbitals can arrange in such a way that there is small overlap, but orbitals are orthogonal, making S_{ij} very small (Figure 1.1).

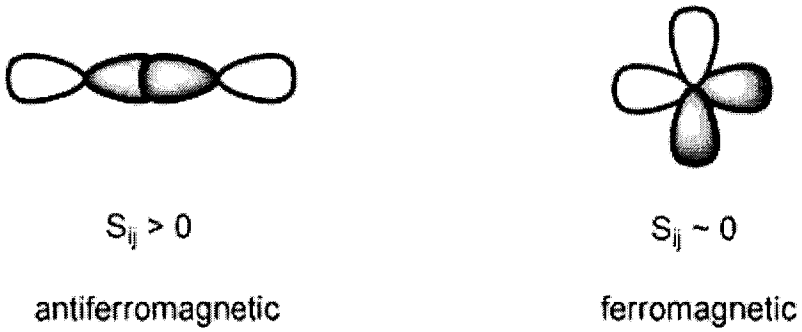

Figure 1.1 - Example of how overlap affects magnetic exchange

Section 1.2 - Magnetic Exchange.

Common types of magnetic exchange interactions in organic systems are through bond (indirect exchange) and through space (direct exchange and dipole-dipole coupling). These magnetic exchanges can occur in five types: direct exchange, which is the coupling of localized magnetic moments in insulators through space; superexchange, which is the coupling of localized magnetic moments in insulators through diamagnetic groups; indirect exchange, which is the coupling of localized magnetic moments in metals with the conducting electrons; itinerant exchange, which is the coupling of itinerant electrons in metals; and double exchange, which is the coupling of localized magnetic moments through an itinerant electron.

In organic systems, direct exchange and superexchange are relevant. In direct exchange, the strength of the magnetic exchange interaction depends roughly on the overlap of the orbitals containing unpaired spin (single occupied molecular orbital or SOMOs) and the distance between the radical centers. The

dependence of the exchange integral on the atomic separation in magnetic materials can be described by the Bethe-Slater curve. (See Figure 1.2)

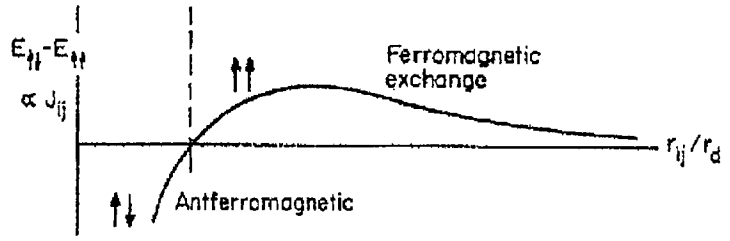

Figure 1.2 - Bethe-Slater curve for energy difference for spatially symmetric and antisymmetric wavefunctions versus atomic separation r_{ij}.[93]

Superexchange is the dominant mechanism of through bond magnetic exchange in molecular systems. Superexchange can be described as the magnetic exchange coupling of spins though diamagnetic atoms[10] and is extremely common since there are a large number of magnetic materials that do not have direct metal-metal bonding.[11,12,13]

One simplified model based on configuration interaction for intermolecular exchange is referred to as spin polarization. Spin polarization (or exchange polarization) can be understood as the polarization of the σ-bonding system through exchange coupling with the unpaired electrons in the π-electron system (see Figure 1.2).[14,7,15] Spin polarization is technically not a mechanism, but a model to account for the mechanism of configuration interaction. Specifically, spin polarization is one of the seven principal contributions in the second order perturbative configuration interaction to the exchange coupling constant. The p-π and sp^2-σ orbitals of a sp^2 hybrid carbon, for example, are orthogonal to each other by symmetry, but have a nonzero overlap integral due to overlap between

the orbitals in the region close to the nucleus. If there is an unpaired electron in the π-orbital, then there are two possible arrangements for the two electrons in the σ-bond: the electron in the sp^2 orbital can have parallel or anti-parallel spin relative to the π electron (see Figure 1.3).

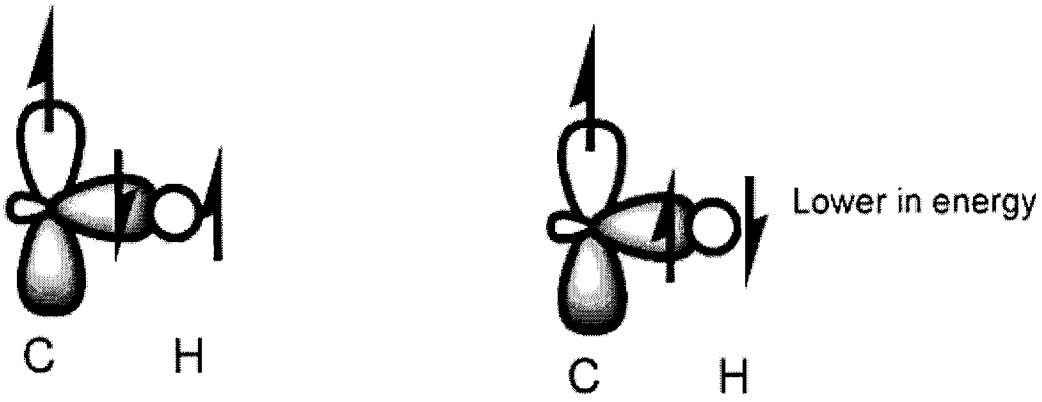

Figure 1.3 - Spin polarization of the π-electron through the σ-bonding electrons

Parallel alignment is preferred because Pauli's exclusion principle forbids electrons of parallel spin from simultaneously occupying the same point in space. If the electrons have the same spin state, they cannot occupy the same point in space and avoid an increase in electron-electron repulsion energy. As a consequence, the spin on the adjacent atom will be of the opposite spin state (α versus β). This phenomenon can be easily observed experimentally by looking at the EPR of organic molecules containing unpaired electrons in the π-system (i.e., the benzene radical anion). Spin density is observed at the hydrogen atom positions, as shown by the nonzero hyperfine coupling constants. The mechanism

of transmission is spin polarization. This phenomenon is therefore distinct from the radical SOMO being delocalized over the hydrogen nucleus.

The spin polarization model can be used to predict the sign of magnetic exchange between radicals in which the unpaired electron is in a π-orbital. When two radicals are bonded to a benzene ring to create a biradical, the positioning on the ring determines the sign of the intramolecular exchange, as seen in Figure 1.4.

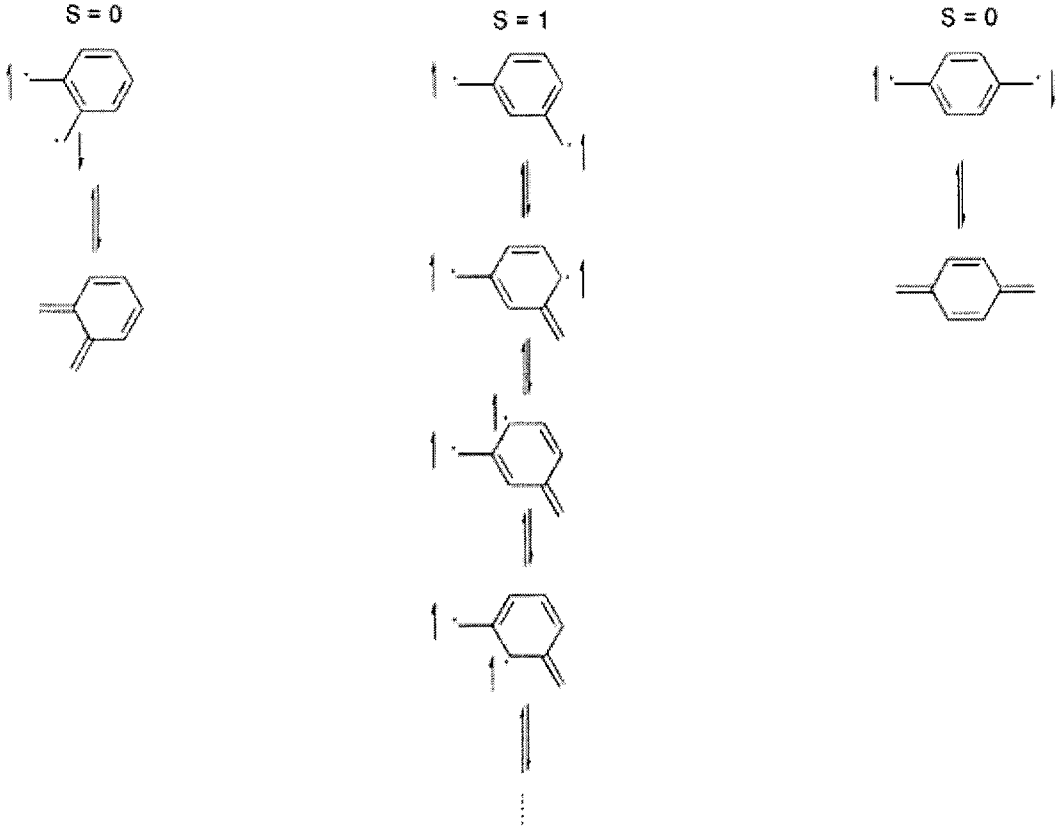

Figure 1.4 - Intramolecular exchange in biradicals

If the radicals are *meta* to each other on the ring, the ground state is the triplet high spin state, and the radicals are said to be ferromagnetically coupled. If the radicals are *para* or *ortho* to each other on the ring, the ground state is the singlet low spin state, and the radicals are said to be antiferromagnetically coupled.

The presence versus absence of non-Kekule structures is a simple way of determining whether ferromagnetic or antiferromagnetic intramolecular exchange dominates. There are several theories that predict whether the singlet or triplet is the ground state. The first such theory is Ovchinnikov's equation, which is based on valence bond theory. This equation determines whether a system is antiferromagnetic or ferromagnetically coupled based on whether the radical system is alternant or non-alternant. The difference between "marked" (starred) or "unmarked" (unstarred) nuclei divided by two determines whether the ground state is high spin or low spin and is described by the following equation:

$$S = (N^* - N) / 2$$

If S is equal to zero, the system is low spin and if S is equal to one, then the system is high spin.

A more advanced way of determining the ground spin state, based on Huckel theory was developed by Borden and Davidson, by examining the non-bonding molecular orbitals (NBMO) of the radical.[16] If the NBMOs do not span both the starred and unstarred atoms, then the biradical is described as being disjoint. If the NBMO covers both the starred and unstarred atoms, then the biradical is described as being non-disjoint. The simplest way of determining if a radical is disjoint or non-disjoint without doing MO calculations is to count the unstarred and starred atoms. If $N^* = N$, then the NBMOs span both the sets of atoms equally, and the radical is disjoint. If $N^* > N$, then the NBMOs can span the N^* more than the N, and the radicals are considered non-disjoint.

Disjoint biradicals gain little energetic advantage by having a triplet state over a singlet state since the unpaired electrons do not occupy the same space. In this case, the ground state can be either a singlet or triplet. Non-disjoint biradicals, with high overlap of NBMOs, are expected to have a large singlet-triplet gap with the high spin state as the ground state, because the exclusion principle keeps the two nonbonding electrons from simultaneously occupying the same region of space.

The topography of the spin distribution is a crucial aspect of intermolecular magnetic exchange. The McConnell I mechanism predicts the sign of the magnetic exchange based on the assumption that through space overlap of spin density is the primary mechanism of exchange. Ferromagnetic exchange is predicted when two odd-alternate radicals, in which the π-spin distribution is characterized by an alternation in signs, have some nonzero overlap through space. [17] (See Figure 1.5.)

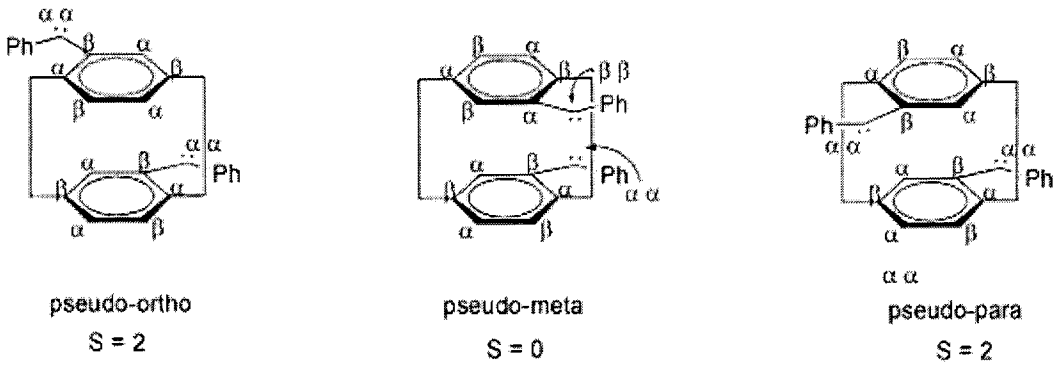

Figure 1.5 - Orientation and spin state of bis(phenylmethylenyl)-[2.2]paracyclophanes

In other words, when π-orbital radicals form π-stacks, giving rise to α (positive) spin overlapping with the β (negative) spin, the net intermolecular interaction between the radicals is predicted to be ferromagnetic. If the net overlap is α-α spin or β- β spin, then the overall intermolecular interaction between the radicals is predicted to be antiferromagnetic.

Section 1.3 – Organic Radicals.

Free organic radicals have often been considered to be reactive species that undergo hydrogen abstraction or decomposition in the presence of oxygen or water. Over the last 30 years, however, several classes of persistent organic radicals that are thermodynamically and chemically (kinetically) stable have been synthesized and shown to be excellent building blocks in the design of molecular materials. The majority of these radical classes are based on π-systems containing nitrogen, oxygen, or sulfur that allow stabilization of the radical by delocalization through the π framework and the electronegativity/lone electron pairs of the heteroatoms. Kinetic stability is provided in some cases by the incorporation of sterically demanding substituents. The design of magnetic materials involves primarily persistent nitronyl nitroxide, verdazyl, and thiazyl radicals.

1.3.1 - Thiazyl Radicals.

One of the first examples of an organic ferromagnet was based on the thiazyl radical.[18] The thiazyl is an example of a π-delocalized radical that exhibits interesting properties in the solid state depending on the nature of the π-stacking

(see Figure 1.6 for thiazyl radical example). The 4-cyanophenylthiazyl radical in the β-phase crystalline state exhibits the properties of a ferromagnet below 34 K. This was the first example of an organic material over 5 K and, to date, the highest temperature organic ferromagnet under ambient pressure.

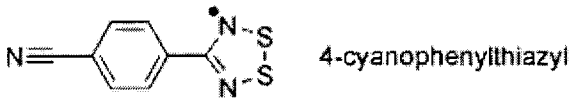

4-cyanophenylthiazyl

Figure 1.6 - Thiazyl radical

Other derivatives, such as the 4-nitrophenylthiazyl, have been determined to also act like a ferromagnet, but unfortunately, at considerately lower temperature (T_c 1.6 K).[19] The 4-cyanophenylthiazyl exemplifies the idea that organic systems can demonstrate magnetic properties once thought to be limited to inorganic systems. More importantly, the idea that an organic ferromagnet is not limited to transition temperatures below 5 K, suggests that organic radical materials in combination with other systems may eventually reach the necessary transition temperatures for practical usage.

1.3.2 - Verdazyl Radicals.

Another class of organic π-radicals is the verdazl radical. This class was first examined in 1973 as potential spin labels,[20] but have recently been reexamined for use in the field of organic magnetic materials. Derivatives of the verdazyl with aromatic groups at the 3-position were found to be stable in the solid state for years. In addition, large spin density delocalization of the unpaired electron through the verdazyl ring was shown (Figure 1.7).[21,22] Magnetic

susceptibility measurements of 1,5-dimethyl-3-(2-pyridyl)-6-oxoverdazyl, co-crystallized with hydroquinone, showed significant antiferromagnetic exchange (J = -58.3 cm^{-1}) when fit with a 1D regular chain model, even though the verdazyl radicals are separated from each other by hydroquinone molecules in the solid state.

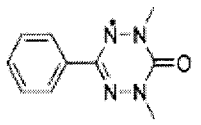

1,5-dimethyl-3-(2-pyridyl)-6-oxoverdazyl

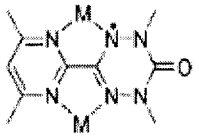

1,5-dimethyl-3-(4,6-dimethyl-2-pyrimidinyl)-6-oxoverdazyl

Figure 1.7 - Verdazyl radicals (M = Mn^{II} and Ni^{II})

The large spin density on nitrogen makes this class of radical ideal for binding to transition metals.[23] Verdazyl radicals with 4,6-dimethyl-2-pyrimidinyl at the 3-position have been shown to chelate two metal atoms of $Mn^{II}(hfac)_2$ and $Ni^{II}(hfac)_2$, producing significant magnetic interactions between the radical and metal, with the magnitude of the interactions $J_{Ni\text{-}rad}$ = 220 cm^{-1} and $J_{Mn\text{-}rad}$ = -48 cm^{-1} using a linear three spin model. In addition to the high ferromagnetic exchange between the Ni and verdazyl radical, the antiferromagnetic interaction between the radical and Mn leads to a net ferromagnetic interaction between the Mn ions. The use of organic radicals as antiferromagnetic coupling units between high spin transition metal ions is a clever way of achieving bulk ferrimagnetism in a molecular material

1.3.3 - Phenalenyl Radicals.

One example of a neutral aromatic radical system that has displayed interesting multifunctional properties in the solid crystalline state is the spiro-biphenalenyl radical.[24] Magnetic susceptibility measurements of a N,N'-dibutyl derivative (Figure 1.8) suggest magnetic behavior that tests the limits of our understanding of molecular magnetism.[25]

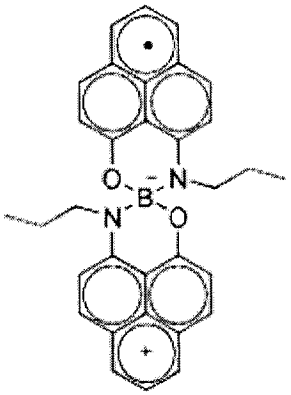

Figure 1.8 – Dibutyl spiro-biphenalenyl radical

The spiro-biphenalenyl compound exists as a diamagnetic dimer at ambient temperatures and undergoes a phase transition to a paramagnetic material when heated to temperatures above 300 K. This phase change is also accompanied by a drop in conductivity by 100 S/cm. The exact solid state dynamics are not completely understood with current solid state band structure and are still being investigated.[25] The existence of such new multifunctional materials highlights the need for greater investigation of purely organic systems and suggests that these systems can possess useful properties at room temperature and in ambient environments.

1.3.4 - Tetramethyl Nitronyl Nitroxide Radical.

Although there are several types of stable organic nitronyl nitroxides that have shown promise due to their ease of synthesis and air/temperature/chemical stability, tetramethylnitronyl nitroxide (**TMNN**) is the most widely investigated.[6,26] Figure 1.9 depicts an example of a **TMNN** radical.

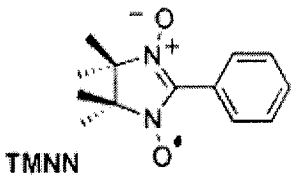

Figure 1.9 – Example of TMNN

TMNN radicals have been investigated extensively as biological spin labels and as a source of spin density in organic polymers,[27,28] inorganic ligands,[29] and solid state crystals.[8] The spin density of **TMNN** is mainly localized to the heteroatoms on the ONCNO moiety, with small alternating positive/negative spin densities on the R-group substituent on C2 (central carbon between NO) through spin polarization.[30,31]

Polarized neutron diffraction[31] and EPR studies[32] comparing with computational work[32] have yielded detailed spin density distribution maps of **TMNN** as a function of substitution. The weak exchange observed in the solid state of **TMNN** is linked to its stability and spin distribution. Most of the spin density is localized on the ONCNO moiety and the bulky tetramethyl groups provide kinetic stability through protection of the delocalized unpaired electron. The dihedral angle between the phenyl and nitronyl nitroxide π-systems and the

negative spin density on the bridge carbon prevent full delocalization of the unpaired electron into the π-system of the 2-position aromatic group.[32] A consequence of this steric interaction is the introduction of unfavorable interactions in the solid state, in which the planar phenyl and tetrahedral methyl moieties do not allow effective stacking. As a result, **TMNN**s do not π-stack, limiting the primary intermolecular interactions to direct overlap of the NO moiety, which has been shown to be quite weak.[30]

Predicting the type of direct magnetic exchange has been problematic, with magnetostructural relationships between stacking arrangements of nitroxides and type of magnetic exchange showing no statistical significance.[30] However, **TMNN** radicals do have the potential for extremely high intramolecular magnetic exchange (Figure 1.10). One example is the NN-SQZnTp^{Cum,Me} biradical which has extraordinarily high intramolecular ferromagnetic exchange between a semiquinone and a nitronyl nitroxide, with the exchange coupling suggested to be higher than room temperature (J > 300 K).[33]

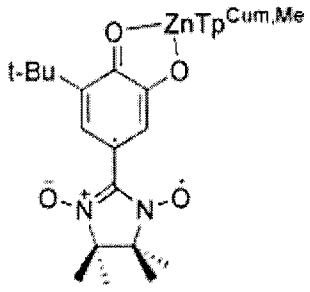

NN-SQZnTp^{Cum,Me}

J > 300K

Figure 1.10 - High ferromagnetic exchange in TMNN radicals

1.3.5 - 2-Phenylbenzimidaozle nitronyl nitroxides.

In 1968, a short communication described the synthesis and brief fitting of the EPR spectra of a 1-hydroxy-2-phenylbenzimidazole 3-oxide.[34] Further analysis of the EPR of phenylbenzimidazole nitronyl nitroxide (**PBNN** or phenylbenzimidazole N,N-oxide PBIDO) was performed 10 years later and showed large hyperfine coupling with protons in the annelated ring.[35] (Examples of **TMNN** and **PBNN** radicals are shown in Figure 1.11.)

Figure 1.11 – TMNN versus PBNN

Analysis of the spin densities calculated from the hyperfine constants and using molecular orbital theory showed that radical spin density was delocalized throughout the benzimidazole ring. The delocalization could be seen by comparing the hyperfine coupling constants of the nitrogen in the nitronyl nitroxide of **TMNN** versus **PBNN**. The a_N for **TMNN** was measured by EPR to be 7.45 G, but the a_N for the nitrogen in **PBNN** was determined to be 4.26 G.

The drop in spin density on the nitrogen is consistent with the delocalization of the unpaired electron into the benzene ring on the benzimidazole. This delocalization into an aromatic ring that is fused to the imidazole ring will be referred to as annelation (or being annelated). In addition to the significantly higher spin density on the protons on the annelated

benzimidazole moiety, the spin was predicted to be positive in sign by computational methods (MO theory, DFT calculations). However, understanding of the unpaired electron distribution of these annelated benzimidazole systems was limited to the phenyl and t-butyl derivatives in solution only.

The **PBNN** radical was finally crystallized 30 years after the original publication of the EPR.[35] Structural deviations from the classical **TMNN** led to organic radicals with orders of magnitude higher magnetic interactions in the solid state yet retaining the general stability of the radical. The crystals were radically different from **TMNN**. For example, **TMNN** radicals are blue in solution, form bright blue crystals, and are easy to crystallize in many solvent systems. On the other hand, the **PBNN** radical was found to only crystallize in dilute n-pentane solution and form dark brown/red crystals. The X-ray structure of the **PBNN** radical showed a dihedral angle near 0° degrees between the imidazole and phenyl rings, allowing for a planar geometry, as may be seen in Figure 1.12.

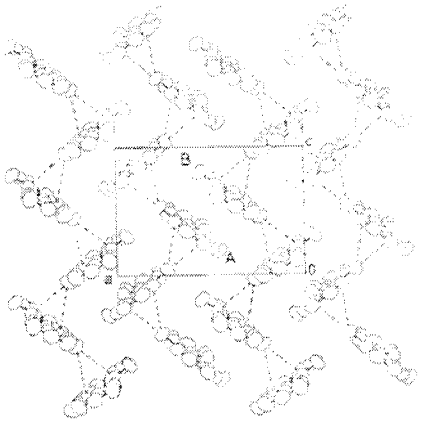

Figure 1.12 - X-ray structure of PBNN[36]

Planar radicals form dimers in the solid state (3.410 Å between the radicals), with the benzimidazole rings stacking on top of each other in a face-to-face overlapping arrangement and strong anti-ferromagnetic magnetic exchange of -40 K through overlapping π-stacks.[36] Changing the tetramethyl structure to a benzimidazole increases the amount of spin delocalization of the unpaired electron and removes the sterically bulky substituents, there by allowing for higher magnetic exchange in the crystal phase by π-stacking (See Figure 1.13.). Even though this is one derivative, the **PBNN** radical showed great potential for being better suited for intermolecular exchange than **TMNN**, with this derivative exhibiting the highest magnetic exchange of any nitronyl nitroxide. However, the **PBNN** radical is the only recorded case of this occurring, so the magnetic exchange could be due to structural factors in this one unique case.

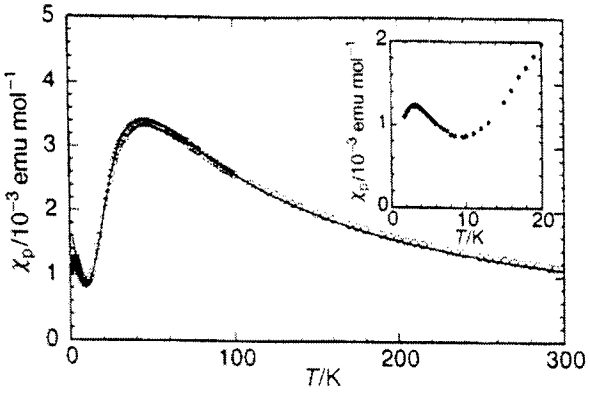

Figure 1.13 - χ_p versus T magnetic susceptibility measurement of polycrystalline PBNN[36]

K. Itoh and T. Nogami in Japan tried to determine if varying the phenyl group to include other functional groups would change the magnetic susceptibility of the radical in the crystalline state.[37] They synthesized a series of BNN radicals

with different substituent groups on the phenyl ring at the para-position. The functional groups included $-NO_2$, $-CO_2C_2H_5$, $-OCH_3$, -Cl, and $-CH_3$, and unfortunately the researchers were unable to grow X-ray quality crystals. This has proven to be a consistent trend with the BNN class of radicals. The solubility of BNN radicals is low in n-pentane, and the radicals tend to form polycrystalline structures when crystallized. Even though the crystal structures were not determined, magnetic susceptibility measurements were taken for the polycrystalline samples. The $-CO_2C_2H_5$, $-OCH_3$, -Cl, and $-CH_3$ derivatives were found to have weak magnetic interactions, being fit to a Curie-Weiss model with Weiss constants of 1.0, -7.5, -11.0, and -6.9 K respectively. However, the $-NO_2$ derivative was found to be strongly antiferromagnetic, with a maximum of χ_p at 120 K, which is even stronger than the magnetic exchange seen in **PBNN**.

Even though the researchers were unsuccessful at fitting the magnetism, the appearance of strong magnetic interactions in the $-NO_2$ derivative effectively proved that the strong magnetic exchange was not an abnormality only seen in the **PBNN** derivative. Clearly, these radicals represent a relatively unexplored class of radicals that show promise of strong magnetic exchange in the solid state.

The work done by Shiomi and coworkers[37] also revisited the phenanthrene derivative of the nitronyl nitroxide, synthesized originally in 1967 by Zimmermann.[38] The 2-phenylphenanthrene nitronyl nitroxide (**PhenaNN**) was found to be much less stable than the benzimidazole. The hyperfine coupling constants to the nitrogen in the imidazole moiety were lower in **PhenaNN** than

PBNN, (4.38 G for **PBNN** versus 3.81 G for **PhenaNN**), showing that the spin density delocalizes into the annelated aromatic system, but reduces the chemical stability. **PhenaNN** was the only example of an extended nitronyl nitroxide that had been synthesized and, thus, it is unknown whether extended annelation leads to a reduction in stability of the radical.

In more recent developments occurring since the start of this thesis in 2000, a series of halogenated phenylbenzimidazole nitronyl nitroxides with the 2-position R-group consisting of 2,6-dichlorophenyl, 2,6-difluorophenyl, 2-chloro-6-fluorophenyl, 2,3,6-trichlorophenyl, 2,3,4,5,6-pentafluorophenyl, and 3-cyanophenyl were synthesized, and the crystal structure and magnetism were measured.[39] The magnetism varied widely based on the packing of the radicals in the crystal, but, like the **PBNN** radical, the radicals adopted a planar arrangement with a small dihedral angle of less than 5 degrees between the benzimidazole and C2 aromatic rings. The 2,6-dichloro, 2,3,4,5,6-pentafluoro, and 3-cyano derivatives exhibited strong long range antiferromagnetic exchange (J/k_B = -84.2, -37.0, and -95.3 K respectively) and showed packing arrangements with the planar radicals forming extended π-stacks. Interestingly, the 2,6-difluoro derivative exhibited strong ferromagnetic exchange (J/k_B = 66.0 K) based on a Pade linear chain model.

The crystal structure of the 2,6-difluoro derivative was different from the other BNN radicals, in that the radicals were perpendicular to each other, with the N-O—O-N distances measured as 3.4 A with an orthogonal arrangement of the π-

systems. This was the first documented example of BNN radicals exhibiting significant ferromagnetic exchange in the solid state, and showed that the high magnetic interaction seen in this class of molecules was not limited to just antiferromagnetic exchange.

The effects of heterocyclic annelation is an unexplored area of this class of radicals. There are no known examples in the literature of the synthesis and characterization of benzimidazole nitronyl nitroxides containing heterocycles as the annelated ring.

Section 1.4 - Organization of the Thesis.

This thesis is divided into four chapters based on the experimental focus. Chapter 2 describes the investigations into the electronic structure of benzimidazole nitronyl nitroxides in which the phenyl moiety has been replaced by a heterocycle. Discussion surrounds the 2'-thienyl, 3'-thienyl, 2'-pyridyl, 4'-pyridyl, and phenyl benzimidazole nitronyl nitroxides being synthesized and the radicals for **TMNN** investigated by ultraviolet-visible absorbance, electron paramagnetic resonance spectrum, magnetic/X-ray crystal structure-function relationships, and computational analysis. Chapter 2 also includes the investigations into the solubility of the precursor imidazole 1-oxyl-3-oxide by examining various functional groups on the 2-position of the benzimidazole moiety.

Chapter 3 focuses on synthetic attempts to make larger annelated nitronyl nitroxide incorporating pyrene, phenanthrene, acenaphthylene and naphthalene and determining how the extended annelated aromatic system affected the overall stability and electronic structure of the radical.

Chapter 4 describes the synthesis of annelated nitronyl nitroxides with heteroaromatics annelated to the radical imidazole moiety (2-phenyl-5-azabenzimidazole nitronyl nitroxide, 2-phenyl-4-azabenzimidazole nitronyl nitroxide, and 2-phenylimidazo[4,5-b]quinoxaline nitronyl nitroxide) in an attempt to understand the effect of incorporating heteroatoms into the annelated ring of BNN radicals.

Chapter 5 describes the attempts to synthesize organic polyradicals with delocalized radicals in the aromatic backbone.

Chapter 2. Synthesis and Electronic Structure of C-2 Heteroaromatic Benzimidazole Nitronyl Nitroxides

Section 2.1- Introduction

Puzic and Gough published the most comprehensive review on the structure of phenylbenzimidazole nitronyl nitroxide in 1976,[35] including a summary of the known methods of preparing the radical precursor and a simulated EPR spectrum of the hyperfine coupling constants of the protons on the entire molecule. Initially, the purpose was to develop generalized methodology that could be used to synthesize a larger class of annelated nitronyl nitroxides. While the literature has focused on the solid state properties of the BNN radical, little was know regarding the electronic structure (Figure 2.1) of this class of radicals as compared to **TMNN.**

Figure 2.1 – Phenylbenzimidazole nitronyl nitroxide and tetramethyl analogue

To explore the structure of these radicals, a series of benzimidazole annelated radicals were synthesized in order to investigate the effect of C-2 heteroaromatic substitution on the electronic structure and stability of **PBNN**. Due to the presence of a node in the SOMO of the radical, small alternating spin densities are observed on the C2 position phenyl group. Determining whether substitution of

this phenyl group with electron rich (thiophene) and electron poor (pyridine) heteroaromatics induced a shift in the spin density distribution, a change in the oxidation or reduction potentials, or changes in intermolecular interactions and magnetic behavior in the solid state became the focus of study and the following radicals were prepared: 2'-phenylbenzimidazole 1-nitronyl nitroxide (**PBNN** or **1a**), 2'-pyridylbenzimidazole nitronyl nitroxide (**2PBNN** or **1b**), 4'-pyridylbenzimidazole nitronyl nitroxide (**4PBNN** or **1c**), 2'-thienylbenzimidazole nitronyl nitroxide (**2TBNN** or **1d**), and 3'-thienylbenzimidazole nitronyl nitroxide (**3TBNN** or **1e**) (Figure 2.2). The synthetic challenge associated with the extremely low solubility of the benzimidazole 1-oxyl-3-oxide precursors was also explored.

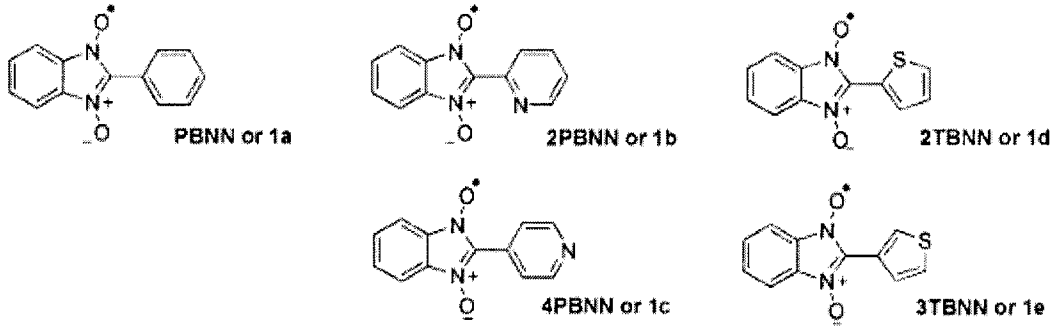

Figure 2.2 - Heterocyclic benzimidazole nitronyl nitroxides

A series of radical precursors were synthesized to investigate if structural changes on the 2-position phenyl would lead to an increase in the solubility of the precursor in organic solvents: 2-4'-t-butylphenylbenzimidazole 1-oxyl-3-oxide (**2i**), 2-2'-hydroxyphenylbenzimidazole 1-oxyl-3-oxide (**2h**), 2-3'-hydroxyphenylbenzimidazole 1-oxyl-3-oxide (**2g**), 2-4'-

diethylaminophenylbenzimidazole 1-oxyl-3-oxide (**2f**), 2-4'-nitrophenylbenzimidazole 1-oxyl-3-oxide (**2j**), 2-4'-hexylphenylbenzimidazole 1-oxyl-3-oxide (**2m**), 2-2',3',4'-trimethoxylphenylbenzimidazole 1-oxyl-3-oxide (**2l**), 2-4'-carboxylatephenylbenzimidazole 1-oxyl-3-oxide (**2n**), and 2-3',4'-dihexyloxylbenzimidazole 1-oxyl-3-oxide (**2k**)(See Figure 2.3 below).

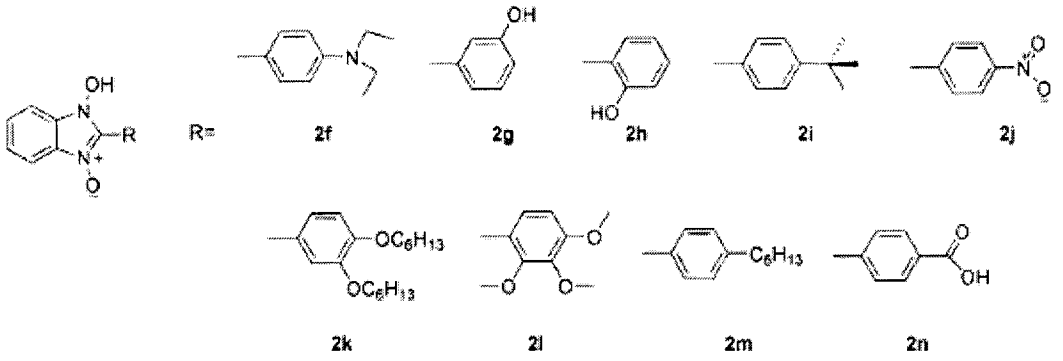

Figure 2.3 - Phenyl substituted benzimidazole 1-oxyl-3-oxide radical precursors

Section 2.2 – Results and Discussion of C2 heteroaromatic BNN radicals

2.2.1 – Synthesis of BNN radicals.

The first reported synthesis of the radical precursor 2'-phenylbenzimidazole 1-oxyl-3-oxide was in 1963 from the reaction of nitrosobenzene and benzonitrile oxide in ether solution at room temperature.[40] Oxidation of 2'-phenylbenzimidazole 1-oxyl-3-oxide with lead (IV) oxide[34] led to the generation of the phenylbenzimidazole nitronyl nitroxide (**PBNN**). The initial interest in this radical class was related to their parent system, **TMNN**, which was being studied extensively by Ullman and others for potential usage as a spin label

using EPR. At that time, spin labels with minimal hyperfine interactions were preferred, like the three line pattern of nitroxides, because their spectra were easier to solve. With the new appearance of computers for solving spectra rich in hyperfine, more complex spectra posed less of a problem and new radicals with more intricate hyperfine coupling could be used. Thus, **PBNN** was first looked at as a potential novel spin label.

Puzic and Gough established the three general synthetic routes for preparation of phenylbenzimidazole nitronyl nitroxide. Their work identified three major pathways for making the **PBNN** radical (Scheme 2.1).[35]

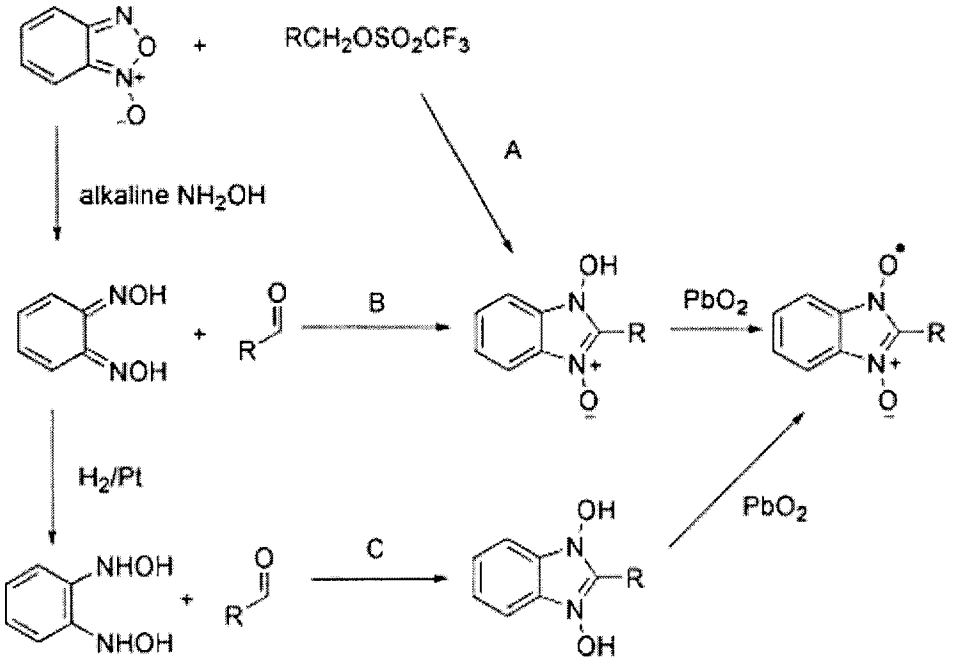

Scheme 2.1 - Summary of Route A, B and C for the synthesis of benzimidazole nitronyl nitroxides.

Route A involved condensation of benzofuroxan with an alkyltriflate under neutral conditions to give the radical 2-arylbenzimidazole 1-oxyl-3-oxide precursor. The disadvantage of this route lies in the cost of generating

alkyltriflates and the reported low reaction yield of 9%.[41] Route B involved acid-catalyzed condensation of a dioxime with appropriately substituted arylaldehydes to give the 2-arylbenzimidazole 1-oxyl-3-oxide in 65 to 91% yeild.[42] Route C involved condensation of the bishydroxylamine with an appropriately substituted arylaldehyde to give the 2-arylbenzimidazole 1-oxyl-3-oxide.

Route C was based on the synthesis of **TMNN** developed by Ullman in which tetramethylbishydroxylamine could be condensed with aldehydes.[6,26] Disadvantages associated with this route lay in the difficulty in generating bis-hydroxylamines in high yield from the readily accessible dioxime or 1,2-diamine. Over reduction of the dioxime often occurred, leading to the 1,2-diamino derivative,[43] while over oxidization of the 1,2-diamine led to the 1,2-dinitro derivative.[44]

An alternative method of generating the 2-phenylbenzimidazole 1-oxyl-3-oxide is from the reaction of benzofuroxan with a phenylnitrone in refluxing benzene to give the desired product and nitrosobenzene[45] at 80% yield. A proposed mechanism for the condensation reaction is shown in Scheme 2.2.

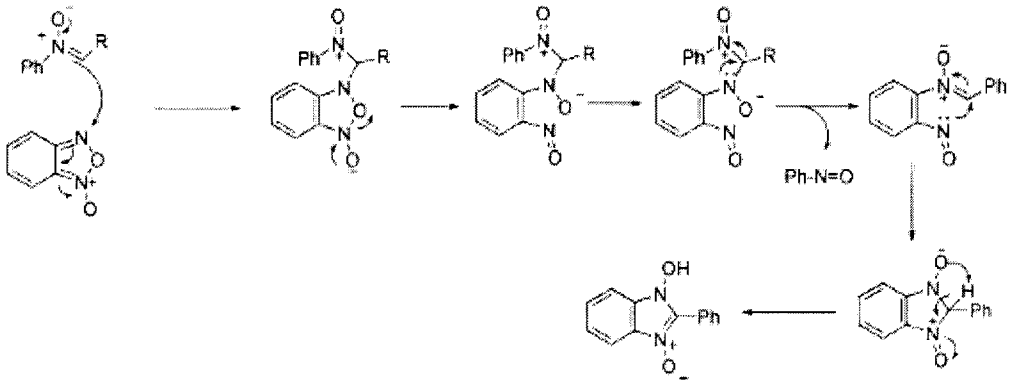

Scheme 2.2 - Route D: Condensation of a benzofuroxan and nitrone

This method gives the product in high yields (50 to 70%) and high purity with a simple workup. The phenylnitrone can be easily synthesized from benzaldehyde and hydroxylaminobenzene. This example was the only reported use of this reaction in the literature and it was not known whether the reaction would be applicable to a larger series of compounds.

Another alternative synthetic route for synthesizing benzimidazole 1-oxyl-3-oxide was examined based on the reaction of primary nitroalkanes with benzofuroxan in the presence of base (typically diethylamine).[46] The synthesizing route is shown in Scheme 2.3.

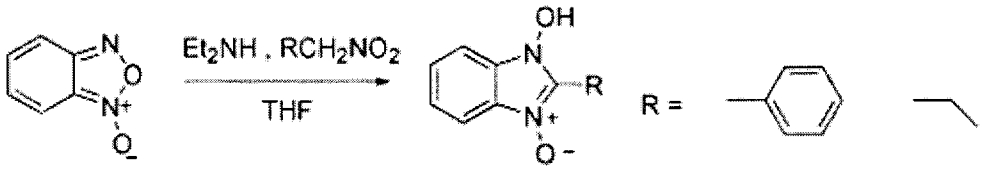

Scheme 2.3 - Route E: Condensation of nitroalkyl and benzofuroxan

There are challenges associated with using Route E to synthesize a larger class of annelated aromatic nitronyl nitroxides. Firstly, some furoxans are base sensitive and diethylamine was found to react in some cases with the furoxan faster than with the nitroalkane. Secondly, the nitroalkane is synthesized from a benzyl bromide, necessitating the synthesis of the halogenated precursor, as opposed to utilizing commercially available aldehydes, as is possible with the previous synthetic routes discussed. Thirdly, the reaction to make the nitroalkane derivative is low yielding, involving an S_N2 reaction of sodium nitrite with benzyl bromide,[47] which produces large quantities of nitrosooxymethyl-benzene along with the nitromethyl-benzene.

The final synthetic pathway considered for the synthesis of 2-phenylbenzimidazole 1-oxyl-3-oxide was the reaction of nitrosobenzene and benzonitrile oxide in ether at room temperature (Scheme 2.4, Route F).[40]

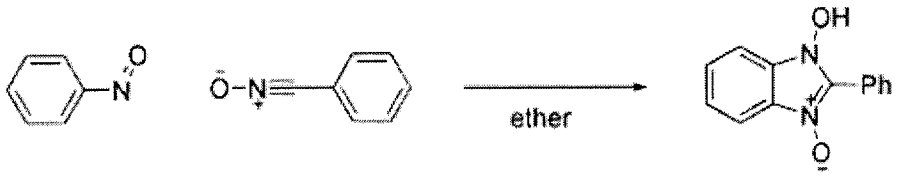

Scheme 2.4 - Route F: Reaction of nitrosobenzene with benzonitrile

Although Route F was the original method of synthesizing the 2-phenylbenzimidazole 1-oxyl-3-oxide, it is inadequate for several reasons. The most important reason is related to the unstable nature of benzonitrile oxides, which dimerize to form the diphenylfuroxan. In addition, the nitroso functional group is more synthetically challenging and is sensitive to oxidation and reduction. For these two reasons, the synthetic flexibility of this reaction pathway is limited and therefore not used in developing generalized synthetic methodology in this thesis.

Route B and Route D were found to be the most versatile. While Route B was found to generate the annelated radicals in consistently good yields (35 to 70%), the route required the use of harsh reaction conditions (3.5 M HCl, reflux, 4-5 hours) to produce the desired product. This led to problems in the synthesis of radicals containing acid sensitive functionality. The nitrone-benzofuroxan synthesis (Route D) was a more versatile synthetic tool. Benzimidazole 1-oxyl-3-oxide compounds made by the nitrone-benzofuroxan method were more pure than Route B, which allowed for simpler purification of the product. The reaction of

benzofuroxan with an arylnitrone in refluxing cyclohexane or benzene gave the product and nitrosobenzene in consistently high yields (50 to 70%) under mild conditions (Route D) with easy work up conditions and high purity (See Scheme 2.5.).

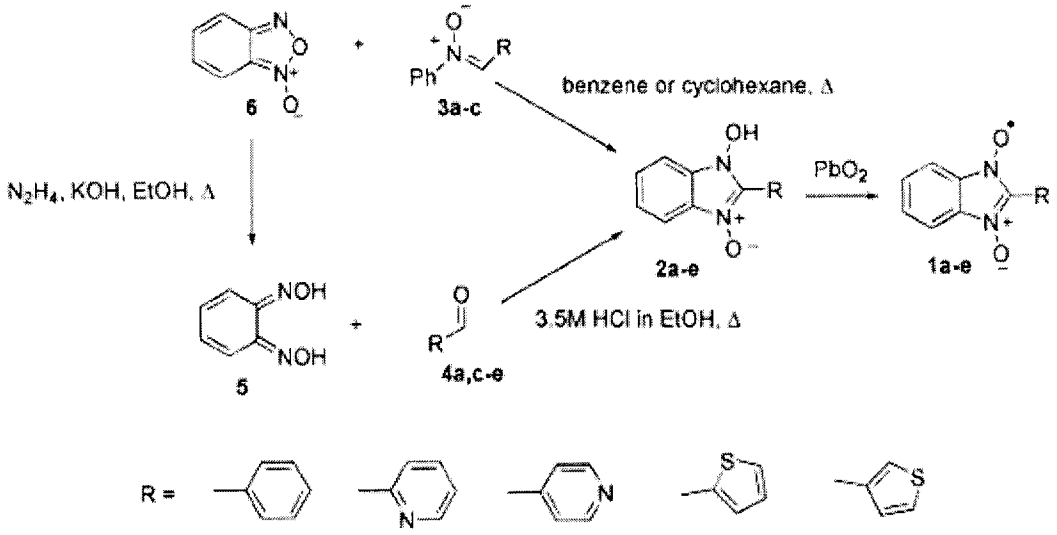

Scheme 2.5 - Synthesis of C2-heteroaromatic BNN

Route B started with the reduction of benzofuroxan to benzo-1,2-dioxime with hydrazine in potassium hydroxide-ethanolic solution in 56% yield. The benzo-1,2-dioxime was then heated in 3.5 M HCl in ethanol for 2 to 4 hours with the appropriate aryl aldehyde and then filtered to isolate the hydrochloric salt of the 2-arylbenzimidazole 1-oxyl-3-oxide. The neutral 2-arylbenzimidazole 1-oxyl-3-oxide compound was obtained by dissolving the salt in methanol/water, adjusting the pH to 10 with aqueous sodium hydroxide, filtering, and adjusting the pH to 7 with aqueous ammonium hydroxide to precipitate the neutral compound in 35 to 70% yield. **2a,c-e** were prepared by Route B.

Route D started with the reduction of nitrobenzene with zinc metal and ammonium chloride in water to synthesize hydroxylaminobenzene. The hydroxylaminobenzene was sonicated immediately with the appropriate arylaldehyde in ethanol to produce the arylnitrone. The arylnitrone was refluxed in benzene or cyclohexane with benzofuroxan to produce the 2-arylbenzimidazole 1-oxyl-3-oxide in 56 to 67% yield. The **2a-c** were prepared by Route D.

A major challenge for the synthesis of annelated nitronyl nitroxides is the low solubility of the precursor, benzimidazole 1-oxyl-3-oxide, in most organic solvents. The ^{1}H-NMR of the benzimidazole 1-oxyl-3-oxide in DMSO, after heating to reflux and sonication, showed decomposition of the compound. Direct probe MS of the decomposition product showed that the benzimidazole 1-oxyl-3-oxide loses oxygen under these conditions to form benzimidazole 1-oxyl and benzimidazole. The solubility could be partially modified by substitution at the C2-carbon. Substitution of the phenyl functional group to pyridyl led to the precursor being soluble in acidic water (pH < 4) due to the protonation site of the pyridyl group. The problem of solubility will be examined in Section 2.3.

The overall kinetic (chemical) stability of the radicals varied depending on the 2-position R-group. The radicals **PBNN, 2TBNN, 3TBNN,** and **4PBNN** were the most stable, slowly decomposing over years in the freezer in the solid state and over a week in solution exposed to air. The radicals proved to be stable in the solid crystalline state. A test was performed in which two crystals of **3TBNN** from the same crystallization attempt were placed in two melting point tubes.

One was left in the freezer, with the open end capped. The other was left on a window sill exposed to air and sunlight. After three months, a MS-direct probe was taken on both samples and the fragmentation patterns were identical. The chemical composition was constant, even when exposed to light and air. The radical **2PBNN** was the most unstable of the heteroaromatic radicals, with the radical decomposing in the solid state and in solution overnight. The rate of decomposition of the radicals in solution will be discussed in depth in Section 2.2.2.

2.2.2 - UV-Vis Spectroscopy.

The UV/Vis absorption spectra of the nitronyl nitroxides were measured in acetonitrile (ACN) and are shown in Figures 2.4 and Appendix 2. Radicals **2a-e** were a bright green/yellow color and exhibited similar spectra, with minor changes in molar absorptivity (ε) and λ_{max} (see Table 2.1).

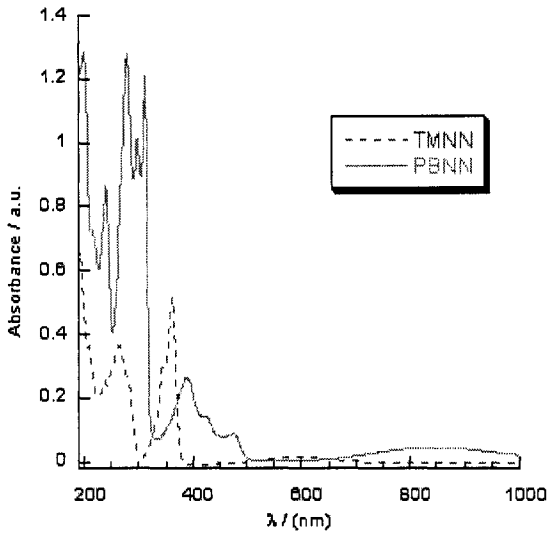

Figure 2.4 - UV/Vis spectrum of PBNN in ACN versus TMNN at 293 K and 10^{-5} M

Table 2-1 - UV-Vis λ_{max}[a] and extinction coefficient[s] (ε) for BNN radicals in ACN.

Radical	Short UV	Long UV	Visible	Near IR
PBNN	200 (21200)	279 (23000)	388 (6480)	825 (1280)
	241 (16500)	298 (18800)	421 (4320)	
		312 (22300)	475 (3220)	
2PBNN[c]	242 (20000)	280 (10000)	392 (5000)	762 (1000)
		308 (10000)	475 (2000)	
4PBNN	243 (13900)	281 (15200)	397 (4440)	831 (450)
		299 (14200)	427 (2010)	
		312 (17400)	483 (740)	
2TBNN	243 (15800)	289 (14900)	390 (4720)	975 (263)
		315 (25500)	433 (2050)	
		331 (36400)	482 (1300)	
3TBNN	240 (17800)	280 (24700)	386 (4970)	930 (432)
		299 (22400)	426 (2350)	
		313 (32200)	476 (1590)	
		330 (4080)		

[a]λ_{max} in nm. [b]ε in $(cm*M)^{-1}$ [c] estimated since radical was unstable in the solid state.

The UV/Vis spectrum of **PBNN** showed strong absorptions in the UV region (four transition from 240 to 330 nm, $\varepsilon \sim 20000$), medium strength absorptions in the visible (three transitions from 380 to 480 nm), and weak absorption in the near-IR (one broad transition at 850 nm).

The UV/Vis absorption bands were assigned using a combination of experimental and theoretical techniques, including TD DFT B3LYP/6-31G* calculations (Figure 2.2), solvatochromism due to changes in dielectric constant (Table 2.2), and molar absorptivity (Table 2.1).

Table 2-2 - Solvatochromism of λ_{max} for PBNN in nanometers

	CCl_4	benzene	ACN
UV λ_{max}	N/A[a]	N/A[a]	241
	286	282	279
	303	301	298
	317	315	312
Visible λ_{max}	400	397	388
	432	431	421
	476	477	475
Near IR λ_{max}	876	881	800

The series of strong absorption ($\varepsilon \sim 16000\text{-}30000$ $(cm*M)^{-1}$) in the UV region for **PBNN** in ACN were assigned as (π to π^*) transitions from the SOMO to $LUMO_3$ of similar A2 symmetry. When the solvent was changed from ACN to a non-polar, low dielectric constant solvent (benzene/CCl_4), the peaks only shift by 1-3 nm. Generally, (π to π^*) transitions are high intensity. The ε for the 240-300 nm transitions were above 10000 $(cm*M)^{-1}$. The TD DFT calculations showed an orbital with the same symmetry within 5.5127 eV of the SOMO (Table 2.3) and this was near the energy of the 241-300 nm (5.0-4.0 eV) transitions. Figure 2.5 shows peak assignment using TD B3LYP/6-31G*.

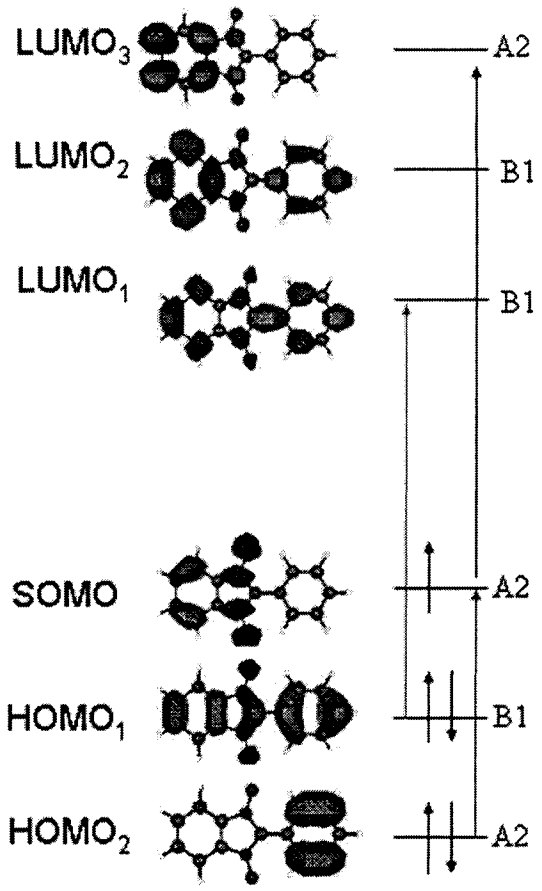

Figure 2.5 - UV/Vis peak assignment using TD B3LYP/6-31G*

Table 2-3 - Assignment of UV/Vis absorption bands based on TD DFT calculations

nm	eV[a]	eV[b]	Transition
241	5.16	5.5127	SOMO to $LUMO_3$
388	3.20	4.4913	$HOMO_1$ to $LUMO_1$
825	1.51	1.3275	$HOMO_2$ to SOMO

[a]Energy of UV/Vis transition from spectrum. [b]Calculated energy of UV/Vis transitions

The next set of bands in the (350 - 450 nm) region were assigned as (n to π^*) transitions with medium to weak intensity (ε~2000-6000 $(cm*M)^{-1}$) from the $HOMO_1$ to $LUMO_1$ with B1 symmetry. These peaks undergo a hypsochromic shift of 10 nm when the solvent was changed from benzene/CCl_4 to ACN. The ε and hypsochromic shifts in high dielectric solvent were consistent with (n to π^*) transitions. The TD DFT calculations showed that there was symmetry-allowed transition from the $HOMO_1$ to $LUMO_1$ that was similar in energy to the observed transition (3.20 eV versus 4.49 eV).

The extremely weak transition (ε~ 1000 $(cm*M)^{-1}$) out at 850 nm was determined to be a (n to π) transition, or HOMO to SOMO, based on the ε and calculations. The transition was low intensity, so initially, it was thought that the transition was a symmetry forbidden transition (n to π^*), but the calculations lacked any possible transitions in the energy range of the absorption. The best hypothesis was that this transition was a $HOMO_2$ to SOMO transition, where an electron was promoted into the half-filled MO. The transition was symmetry-allowed (both were A2), and the calculated energy for this transition was 1.3275 eV, which was close to the experimental energy of 1.51 eV. This transition into the half-filled orbital was consistent with the literature example of the UV-Vis spectrum of triphenylmethane radical, which has a weak transition at 500 nm that was assigned to a HOMO to SOMO transition.[48]

The rate of decomposition of the radical could be monitored using UV-Vis and was solvent dependent. For example, methanol caused the radical to decay slowly over several hours (Figure 2.6).

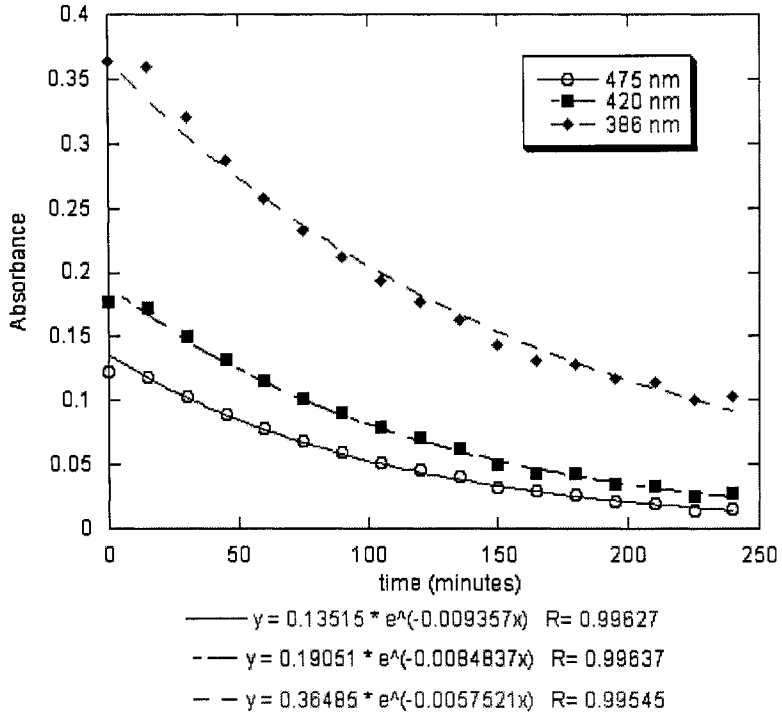

Figure 2.6 - Decay of PBNN in methanol over 4 hours

The rate of decay is approximated by a simple first order rate law with the average τ_1= 0.000131 s^{-1} and a half life of 5290 seconds (88.1 minutes). Fortunately, the radical is much more stable in non-polar solvents. The radical is stable in benzene for days with exposure to air.

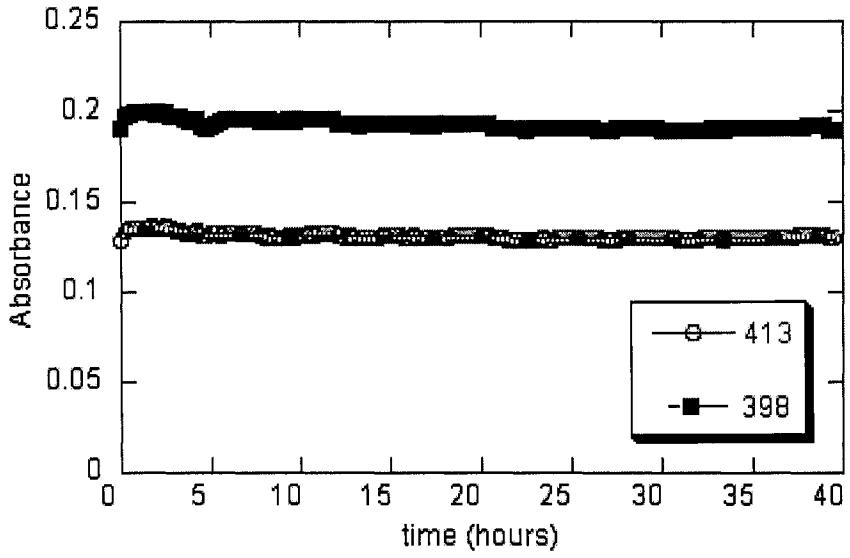

Figure 2.7 - Decay of PBNN in benzene over 40 hours

Unfortunately, when attempting to crystallize the radical, only n-pentane yielded crystals. Other solvents and combinations, such as benzene, toluene, DCM, petroleum ether, and diethyl ether, yielded a fine powder instead.

2.2.3 - Cyclic Voltametry.

Cyclic voltammograms were recorded between -1.5 V and 1.5 V versus $Ag/AgNO_3$ in 0.1 M n-Bu_4NPF_6/ACN at 25 °C using a Princeton Applied Research Powerstat 2263 Advanced Electrochemistry System and PowerSuite v2.33.0 and are reported in Figures 2.8 and Appendix for Chapter 2. Ferrocene was used as an external standard to check the calibration of the apparatus. Radical solutions were made at 2-5.0 mM concentrations. The cathodic and anodic sweep potentials are reported in Table 2.4.

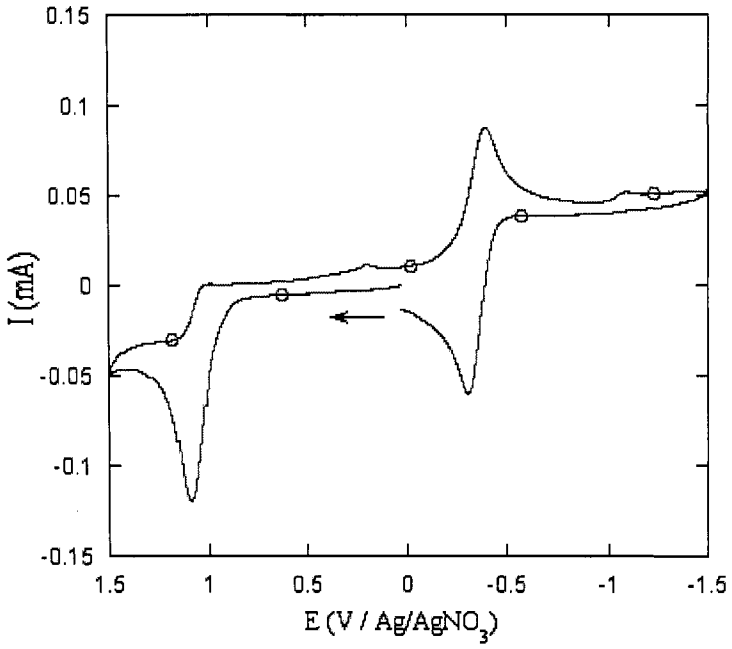

Figure 2.8 - Cyclic voltammogram of PBNN in 0.1 M TBAHFP dry ACN versus $Ag/AgNO_3$

Table 2-4 - Cyclic voltametry data of BNN radicals

Radical	$E_{an}(1)$ (V)	$E_{ca}(1)$ (V)	$E^{1/2}$ (V)	ΔE (mV)	$E_{an}(2)$ (V)
PBNN	-0.396	-0.308	-0.352	88	1.086
4PBNN	-0.2	n/a	n/a	n/a	1.220
2TBNN	-0.397	-0.289	-0.343	108	1.048
3TBNN	-0.384	-0.300	-0.342	84	1.082

vs 0.01M $Ag/AgNO_3$ in dry ACN with 0.1 M TBAHFP, glassy carbon working electrode, Pt wire auxiliary electrode, scan speed 50 mV/s, rt.

The radicals could be separated into two groups based on the cyclic voltammograms: **PBNN/2TBNN/3TBNN** and **4PBNN**. Both groups showed some degree of decomposition during CV in the form of a brown solid that was determined to be the benzimidazole 1-oxyl-3-oxide precursor by MS and ^{1}H-NMR. The **4PBNN** was much more dramatic, which would cause a drop in current after one cycle as it coated the electrochemical cell (Figure 2.8).

The radicals **PBNN/2TBNN/3TBNN** showed two one-electron transitions at -0.3 V and 1.1V versus $Ag/AgNO_3$. **4PBNN** showed two transitions at -0.200 V and 1.22 V, but both transitions were completely irreversible. Figures 2.9 and 2.10 show these cyclic voltammograms.

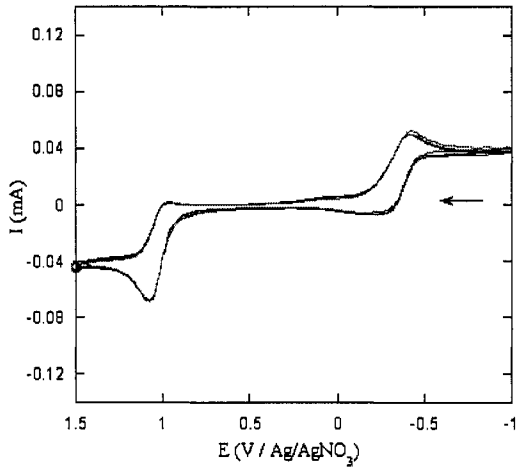

Figure 2.9 - Cyclic voltammogram of PBNN in 0.1 M TBAHFP dry ACN versus $Ag/AgNO_3$ after 5 cycles

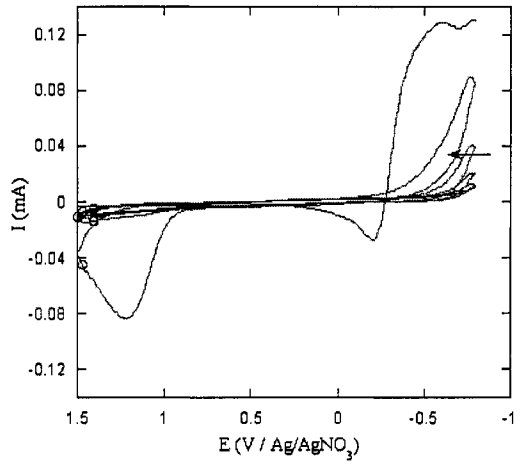

Figure 2.10 - Cyclic voltammogram of 4PBNN in 0.1 M TBAHFP dry ACN versus $Ag/AgNO_3$ after 5 cycles

For the **PBNN/3TBNN/2TBNN** radicals, the quasi-reversible wave at -0.3 V was determined to be quasi-reversible by looking at the ΔEs and by varying the scan rate. Fully reversible diffusion controlled processes ideally have a ΔE between anodic and cathodic peaks of 58 mV. The ΔEs for the transition at -0.300 V for **PBNN/3TBNN/2TBNN** were all between 80-110 mV, indicating that they were not completely reversible. The plot of the peak current against the square root of the scan rate for **3TBNN** was linear (Figure 2.12) and the potential versus the log of the scan rate for **3TBNN** did not change (Figure 2.11).

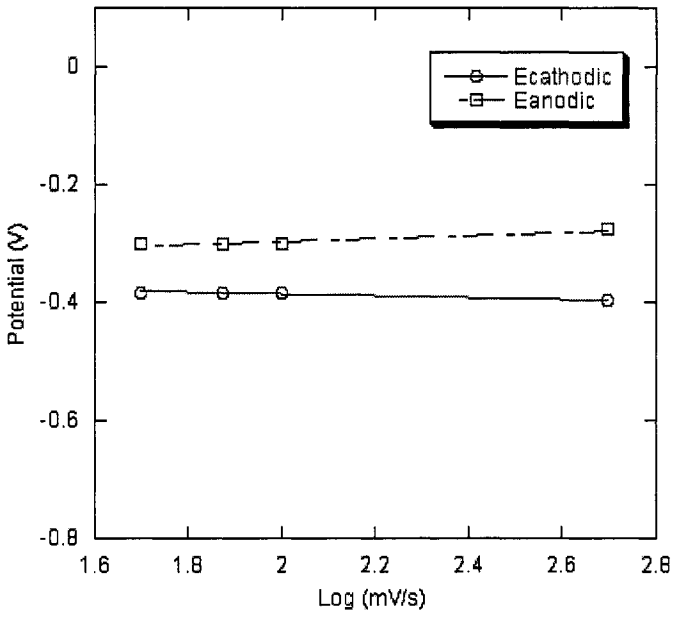

Figure 2.11 - Peak current potential versus scan rate for 3TBNN in 0.1 M TBAHFP dry ACN versus $Ag/AgNO_3$

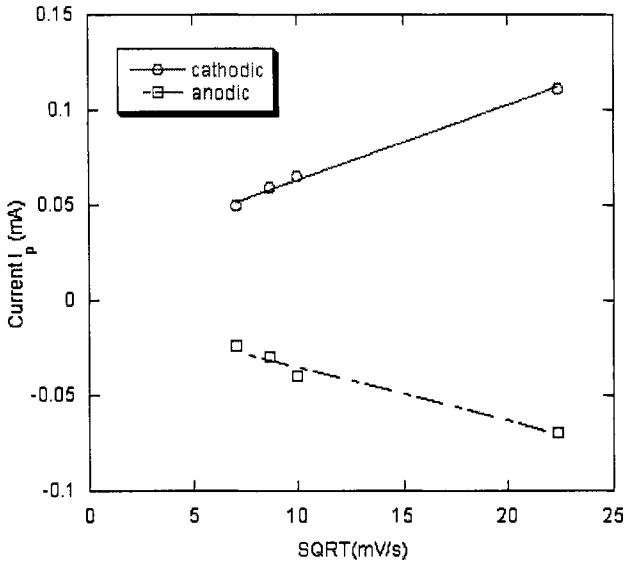

Figure 2.12 - Current versus the square root of the scan rate for 3TBNN in 0.1 M TBAHFP dry ACN versus $Ag/AgNO_3$

2TBNN and **PBNN** exhibited similar trends. These were properties of a reversible process, and with $\Delta E \sim 100mV$ for the three radicals, the transition was quasi-reversible. In addition to being quasi reversible, the transition at -0.300 V was determined to be a reduction potential since the radicals reacted with ascorbic acid in ACN (E_{ox} = +0.168 V versus Ag/AgCl) or TTF (E_{ox} = +0.340[49] versus Ag/AgCl) (Figure 2.13).

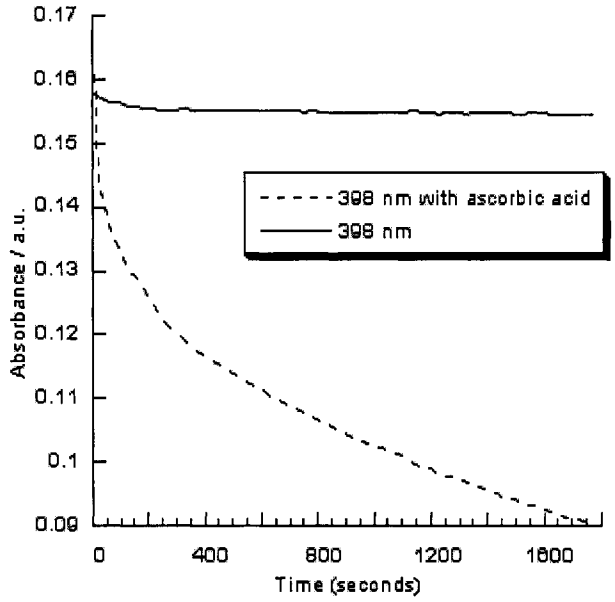

Figure 2.13 - Decay of PBNN in ACN due to addition of ascorbic acid in benzene

The low reduction potential makes the benzimidazole nitronyl nitroxide an extremely good electron acceptor, similar to the widely used TCNE ($E^{1/2}$ = -0.32 versus Ag/AgCl).[50] The second wave at 1.086 V was determined to be completely irreversible. There was no cathodic wave at 50 mV/s. If the scan rate was increased to 500 mV/s, the cathodic wave started to appear but not in a linear relationship with the scan rate. The benzimidazole 1,3-oxide cation was extremely unstable and decayed irreversibly.

Another useful property when considering electronic properties was the band gap between HOMO and LUMO. This band gap has been shown to have an influence on the conducting properties of the material in the solid state. The electrochemical band gap in solution for **PBNN** was measured to be 1.438 V (or 862 nm), which corresponded to the optically measured band gap of 1.50 V (or

825 nm) in ACN. Generally, the band gap of a material needs to be less than 1 V in order for it to be a good conductor, so this predicted that these radicals will be semiconductors in the solid state.

Based on the cyclic voltammogram, BNN radicals were harder to oxidize and easier to reduce than the parent **TMNN**. This represented a large change in electronic structure upon substitution of tetramethyl to benzimidazole. The change in electronic structure resulting from the annelation of the nitronyl nitroxide could be compared by examining the redox potentials of **PBNN** to the parent **TMNN** compound. The cyclic voltammogram of **TMNN** was measured by the same methodology and was found to have a reversible one-electron oxidation at 0.573 V versus $Ag/AgNO_3$ (ΔE = 87 mV) and irreversible one-electron reduction at -1.18 V versus $Ag/AgNO_3$ (ΔE = 500 mV). Annelation shifted the reduction potential of **PBNN** by 0.831 V and the oxidation potential by 0.513 V compared to **TMNN**. This large shift in energy of the SOMO of the annelated radical illustrated an overall drop in energy due to the addition of the annelated ring, which made the radical more prone to reduction but more stable to oxidative conditions. This was in agreement with experimental evidence. The band gap was determined electrochemically for **TMNN** to be 1.753 V compared to 1.50 V for **PBNN**.

2.2.4 – Fluorescence.

Fluorescence measurements were taken on a Perkin Elmer LS-50B Luminescence Spectrometer in the UW Spectroscopic and Analytical

Instrumentation Facility. The samples were prepared by dissolving crystalline samples of the radicals **PBNN/2TBNN/3TBNN/4PBNN** in benzene, blanking the spectrometer against benzene, and measuring the emission spectrum when exciting at 300 nm (see Figure 2.14).

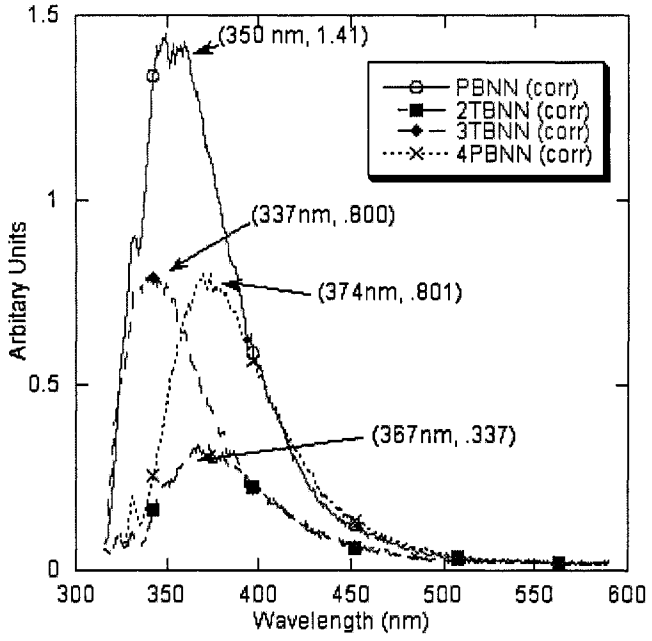

Figure 2.14 - Fluorescence Measurements of the PBNN/2TBNN/3TBNN/4PBNN in benzene (excitation at 300nm, corrected by concentration)

Initially, it was found that all radicals **PBNN, 2TBNN, 3TBNN,** and **4PBNN** fluoresced in the 350 – 375 nm range when excited at 300 nm, with the fluorescence maximum shifting depending on the aromatic group. This is extremely unusually since radicals classically inhibit fluorescence. Unpaired electrons provide a method of non-radiative decay by dipolar coupling with the excited state of the fluorescent species, causing the fluorescence to be quenched. Initially, it was unknown if the radical was responsible for the observed

fluorescence or some extremely efficient fluorescent impurity that was being excited by the same wavelength as the π to π^* absorption of the radical's UV-Vis spectrum. We set out to determine if the radical was the cause of the fluorescence.

According to the literature, the parent **TMNN** does not fluoresce and there was no recorded fluorescence data for **PBNN**. Previous experiments had indicated that the **PBNN** radical reacts with ascorbic acid to form an EPR silent material. Ascorbic acid does not exhibit fluorescence at 300 nm either. To determine if the radical was the primary fluorescent species, an experiment was set up in which the fluorescence was measured before and after the radical was reacted with ascorbic acid. Figure 2.15 shows the results of those measurements.

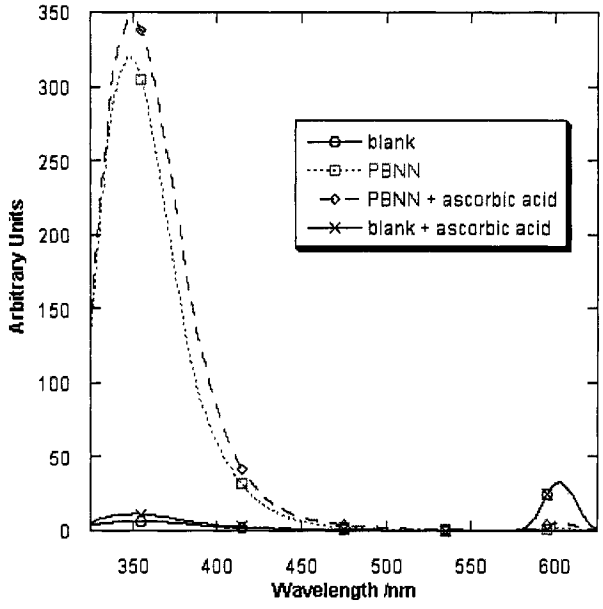

Figure 2.15 - Fluorescence Measurement of PBNN before and after the addition of ascorbic acid in ACN (300nm excitation)

The radical was found to not be responsible for the high fluorescence seen in the solution. The highly fluorescent compound was a trace impurity of the compound that was stable towards the ascorbic acid. It was hard to isolate, being one of many compounds that appeared after the decomposition of the radical. In addition, the compound did not appear in all samples of the radical.

After running a preparative TLC on a sample of decomposed **PBNN** in 95:5 DCM/MeOH with the fluorescent peak present, the compound was finally extracted with DCM, and an electrospray MS was run on the extract in ACN. The MS determined the primary molecular ion of the fluorescent impurity was 194 m/z (193 m/z in negative mode and 195 m/z in positive mode), which corresponded to deoxygenated 2-phenylbenzimidazole which undergoes fluorescent emission at 350-370 nm when excited at 305 nm.[51] This was consistent with the fluorescence impurity seen in the decomposed radical sample and, based on the fragmentation pattern of the direct probe MS spectra of the radicals and radical precursors and the loss of the di-oxygen functionality, was extremely reasonable.

2.2.5 - EPR Analysis.

The EPR spectra of annelated nitronyl nitroxides (Figures 2.16 to 2.20) were measured in degassed benzene. Analysis of the spectra showed the expected 5-line signal in a 1:2:3:2:1 hyperfine coupling constant (hfcc) pattern consistent with the coupling to two equivalent nitrogen. Superhyperfine coupling constants

could be resolved for coupling with the two sets of equivalent hydrogen on the annelated ring and the different hydrogen on the substituent rings.

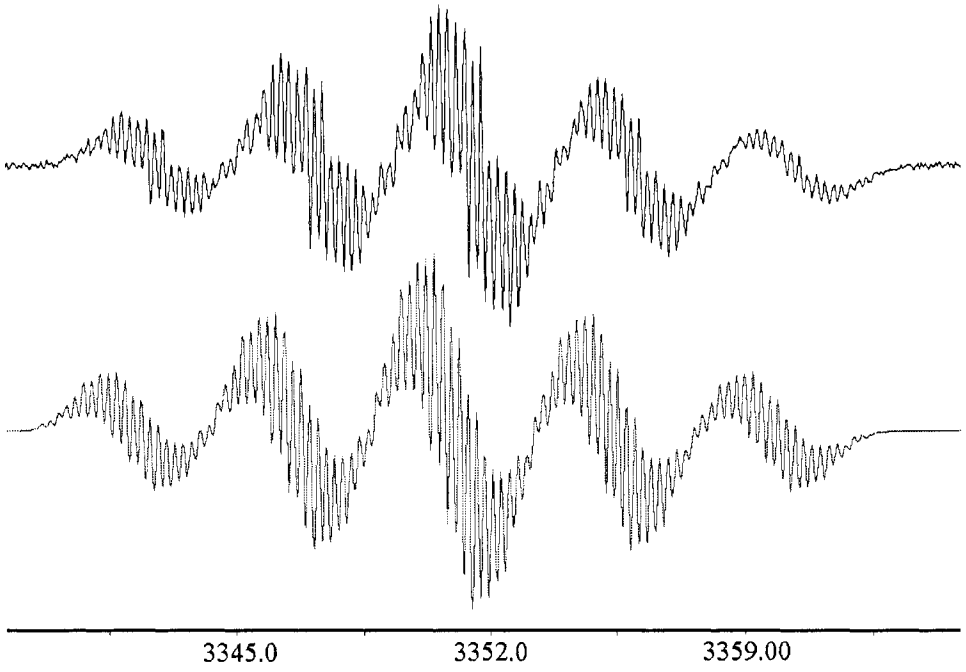

Figure 2.16 - EPR of PBNN in degassed benzene (top = experimental: bottom = simulated) at RT and ~10^{-5} M.

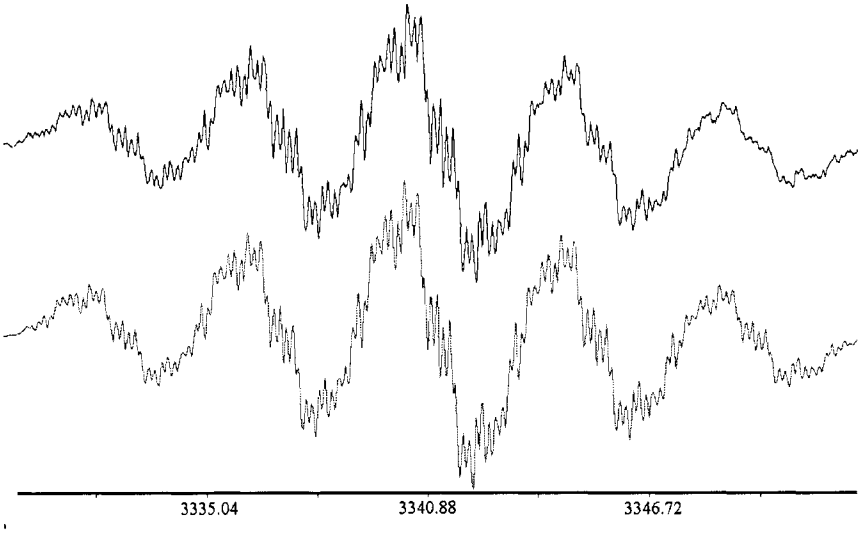

Figure 2.17 - EPR of 2PBNN in degassed benzene (top = experimental: bottom = simulated) at RT and ~10^{-5} M.

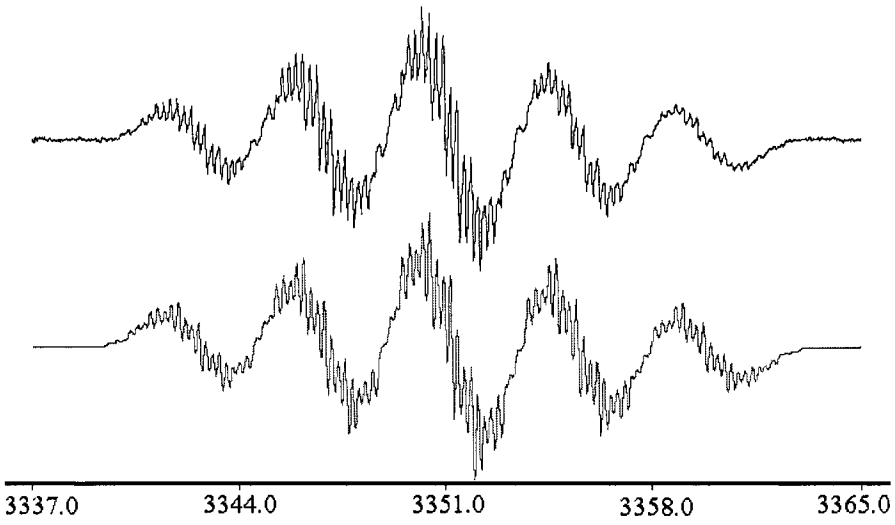

Figure 2.18 - EPR of 4PBNN in degassed benzene (top = experimental: bottom = simulated) at RT and ~10^{-5} M.

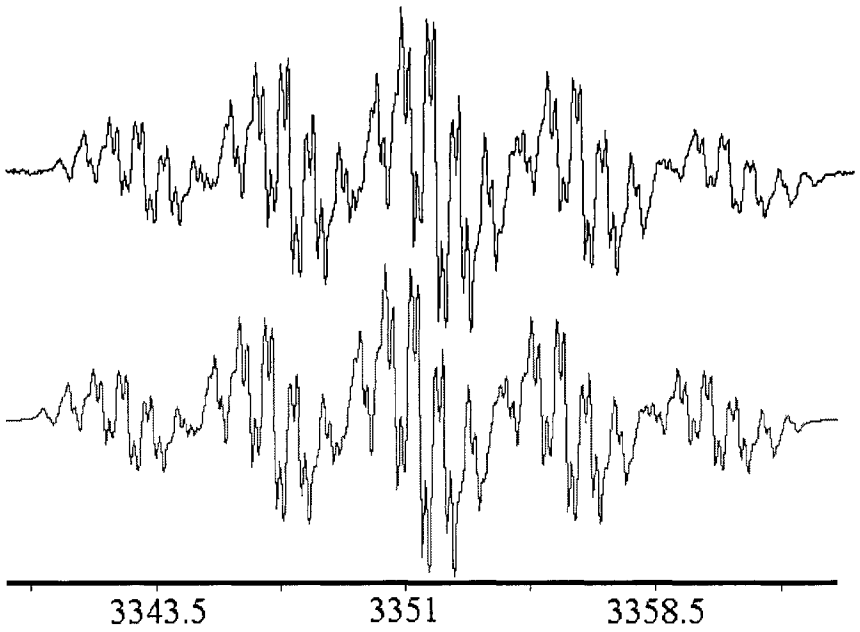

Figure 2.19 - EPR of 2TBNN in degassed benzene (top = experimental: bottom = simulated) at RT and ~10^{-5} M.

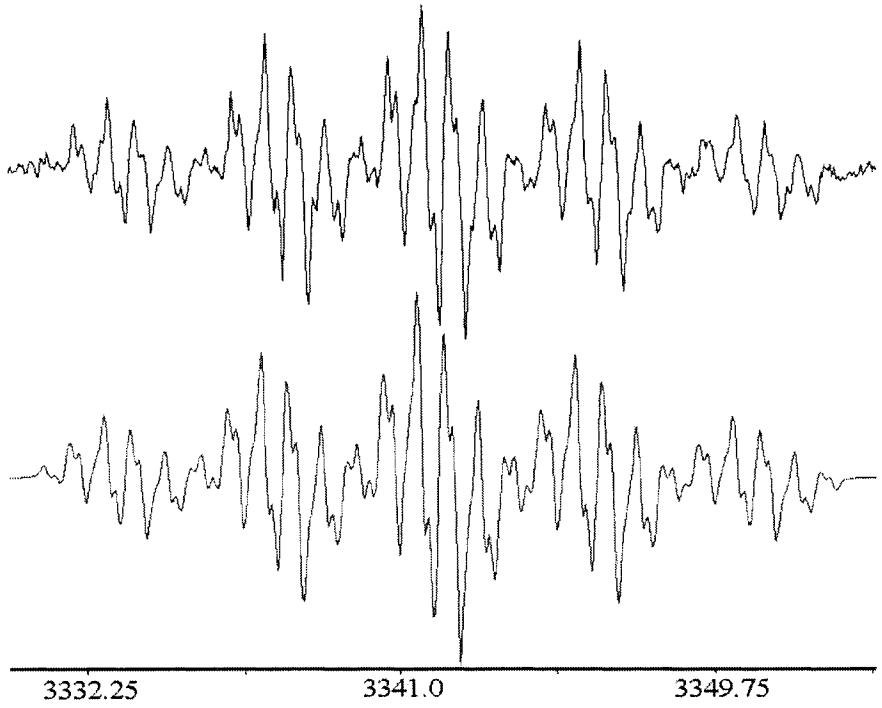

Figure 2.20 - EPR of 3TBNN in degassed benzene (top = experimental: bottom = simulated) at RT and ~10^{-5} M.

The g-value of the radicals were measured relative to the standard DPPH, with the g value for all the radical derivatives being approximately 2.0070. [52] Hfccs were simulated with WinSim using the nitroxide simulation type and DFT calculations as an rough estimate of hffcs. A summary of the hfcc is reported in Table 2.5. Assignments of the hfccs to individual atoms were made by referencing the spin density distribution generated by the DFT calculations. The EPR of the annelated benzimidazole nitronyl nitroxide showed that the structural change of tetramethyl to annelated benzene produced greater spin delocalization onto the annelated ring.

Table 2-5 - EPR hfcc (in Gauss) of heterocyclic BNN in degassed benzene

atom	PBNN	2PBNN	4PBNN	2TBNN	3TBNN	TMNN[1]
N	4.370	4.260	4.260	4.372	4.378	7.435
H-α	0.930	0.920	0.910	0.991	0.957	----
H-β	0.650	0.690	0.730	0.742	0.698	----
H-o	0.490	0.230	0.410	----	----	0.495
H-m	0.220	0.200	0.220	----	----	0.173
H-p	0.410	0.450	----	----	----	0.421
H-m'	----	0.200	----	----	----	----
N-pyr	----	0.690	0.690	----	----	----
H2-thio	----	----	----	----	0.723	----
H3-thio	----	----	----	0.728	----	----
H4-thio	----	----	----	0.544	0.269	----
H5-thio	----	----	----	0.174	0.079	----

[1] [32] in CCl_4

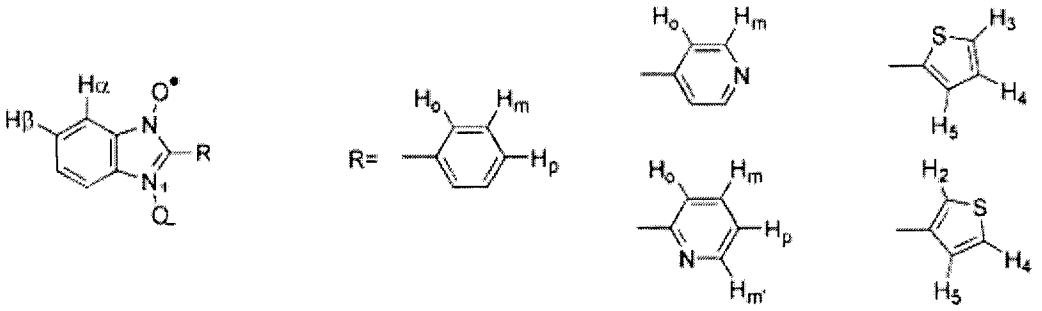

The hfcc for the 2-position phenyl group for **PBNN** was almost identical to the **TMNN**, showing that the annelation does not change the spin polarization mechanism through the center carbon in the nitronyl nitroxide moiety. The hfcc on the nitrogen in the nitronyl nitroxide dropped dramatically from the **TMNN** to **PBNN**, with the unpaired spin density being delocalized into the annelated benzene ring.

The hfccs on the annelated aromatic positions H-α and H-β were consistently higher than hyperfines associated with the phenyl ring. The change of heterocyclic aromatic R-group did not significantly change the spin populations

on the annelated moiety of the molecule (N, H_α, and H_β). This showed that the 2-position R-group did not have a large influence on the SOMO, consistent with the similar UV-Vis spectra and cyclic voltammograms.

The hfcc for the nitrogen in the nitronyl nitroxide moiety of the **BNN** series of radicals was found to be an average of 4.328 +/- 0.062. All **BNN** radicals had large hfcc's with the 4 protons on the annelated benzene with the magnitude of the hfcc varying little with the different aromatic groups (H_α = 0.942 +/- 0.033 and H_β = 0.702 +/- 0.036). The **2TBNN/3TBNN** EPR spectrum looked different from the **PBNN**, but the difference was found to be due to a change in the number of protons and competing spin polarization pathways out through the thiophene ring. Unlike six membered rings, spin polarization on a non-symmetrical 5-membered thienyl ring leads to destructive and constructive overlap since there are an odd number of atoms in the ring. Spin polarization of the electrons through bonds happens differently depending on which bonds (C-C versus S-C) transfer the spin more effectively.

2.2.6 - Computations of BNN radicals

Experimental EPR spin populations are commonly used to evaluate the effectiveness of computational analytical methods in predicting spin populations. In this experiment, hfccs were converted to spin densities using the McConnell equation[35] with Q_{CH}^{H} = 23.7 G and Q_N^N = 25 G. Table 2.6 shows that one can evaluate how accurately the B3LYP/6-31G* computations were at estimating the spin populations.

Table 2-6 - Comparison of calculated and simulated spin densities

EPR
Comp*

	C-β	C-α	N	X1	X2	X3	X4	X5
TMNN			0.298	0.021	0.007	0.018		
			0.263	*-0.048*	*0.028*	*-0.043*		
PBNN	0.029	0.04	0.175	0.018	0.007	0.018		
	0.024	*0.033*	*0.184*	*-0.046*	*0.025*	*-0.045*		
2PBNN	0.029	0.038	0.166	0.0136	0.006	0.0133	0.005	*0.0192*
	0.025	*0.032*	*0.169*	*-0.039*	*0.019*	*-0.038*	*0.018*	*-0.03*
4PBNN	0.032	0.038	0.17	0.018	0.009	*0.017*		
	0.023	*0.034*	*0.181*	*-0.045*	*0.021*	*-0.035*		
2TBNN	0.031	0.042	0.172	*S*	0.023	0.007	0.031	
	0.025	*0.036*	*0.185*	*-0.008*	*0.029*	*-0.007*	*-0.061*	
3TBNN	0.029	0.04	0.175	0.032	*S*	0.0035	0.0107	
	0.022	*0.036*	*0.179*	*-0.071*	*-0.011*	*0.017*	*-0.021*	

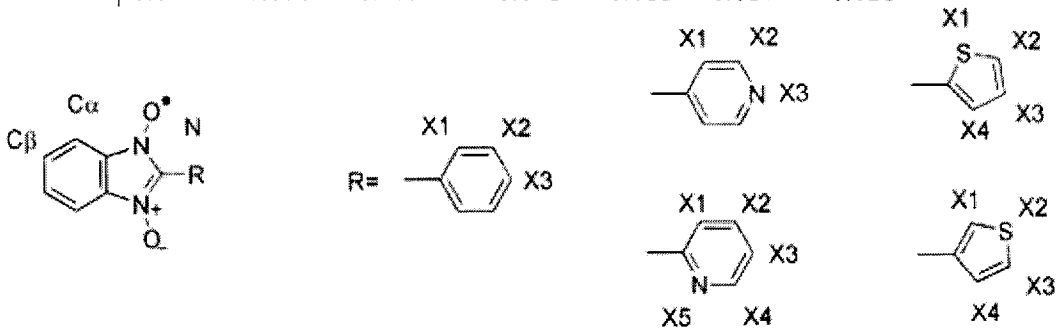

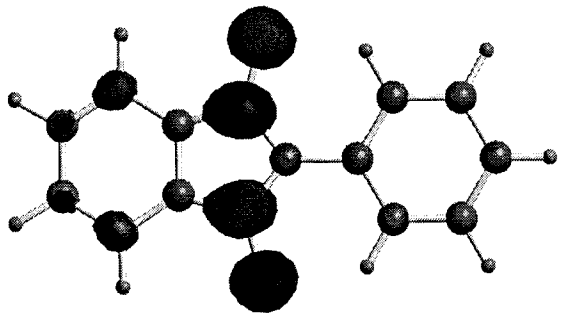

Figure 2.21 - SOMO of PBNN generated at B3LYP/6-31G* with CubGen (isocontour = 40, scaling factor = 0.18) and visualized with Chem3D

There were several problems that were consistent with previous studies in comparing spin density from neutron diffraction studies with various computational methods.[31,32] The amount of spin density on the R-group was consistently overestimated by the calculations compared to the experimental spin densities. The change of heterocyclic aromatic group did not significantly change the spin populations on the annelated moiety of the molecule, indicating that the 2-position R-group did not have a large influence on the SOMO. Examination of the computationally determined SOMOs (Figure 2.21 and Appendix Figures 2.39-2.42) confirmed these experimental results. All BNN radicals had large hfccs with the 4 protons on the annelated benzene.

The experimental EPR spin populations could be used to evaluate the effectiveness of computational analytical methods in predicting spin populations. Table 2.6 made it clear that the B3LYP[15]/6-31G*[16] did an adequate job at estimating the spin populations. Consistent with previous studies comparing spin density from neutron diffraction studies with various computational methods, [31,32] the amount of spin density on the nitrogen and R-group were overestimated by the calculations. However, the spin on the annelated ring was repeatedly underestimated. The reason that the calculations consistently distort the spin distribution may result from the fact that the radical was free to rotate in solution, taking the R-group and benzimidazole π-systems out of phase with each other. The computation minimum was fixed in a geometry optimized planar position when molecular orbitals were being computed and that the B3LYP method has

been shown to overestimate the magnitude of dihedral rotation energy barrier by 1-2 kcals in alkylbenzene radicals.[13] The geometry-optimized calculations would better describe the solid-state spin distribution than EPR in solution.

Comparing the **PBNN** to **TMNN**, the major difference was in how the annelated aromatic system changed the spin density on the O-N-C-N-O segment. There was 41% less spin density on the nitrogen of **PBNN** than **TMNN**, stemming from the extra delocalization on the annelated benzene ring. The annelated ring showed large spin populations, twice as often as the phenyl R-group. The spin population on the different R-groups alternated in sign while all the values on the annelated ring were positive.

Alternation of spin signs on neighboring atoms indicated spin polarization as the mechanism for spin propagation. Due to the relative magnitudes from experimental spin populations and sign of spin populations from computational analysis, it was clear that the computationally derived SOMO correlated with the spin distributions on the annelated benzene, while the R-group's spin populations were due to spin polarization through the central carbon in the ONCNO moiety.

It was possible that the calculations consistently distort the spin distribution, because the radical was free to rotate in solution, taking the R-group and benzimidazole π-systems out of phase with each other. To prove that the lowest energy geometry optimized configuration does not reflect spin populations of the radical in solution state, a series of single point calculations were performed, changing the amount of π-conjugation with the R-group by altering

the dihedral (and therefore the overlap) between rings. These calculations used the planar optimized geometry of the molecule, but each point in the series resulted in a change in the dihedral angle between the phenyl and benzimidazole portions of the radical from the ~5° optimized configuration to 90° between rings (Figure 2.22).

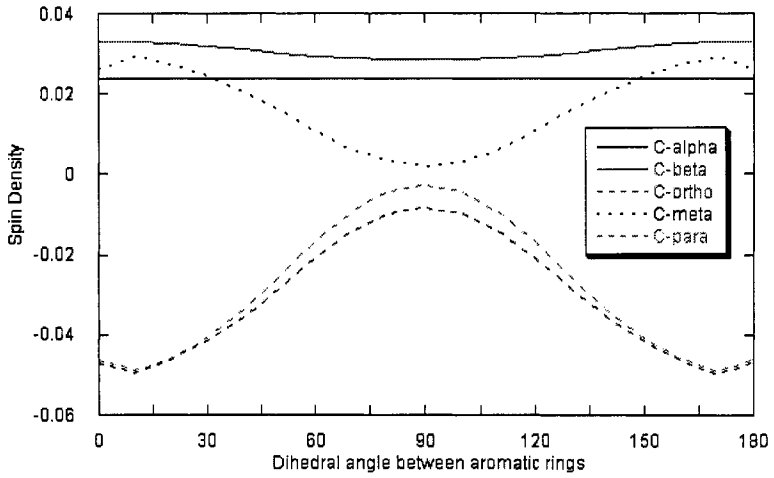

Figure 2.22 - Spin Density dependence on the Dihedral Angle between Aromatic Moieties in PBNN

As shown in Figure 2.22, a drop in spin density on the R-group carbon was seen as the π-conjugation was disrupted. The computations overestimate the amount of spin density on the R-group by assuming the molecule was almost planar in arrangement, when this was not consistent in solution. The computational dihedral angle that corresponded to EPR experimental values was 50-60°.

2.2.7 - X-ray Crystallographic Analyses.

Slow evaporation of saturated radical solution in n-pentane yielded X-ray quality crystals of **2TBNN** and **3TBNN**. After multiple attempts using this and other methods, X-ray quality crystals for **4PBNN** could not be obtained, mainly due to twinning or formation of polycrystalline material. X-ray measurements were taken on a Nonius KappaCCD (1997) diffractometer. X-ray crystal data and structure refinement parameters are listed in Table 2.9. The ORTEP diagrams for the two thienyl radicals are illustrated in Figure 2.20 (page 48). Selected bond lengths and angles are shown in Table 2.8 on page 60, compared with the geometry optimized conformations of the radicals using B3LYP density functional theory and 6-31G* basis set with Gaussian 98 software package.

Both radicals demonstrated a large amount of disorder of the molecules in their orientation in the lattice (Figure 2.23). This was illustrated in the larger than expected electron density on the C1 atom in the **3TBNN** and C2 atom in the **2TBNN**. In the case of **3TBNN**, the molecule had approximately 28% of the molecules rotated 180° along the perpendicular z-axis, with the S1 atom occupying the same position as the C1. In the **2TBNN** crystal, 50% of the radicals were in one orientation, and 50% of the molecules were arranged in a way that had an 180° rotation along the long y-axis. Thus, the C2 atom had significantly more electron density than it normally would, since half the time a sulfur atom was in that position. The type of disorder in each compound was extremely important and had dramatic effects on the magnetic behavior.

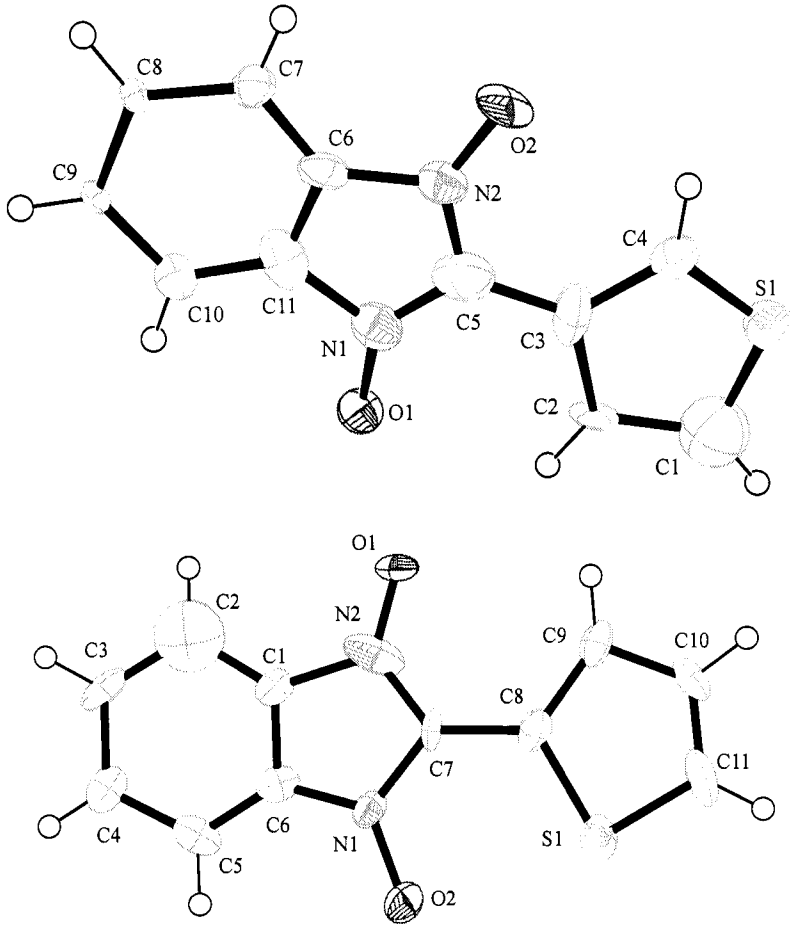

Figure 2.23 - ORTEP diagram for 2TBNN and 3TBNN showing 50% probability thermal ellipsoids

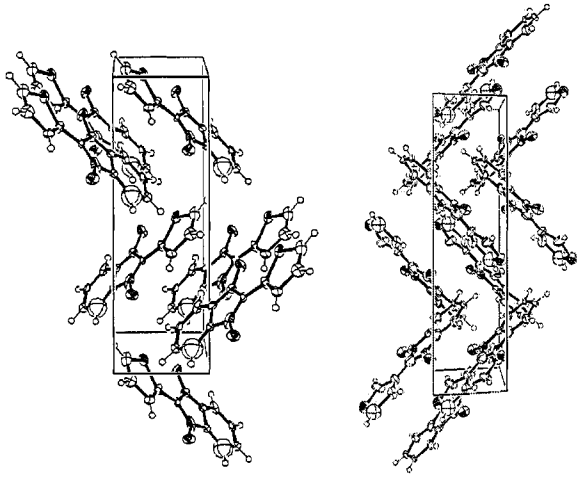

Figure 2.24 - Unit cells of 2TBNN and 3TBNN radicals in the crystalline state

Table 2-7 - Crystallographic Data for 2TBNN and 3TBNN

	2TBNN	**3TBNN**
Empirical formula	$C_{11}H_7N_2O_2S_1$	$C_{11}H_7N_2O_2S_1$
Formula weight	231.25	231.25
a/ Å	7.331(1)	4.800(1)
b/ Å	4.6370(5)	17.022(4)
c/ Å	14.750(3)	12.520(2)
α/deg	90	90
β/deg	104.331(5)	111.273(6)
γ/deg	90	90
Volume/ A^3	485.81(13)	953.3(3)
Z	2	4
Crystal system, space group	Monoclinic, *P c* (No. 7)	Monoclinic, *P* $2_1/c$ (No. 14)
Crystal size/mm	0.48 x 0.12 x 0.02	0.41 x 0.05 x 0.02
Temperature/K	130(2)	130(2)
Wavelength/ Å	0.71073	0.71073
Calculated ρ/ mg/m^3	1.581	1.611
Absorption coefficient (μ)/mm^{-1}	0.316	0.322
R [I>2σ(I)][a]	0.0630	0.0638
wR^2 [b]	0.1535	0.1786

[a] $R1 = \Sigma||F_o|-|F_c||/\Sigma|F_o|$

[b] $wR2 = sqrt(\Sigma(wDD)/\Sigma(wF_oF_o))$, where $D = (F_oF_o - F_cF_c)$, calc $w = 1/[s^2(F_o^2)+(0.0615P)^2+0.0000P]$ and $P=(F_o^2+2F_c^2)/3$.

The bond lengths and angles for the **2TBNN** and **3TBNN** X-ray structure compared to computational optimized geometry were significantly different, further illustrating the disorder in the crystal state.

In Table 2.8, the benzimidazole bonds for the X-ray structure and computations of **3TBNN** are similar, but the bond lengths and angles on the thienyl moiety are significantly different between the computations and X-ray structure. This is in perfect agreement with the observed disorder in the crystal. On the other hand, the **2TBNN** had significant differences throughout the entire molecule, demonstrating how much more the rotation distorts the packing and neighboring interactions in the lattice from the expected computationally derived conformation.

The planar conformation of **2TBNN** and **3TBNN** in the solid state were in stark contrast with the solid state packing of the structurally similar 3-thienyl **TMNN**.[53] The dihedral angle between the thienyl and benzimidazole rings was almost zero in both **2TBNN/3TBNN** derivatives' X-ray structures. This was unusual since the standard dihedral angle between aromatic rings was around 33°. The observed dihedral angle in the 3-thienyl **TMNN** X-ray structure was 16.4°. The magnetism for the 2-thienyl **TMNN** was measured, but the X-ray structure for 2-thienyl was never determined.[54] This planar conformation allowed for the slipped stack solid state packing arrangement that was not available in the **TMNN** derivatives, due to the tetrahedral tetramethyl moiety.

Table 2-8 - Comparision of calculated bond lengths, angles and dihedral angles and X-ray structure for 2TBNN and 3TBNN

	2TBNN	2TBNN
Bond Distances	X-ray	B3LYP 6-21 G*
S(1)-C(8)	1.76(2)	1.759
C(8)-C(9)	1.487(10)	1.386
C(9)-C(10)	1.411(11)	1.418
C(10)-C(11)	1.356(12)	1.371
S(1)-C(11)	1.673(14)	1.73
C(7)-C(8)	1.461(18)	1.428
N(1)-C(7)	1.392(18)	1.375
N(1)-C(6)	1.32(2)	1.412
O(1)-N(2)	1.255(16)	1.274
C(1)-C(6)	1.33(2)	1.395
C(5)-C(6)	1.319(14)	1.386
C(4)-C(5)	1.403(8)	1.399
C(4)-C(3)	1.392(8)	1.405
Bond Angles		
C(11)-C(10)-C(9)	118.2(12)	112.778
C(10)-C(11)-S(1)	113.8(10)	112.651
C(11)-S(1)-C(8)	89.9(8)	90.74
C(7)-C(8)-S(1)	120.3(14)	121.663
N(2)-C(7)-N(1)	104.8(15)	107.875
C(6)-N(1)-O(2)	125.3(14)	124.829
C(6)-N(1)-C(7)	111.8(16)	109.175
O(2)-N(1)-C(7)	122.9(12)	125.994
N(1)-C(6)-C(1)	107.5(13)	106.947
C(5)-C(6)-C(1)	119.0(14)	122.241
C(5)-C(6)-N(1)	132.9(17)	130.811
C(6)-C(5)-C(4)	122.0(11)	116.169
Dihedrals		
N(1)-C(7)-C(8)-S(1)	**0.3**	**0**

Continue Table 2-9 - Comparision of calculated bond lengths, angles and dihedral angles and x-ray structure for 2TBNN and 3TBNN

	3TBNN	**3TBNN**
Bond Distances	X-ray	B3LYP 6-21 G*
S(1)-C(1)	**1.633(5)**	**1.738**
C(1)-C(2)	1.545(12)	1.362
C(2)-C(3)	1.514(15)	1.443
C(3)-C(4)	1.458(14)	1.384
S(1)-C(4)	1.526(13)	1.723
C(3)-C(5)	1.445(17)	1.442
N(1)-C(5)	1.288(17)	1.38
N(1)-C(11)	1.459(15)	1.413
O(1)-N(1)	1.254(10)	1.275
C(6)-C(11)	1.297(12)	1.393
C(6)-C(7)	1.386(16)	1.386
C(7)-C(8)	1.429(13)	1.399
C(8)-C(9)	1.432(11)	1.406
Bond Angles		
C(3)-C(2)-C(1)	110.5(7)	112.441
C(4)-S(1)-C(1)	106.2(50)	91.806
C(2)-C(1)-S(1)	103.4(4)	111.936
C(4)-C(3)-C(2)	108.8(10)	112.179
C(5)-C(3)-C(4)	129.0(11)	123.525
N(1)-C(5)-N(2)	110.5(13)	107.61
C(5)-N(2)-C(6)	107.5(11)	109.15
N(2)-C(5)-C(3)	121.5(13)	125.856
C(11)-C(6)-N(2)	108.0(11)	107.085
C(11)-C(6)-C(7)	120.2(12)	122.227
C(6)-C(7)-C(8)	120.2(10)	116.17
C(7)-C(8)-C(9)	118.2(9)	121.596
Dihedrals		
C(4)-C(3)-C(5)-N(2)	**-5.1**	**0**

This planar stacking, with low dihedral angle between 2-position aromatic moiety and benzimidazole, had been observed in the crystal structure of the **PBNN**, but the three dimensional arrangements of the **2TBNN** and **3TBNN**

molecules were completely different from the **PBNN**. The molecules of **PBNN** crystals formed dimers, with each dimer pair stacking at an almost 90° angle to the next one in the lattice. The **2TBNN** and **3TBNN** formed slipped stacks in the crystalline state, with the potential for long range magnetic ordering.

2.2.8 - Magnetic Susceptibility Measurements.

Magnetic susceptibility (χ) measurements were carried out on polycrystalline radical samples using a Quantum Design SQUID magnetometer in the temperature range of 2-300 K at a field of 0.1 Gauss. The polycrystalline samples were prepared by the macroscale evaporation of a saturated radical n-pentane solution over several days, followed by triturating the crystals with n-pentane and methanol, and drying under vacuum for several days. The solubility of the radicals in n-pentane was low and required 2 L of n-pentane to dissolve 50 mg of radical. Diamagnetic corrections were determined by either solving for the slope of the uncorrected χT versus T in the high temperature paramagnetic region (200 to 300 K) or by subtracting the experimentally measured χ_{dia} of the gel capsule and calculated Pascal's constants. The results of the magnetic susceptibility measurements are summarized in Table 2.9.

Table 2-10 - Summary of Magnetic Susceptibility Data for 2TBNN, 3TBNN, and 4PBNN

	Θ (K)	J (cm^{-1})
2TBNN[a]	-7.69	
3TBNN[b]	3.23	-42.4
4PBNN[a]	-1.68	

(a) Curie-Weiss Law: (b) one dimensional Heisenberg chain model with mean field parameter.

The magnetic susceptibility for **4PBNN** could be modeled with the Curie-Weiss Law and was fitted using a χ_p^{-1} versus T plot with a Weiss constant of -1.68 K (see Figure 2.25).

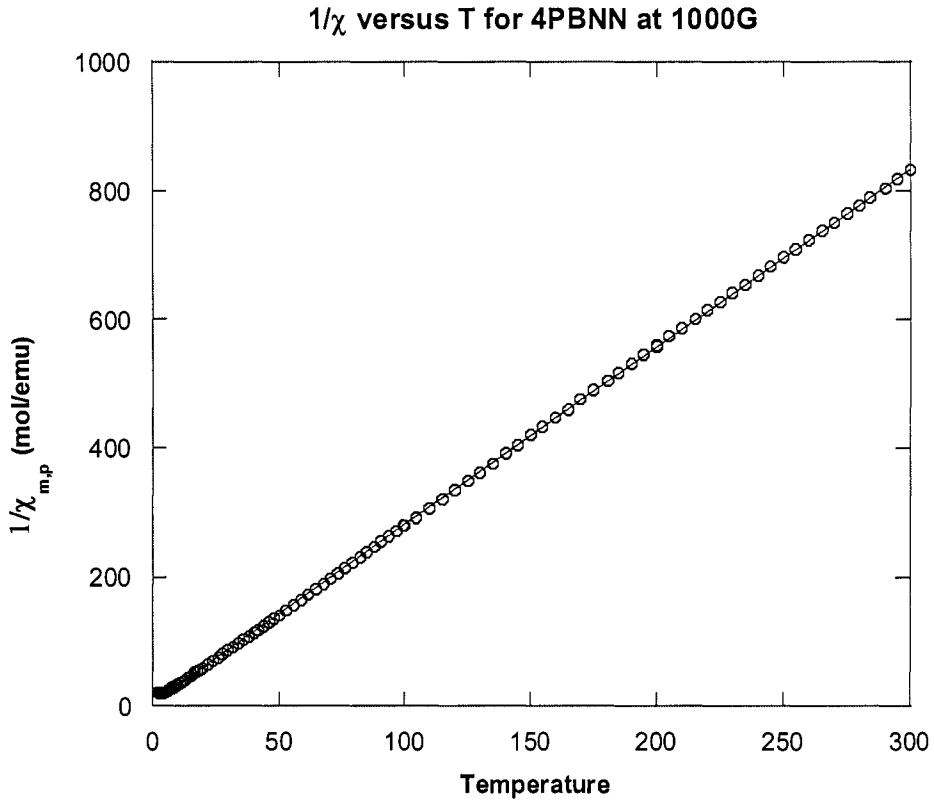

Figure 2.25 - Temperature Dependences of $1/\chi$ versus T for polycrystalline sample of 4PBNN.

The diamagnetic correction used was the high temperature uncorrected χT versus T slope method. From 50 K to 300K, $\chi T_{p,m}$ was a constant .366 $cm^3/(mol*K)$, consistent with an isolated spin ½ system. As the temperature fell below 50 K, the $\chi T_{p,m}$ dropped off dramatically, indicating antiferromagnetic interactions. The χ_p^{-1} versus T was fitted using the Curie-Weiss Law and a Weiss constant of -1.68 K was found. This result was found to be substantially lower

than **PBNN** but similar in magnitude to other derivatives of the BNN class of planar stable organic radicals. Unfortunately, the exact nature of this magnetic interaction was a matter of speculation, since repeated attempts to obtain X-ray quality crystals were unsuccessful. Based on the X-ray structure of the **2TBNN**, **PBNN**, and **3TBNN**, the primary magnetic exchange in the crystalline state for benzimidazole nitronyl nitroxides was the result of a direct overlap of neighboring radicals' π-conjugated SOMOs, giving rise to positive spin density overlap and antiferromagnetic interactions. The **4PBNN** radical followed this pattern, and it may be assumed that this was the primary method of magnetic interactions.

The magnetic susceptibility data for **2TBNN** could be modeled with the Curie-Weiss Law. The data was fitted using a χ_p^{-1} versus T plot with a Weiss constant of -7.69 K (see Figure 2.26).

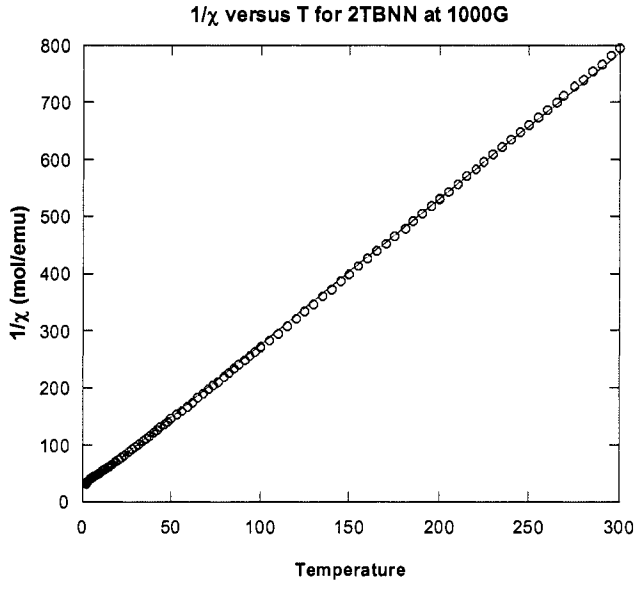

Figure 2.26 - Temperature Dependences of 1/χ versus T for polycrystalline sample of 2TBNN

The diamagnetic correction used was the high temperature uncorrected χT versus T slope method. The room temperature $\chi T_{p,m}$ was low (0.337 $cm^3/(mol*K)$) for an isolated spin ½ system but was constant above 100 K, suggesting the diamagnetic correction was off or the sample had a substantial amount of diamagnetic impurities. Decomposition of the radicals in the solid state or during crystallization was a common problem that is often associated with organic radicals. Assuming that 7% of the **2TBNN** radical had decomposed (e.g., the diamagnetic correction was incorrect for the mass of the sample), the $\chi T_{p,m}$ was 0.377 $cm^3/(mol*K)$, consistent with an isolated spin ½ system. This was a reasonable assumption considering **2TBNN** yielded small crystals and the radical did decay during the evaporation. The exchange was clearly antiferromagnetic, with a positive y-intercept in the χ_p^{-1} versus T plot and the $\chi T_{p,m}$ going towards zero when approaching low temperature.

The antiferromagnetic exchange could be explained by examining the X-ray crystal structure. The molecules in the solid state were arranged in a slipped stack configuration, in which the radicals adopted a planar confirmation. The closest intermolecular contacts were the Van der Waals π to π contacts between radicals in the slipped stack at less than 3.40 A. This led to an antiferromagnetic interaction based on a McConnell II mechanism. The positive spin density of the π-conjugated SOMO overlapped with the positive spin density of its neighbor's π-conjugated SOMO in the slipped stack. The magnetic interaction was weak since the **2TBNN** crystal was highly disordered and the neighbors in the stacks

were not completely overlapped. This disorder could be seen in the ORTEP by the unusually large electron density associated with C2, because the molecule was rotated 180° along the z-axis (perpendicular axis to the plane of the molecule) approximately 28% of the time and the sulfur occupied that position in the lattice. This disorder prevented any consistent long range interaction and the experimental data did not fit to any linear chain models.

The magnetic susceptibility data for **3TBNN** exhibited strong magnetic interactions for an organic system. Using a linear chain Heisenberg model with a mean field parameter for a spin = ½ system, J between radicals were calculated to be -42.2 cm^{-1} with a mean field parameter (Weiss constant) of 3.23 K (Figures 2.27a through 2.27c).

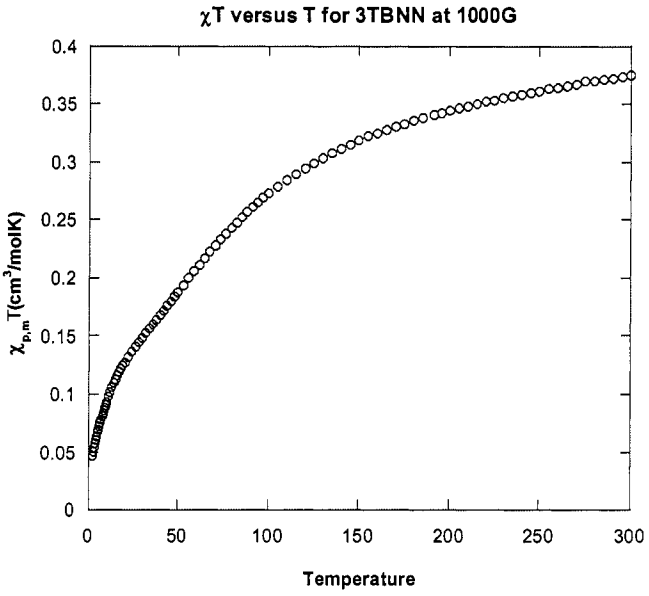

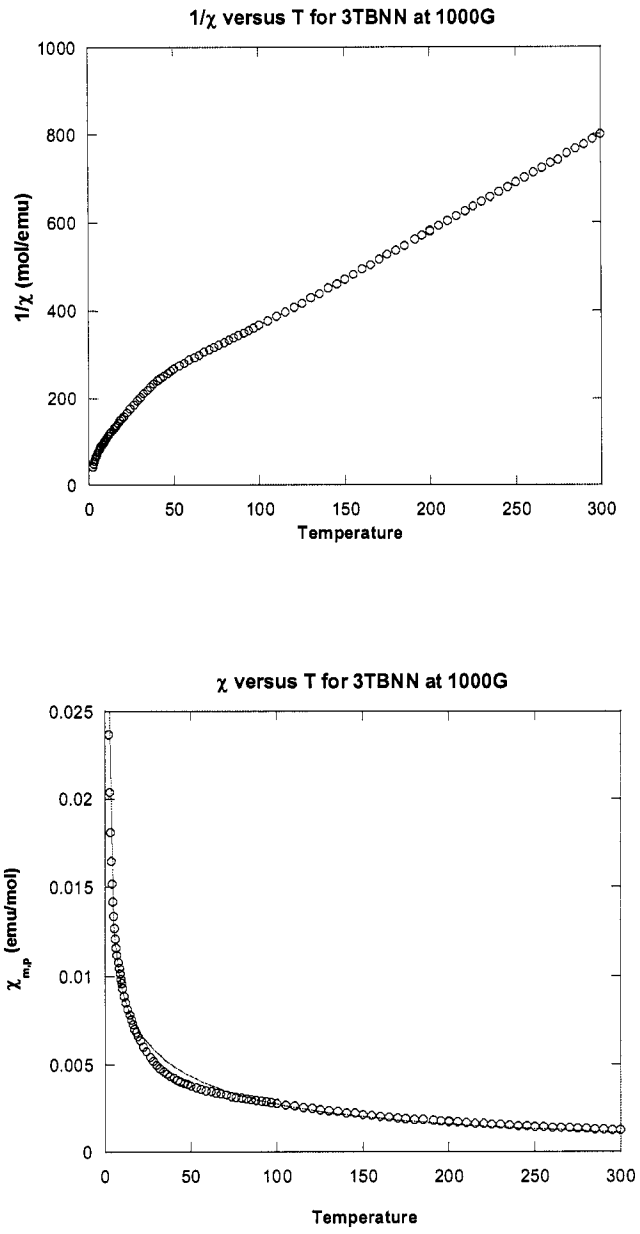

Figure 2.27 - Temperature Dependences of $1/\chi$, χ, and χT for polycrystalline sample of 3TBNN

The diamagnetic correction was accomplished by subtracting the experimentally measured χ_{dia} of the gel capsule and calculated Pascal's constants. The magnetic exchange was strong enough that the χT at 200-300 K was not

linear, and the χT only leveled out near 300 K at a value of 0.370 $cm^3/(mol*K)$. The χT distinctly demonstrated two changes in curvature at ~50K and another one at ~5 K. These two transitions were also seen in the non-linear χ_p^{-1} versus T plot. The measured magnetic data was difficult to model, but the best fit was obtained by fitting the χ versus T plot with the following Hamiltonian and equations for the infinite chain model proposed by Fischer.[55]

$$H = -J \Sigma S_{Ai} * S_{Ai+1} \quad (1)$$

$$\chi_m = [Ng^2\beta^2 S_A(S_A+1)/3k(T-\Theta)][(1+u)/(1-u)] \quad (2)$$

$$u = \coth [J S_A(S_A+1)/kT] - [kT/ (J S_A(S_A+1))] \quad (3)$$

The parameters from the experimental fit, using g = 2 and S_A = ½, were found to be Θ = 3.23 K and J = -42.2 cm^{-1}. The R value for the experimental fit was 0.9963, which indicated that there were other exchange mechanisms or phase transitions that were not completely taken into account by the model. The main intermolecular magnetic interaction was the long range antiferromagnetic exchange of -42.2 cm^{-1} along the planar slipped stack, while the ferromagnetic mean field of 3.23 K may have arisen from interactions between molecules within the stacks. The crystal structure of the **3TBNN** was similar to the **2TBNN** isomer, but with key differences that explained the difference in magnetic interactions in the solid state. (See Figures 2.28 to 2.29.)

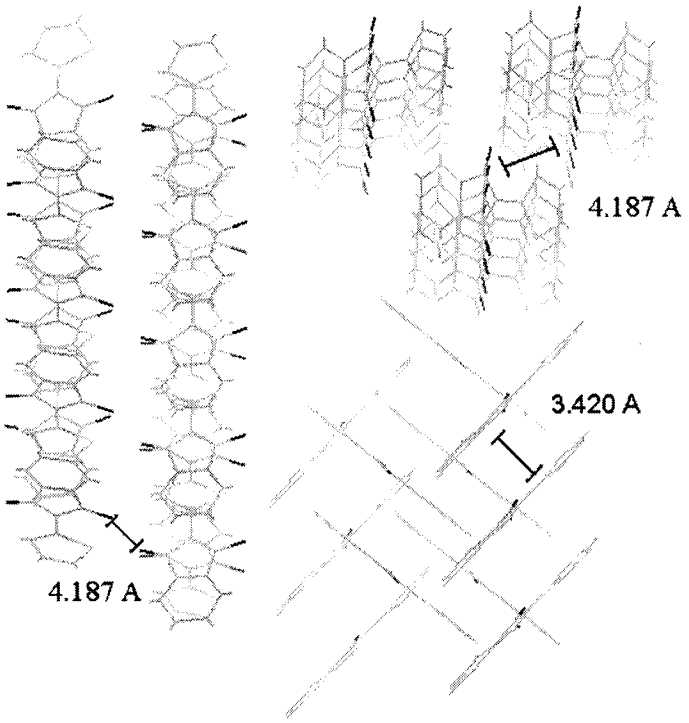

Figure 2.28 - Intermolecular interactions in 2TBNN

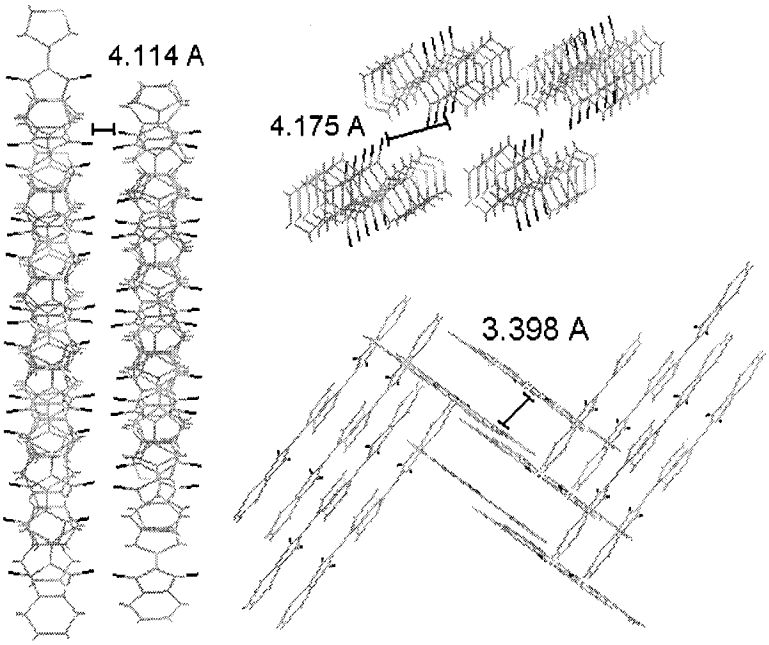

Figure 2.29 - Intermolecular Interactions in 2TBNN

2TBNN and **3TBNN** formed disordered slipped stacks. The distances between radical stacks were above 4.0 Å for **2TBNN** and **3TBNN,** meaning that the inter-chain magnetic interaction due to direct overlap was weak. Spin densities of these radicals, based on computations (see Figure 2.42 and 2.43 in Chapter 2 Appendix for SOMO of benzimidazole radicals) and EPR measurements, placed large amounts of spin density on the ONCNO moiety, with significant positive spin density on the benzimidazole and alternating positive/negative spin density on the thienyl due to spin polarization through the C2 carbon. The primary pathway for magnetic exchange was between the neighboring radicals in the stack by a McConnell I mechanism, and the distance between the radicals was about 3.4 Å in both crystal structures. This was within Van der Waals distances for π–π interactions. The difference between the **2TBNN** and **3TBNN** was a consequence of the crystal packing.

The key differences in the crystal structure that account for the radically different magnitude of magnetic exchange were the disorder in the crystal and the overlap between the neighboring radicals. The molecules in the slipped stacks had greater overlap with each other in **3TBNN** than the **2TBNN** (see Figure 2.30 and 2.31).

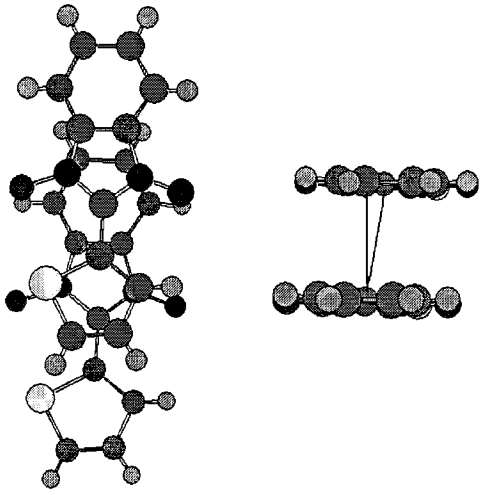

Figure 2.30 Stacking in 2TBNN in crystalline state

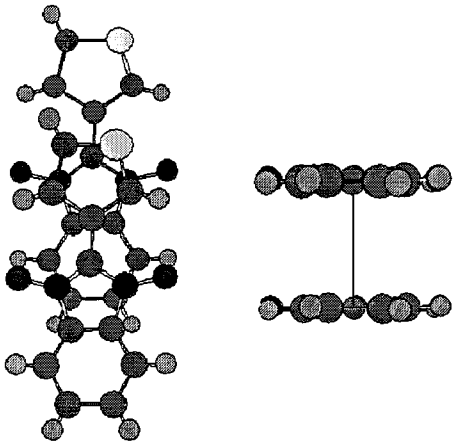

Figure 2.31 - Stacking in 3TBNN in crystalline state

The area of highest spin density was located around the nuclei, and only the **3TBNN** crystal structure demonstrates direct overlap. The disorder in **3TBNN** was along the long axis of the molecule so it does not greatly disrupt the interactions between neighboring radicals in the chain versus the large disorder induced by the rotation of **2TBNN** along the short axis. The disorder could be

observed in the ORTEP diagram in the form of a rotation on the long y-axis, leading to an unusually large amount of spin density on the C1 on the thienyl ring since half the time, sulfur was in that position. This rotation did not change how the molecule interacted with the ones above and below it in the stack. Since the thienyl ring stacked on the symmetrical benzimidazole of the neighboring radical, the interaction between neighbors was conserved with the rotation along the y-axis.

Section 2.3 – Examining problems with solubility of the radical precursor

2.3.1 - Synthesis and characterization of alkyl derivative ethylbenzimidazole nitronyl nitroxide.

The ethylbenzimidazole nitronyl nitroxide (**EthNN** or **1o**) was synthesized by Route E, with the ethylbenzimidazole 1-oxyl-3-oxide (**2o**) being synthesized by the reaction of 1-nitropropane and benzofuroxan in diethylamine and THF (Figure 2.32). **2o** was surprisingly soluble compared to the phenyl derivatives, with recrystallization possible using methanol. **2o** dissolves in several common polar organic solvents like DMF, DMSO, and ACN.

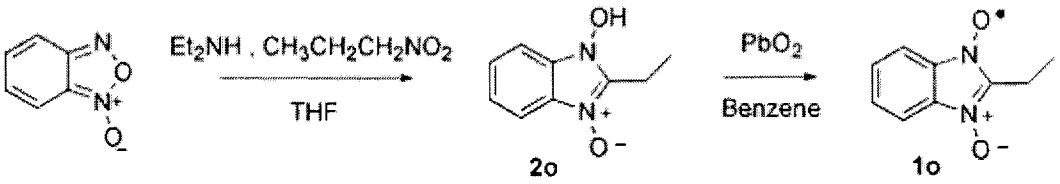

Figure 2.32 – Synthesis of EthBNN

The UV-Vis spectrum of **EthBNN** was similar to **PBNN**, with the same pattern of strong absorbance in the UV, medium absorbance in the visible range, and weak absorbance in the near IR (See Figures 2.33 and 2.34 and Table 2.10).

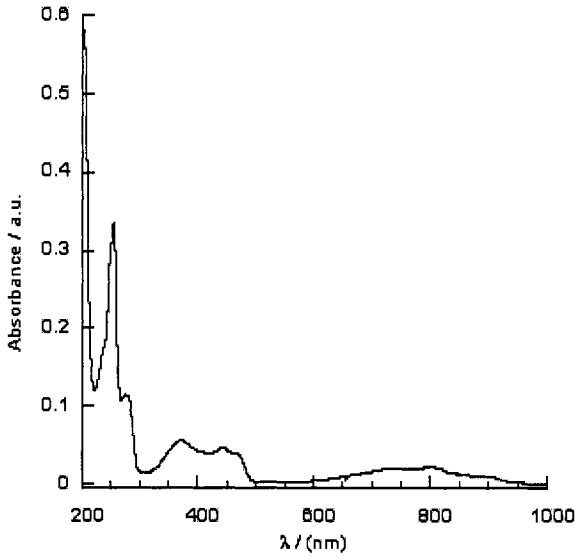

Figure 2.33 UV-Vis of EthBNN in ACN at RT and 10^{-5} M

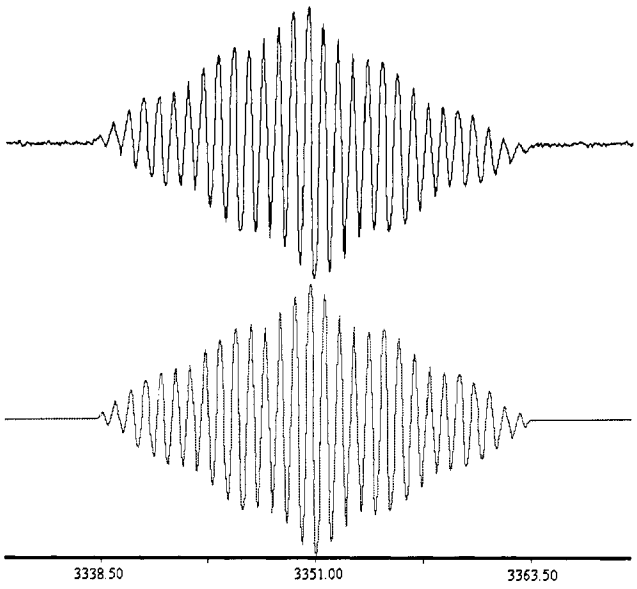

Figure 2.34 - EPR of 1o in degassed benzene (top = experimental: bottom = simulated) at RT and ~10^{-5} M.

Table 2-11 - Hfcc of EthBNN in degassed benzene

	ethyl	phenyl
N	4.310	4.370
H-α	0.950	0.930
H-β	0.690	0.650
$-CH_2-$	1.830	
H-ortho		0.490
H-meta		0.220
H-para		0.407

Analysis and fitting of the EPR spectrum shows that the coupling constants to the benzimidazole moiety of the molecule are unperturbed by the change from ethyl to phenyl (N = 4.310 for **EthBNN** versus 3.372 for **PBNN**). The large coupling constants to the $-CH_2-$ protons on the ethyl group blur the 5 line splitting pattern, but the fit is consistent with the aromatic benzimidazole nitronyl nitroxides. **EthBNN** was not stable in the solid state and decayed slowly in non-polar solvents over 12 hours when left exposed to air. The color of the radical in solution was a green-yellow color, comparable to the aromatic BNN derivatives.

2.3.2 - Solubility effects by adding functional groups to the R-group.

The heteroaromatic and 2-phenylbenzimidazole 1-oxyl-3-oxide compounds were extremely insoluble in organic solvents (including chlorinated solvents, EtOH, ethyl acetate, DMF, THF, MeOH, DMSO, pyridine, diglyme, 2-propanol, diethyl ether, pentane, hexanes, benzene, toluene, and ACN) and water, even after extensive heating and sonication. The 2-phenylbenzimidazole 1-oxyl-3-oxide was observed to decompose when heated in high boiling solvents (+150 °C), as seen in experiments involving ^{1}H-NMR spectrum in d_6-DMSO and in the direct probe MS. The only solvent that 2-phenylbenzimidazole 1-oxyl-3-oxide

dissolved was in 0.1 M KOH in H_2O. This is not a convenient solvent to use for synthetic chemistry, and this limitation removed most common methods of separating and purifying organic compounds.

An attempt was made to increase the solubility on the benzimidazole 1-oxyl-3-oxide by attaching functional groups to the 2-position aromatic group. This synthetic technique had worked and been referred to on many occasions in the literature (e.i., the dramatic solubility increase of poly-(3-hexylthiophene) over polythiophene[56,57] or the addition of t-butyl groups to dimethyldihydropyrene-dehydrobenzoannulene system[58,59]). In addition, the 2-ethylbenzimidazole 1-oxyl-3-oxide was found to be soluble in many organic solvents and recrystallizable in methanol. This change in solubility due to the simple ethyl group moiety substitution suggested that a functional group change on the 2-position phenyl group might increase the solubility of the benzimidazole precursor.

To test this method of increased solubility, a series of benzimidazole 1-oxyl-3-oxide precursors were synthesized (Scheme 2.6): 2-4'-t-butylphenylbenzimidazole 1-oxyl-3-oxide (**2i**), 2-2'-hydroxyphenylbenzimidazole 1-oxyl-3-oxide (**2h**), 2-3'-hydroxyphenylbenzimidazole 1-oxyl-3-oxide (**2g**), 2-4'-diethylaminophenylbenzimidazole 1-oxyl-3-oxide (**2f**), 2-4'-nitrophenylbenzimidazole 1-oxyl-3-oxide (**2j**), 2-4'-hexylphenylbenzimidazole 1-oxyl-3-oxide (**2m**), 2-2',3',4'-trimethoxylphenylbenzimidazole 1-oxyl-3-oxide

(**2l**), 2-4'-carboxylatephenylbenzimidazole 1-oxyl-3-oxide (**2n**), and 2-3',4'-dihexyloxylbenzimidazole 1-oxyl-3-oxide (**2k**).

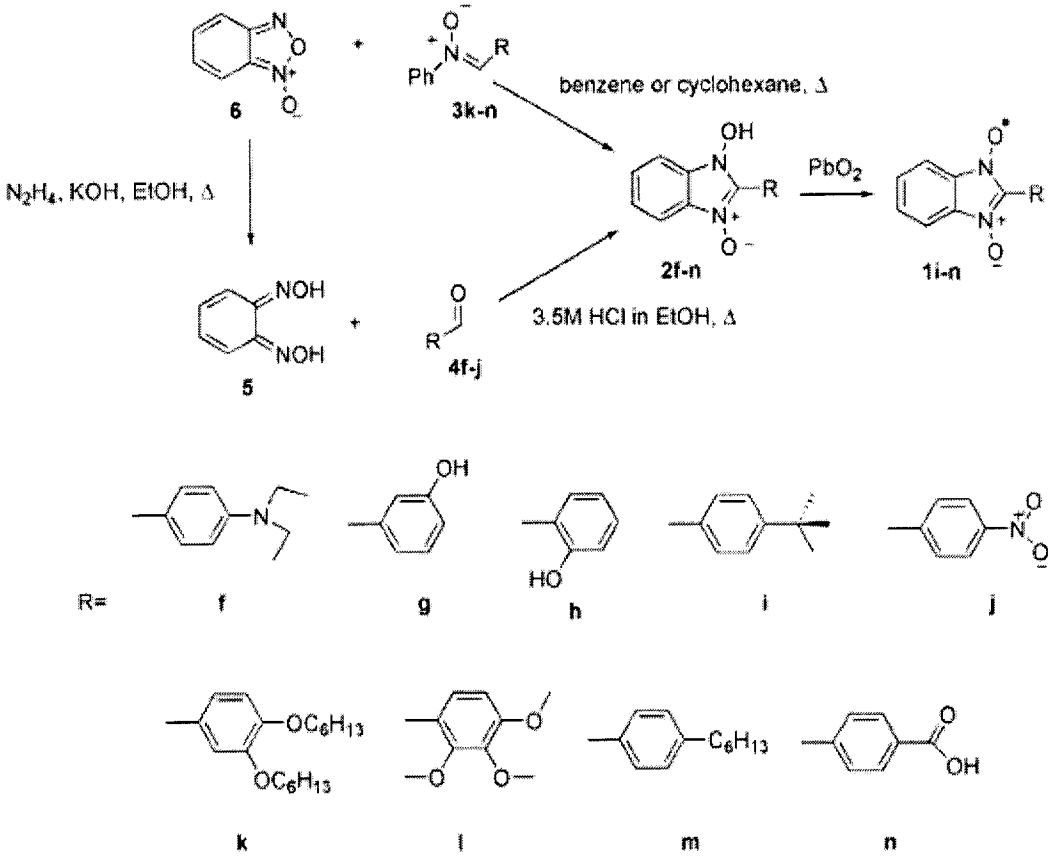

Scheme 2.6 - Synthesis of a series of benzimidazole 1-oxyl-3-oxides in attempts to increase their solubility.

The compounds were then tested to see if the resulting radical was stable and whether the addition of the functional group increased the stability of the radical. The synthetic preparation was based on methodologies used in making the thienyl and pyridyl derivatives: the acid-catalyzed condensation of benzo-1,2-dioxime with an aryl aldehyde or the reaction of benzofuroxan and appropriate nitrone. **2f-j** were prepared by Route B. **2k-n** were prepared by Route D.

Oxidation of **2f-h** with lead(IV) oxide gave an unstable radical with no detectable EPR signal (2-hydroxyl and 3-hydroxyl) or extremely weak signal that degraded quickly (diethylamino derivative). Hydroxyl and amine groups are known to have low oxidation potentials and, based on the electrochemistry, the benzimidazole radicals were excellent electron acceptors. The reason that these radicals were unstable could be due to intramolecular electron transfer followed by decomposition of the unstable intermediate. Oxidation of **2i-n** gave stable radicals with the expected five line pattern (see Figure 2.35 and Chapter 2 Appendix).

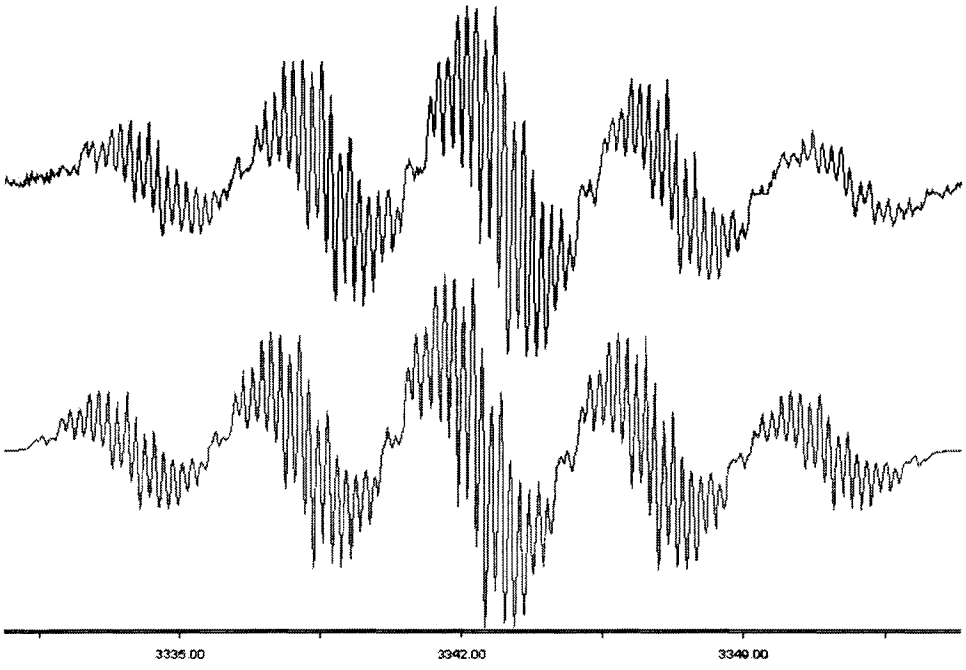

Figure 2.35 - EPR of 2j (R=p-nitrophenyl) in degassed benzene (top = experimental: bottom = simulated) at RT and ~10^{-5} M.

These radicals had EPR spectra and UV-Vis spectra consistent with the phenyl derivative. Unfortunately, none of the benzimidazole 1-oxyl-3-oxide precursors

showed any improvement in solubility in organic solvents compared to the phenyl derivative. The changes in functionality of the 2-position aromatic R-group did not improve the solubility of the precursor, and the solubility increase due to the substitution from phenyl to ethyl in 2-ethylbenzimidazole 1-oxyl-3-oxide was isolated to just to the alkyl derivative.

Section 2.5 – Conclusions

The following series of heteroaromatic BNN radicals were successfully synthesized, and the effect of substitution on the 2-position was investigated: 2'-phenylbenzimidazole 1-nitronyl nitroxide (**PBNN**), 2'-pyridylbenzimidazole nitronyl nitroxide (**2PBNN**), 4'-pyridylbenzimidazole nitronyl nitroxide (**4PBNN**), 2'-thienylbenzimidazole nitronyl nitroxide (**2TBNN**), and 3'-thienylbenzimidazole nitronyl nitroxide (**3TBNN**). The 2-position group was found to have had little effect on electronic structure and overall spin distributions. In the process of synthesizing derivatives of the BNN, the versatility of the known nitrone-furoxan coupling was explored, and the reaction was found to be robust and useful in synthesizing a wide range of derivatives.

An attempt was made to increase the solubility of the benzimidazole 1-oxyl-3-oxide by investigating how different functional groups on the 2-position aromatic group responded. This was accomplished by synthesizing the following series of radicals: 2-4'-t-butylphenylbenzimidazole 1-oxyl-3-oxide (**2i**), 2-2'-hydroxyphenylbenzimidazole 1-oxyl-3-oxide (**2h**), 2-3'-

hydroxyphenylbenzimidazole 1-oxyl-3-oxide (**2g**), 2-4'-diethylaminophenylbenzimidazole 1-oxyl-3-oxide (**2f**), 2-4'-nitrophenylbenzimidazole 1-oxyl-3-oxide (**2j**), 2-4'-hexylphenylbenzimidazole 1-oxyl-3-oxide (**2m**), 2-2',3',4'-trimethoxylphenylbenzimidazole 1-oxyl-3-oxide (**2l**), 2-4'-carboxylatephenylbenzimidazole 1-oxyl-3-oxide (**2n**), and 2-3',4'-dihexyloxylbenzimidazole 1-oxyl-3-oxide (**2k**). The addition of traditional functional groups that increase solubility in previous aromatic systems did not improve the solubility of the benzimidazole, and the radicals were unstable if the functional group was a diethylamine or hydroxyl group.

The structural change from tetramethyl to benzimidazole had a dramatic effect on the electronic properties of the nitronyl nitroxide, shifting the reductive potential to -0.300 V and raising the oxidation potential to 1.1 V. This was a low reduction potential for an organic molecule and could lead to charge transfer salts based on the **PBNN** radical. The band gap for BNN radical's SOMO and LUMO was found to be 1.5 eV, consistent with both electrochemical and UV-Vis spectroscopy techniques. Calculations did an adequate job of predicting the spin density on the radicals, but underestimated the delocalization into the benzimidazole ring and overestimated the spin polarization onto the 2-position aromatic group. Analysis of the EPR and calculations showed that the radical had a delocalized SOMO on the benzimidazole, with high spin density on the annelated benzene ring.

The X-ray crystal structure and magnetic susceptibility measurements for **2TBNN** and **3TBNN** allowed for structure-function analysis on the solid state magnetism. The slipped stacks for **2TBNN** and **3TBNN** differed from the solid state packing of **PBNN**. The magnetic susceptibility for **2TBNN** was found to be antiferromagnetic and weak, consistent with the X-ray structure showing a disordered and unfavorable overlap of the radicals in the slipped stacks. The magnetic susceptibility of **3TBNN** was found to be strong for an organic system, with long range antiferromagnetic exchange occurring along the slipped stacks in the crystalline state. In addition, a magnetic anomaly at 50 K was observed which may have been due to a phase transition. Further work will be needed to identify the nature of this transition.

Section 2.6 - Experimental

All solvents used in reactions were ACS grade unless specifically dried or purified. All chemicals were purchased from Aldrich or Arcos. ^{1}H-NMR spectra were obtained on a 200 MHz Bruker Spectrospin 4.7 T superconducting magnet. Mass spectra for routine characterization were obtained on either a Bruker Esquire~LC Ion Trap Electrospray Mass Spectrometer or a Kratos Profile HV-3 Direct Probe Mass Spectrometer. Infrared spectra were recorded on a Perkin Elmer 1720 FTIR spectrophotometer in KBr pellets. X-band ESR spectra were taken on a 9GHz continuous wave Bruker EMX ESR spectrometer. UV-Vis absorption spectra of the radicals were recorded on an Agilent 8453 UV/Vis

spectrometer. These experimental characterization conditions were consistent though all chapters.

Hydroxylaminobenzene (43).[60] A solution of NH_4Cl (2.5 g, 0.047 mol), nitrobenzene (4.16 mL, 0.041 mol), and 80 mL of H_2O was stirred in a flask. With constant stirring and monitoring of the temperature to ensure the reaction did not exceed 60 °C, Zn dust (6.2 g, 0.081 mol) was added over 10 minutes. The temperature was stabilized at 58 °C for 5 minutes. After the solution started to cool, it was filtered with suction and the zinc oxide was washed with 10 mL of boiling H_2O. While still warm, the solution was saturated with NaCl (~20 g), and cooled in an ice-water bath for an hour. A pale yellow solid precipitated out of solution. This was filtered with suction, washed with hexanes, and placed under vacuum to give a white crystalline solid (2.7 g, 60.4%). mp 82 °C (lit.[60] 79.8 °C). ^{1}H-NMR (200MHz, *d6*-DMSO, δ): 9.97 (t, 2H, J = 8.4, 6.9 Hz Ar-H), 8.17 (d, 2H, J = 8.4 Hz, Ar-H), 7.95 (t, 1H, J = 6.9 Hz, Ar-H), 5.3 (s, 1H, N-H).

Benzo-1,2-dioxime(5).[61] Benzofuroxan (2.400 g, 0.015 mol) was added to 15 mL of 100% EtOH, 15 mL of H_2O, and 20 mL of 25% KOH in 100% EtOH. Hydrazine hydrochloride (1.0 mL, 0.019 mol) was added and the reaction was heated to 60 °C for 2 hours. The reaction solution was evaporated under reduced pressure to half volume, diluted with 25 mL of water, and cooled in ice. The solution was acidified with conc. acetic acid, filtered with suction, washed with

water, and dried under vacuum (1.16 g, 56%). mp 145-6 °C (lit.[62] 145-6 °C). MS (negative-mode in MeOH): 137 $[M-1]^-$. ^{1}H-NMR (200MHz, *d6*-DMSO, δ): 7.1 (dd, 2H, J = 3.2, 7.9 Hz, Ar-H), 6.7 (broad s, 2H, NOH), 6.45 (dd, 2H, J = 3.2, 7.9 Hz Ar-H).

3-Thienylcarbonaldehyde (4e). 3-Bromothiophene (0.8 mL, 8.5 mmol) was added to 40 mL of dry THF under N_2. The solution was cooled to –78 °C in an acetone/$CO_{2(s)}$ bath and 3.4 mL of 2.5M *n*-butyl lithium (8.5 mmol) in hexanes was added dropwise. The solution was stirred at –78 °C for one hour, followed by the addition of 1.3 mL of DMF (19.5 mmol), and stirred overnight at room temperature. The next day, the reaction was poured over 80 mL of 5% $HCl_{(aq)}$ in an ice bath. The aqueous layer was extracted with DCM, dried with $MgSO_4$, and solvent evaporated under reduced pressure. The resulting liquid was purified with column chromatography (silica, 1:1 hexanes/DCM). Evaporation of the solvent under reduced pressure yielded a clear oil (0.902 g, 95.7%). ^{1}H-NMR (200MHz, $DCCl_3$, δ): 9.97 (s, 1H, aldehyde), 8.17 (dd, 1H, J = 2.8, 1.2 Hz, Ar-H), 7.95 (dd, 1H, J = 5.2, 2.8 Hz, Ar-H), 7.40 (dd, 1H, J = 5.2, 1.2 Hz, Ar-H).

3,4-Dihexyloxylbenzaldehyde (4k). A solution of benzaldehyde (0.89 g, 0.0065 mol), potassium carbonate (1.823 g, 0.0132 mol), and 1-bromohexane (2.3 mL, 0.014 mol) in 25 mL of DMF was refluxed for 4.5 hours. The starting material had disappeared by TLC (95/5 DCM/MeOH). DMF was evaporated under a

vacuum, leaving a brown oil. To the oil was added 50 mL of ether and this was extracted with 3 x 50 mL of water and 2 x 20 mL of brine. The organic layer was dried with $MgSO_4$ and evaporated under reduced pressure to give a brown solid (1.57 g, 78.8%). ^{1}H-NMR (200MHz, $DCCl_3$, δ): 9.872 (s, 1H, -CHO), 7.48 (d, 1H, J = 8.2 Hz, Ar-H), 7.30 (s, 1H, Ar-H), 7.00 (d, 1H, J = 8.2 Hz, Ar-H), 4.18 (d, 2H, O-C*H*$_2$-CH_2), 4.15 (d, 2H, O-C*H*$_2$-CH_2), 1.7 (m, 4H, O-CH_2-C*H*$_2$-CH_2-), 1.45 (m, 12H, -C*H*$_2$-C*H*$_2$-C*H*$_2$), 0.97 (t, 6H, -CH_2-C*H*$_3$).

4-Hexylbenzaldehyde (4m). [63] A mixture of hexylbenzene (9.5 mL, 0.0504 mol) and hexamethylenetetramine (7.7 g, 0.0553 mol) was heated in 50 mL of trifluoroacetic acid for 13 hours at 80 °C, while being monitored by TLC. The solution was then neutralized with $NaHCO_3$ and extracted with 4 x 50 mL of ethyl ether. The organic layer was washed with 2 x 100 mL of H_2O, dried with $MgSO_4$, and evaporated under reduced pressure. The brown oil was placed under vacuum for 24 hours and yielded a brown liquid (8.06 g, 85.4%). ^{1}H-NMR (499MHz, $DCCl_3$, δ): 9.99 (s, 1H, -COH), 7.82 (d, 2H, J = 8 Hz, Ar-H), 7.35 (d, 2H, J = 8.0 Hz, Ar-H), 2.70 (t, 2H, J = 7.5 Hz, Ar-CH_2-C), 1.67 (m, 2H, C-CH_2-C), 1.33 (m, 6H, C-$(CH_2)_3$-C), 0.91 (s, 3H, -CH_3).

***C*-2'-pyridyl-*N*-phenylnitrone (3b).** A solution of hydroxylaminobenzene (2.1906 g, 0.0198 mol) and 2-pyridylcarbaldehyde (2.4 mL, 0.0198 mol) in 15 mL of 100% ethanol was heated briefly to reflux. The solution was then sonicated,

capped with a rubber stopper, and placed in a dark place for 12 hours. The solution was then evaporated under reduced pressure to give a yellow oil. The oil was dissolved in ~150 mL of hot hexanes, cooled in freezer, filtered with suction, washed with hexanes, and placed under vacuum to give a yellow crystalline solid (2.50 g, 74.6%). mp 68-9 °C (lit.[64] 75-77 °C). ^{1}H-NMR (200MHz, $DCCl_3$, δ): 9.4 (d, 1H, J = 8.0 Hz, Ar-H), 8.7 (d, 1H, J = 4.0 Hz, Ar-H), 8.3 (s, 1H, NOCH), 7.9 (m, 3H, Ar-H), 7.5 (m, 3H, Ar-H), 7.4 (m, 1H, Ar-H). MS (direct probe) m/z: 198 $[M]^+$, 182 $[M\text{-}O]^+$. HRMS-EI (70eV) m/z: $[M]^+$ calcd for $C_{12}H_{10}N_2O$, 198.07931; found, 198.07899.

***C*-4'-pyridyl-*N*-phenylnitrone (3c)**. A solution of hydroxylaminobenzene (2.0974 g, 0.0192 mol) and 2-pyridylcarbaldehyde (2.5 mL, 0.0192 mol) in 15 mL of 100% ethanol was heated briefly to reflux. The solution was then sonicated, capped with a rubber stopper, and placed in a dark place for 12 hours. A large amount of white precipitate formed. The slurry was filtered with suction, washed with hexanes, recrystalized with EthOH, and placed under vacuum to give a white crystalline solid (2.80 g, 71.4%). mp 137-9 °C (lit.[64] 140-2 °C). ^{1}H-NMR (200MHz, $DCCl_3$, δ): 8.8 (d, 2H, J = 6.0 Hz, Ar-H), 8.2 (d, 2H, J = 6.0 Hz, Ar-H), 8.0 (s, 1H, NOCH), 7.80 (m, 2H, Ar-H), 7.57 (m, 3H, Ar-H). MS (direct probe) m/z: 198 $[M]^+$, 182 $[M\text{-}O]^+$.

***C*-phenyl-*N*-phenylnitrone(3a).**[65] A solution of hydroxylaminobenzene (1.187 g, 0.0108 mol) and benzaldehyde (1.10 mL, 0.0108 mol) in 6 mL of 100% ethanol was heated briefly to reflux. The solution was then sonicated, capped with a rubber stopper, and placed in a dark place for 12 hours. The solution was evaporated under reduced pressure to give a brown oil. The oil was dissolved in ~100 mL of hot hexanes, cooled in freezer, filtered with suction, washed with hexanes, and placed under vacuum to yield a light brown flaky crystalline solid (3.1 g, 70.4%). mp 112-3 °C (lit. [65] 112-4). ^{1}H-NMR (200MHz, $DCCl_3$, δ): 8.4 (m, 2H, Ar-H), 7.9 (s, 1H, NOCH), 7.80 (m, 2H, Ar-H), 7.52 (m, 6H, Ar-H).

***C*-4'-hexylphenyl-*N*-phenylnitrone (3m).** A solution of hydroxylaminobenzene (2.7g, 0.0247 mol) and 4-hexylbenzaldehyde (6.0 g, 0.0315 mol) in 7.0 mL of 100% ethanol was heated briefly to reflux. The solution was then sonicated, capped with a rubber stopper, and placed in a dark place for 12 hours. A large amount of white precipitate had formed. The slurry was filtered with suction, washed with hexanes, recrystalized with EthOH, and placed under vacuum to give a white crystalline solid (1.7 g, 25%). ^{1}H-NMR (200MHz, *d6*-DMSO, δ): 8.47 (s, 1H, NOCH), 8.43 (d, 2H, J = 3.4 Hz, Ar-H), 7.92 (d, 2H, J = 2.8 Hz, Ar-H), 7.55 (m, 3H, Ar-H), 7.35 (d, 2H, J = 3.4 Hz, Ar-H),), 2.70 (t, 2H, J = 7.5 Hz, Ar-CH_2-C), 1.67 (m, 2H, C-CH_2-C), 1.33 (m, 6H, C-$(CH_2)_3$-C), 0.91 (t, 3H, -CH_3). MS (direct probe) m/z: 281 $[M]^+$, 265 $[M\text{-}O]^+$.

***C*-3,4-dihexyloxylphenyl-*N*-phenylnitrone (3k).** A solution of hydroxylaminobenzene (0.601 g, 0.0055 mol) and 3,4-dihexyloxylbenzaldehyde (1.57, 0.0052 mol) in 30 mL of 100% ethanol was heated briefly to reflux. The solution was then sonicated, capped with a rubber stopper, and placed in a dark place for 12 hours. The solution was evaporated under reduced pressure to give a brown oil and the oil was purified by column chromatography (silica , 2:1 EA/hexanes) and isolation of the low R_f spot yielded a white solid (0.865 g, 39.3%). mp 50-2 °C. ^{1}H-NMR (200MHz, $DCCl_3$, δ): 8.51 (s, 1H, Ar-H), 7.9 (s, 1H, NOCH), 7.80 (m, 2H, Ar-H), 7.70 (m, 2H, Ar-H), 7.52 (m, 3H, Ar-H), 7.00 (d, 1H, Ar-H), 4.18 (d, 2H, O-C*H*$_2$-CH$_2$), 4.15 (d, 2H, O-C*H*$_2$-CH$_2$), 1.7 (m, 4H, O-CH$_2$-C*H*$_2$-CH$_2$-), 1.45 (m, 12H, -C*H*$_2$-C*H*$_2$-C*H*$_2$), 0.97 (t, 6H, -CH$_2$-C*H*$_3$). MS (direct probe) m/z: 398 $[M]^+$, 382 $[M-O]^+$.

***C*-2,3,4-trimethoxylphenyl-*N*-phenylnitrone (3l).** A solution of hydroxylaminobenzene (0.230 g, 0.002 mol) and 2,3,4-trimethoxylbenzaldehyde (0.400 g, 0.002 mol) in 30 mL of 100% ethanol was heated briefly to reflux. The solution was then sonicated, capped with a rubber stopper, and placed in a dark place for 12 hours. The solution was evaporated under reduced pressure to give a brown oil. The oil was purified with column chromatography (silica, 1:1 EA/hexanes) and isolation of the low R_f spot yielded a yellow solid (0.330 g, 58.4%). ^{1}H-NMR (200MHz, $DCCl_3$, δ): 9.31 (d, 1H, Ar-H), 8.26 (s, 1H, NOCH), 7.88 (m, 2H, Ar-H), 7.55 (m, 3H, Ar-H), 6.81 (d, 1H, Ar-H), 3.98 (s, 3H,

O-C*H*$_3$), 3.94 (s, 3H, O-C*H*$_3$), 3.92 (s, 3H, O-C*H*$_3$). MS (direct probe) m/z: 287 $[M]^+$, 271 $[M\text{-}O]^+$, 256 $[M\text{-}OCH_3]^+$, 240 $[M\text{-}O_2CH_3]^+$. IR (KBr, pellet) cm^{-1}: 2938 (C-H), 2836 (C-H), 1587 (C=N), 1301 (N-O), 1092 (C-O, ether).

Acid catalyzed coupling of benzodioxime and aldehyde.[42] A solution of aldehyde (0.0036 mol) and benzodioxime (0.0036 mol) in 3.5 M ethanolic HCl (6.0 mL) was refluxed for 3-5 hours until red color had disappeared. The solution was cooled in ice, filtered with suction, and suspended in 20 mL of H_2O/MeOH. The solution was made basic with 1.0 M $NaOH_{aq}$, filtered with suction, and the pH was adjusted to 7 with NH_4OH_{aq}. A cloudy grey/white solid precipitated out and was filtered with suction and dried under vacuum. Identifications were done by MS in negative ion mode in 1M $NaOH_{(aq)}$ or by direct probe, melting point, and ^{1}H-NMR in 0.1M KOH in D_2O or *d6*-DMSO.

2-phenylbenzimidazole 1-oxyl-3-oxide (2a). Grey solid (56%). mp 224-225 °C (lit. [42] 223-5 °C). MS m/z: 225 $[M\text{-}H]^-$, 210 $[M\text{-}OH]^-$. ^{1}H-NMR (499MHz, .1M KOH in D_2O, δ): 7.81 (m, 2H, Ar-H), 7.62 (dd, 2H, J= 6.3, 3.0 Hz, Ar-H), 7.57 (m, 3H, Ar-H), 7.35 (dd, 2H, J= 6.3, 3.0 Hz, Ar-H).

2-4'-pyridylbenzimidazole 1-oxyl-3-oxide (2c). Brown-grey solid (67.7%). mp 228 °C. MS m/z: 226 $[M\text{-}H]^-$, 210 $[M\text{-}HO]^-$. ^{1}H-NMR (499MHz, .1M KOH in D_2O, δ): 8.71 (s, 2H, Ar-H), 8.08 (s, 2H, Ar-H), 7.66 (d, 2H, J = 3.0 Hz, Ar-H), 7.39 (d, 2H, J= 3.0 Hz, Ar-H). Anal. Calcd for $C_{12}H_9N_3O_2$: C, 63.43; H, 3.99; N, 18.49. Found: C, 62.79; H, 3.35; N, 17.64.

2-2'-thienylbenzimidazole 1-oxyl-3-oxide (2d). White-grey solid (34%). mp 218-9 °C (lit. [42] 183-5 °C). MS m/z: 230 $[M-H]^-$, 214 $[M-OH]^-$, 198 $[M-O_2H]^-$. ^{1}H-NMR (499MHz, .1M KOH in D_2O, δ): 8.59 (d, 1H, J = 2.7 Hz, Ar-H), 8.08 (s, 1H, J = 4.8 Hz, Ar-H), 7.62 (d, 2H, J = 6.3 Hz, Ar-H), 7.32 (d, 2H, J= 6.3 Hz, Ar-H), 7.29 (t, 1H, J = 4.8, 2.7 Hz, Ar-H) .

2-3'-thienylbenzimidazole 1-oxyl-3-oxide (2e). White/gray solid (64%). mp 233-235 °C. MS m/z: 230 $[M-H]^-$, 214 $[M-OH]^-$, 198 $[M-O_2H]^-$. ^{1}H-NMR (499MHz, .1M KOH in D_2O, δ): 8.00 (d, 1H, J = 5.0 Hz, Ar-H), 7.63 (d, 2H, J = 2.5 Hz, Ar-H), 7.60 (d, 1H, J = 5.0 Hz, Ar-H), 7.32 (m, 3H, Ar-H). IR (KBr, pellet) cm^{-1}: 3122 (CH, thiophene), 1255 (NO), 736 (N-O---H-O).

2-4'-t-butylphenylbenzimidazole 1-oxyl-3-oxide (2i). White/pink solid (53.6%). Recrystalized in MeOH. mp 213-4 °C. MS (electrospray, negative mode) m/z: 281 $[M-H]^-$, 265 $[M-OH]^-$. ^{1}H-NMR (200 MHz, 0.1 M KOH in D_2O, δ): 7.84 (d, 2H, J = 8.6 Hz, Ar-H), 7.68 (d, 2H, J = 8.6 Hz, Ar-H), 7.63 (dd, 2H, J = 3.2, 6.4 Hz, Ar-H), 7.36 (dd, 2H, J = 3.2, 6.4 Hz, Ar-H), 1.25 (s, 9H, -C$(CH_3)_3$). IR (KBr, pellet) cm^{-1}: 2961 (C-H), 1269 (N-O), 748 (N-O---H-O).

2-2'-hydroxylphenylbenzimidazole 1-oxyl-3-oxide (2h). White/orange solid (47.5%). Recrystalized in EtOH. mp 214.0 °C (lit. [42] 180-5 °C). MS (electrospray, negative mode) m/z: 241 $(M-H)^-$, 225 $(M-OH)^-$, 209 $(M-O_2H)^-$. ^{1}H-NMR (200MHz, .1M KOH in D_2O, δ): 7.62 (dd, 2H, J = 3.0, 6.2 Hz, Ar-H), 7.35 (dd, 2H, J = 3.0, 6.2 Hz, Ar-H), 7.27 (t, 1H, J = 7.4, 8.4 Hz, Ar-H), 7.06 (d, 1H, J = 6.2Hz, Ar-H), 6.66 (d, 1H, J = 8.4 Hz, Ar-H), 6.59 (t, 1H, J = 6.2, 7.4 Hz, Ar-H).

2-3'-hydroxylphenylbenzimidazole 1-oxyl-3-oxide (2g). brown solid (51.2%). mp 234-6.0 °C. MS m/z (direct probe): 242 $[M]^+$, 226 $[M-O]^+$, 210 $[M-O_2]^+$. ^{1}H-NMR (200MHz, .1M KOH in D_2O, δ): 7.62 (dd, 2H, J = 3.0, 6.2 Hz, Ar-H), 7.35 (dd, 2H, J = 3.0, 6.2 Hz, Ar-H), 7.27 (d, 1H, J = 8.4 Hz, Ar-H), 6.96 (d, 1H, J = 1.8 Hz, Ar-H), 6.88 (t, 1H, J = 8.2, 8.4 Hz, Ar-H), 6.59 (m, 1H, J = 8.2, 1.8 Hz, Ar-H). IR (KBr, pellet) cm^{-1}: 3103 (broad, O-H), 1214 (N-O), 741 (N-O---H-O).

2-4'-diethylaminophenylbenzimidazole 1-oxyl-3-oxide (2f). White solid (52.9%). Recrystalized in EtOH. mp 226-7 °C (lit. [42] 227-8). MS (direct probe) m/z: 298 $[M]^+$, 281 $[M-OH]^+$, 264 $[M-O_2H_2]^+$. ^{1}H-NMR (200MHz, 0.1 M KOH in D_2O, δ): 7.82 (d, 2H, J = 9.0 Hz, Ar-H), 7.63 (dd, 2H, J = 3.2, 6.4 Hz, Ar-H), 7.35 (dd, 2H, J = 3.2, 6.4 Hz, Ar-H), 6.95 (d, 2H, J = 9.0 Hz, Ar-H), 3.40 (q, 4H, J = 7.0 Hz, $N(\mathit{CH_2}CH_3)_2$), 1.15 (t, 6H, J = 7.0 Hz, $N(CH_2\mathit{CH_3})_2$). IR (KBr, pellet) cm^{-1}: 3057 (C-H), 2964 (C-H), 1274 (N-O), 743 (N-O---H-O).

2-4'-nitrophenylbenzimidazole 1-oxyl-3-oxide (2j). Brown solid (69.7%). mp 222-3 °C. MS (direct probe) m/z: 271 $[M]^+$. ^{1}H-NMR (500MHz, 0.1 M KOH in D_2O, δ): 8.52 (d, 2H, J = 9.5 Hz, Ar-H), 8.38 (d, 2H, J = 9.5 Hz, Ar-H), 7.81 (dd, 2H, J = 3.0, 6.0 Hz, Ar-H), 7.52 (dd, 2H, J = 3.0, 6.0 Hz, Ar-H).

Nucleophilic attack of nitrone on furoxan.[66] A solution of nitrone (0.0085 mol) and furoxan (0.0085 mol) in 120 mL of cyclohexane (or 40 mL of benzene) was heated to just below reflux, preventing lose of solvent over long heating times.

The solution was heated for 24 hours, filtered hot with suction, and washed with cyclohexane, acetone, and benzene.

2-phenylbenzimidazole 1-oxyl-3-oxide (1a). Yellow/white solid (56%). Product was consistent with previous method of making.

2-4'-pyridylbenzimidazole 1-oxyl-3-oxide (1c). Brown solid (67.7%). Product was consistent with previous method of making.

2-2'-pyridylbenzimidazole 1-oxyl-3-oxide (1b). Brown solid (53.9%). mp 209 °C. MS m/z: 226 $[M-H]^-$, 210 $[M-HO]^-$. ^{1}H-NMR (499MHz, .1M KOH in D_2O, δ): 8.76 (d, 1H, J = 5.0 Hz, Ar-H), 8.06 (triplet, 1H, J = 7.8, 7.8 Hz, Ar-H), 7.88 (d, 1H, J = 7.8 Hz, Ar-H), 7.68 (dd, 2H, J = 3.2, 6.4 Hz, Ar-H), 7.58 (triplet, 1H, J = 7.8, 5.0 Hz, Ar-H), 7.33 (dd, 2H, J = 3.2, 6.4 Hz, Ar-H). Anal. Calcd for $C_{12}H_9N_3O_2$: C, 63.43; H, 3.99; N, 18.49. Found: C, 62.86; H, 3.88; N, 18.13. IR (KBr, pellet) cm^{-1}: 3075 (C-H), 1251 (N-O), 745 (N-O---H-O).

2-4'-hexylphenylbenzimidazole 1-oxyl-3-oxide (1m). White fluffy solid (25%). ^{1}H-NMR (499MHz, 0.1M KOH in D_2O/d_6-DMSO, δ): 8.2 (d, 2H, J = 8.5Hz, Ar-H), 7.62 (dd, 2H, J = 6.3, 3.0 Hz, Ar-H), 7.57 (d, 2H, J = 8.5 Hz , Ar-H), 7.35 (dd, 2H, J = 6.3, 3.0 Hz, Ar-H), 2.70 (t, 2H, J = 7.5 Hz, Ar-CH_2-C), 1.67 (m, 2H, C-CH_2-C), 1.33 (m, 6H, C-$(CH_2)_3$-C), 0.91 (t, 3H, -CH_3). HRMS-ESI (m/z): $[M - H]^-$ calcd for $C_{19}H_{22}N_2O_2$, 309.1603; found, 309.1610.

2-3',4'-dihexyloxylbenzimidazole 1-oxyl-3-oxide (2k). White/brown solid (40.0 %). MS m/z (direct probe): 410 $[M-O]^+$, 394 $[M-O_2]^+$. ^{1}H-NMR (200MHz, d_6-DMSO, δ): 7.88 (m, 2H, Ar-H), 7.63 (m, 1H, Ar-H), 7.53 (m, 1H,

Ar-H), 7.32 (m, 2H, Ar-H), 7.17 (m, 1H, Ar-H), 4.18 (t, 4H, O-C*H*$_2$-CH$_2$), 1.7 (m, 4H, O-CH$_2$-C*H*$_2$-CH$_2$-), 1.45 (m, 12H, -C*H*$_2$-C*H*$_2$-C*H*$_2$), 0.97 (t, 6H, -CH$_2$-C*H*$_3$).]$^+$. IR (KBr, pellet) cm^{-1}: 2931 (C-H), 2858 (C-H), 1271 (N-O), 1098 (C-O, ether), 744 (N-O---H-O).

2-2'-3',4'-trimethoxylbenzimidazole 1-oxyl-3-oxide (2l). White fluffy solid (57.0 %). ^{1}H-NMR (200MHz, 0.1M KOH in D_2O, δ): 7.66 (dd, 2H, J = 6.4, 3.2 Hz, Ar-H), 7.40 (dd, 2H, J = 6.4, 3.2 Hz, Ar-H), 7.20 (d, 1H, J = 8.8 Hz, Ar-H), 7.0 (d, 1H, J = 8.8 Hz, Ar-H), 3.90 (s, 3H, O-CH$_3$), 3.85 (s, 3H, O-CH$_3$), 3.57 (s, 3H, O-CH$_3$). MS m/z (direct probe): [M-O]$^+$, [M-O$_2$]$^+$. IR (KBr, pellet) cm^{-1}: 2944 (C-H), 1300 (N-O), 1093 (C-O, ether), 749 (N-O---H-O). HRMS-ESI (m/z): [M-H]$^-$ calcd for $C_{16}H_{16}N_2O_5$, 315.0982; found, 315.0982.

2-4'-carboxylatephenylbenzimidazole 1-oxyl-3-oxide (2n). Brown solid (35.5%). ^{1}H-NMR (200MHz, 0.1M KOH in D_2O, δ): 7.93 (d, 2H, J= 8.6 Hz, Ar-H), 7.89 (d, 2H, J= 8.6 Hz, Ar-H), 7.61 (dd, 2H, J= 6.4, 3.2 Hz , Ar-H), 7.35 (dd, 2H, J= 6.4, 3.2 Hz, Ar-H). IR (KBr, pellet) cm^{-1}: 3500 (OH), 3035 (O-H), 1696 (C=O), 1284 (N-O), 694 (N-O-H-O). HRMS-ESI (m/z): [M-H]$^-$ calcd for $C_{14}H_{10}N_2O_4$, 269.0562; found, 269.0570.

2-ethylbenzimidazole 1-oxyl-3-oxide(2o).[46] A solution of benzofuroxan (1.0g, 0.0073 mol) in 8 mL of dry THF under nitrogen was stirred. To this was added 1-nitropropane (0.78 mL, 0.0088 mol), and then diethyl amine (0.90 mL, 0.0088 mol) was added dropwise over 15 minutes. The color changed slowly from an

orange yellow to a red/orange. Precipitate was present after 2 hours. The reaction was stirred overnight and, the next day, the white precipitate was filtered with suction and recrystalized in MeOH (200 mL for ~1 g). White solid (0.44 g, 33.8%). mp 195-195.5 °C (lit. [46] 194-5 °C). ^{1}H-NMR (200MHz, *d6*-DMSO, δ): 7.65 (dd, 2H, J = 3.1, 6.2 Hz, Ar-H), 7.49 (dd, 2H, J = 3.1, 6.2 Hz, Ar-H), 3.33 (q, 2H, J = 7.5 Hz, -CH_2CH$_3$), 1.43 (t, 3H, J = 7.5 Hz, -CH$_2$$CH_3$).

General Oxidation Procedure.[36] Before oxidation, 2-phenylbenzimidazole 1-oxyl-3-oxide **2a** (0.300 g, 0.0013 mol) was dissolved in 20 mL of 15% $NaOH_{(aq)}$, filtered with suction, acidified with 12M HCl, and refiltered with suction. The wet clay was then suspended in 80 mL of 99:1 DCM/methanol. The solution was sonicated and stirred for an hour before the addition of lead. Lead (IV) oxide (11 g) was added to the solution, stirred for 10 minutes, allowed to settle, and the green solution with suspended lead oxide/benzimidazole was filtered with suction. The filtrate was bright green/yellow color and was stored in the freezer. The lead/imidazole solid was re-suspended in 80 mL of 98:2 DCM/methanol. This was repeated 3 times until the solution was clear after filtration. The collected filtrate was then removed from the freezer, filtered with suction a second time, and the solvent was removed under vacuum. A brown solid was obtained (0.220 g, 73%). UV-Vis (ACN) λ_{max}, nm (ε): 200 (21200), 241 (16500), 279 (23000), 298 (18800), 312 (22300), 388 (6480), 421 (4320), 475 (3220), 825 (1280).

4-Pyridylbenzimidazole nitronyl nitroxide (4PBNN, 1c): 2-4'-pyridylbenzimidazole 1-oxyl-3-oxide (0.308 g, 1.4 mmol) was oxidized with PbO_2 to yield a brown solid (0.226 g, 73.4%) after 5 filtration cycles. UV-Vis (ACN) λ_{max}, nm (ε): 243 (13900), 281 (15200), 299 (14200), 312 (17400), 397 (4440), 427 (2010), 483 (740), 831 (450).

2-Thienylbenzimidazole nitronyl nitroxide(2TBNN, 1d): 2-2'-thienylbenzimidazole 1-oxyl-3-oxide (0.202 g, 0.87 mmol) was oxidized with PbO_2 to yield a brown solid (0.119 g, 58.9%) after 4 filtration cycles. UV-Vis (ACN) λ_{max}, nm (ε): 243 (15800), 289 (14900), 315 (25500), 331 (36400), 390 (4720), 433 (2050), 482 (1300), 975 (263).

3-Thienylbenzimidazole nitronyl nitroxide (3TBNN, 1e): 2-3'-thienylbenzimidazole 1-oxyl-3-oxide (0.266 g, 1.2 mmol) was oxidized with PbO_2 to yield a brown solid (0.148 g, 56.0%) after 3 filtration cycles. UV-Vis (ACN) λ_{max}, nm (ε): 240 (17800), 280 (24700), 299 (25400), 313 (32200), 330 (4080), 386 (4970), 426 (2350), 476 (1590), 930 (432).

2-Pyridylbenzimidazole nitronyl nitroxide (2PBNN, 1b): Before oxidation, 2-2'-pyridylbenzimidazole 1-oxyl-3-oxide (0.004 g, 0.1 mmol) was suspended in 10 mL of benzene. Lead (IV) oxide (~0.5 g) was added to the solution under nitrogen and the solution was stirred for 1 hour. The bright green solution was filtered through a Celite-545 plug, diluted, and degassed with N_2 to prepare EPR samples. UV-Vis (ACN) λ_{max}, nm: 242, 280, 308, 392, 475, 762.

Ethylbenzimidazole nitronyl nitroxide (EthBNN, 1o).[35] Before oxidation, 2-ethylbenzimidazole 1-oxyl-3-oxide (0.020 g, 0.12 mmol) was suspended in 20 mL of benzene. Lead (IV) oxide (~0.8 g) was added to the solution under nitrogen and the solution was stirred for 3 hours. The bright green solution was filtered through a Celite-545 plug, diluted, and degassed with N_2 to prepare EPR samples. UV-Vis (ACN) λ_{max}, nm: 254, 275, 371, 441, 797.

Section 2.7 – Appendix for Chapter 2

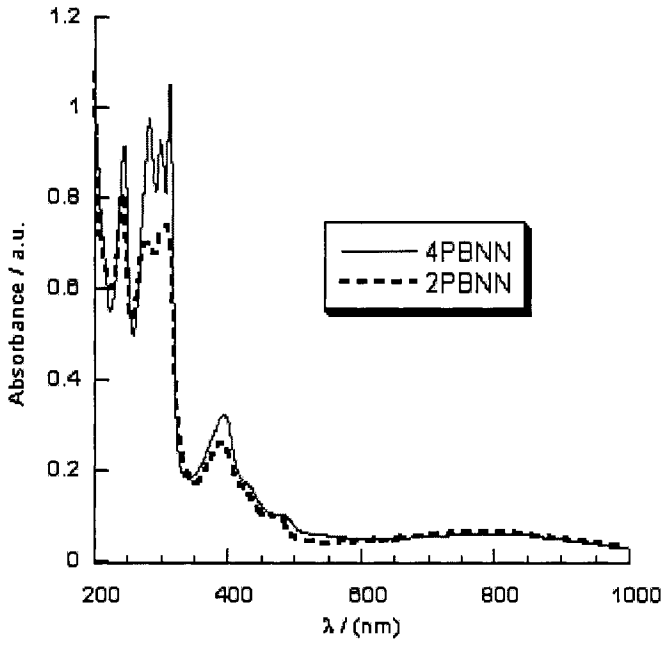

Figure 2.36 - UV/Vis spectrum of 2PBNN and 4PBNN in ACN at RT and ~10^{-5} M

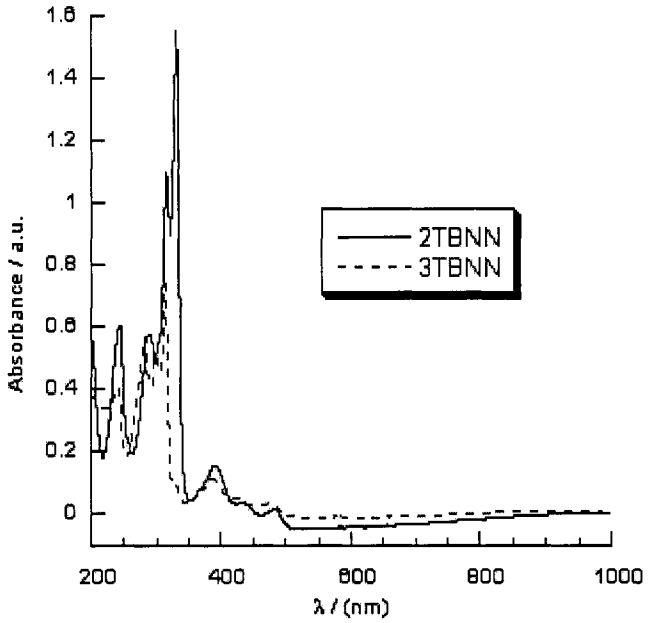

Figure 2.37 - UV/Vis spectrum of 2TBNN and 3TBNN in ACN at RT and ~10^{-5} M

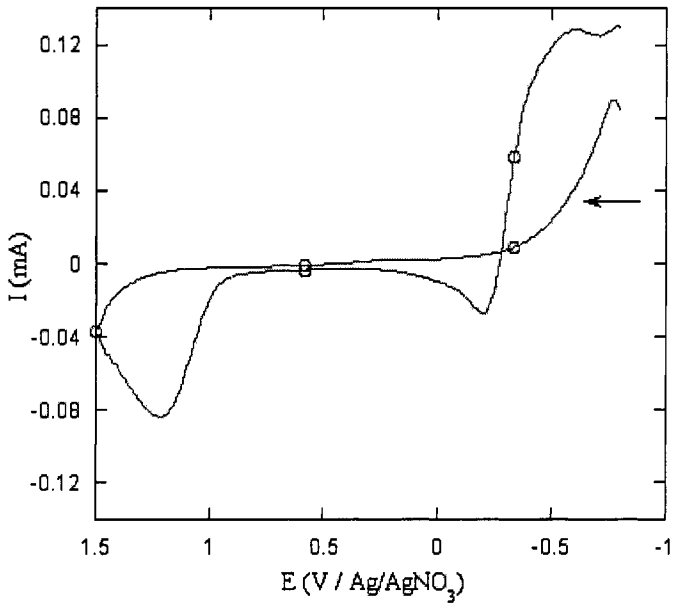

Figure 2.38 - Cyclic voltammogram of 5.0 mM 4PBNN in 0.1 M TBAHFP dry ACN versus $Ag/AgNO_3$ at RT

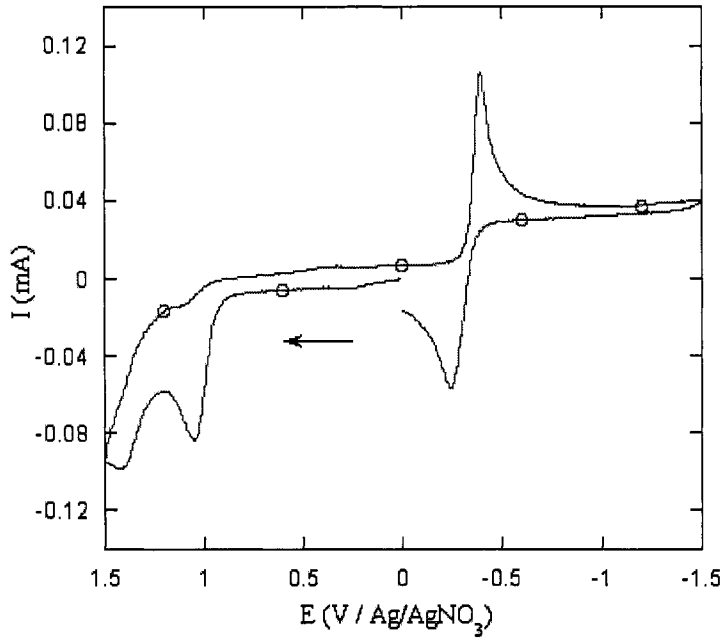

Figure 2.39 - Cyclic voltammogram of ~5.0 mM 2TBNN in 0.1 M TBAHFP dry ACN versus $Ag/AgNO_3$ at RT

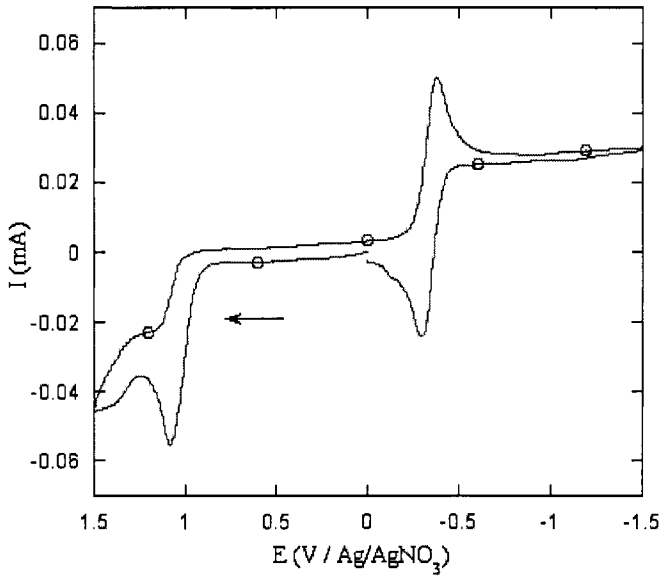

Figure 2.40 - Cyclic voltammogram of ~5.0 nM 3TBNN in 0.1 M TBAHFP dry ACN versus $Ag/AgNO_3$ at RT

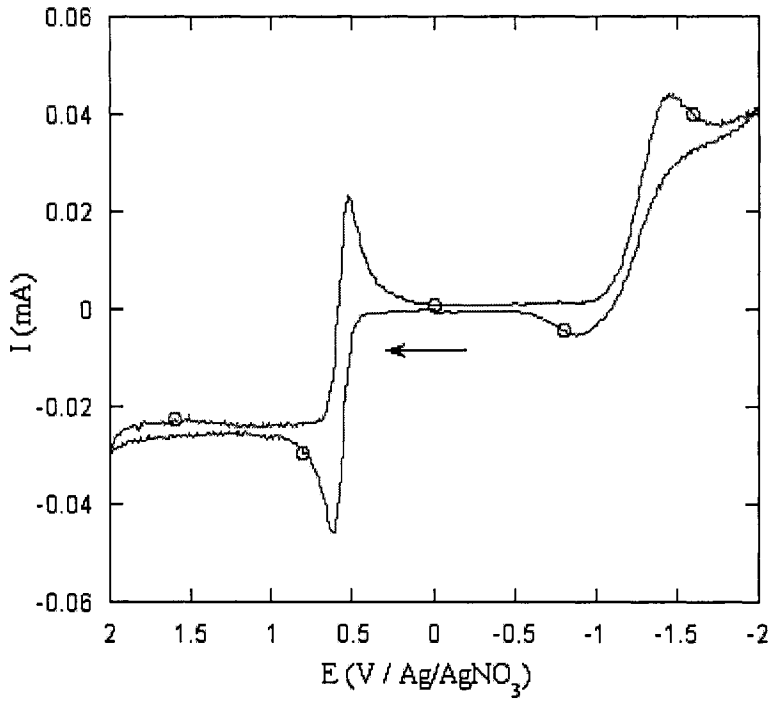

Figure 2.41 - Cyclic voltammogram of ~5.0 mM TMNN in 0.1 M TBAHFP dry ACN versus $Ag/AgNO_3$ at RT

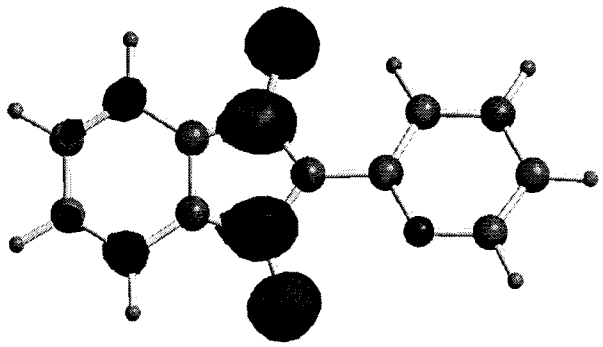

Figure 2.42 - SOMO of 2PBNN generated at B3LYP/6-31G* with CubGen (isocontour = 40, scaling factor = 0.18) and visualized with Chem3D

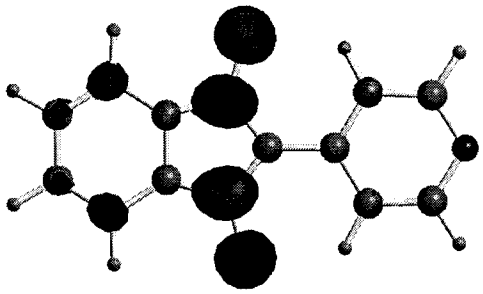

Figure 2.43 - SOMO of 4PBNN generated at B3LYP/6-31G* with CubGen (isocontour = 40, scaling factor = 0.18) and visualized with Chem3D

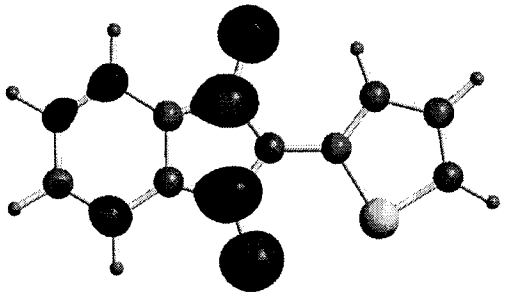

Figure 2.44 - SOMO of 2TBNN generated at B3LYP/6-31G* with CubGen (isocontour = 40, scaling factor = 0.18) and visualized with Chem3D

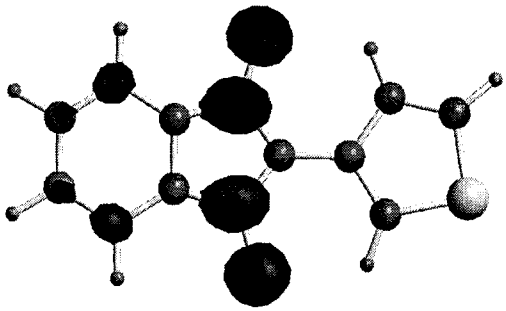

Figure 2.45 - SOMO of 3TBNN generated at B3LYP/6-31G* with CubGen (isocontour = 40, scaling factor = 0.18) and visualized with Chem3D

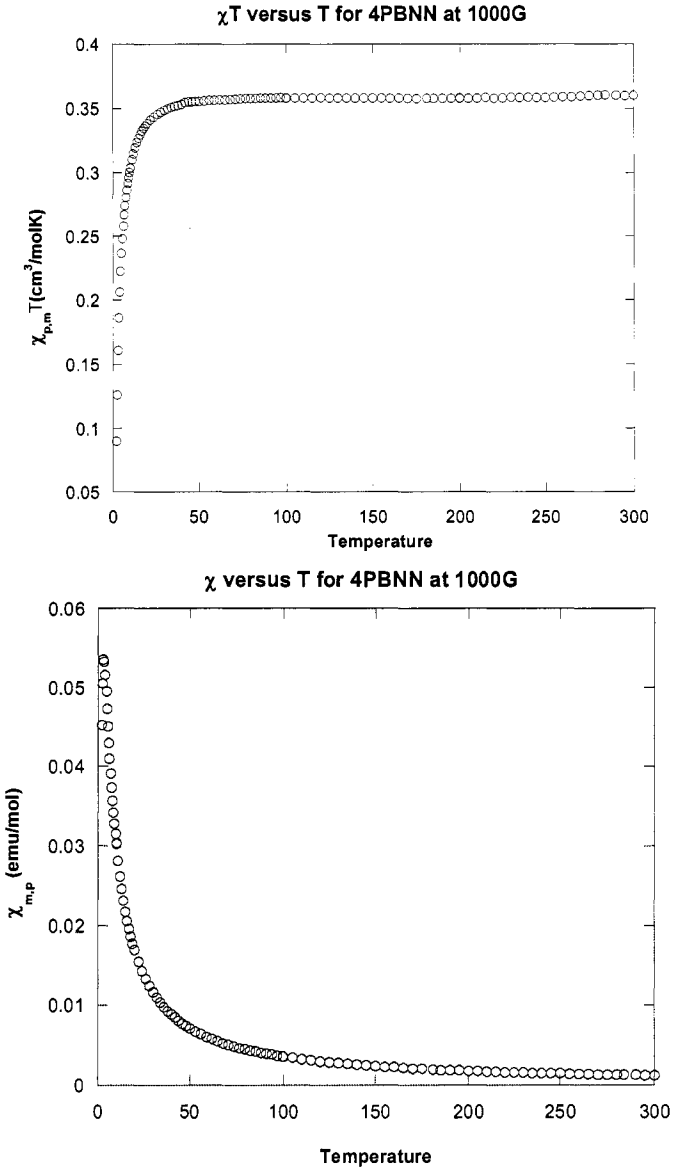

Figure 2.46 - Temperature Dependences of χ and χT versus T for polycrystalline sample of 4PBNN.

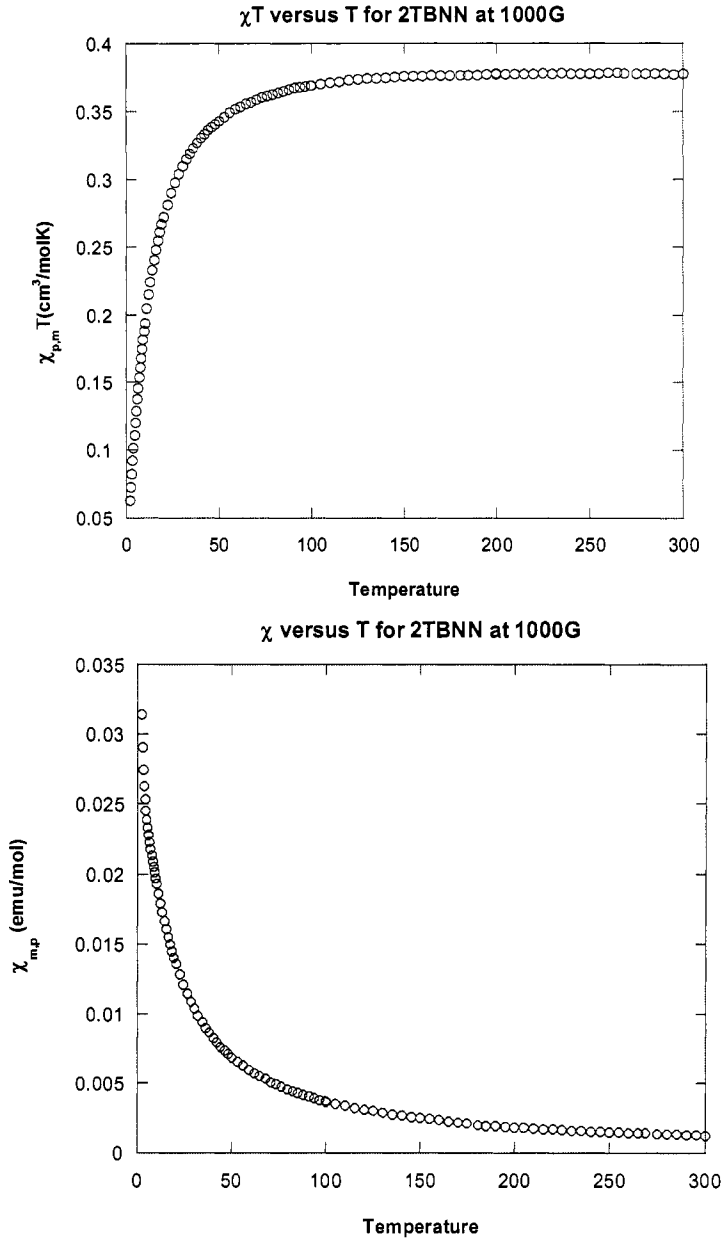

Figure 2.47 - Temperature Dependences of $1/\chi$, χ, and χT versus T for polycrystalline sample of 2TBNN

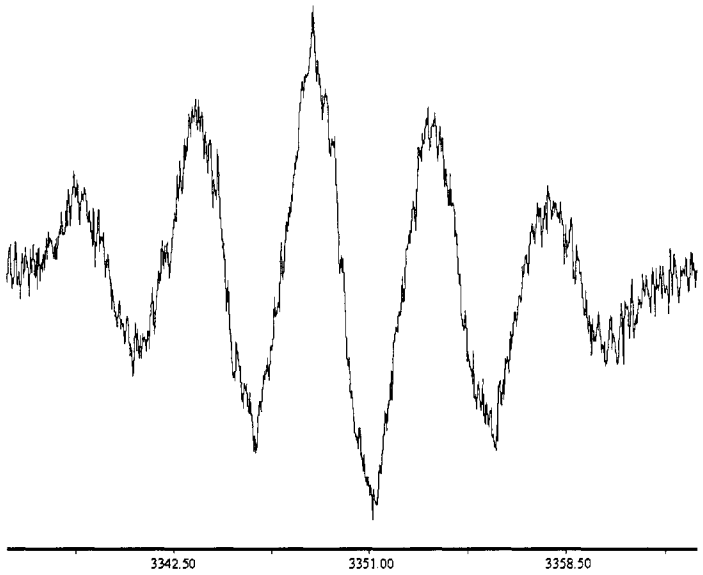

Figure 2.48 - EPR of 1f in degassed benzene at RT and ~10^{-5} M

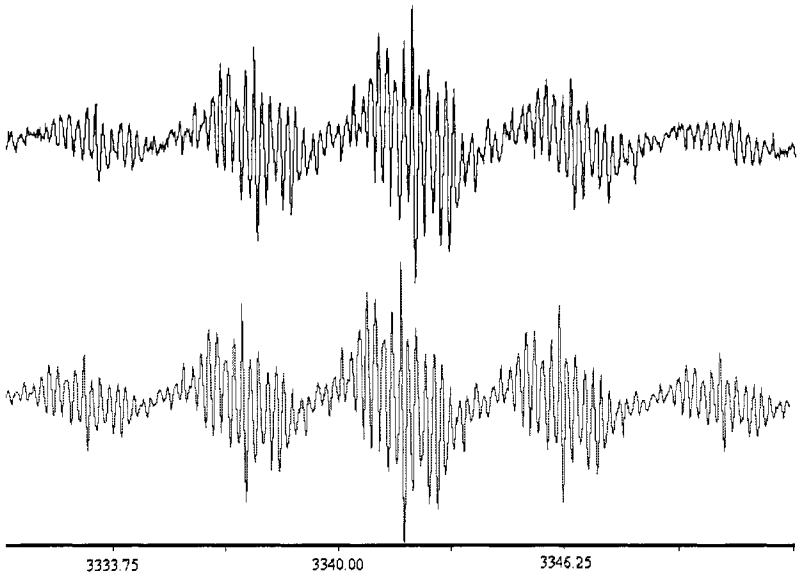

Figure 2.49 - EPR of 2m in degassed benzene (top = experimental: bottom = simulated) at RT and ~10^{-5} M.

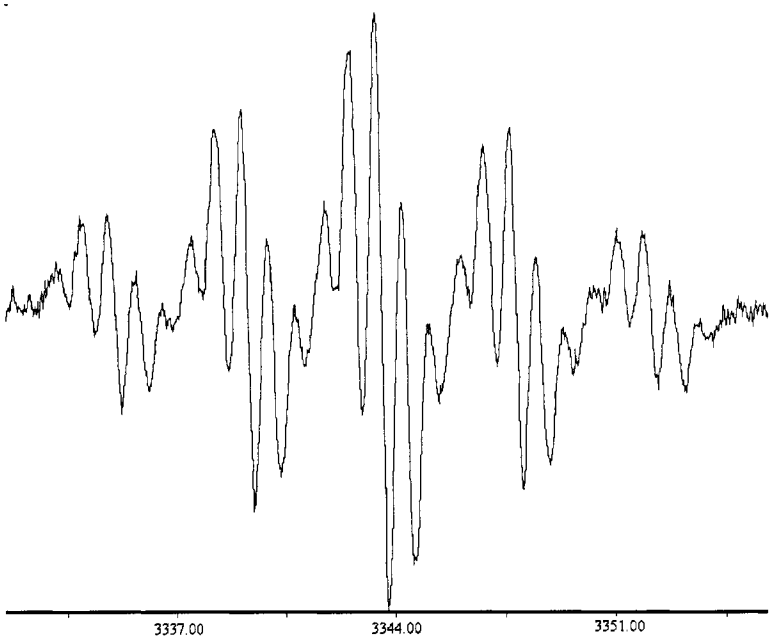

Figure 2.50 - EPR of 2l in degassed benzene at RT and ~10^{-5} M

Chapter 3. - Investigations into Extended Aromatic Nitronyl Nitroxides.

Section 3.1 - Introduction

The effects of conjugation on closed shell systems are an increase in reactivity, a bathochromic shift in the ultraviolet absorption bands, an increase in the extinction coefficient, and propagation of electronic effects through the atoms of the conjugated system. Such effects are due to a rising of the HOMO and lowering of the LUMO upon increased conjugation. The effect of conjugation on the stability and spin distribution of open shell systems is not understood well, especially with respect to non-alternant aromatic radicals.[14]

The substitution of the annelated benzene ring with either an alkene, or larger aromatic such as phenanthrene, was found to lead to a decrease in stability of this class of radicals, as demonstrated from the synthesis and characterization 2,4,5-triphenylimidazole N,N-dioxide[38], 2,4,5-trimethylimidazole N,N-dioxide[38], and 2-phenylphenanthrenimidazole nitronyl nitroxide (Figure 3.1).

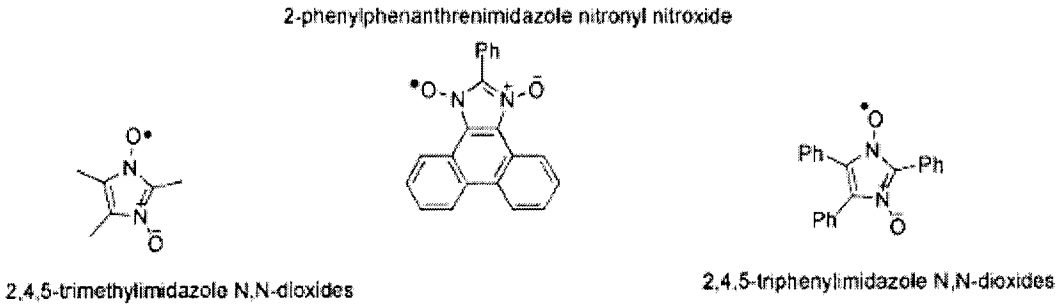

Figure 3.1 - Unstable alkene-based nitronyl nitroxides

Generation of the 2,4,5-triphenylimidazole N,N-dioxide and 2,4,5-trimethylimidazole N,N-dioxide from the alkali salt by oxidation with chlorine led to rapid rate of radical decomposition. The EPR spectra of the radical 2-phenylphenanthrenimidazole nitronyl nitroxide was recorded in which a hyperfine coupling constant to the nitrogen of 3.89 G and g = 2.0007 was observed. The nitrogen hyperfine coupling constant was smaller than that of BNN (4.370 G), indicating that the unpaired spin density was more heavily distributed into the aromatic phenanthrene than in the annelated aromatic of BNN.

The phenylphenanthrenimidazole nitronyl nitroxide was more stable than the 2,4,5-triphenylimidazole N,N-dioxide and 2,4,5-trimethylimidazole N,N-dioxide, but much less stable than the BNN. Traditionally, the idea that electron delocalization is expected to lead to a stabilization of the radical contradicts this result. It was therefore of interest to determine what structural and electronic factors governed the spin distribution and stability of annelated radicals.

In order to determine the effects of annelated structure on radical stability, the following series of extended aromatic nitronyl nitroxides 2-phenylphenanthrenimidazole nitronyl nitroxide (**PhenaNN** or **7a**), 2-phenylpyrenimidazole nitronyl nitroxide (**PyrNN** or **7b**), 2-phenylnaphthylimidazole nitronyl nitroxide (**NaphNN** or **7c**), and 2-phenylacenaphthylenimidazole nitronyl nitroxide (**AceNN** or **7d**) was investigated. Figure 3.2 depicts the extended annelated hydrocarbon aromatic nitronyl nitroxides.

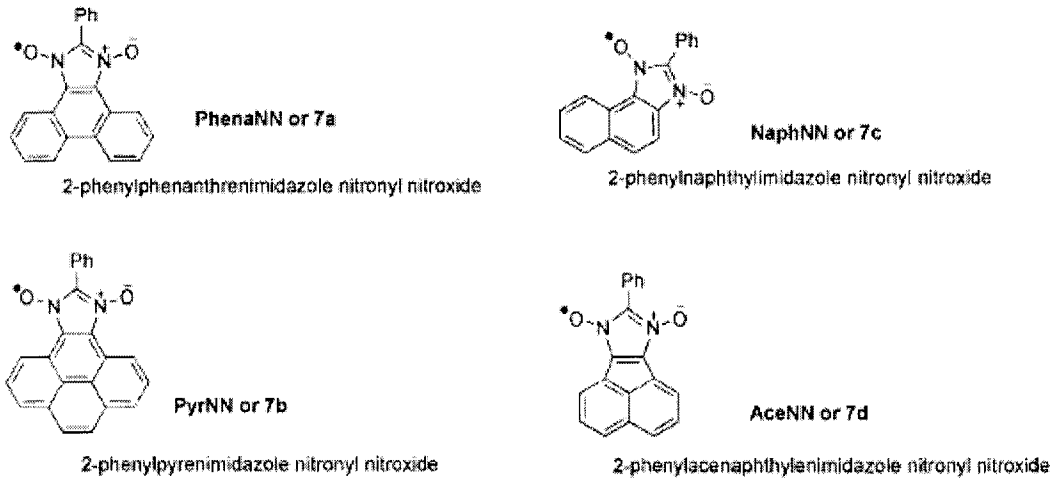

Figure 3.2 - Extended annelated hydrocarbon aromatic nitronyl nitroxides

The 2-phenylphenanthrenimidazole nitronyl nitroxide was determined to be the only derivative stable enough to measure an EPR spectrum. The 2-phenylpyrenimidazole nitronyl nitroxide precursor, 2-phenylpyren[4,5-b]imidazole 1-oxyl-3-oxide (**8b**), was successfully synthesized but the radical **PyrNN** was too unstable to be characterized. The spin distributions and orbital energies of the parent systems were investigated by DFT B3LYP theory at the 6-31G* basis set.

Section 3.2 - Results and Discussion

3.2.1 - Synthesis of 2-phenylphenanthrenimidazole nitronyl nitroxide.

While the EPR and UV-Vis of **PhenaNN** are reported in the literature,[38] the reported synthesis for this radical was poorly described, necessitating the development of new synthetic methodology for this radical precursor. The first step involved the synthesis of phenanthrene-5-oxime-6-one (**9a**) from phenanthrene-5,6-dione by condensation with hydroxylamine hydrochloride and

barium carbonate in ethanol (Scheme 3.1) This was followed by condensing **9a** with benzaldoxime in the presence of excess anhydrous hydrochloride acid in anhydrous ethanol to yield the radical precursor **8a**. The radical was generated by oxidation of the 2-phenylphenanthrimidazole 1-oxyl-3-oxide with lead (IV) oxide in benzene. The radical was deep blue in color and decomposed quickly to a compound that was yellow. Decomposition was supported by EPR and UV-Vis and observed under nitrogen in dry benzene in the absence of residual lead (IV) oxide.

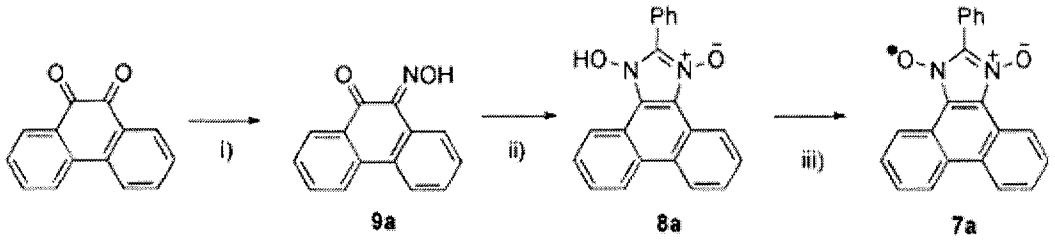

Scheme 3.1 - Synthesis of PhenaNN

Reagents and conditions: 1) H_3NOHCl, $BaCO_3$, EtOH, Δ, 86.6% ii) PhC=NOH, HCl, ethanol, 79% iii) PbO_2, benzene

Previous reports of the EPR of radical **PhenaNN** involved using an EPR apparatus with a streaming flow technique[38] which was not available for this study. The radical precursor **8a** was oxidized with lead (IV) oxide in degassed benzene, filtered, and taken to the pre-tuned instrument as quickly as possible. The time elapsed between oxidation and sample measurement was approximately 10 minutes. Even though the experimental conditions were different than in previous studies, the EPR of the radical was consistent with that reported in the literature[38], with a decay described by the equations $dc/dt = -k * c^{5/2}$ with k = 3.6

x 10^3 $1/(mol^{3/2} * s)$, a_N = 3.89 G , g = 2.007, and a lack of resolvable hyperfine coupling to the set of aromatic hydrogen in the phenanthrene and phenyl substituent. (See Figure 3.3.)

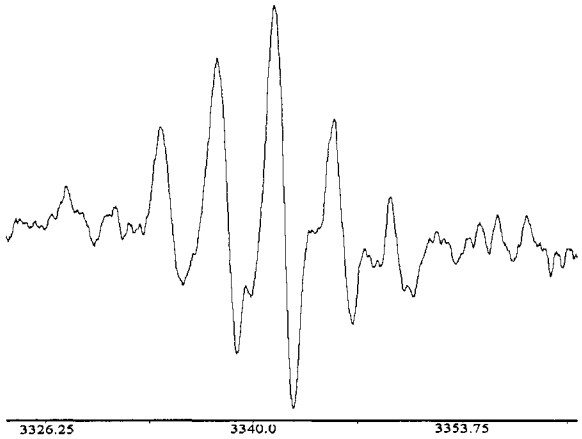

Figure 3.3 - EPR of PhenaNN in degassed benzene

The **PhenaNN** was a bright blue color, which differed from the green/yellow color of the **PBNN** derivatives. The absorption spectrum of **PhenaNN** was measured in benzene and the radical exhibited absorption bands at λ_{max} = 320, 560, and 613 nm. Extinction coefficients were not determined due to the low stability of the radical. The reported spectrum of **PhenaNN** was λ_{max} = 613 nm in DMF, which was consistent with our experimentally determined spectrum in benzene. (See Figure 3.4.)

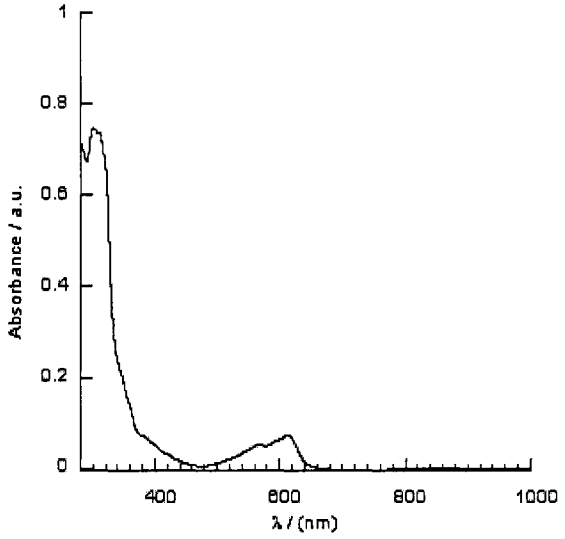

Figure 3.4 - UV/Vis of PhenaNN in benzene

PhenaNN lacked the three resolvable characteristic absorption peaks at 300 nm, with a large unresolvable absorption in the UV region being present. The λ_{max} in the visible region was shifted from 420 nm to 600 nm. Interestingly, the **PhenaNN** did not have the weak intensity absorption at λ_{max} 850 nm as was expected. The larger aromatic system and increased conjugation resulted in a red shift in the absorbance bands, consistent with the effects of conjugation on closed shell molecules. This suggested a decrease in the energy gap between frontier orbitals. The decay of the **PhenaNN** was followed by UV-Vis in benzene and monitored at 569 nm and 613 nm (Figure 3.5). The decay of the radical was best fitted to a bi-exponential decay curve with the following formula: $t(s) = k + c_1 * \exp(-\tau_1 * x) + c_2 * \exp(-\tau_2 * x)$.

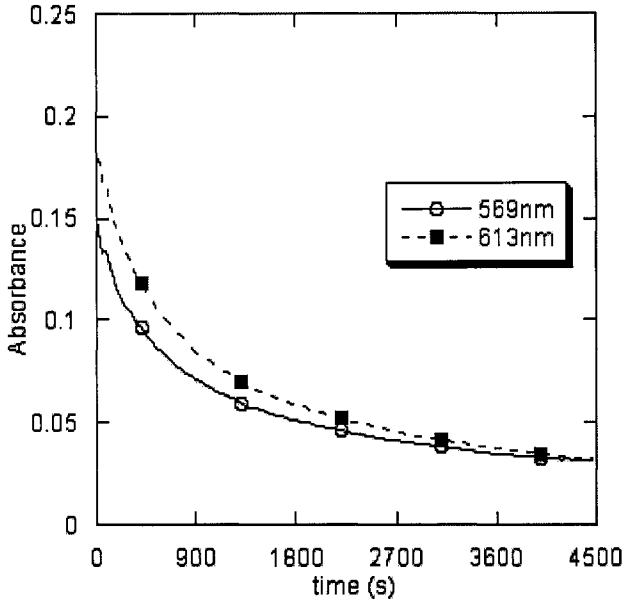

Figure 3.5 - Decay rate of PhenaNN in benzene, monitored at 569 nm and 613 nm

The lifetimes for the radical decay, averaged over three runs, were found to be τ_1= .00323 s^{-1} and τ_2= .000581 s^{-1} with R = 99988 at 569 nm and τ_1= .00291 s^{-1} and τ_2= .000546 s^{-1} with R = 99995 at 613 nm. The fit of a bi-exponential to the decay kinetics indicated that there was more than one pathway for decay. In this case, using 613 nm, there was one major pathway represented by the faster τ_1 with a pre-exponential factor (c_1) of 0.0295 (27.3 %), which was an order of magnitude faster than the second decay pathway with a pre-exponential factor (c_2) of .0785 (72.7 %). This matched experimental observations by TLC of more than one spot appearing during the decay of the radical. The fast rate constant for radical decay was consistent with a decrease in stability of the radical.

3.2.2 - Synthesis of 2-phenylpyrenimidazole 1-oxyl-3-oxide.

The 2-phenylpyrenimidazole 1-oxyl-3-oxide was synthesized from pyrene, based on a literature reaction by Funk,[67] to generate the pyrenedione and coupling reaction conditions used in the making of the phenanthrene radical. Pyrene was selectively oxidized with 50% H_2O_2 in the presence of Na_2WO_4 to give 1,10-dicarboxylatephenanthrene.[67] This was followed by reaction of the carboxylic acid with methyl iodide to generate a diester, which was then reacted with sodium metal in THF to give the pyrenedione. The pyrenedione (**10**) was converted to the monoxime (**9a**) by reacting with one equivalent of hydroxylamine under basic conditions. The monoxime **9a** was then reacted with benzaldoxime in anhydrous ethanol with anhydrous hydrochloric acid. The precipitate was isolated and characterized by high resolution mass spectroscopy and ^{1}H-NMR as the precursor to the radical, 2-phenylpyrenimidazole 1-oxyl-3-oxide (Scheme 3.2).

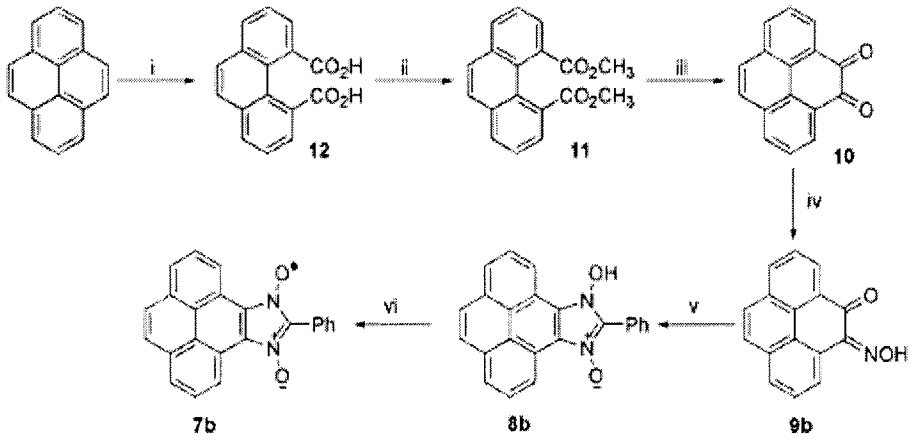

Scheme 3.2 - Synthetic pathways in the preparation of 2-phenylpyrenimidazole 1-oxyl-3-oxide

Reagents and conditions: i) Na_2WO_4, 50% H_2O_2, H_3PO_4, chlorobenzene, 65% ii) CH_3I, $NaHCO_3$, DMF, 71% iii) Na, THF, 75% iv) H_3NOHCl, $BaCO_3$, EtOH, Δ, 89% v) PhC=NOH, HCl, ethanol, 17% vi) PbO_2, benzene

Even though the MS and H-NMR of **8b** were consistent with the expected values, successful measurement of an EPR of the radical when oxidized with lead (IV) oxide was not obtained. When oxidized, the solution turned an immediate yellow color and the EPR of the yellow solution in degassed benzene showed no detectable signal. The change in color was indicative of oxidation occurring, followed by decay, as in past experiments. All of the phenanthrene and benzimidazole radical derivatives decomposed to give a yellow solution as well.

The conclusion, based on the correct characterization of **8b** and the change in color, was that the **PyrNN** was extremely unstable and decayed too quickly to detect the signal by the study's methodologies. An in-situ generation of the radical by EPR using a streaming technique[38] might be an alternate method of determining the lifetime and EPR spectrum of this radical.

3.2.3 - Attempted synthesis of AceNN

AceNN proved to be a challenge to synthesize. After attempting all the methodologies used in the synthesis of the benzimidazole and phenanthrenimidazole nitronyl nitroxides, including unattempted synthetic strategies, 2-phenylacenaphthylenimidazole 1-oxyl-3-oxide was not successfully synthesized. The reaction pathways tried included the following (see Scheme 3.3): acid catalyzed condensation of dioxime and benzaldehyde, acid catalyzed condensation of monoxime and benzaldoxime, base catalyzed condensation of nitromethyl-benzene and furoxan, and reaction of furoxan and phenyl nitrone.

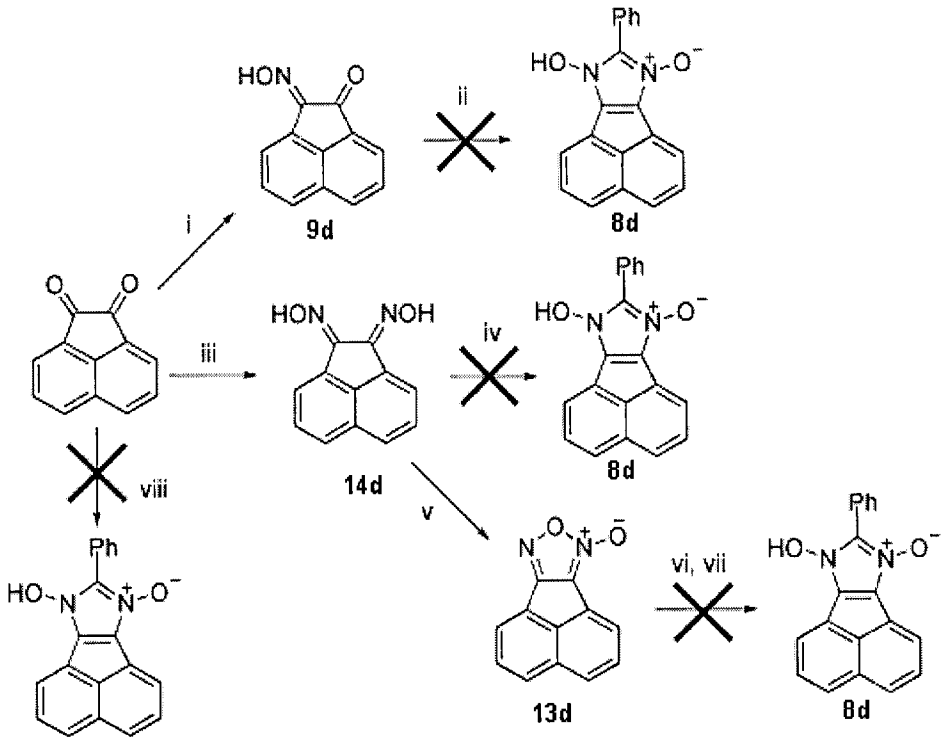

Scheme 3.3 - Synthetic pathways attempted in the preparation of 2-phenylacenaphthylenimidazole 1-oxyl-3-oxide

Reagents and conditions: i) H_3NOHCl, $BaCO_3$, EtOH, Δ, 88% ii) PhC=NOH, HCl_g, 100% ethanol, 0% iii) 2eq H_3NOHCl, $BaCO_3$, EtOH, Δ, 94.6% iv) benzaldehyde, EtOH, 70% $HClO_4$, 80 °C, 0% v) NaOH, 6% NaOCl, 75.0% vi) *C*-phenyl-*N*-phenylnitrone, cyclohexane, benzene, Δ, 0% vii) $PhCH_2NO_2$, triethylamine, THF, RT, 0% viii) 2 NH_3OHCl, benzaldehyde, MeOH, RT, 40 hours, 0%.

The monoxime **9d** was generated by reaction with hydroxylamine hydrochloride and barium carbonate in ethanol. Acid catalyzed condensation with benzaldoxime with anhydrous hydrogen chloride in anhydrous ethanol at room temperature did not lead to the radical precursor **8d**. MS and ^{1}H-NMR on the reaction product showed that it consisted of acenaphthylene-4-monoxime-5-one. The dioxime of acenaphthylene-1,2-dione was synthesized by reaction with two equivalents of hydroxylamine hydrochloride and barium carbonate in ethanol.

Acid catalyzed condensation with benzaldehyde with 70% $HClO_4$ in ethanol under reflux condition did not lead to the radical precursor **8d**. MS and ^{1}H-NMR revealed that the reaction did not occur, and the acenaphthylene-4,5-dioxime starting material was recovered.

The furoxan of acenaphthylene-1,2-dione was synthesized by oxidizing the acenaphthylene-1,2-dione with 6% aqueous sodium hypochlorite. Condensation of nitromethyl-benzene and acenaphthylene[4,5]furoxan in THF and triethylamine, or the acenaphthylene[4,5]furoxan and phenyl nitrone in refluxing cyclohexane/benzene, did not lead to the radical precursor x, using MS and ^{1}H-NMR to show the reaction did not occur.

In addition, a reaction, from the literature based on a synthetic preparation by Panda[45], was attempted and was found to be unsuccessful. Panda's procedure called for the synthesis of the 2-phenylacenaphthylenimidazole 1-oxyl-3-oxide from acenaphthylene-1,2-dione, 2 equivalence of hydroxylamine hydrochloride, and benzaldehyde in methanol stirring at room temperature. Attempts to reproduce their experimental reaction conditions did not yield the supposed product, with MS and H-NMR of reaction revealing that the reaction produced a mixture of acenaphthylenedioxime and acenaphthylene-4-monoxime-5-one instead. The reason why the 2-phenylacenaphthylenimidazole 1-oxyl-3-oxide could not be synthesized was not entirely clear. The reaction pathways monoxime/benzaldoxime worked for derivatives that were structurally similar to the acenaphthylene, such as the 2-phenylphenanthrenimidazole 1-oxyl-3-oxide and 2-phenylpyrenimidazole 1-oxyl-3-oxide.

3.2.4 - Attempted synthesis of NaphNN.

NaphNN proved to be another example of how challenging these extended imidazole 1-oxyl-3-oxide systems were to synthesize. After attempting the methodologies used in the synthesis of the benzimidazole and phenanthrenimidazole nitronyl nitroxide, 2-phenylnaphtho[1,2-*d*]imidazole 1-oxyl-3-oxide was not successfully synthesized. The reaction pathways tried included the following (see Scheme 3.4): acid catalyzed condensation of monoxime and benzaldoxime and the reaction of furoxan and phenyl nitrone.

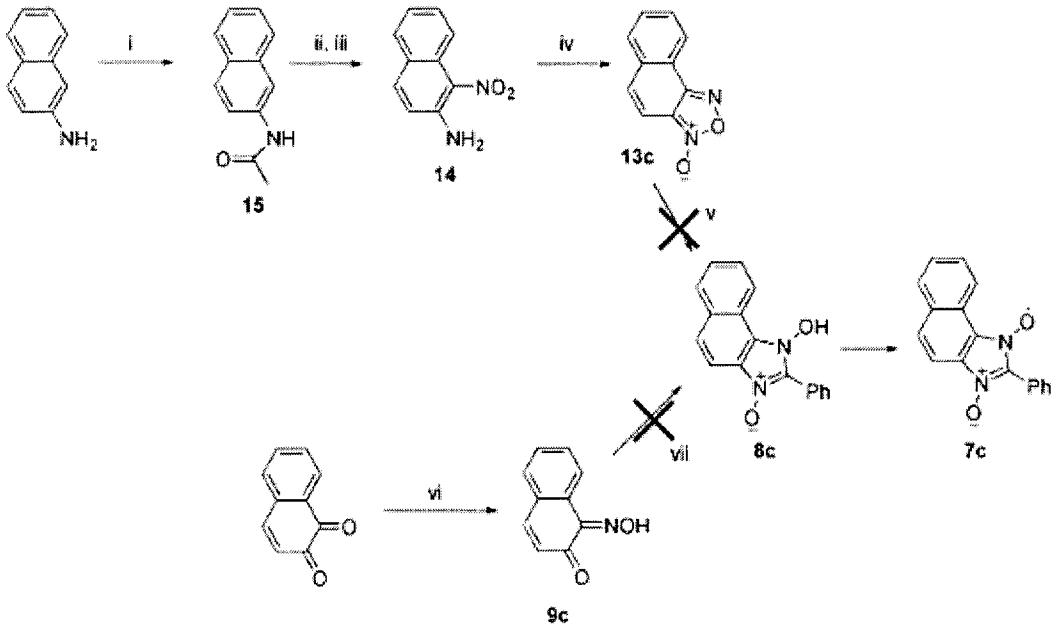

Scheme 3.4 - Synthetic pathways attempted in the preparation of phenylnaphtho[1,2-*d*]imidazole 1-oxyl-3-oxide

Reagents and conditions: i) acetic anhydride, acetic acid, 95% ii) acetic acid, conc. nitric acid iii) HCl, EtOH, Δ iv) NaOH, 6% NaOCl, 14% v) *C*-phenyl-*N*-phenylnitrone, cyclohexane, benzene, Δ, 0% vi) H_3NOHCl, $BaCO_3$, EtOH, Δ, vii) PhC=NOH, HCl_g, 100% ethanol, 0%

The furoxan of naphthalene was synthesized from 2-aminonaphthlene by protecting the amino group with an acetyl protecting group using acetic anhydride in acetic acid. The protected 2-acetamidenaphthalene was then nitrated with nitric acid in acetic acid, followed by deprotection in hydrochloric acid, and oxidation with 6% aqueous sodium hypochlorite. All of the reactions attempted to synthesize the 2-phenylnaphtho[1,2-*d*]imidazole 1-oxyl-3-oxide yielded starting material.

The reason why the 2-phenylnaphtho[1,2-*d*]imidazole 1-oxyl-3-oxide could not be made was not entirely clear. The reaction pathways worked for derivatives that were extremely structurally similar to the naphthalene. The phenanthrene-5-monoxime,6-one molecule was essentially the naphtho-1-monoxime,2-one with an extra polycyclic phenyl ring on the 3,4-position. Their steric interactions and reactivities should have been similar, yet the monoxime/benzaldoxime coupling did not work.

3.2.5 - Computational Calculations of PhenaNN and PyrNN.

Calculations were performed on the two radicals, **PhenaNN** and **PyrNN**, with standard DFT B3LYP/6-31G* method using Gaussian 98 software package. The main reason behind performing calculations on the extended aromatic nitronyl nitroxides was to determine if possible changes in spin density distribution or energy of the frontier orbitals would yield insight into an apparent decrease in stability from the **PBNN** radical.

The SOMO of **PyrNN** and **PhenaNN** are shown in Figure 3.6, visualized with Cubgen at an isocontour value of 40 and scaling factor of 0.18. The SOMO

of the extended radicals shared the same symmetry group and large spin density on the ONCNO moiety as the parent **PBNN**. In Figure 3.7, the total spin-densities of **PyrNN** and **PhenaNN** are displayed.

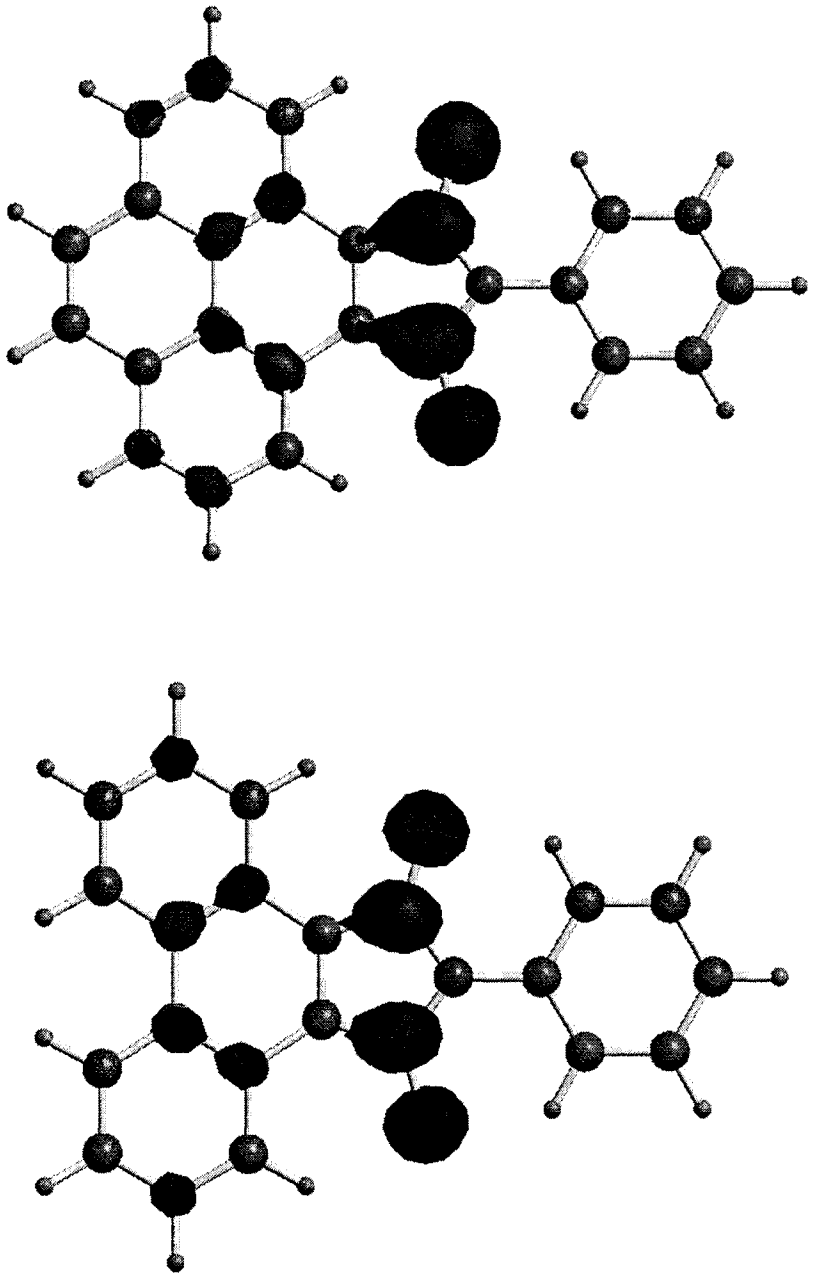

Figure 3.6 - SOMO of PyrNN and PhenaNN generated at B3LYP/6-31G* with CubGen (isocontour = 40, scaling factor = 0.18) and visualized with Chem3D

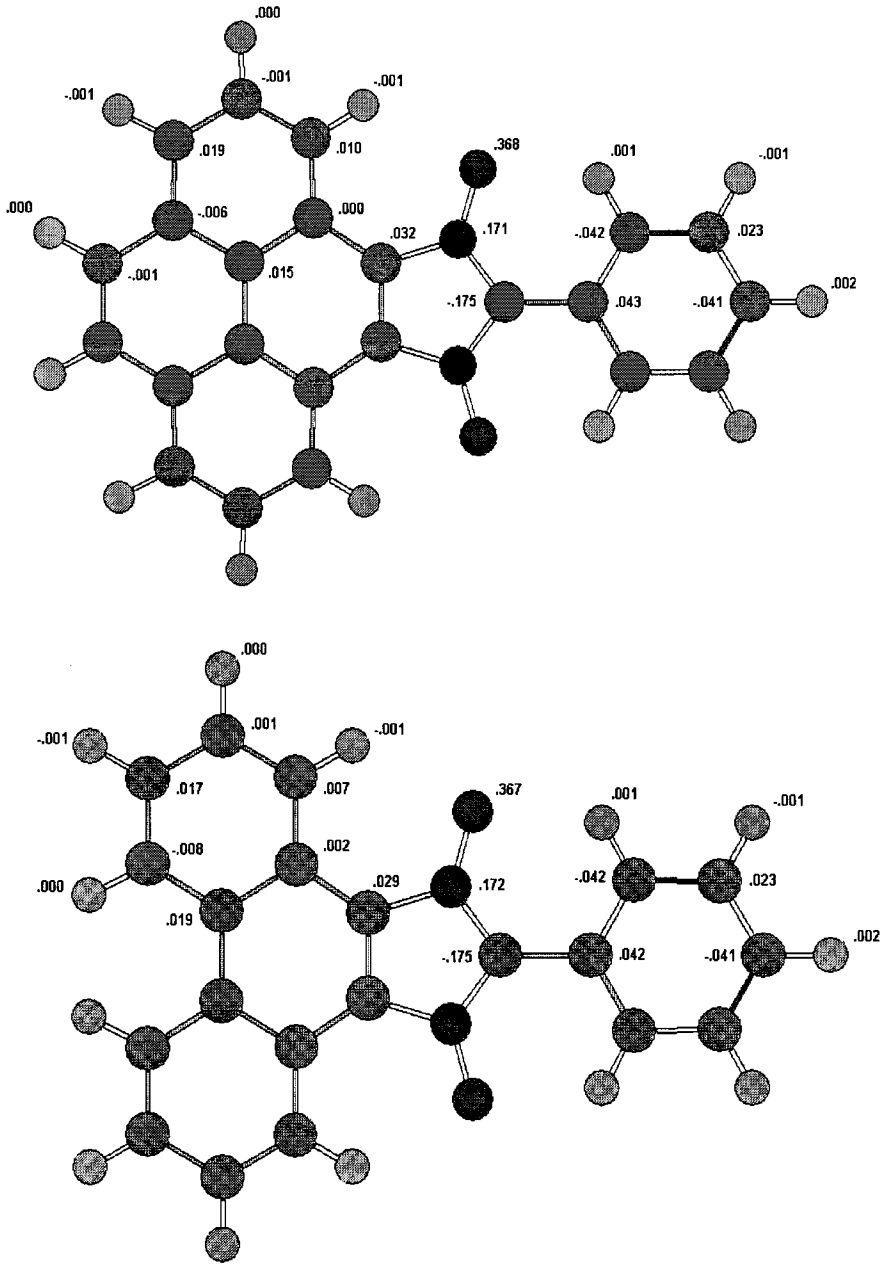

Figure 3.7 - Spin density distribution of PyrNN and PhenaNN generated at B3LYP/6-31G* with CubGen (isocontour = 40, scaling factor = 0.18) and visualized with Chem3D

The predicted spin density on the C2- phenyl substituent of the extended aromatics pyrene and phenanthrene was found to be close to the predicted values for **PBNN**. The predicted spin density on the ortho carbon on the C2-phenyl

group was predicted to be -0.041, -0.041, and -0.0448 for phenanthrene, pyrene, and **PBNN** respectively. The experimental values for the phenyl group on the pyrene and phenanthrene were not measurable, but this overestimation of the phenyl spin distribution follows a trend for all BNN radicals studied to date.

The predicted spin density on the ONCNO moiety did not change, with a calculated value of 0.172 for the nitrogen on the extended aromatic being similar to the value of 0.175 for the **PBNN** radical. This value is larger than that found experimentally, where the hfcc for **PhenaNN** was found to be 0.1556 (3.89 G). The computations appeared to underestimate the spin density on the ONCNO moiety. This showed that the calculations were underestimating the spin density distributed into the phenanthrene system.

The most significant difference between the extended radicals and **PBNN** was the spin density on the bridge carbons where the imidazole ring was connected to the pyrene/phenanthrene versus benzene at C_x and C_y, (i.e. the point of annelation). Figure 3.8 shows these positions.

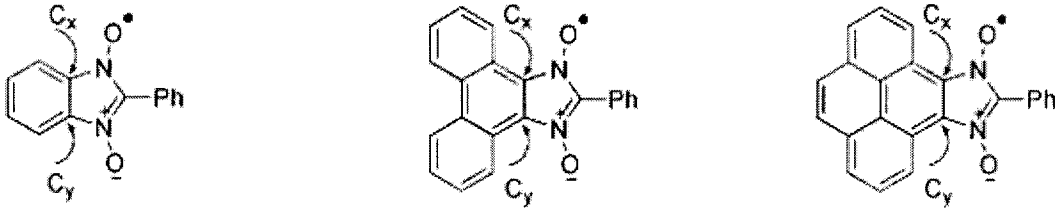

Figure 3.8 - Position of the bridged carbons in annelated nitronyl nitroxides

The BNN radical calculations predicted low spin The BNN radical calculations predict low spin density at these positions (C_x and C_y = -0.00398) but the extended pyrene and phenanthrene had ten times the predicted total spin density (C_x and C_y = 0.032 and 0.029) at these positions. Large spin density at these

bridge head carbons could be a primary reason why the extended radicals were unstable.

Besides the change in spin density distributions, a potential explanation of why the extended radicals were the most unstable could be that the extra delocalization further lowered the reduction potential of the radical, making it unstable toward any reducing species in the solvent. This did not seem likely, however, since the radicals decomposed in the presence of the lead (IV) oxide oxidizing agent. The presence of oxygen was not a factor, with the radical decaying just as quickly when oxidized under ambient conditions as under an inert atmosphere (N_2 environment).

Section 3.4 - Conclusion.

The synthesis of hydrocarbon-based extended nitronyl nitroxide radicals was attempted to explore whether extending the conjugation of the radical would lead to a more stable radical. The synthesis of these extended radicals further elucidated the reactivity of this class of extended dioxime, mono-oximes, and furoxans. **AceNN** and **NaphNN** were not successfully synthesized after numerous attempts. **PhenaNN** and **PyrNN** were successfully synthesized and were found to be extremely unstable. These instabilities defy conventional ideas in organic chemistry, which state that delocalization of radicals increases the overall stability of the system.

The low stability exhibited by this class of radicals might have been rationalized with computational analysis, but the calculations did not demonstrate

any large deviations that would predict instability of the radicals. Overall, the calculations suggested that there was little deviation in spin density distribution or reduction potential from that of **PBNN.** As well, the calculations tended to overestimate the spin density on the phenyl ring and underestimate the delocalization out into the extended aromatic system.

Section 3.5 - Experimental.

Phenanthrene-5-oxime-6-one (9a). A suspension of phenanthrene-5,6-dione (1.0 g, 0.0048 mol) and $BaCO_3$ (0.5 g, 0.0046mol) in 80 mL of EtOH was stirred at RT. To this was added NH_3OHCl (0.32 g, 0.0046 mol). The reaction was refluxed for 30 hours. The solution was evaporated under vacuum, 80 mL of 0.2M HCl was added, and the suspension was stirred for 45 minutes. The solution was filtered with suction and the solid was washed with H_2O, ethanol, hexanes, and ether to give an off-white powder (0.87 g, 86.6%). ^{1}H-NMR (200MHz, $DCCl_3$, δ): 8.40 (m, 2H, Ar-H), 8.20 (m, 2H, Ar-H), 7.83 (m, 2H, Ar-H), 7.51 (m, 2H, Ar-H).

Benzaldoxime.[68] A solution of benzaldehyde (5.0 g, 5.2 mL, 0.0469 mol), hydroxylamine hydrochloride (3.30 g, 0.0475 mol), and sodium acetate (3.90 g, 0.0475 mol) in 200 mL of ethanol were refluxed for 2 hours. The reaction was evaporated under vacuum and the solid was washed with water. The crude solid was purified by column chromatography (silica, DCM) to give a clear brown oil

(2.952 g, 52.5%). ^{1}H-NMR (200MHz, $DCCl_3$, δ): 8.2 (s, 1H, -C*H*N=OH), 7.9 (broad s, 1H, N=OH), 7.65 (m, 2H, Ar-H), 7.45 (m, 3H, Ar-H).

2-phenylphenanthrimidazole 1-oxyl-3-oxide (8a). A solution of **9a** (2.2 g, 0.00487 mol) and benzaldoxime (1.2 g, 0.0049 mol) in 25 mL of absolute ethanol was stirred at RT. The solution was made acidic by bubbling HCl though the ethanol for one hour (a concentrated HCl drip into concentrated sulfuric acid was used as the source of HCl gas). The reaction was stirred at RT for 24 hours and the precipitate was filtered with suction and washed with 10% $NaHCO_3$, water, and hexanes. The tan-brown clay was dried and weighted (2.5 g, 79%). MS m/z (direct probe): 310 $[M-O]^+$, 294 $[M-O_2]^+$. ^{1}H-NMR (500MHz, 0.1 M KOH in D_2O, δ): 8.88 (t, 2H, Ar-H), 8.04 (d, 2H, Ar-H), 7.61 (m, 7H, Ar-H), 7.02 (d, 2H, Ar-H).

2-phenylphenanthrenimidazole nitronyl nitroxide (PhenaNN, 7a). Before oxidation, 2-phenylphenanthrimidazole 1-oxyl-3-oxide (0.002 g, <0.1 mmol) was suspended in 20 mL of degassed benzene. Lead (IV) oxide (0.4 g) was added to the solution under nitrogen, and solution was stirred for 1 minute. The bright blue solution was filtered through a Celite-545 plug, diluted, and degassed with N_2 briefly to prepare EPR samples. The UV-Vis samples were filtered through a Celite-545 plug and diluted to appropriate concentration. UV-Vis (benzene) λ_{max}, nm (~ε): 277, 569, 613.

1,10-dicarboxylatephenanthrene (12).[67] A suspension of pyrene (6.0 g, 0.0296 mol), Aliquat 336(0.50 mL), Na_2WO_4 (0.405 g, 0.0012 mol), and 0.28 mL of 10% H_3PO_4 in 16 mL of chlorobenzene was stirred at RT. To this was added slowly 17 mL of 50% H_2O_2. The reaction was heated to 80 °C. After one hour, the solution turned a dark brown/red color. After 6 hours at reflux, the dark brown solution was cooled to 0 °C, filtered with suction, and the mud brown crude solid was dissolved in 0.4 L of 1.25 M NaOH. The red/brown solution was decolorized with activated carbon, and filtered with suction. The solution was acidified to pH = 4 with acetic acid and filtered with suction to give a light-colored red/brown solid (3.81 g, 53.1%). mp 249-52 °C (lit. [67] 248-50). ^{1}H-NMR (200MHz, d_6-DMSO, δ): 12.9 (broad s, 2H, -CO_2H), 8.14 (d, 2H, J= 7.5 Hz, Ar-H), 8.01 (d, 2H, J= 7.6 Hz Ar-H), 7.91 (s, 2H, Ar-H), 7.67 (t, 2H, J= 7.6, 7.5 Hz, Ar-H).

1,10-dimethyoxycarboxylatephenanthrene (11).[67] A suspension of 1,10-dicarboxylatephenanthrene (3.65 g, 0.0137 mol) and $NaHCO_3$ (6.0 g, 0.0714 mol) in 75 mL of DMF was stirred at RT while methyl iodine (11 mL, 0.176 mol) in 22 mL of DMF was added. The red/brown solution was stirred at RT for 48 hours. The reaction was diluted with 250 mL of EA, extracted with 5 x 130 mL of H_2O and 70 mL of brine, dried with $MgSO_4$, and the solvent was evaporated under vacuum to give 3.4 g of a brick red/yellow solid. The crude solid was columned on silica (gradient column, silica, 2:1 DCM/hexanes to 100% DCM) to give a white/yellow solid (3.052 g, 75.0%). mp=165 °C. ^{1}H-NMR (200MHz, $DCCl_3$,

δ): 8.09 (d, 2H, J= 7.9 Hz, Ar-H), 8.01 (d, 2H, J= 7.3 Hz Ar-H), 7.79 (s, 2H, Ar-H), 7.69 (t, 2H, J= 7.3, 7.9 Hz, Ar-H), 3.88 (s, 6H, $-CO_2CH_3$).

Pyrene-4,5-dione (10).[67] A solution of Na metal (0.90 g, 0.04 mol) in 22 mL of dry THF was refluxed for 15 minutes under N_2 and to this was 1,10-dimethyoxycarboxylatephenanthrene (2.6766 g, 0.00909 mol) in 40 mL of dry THF. The solution was kept at reflux and, after 1 hour, a second chip of Na was added (~0.50 g, 0.0021 mol). The reaction was refluxed for another 2 hours. Analysis by TLC after 3.5 hours showed no more starting material and a bright yellow new spot at a slightly lower R_f. The reaction was poured into 120 mL of EA and 40 mL of H_2O. The black emulsion was left to separate for two days. The organic layer was separated and the aqueous layer was extracted with 3x75 mL of EA. The organic layer was then dried with $MgSO_4$ and evaporated under vacuum to give a dark orange/brown solid. This was purified by column chromatography (silica, DCM) and, after evaporation, the solid was isolated as a bright orange solid (1.807g, 85.5%). ^{1}H-NMR (200MHz, $DCCl_3$, δ): 8.56 (d, 2H, J= 7.4 Hz, Ar-H), 8.24 (d, 2H, J= 7.4 Hz Ar-H), 7.90 (s, 2H, Ar-H), 7.80 (t, 2H, J= 7.7, 7.4 Hz, Ar-H).

Pyrene-4-oxime,5-one (9b). A suspension of pyrene-4,5-dione (0.2325 g, 0.001 mol) and $BaCO_3$ (0.1974 g, 0.001 mol) in 10 mL of EtOH was stirred at RT. The reaction was cloudy and bright orange. Pyrene-4,5-dione's solubility was low in EtOH. To this was added NH_3OHCl (0.0695 g, 0.001 mol). The reaction was

sonicated for 15 minutes until the solution had turned a bright yellow color. The reaction was refluxed for 12 hours. The solvent was evaporated under reduced pressure, 25 mL of 0.1M HCl was added, and the suspension was stirred for 30 minutes. The bright yellow solid with a different R_f than the starting material was filtered with suction and air-dried to yield a bright yellow powder (0.236 g, 95.4%). MS (direct probe) m/z: 247 $[M]^+$, 231 $[M-O]^+$, 215 $[M-NOH]^+$.

2-phenylpyren[4,5-b]imidazole 1-oxyl-3-oxide (8b). An acidic anhydrous solution of ethanol was prepared by bubbling HCl though 10 mL of ethanol (a concentrated HCl drip into concentrated sulfuric acid was used as the source of HCl gas). To this was added pyrene-4-oxime-5-one (0.5 g, 0.00202 mol) and benzaldoxime (0.025 g, 0.00202 mol). The reaction was stirred at RT for 48 hours. The precipitate was filtered with suction and washed with 10% $NaHCO_3$, water, and hexanes. The brown solid was dried and weighted (0.026 g, 36.8%). MS m/z (electrospray, + mode): 351 $[MH]^+$, 335 $[MH-O]^+$, 319 $[MH-O_2]^+$. ^{1}H-NMR (500MHz, 0.1 M KOH in D_2O, δ): 8.88 (t, 2H, Ar-H), 8.04 (d, 2H, Ar-H), 7.61 (m, 7H, Ar-H), 7.02 (d, 2H, Ar-H). HRMS-ESI (m/z): $[M + H]^+$ calcd for $C_{23}H_{15}N_2O_2$, 351.1134; found, 351.1142.

Attempt at 2-phenylacenaphthylenimidazole 1-oxyl-3-oxide from acenaphthylenequinone and benzaldehyde.[45] A suspension of acenaphthylene-1,2-dione (0.455 g, 0.0025 mol) and benzaldehyde (0.250 mL, 0.0025 mol) in 20

mL of MeOH was sonicated at RT. The reaction was cloudy and yellow. To this was added NH_3OHCl (0.343g, 0.005 mol). The reaction was sonicated for an additional 15 minutes until the solution had taken a bright yellow color. After 40 hours stirring at RT, the solution was filter to obtain a white clay-like solid. The initial weight of the solid was 0.173 g after drying under vacuum. The yellow/orange solution was neutralized with K_2CO_3 and saturated $NaHCO_3$. The methanol was evaporated under vacuum, filtered with suction, washed with water and hexanes, and weighted to give a pale orange/brown solid. The weight was 0.2588 g after drying under vacuum. MS and H-NMR of both solids revealed that the solids consisted of acenaphthylenedioxime and acenaphthylene-4-monoxime-5-one. Coupling did not occur.

Acenaphthylene-4,5-dioxime (14d). A suspension of (1.019 g, 0.0056 mol) acenaphthylene-1,2-dione and $BaCO_3$ (1.182 g, 0.0116 mol) in 50 mL of EtOH was stirred at RT. To this was added NH_3OHCl (0.778 g, 0.0112mol), which was refluxed overnight. The reaction was cooled the next day and the EtOH was evaporated under vacuum. To the tan/white paste was added 50 mL of 0.1 M HCl in H_2O and this was stirred at RT for an hour. The light tan solution was filtered with suction, washed with 0.1M HCl, 0.5M Na_2CO_3, water, Et_2O, and hexanes to give a light brown/tan solid (1.1213 g, 94.6%). ^{1}H-NMR (200MHz, d_6-DMSO, δ): 11.6 (broad s, 2H, N=OH), 7.90 (d, 2H, J= 5.6 Hz, Ar-H), 7.64 (d, 2H, J= 6.6 Hz Ar-H), 7.40 (t, 2H, J= 6.6, 5.6 Hz, Ar-H).

Attempt at 2-phenylacenaphthylenimidazole 1-oxyl-3-oxide from acenaphthylene-4,5-dioxime and benzaldehyde. A suspension of benzaldehyde (0.050 mL, 0.5 mmol) and acenaphthylene-4,5-dioxime (0.106 g, 0.5 mmol) in 2 mL of EtOH was stirred at RT. To this was carefully added 0.200 mL of 70% $HClO_4$ in H_2O (~0.0022 mol of $HClO_4$). The solution was then heated to 80 °C overnight. The next day the solution was cooled to RT, diluted with 2 mL of ice water, and neutralized with NH_4OH. A brown precipitate was collected, washed with water and hexanes, and dried to constant weight (0.068 g). MS and H-NMR revealed that the solid consisted of acenaphthylene-4,5-dioxime starting material. Coupling did not occur.

Acenaphthlene-4-monoxime-5-one (9d). A suspension of acenaphthylenequinone (1.010 g, 0.00554 mol) and $BaCO_3$ (1.182 g, 0.00642 mol) in 50 mL of EtOH was stirred at RT. The reaction was cloudy and yellow. To this was added NH_3OHCl (0.343 g, 0.00549mol). The reaction was sonicated for 15 minutes until the solution had turned a bright yellow color. TLC of the reaction showed the reaction was almost complete after 15 minutes. The solution was sonicated for another 15 minutes and the ethanol was evaporated under vacuum. The pale white paste was suspended in 25 mL of water and then neutralized with 6M HCl. Once at pH = 7, the reaction was filtered with suction to give a pale brown solid, which was washed with water and ether to give a fluffy, pale yellow solid (0.785 g, 71.1%). ^{1}H-NMR (200MHz, d_6-DMSO, δ): 13.3 (broad s, 1H, N=OH), 8.34 (d, 2H, J= 7.5 Hz, Ar-H), 8.21 (d, 1H, J= 8.2 Hz

Ar-H), 8.08 (d, 1H, J= 7.9 Hz Ar-H), 7.88 (t, 1H, J= 7.9, 7.2 Hz, Ar-H), 7.82 (t, 1H, J= 7.4 , 8.0 Hz, Ar-H).

Attempt at 2-phenylacenaphthylenimdiazole 1-oxyl-3-oxide from acenaphthylene-4-monoxime-5-one and benzaldoxime. A suspension of acenaphthylene-4-monoxime-5-one (0.075 g, 0.38 mmol) and benzaldoxime (0.045 g, 0.371 mmol) in 6 mL of ethanol was stirred at RT. HCl_g was bubbled through the solution by H_2SO_4/HCl drip until the solution had fully dissolved. The yellow solution was stirred at RT for three days. The temperature was increased to 40 °C on the third day and the solution was stirred for another four days. No precipitate or change in TLC was observed. The solution was filtered with suction after 7 days of stirring and the ethanol was evaporated under vacuum. MS and H-NMR revealed that the solid consisted of acenaphthylene-4-monoxime-5-one. Coupling did not occur.

Acenaphthylene[4,5]furoxan (13d). A solution of acenaphthylene-4,5-dioxime (0.205 g, 0.967 mmol) in 50 mL of 0.75 M NaOH was added to 50 mL of 6% aqueous NaOCl. Precipitate formed almost instantaneously and the pink precipitate was collected by filtration under vacuum, washed with water and hexanes, and recrystalized in EtOH to produce pink needle-like crystals (0.153 g, 75.0%). ^{1}H-NMR (200MHz, $DCCl_3$, δ): 8.09 (m, 4H, Ar-H), 7.77 (m, 2H, Ar-H). IR (KBr pellet, cm^{-1}): 1673 (s, C=N(furoxan)), 1412 (s, C=N(furoxan)), 1361 (s, N-O(furoxan)). MS (direct probe) m/z: 210 $[M]^+$, 194 $[M-O]^+$, 178 $[M-O_2]^+$, 164 $[M-NO_2]^+$, 152 $[M-CNO_2]^+$.

Attempt at 2-phenylacenaphthylenimidazole 1-oxyl-3-oxide from acenaphthylene[4,5]furoxan and *C*-phenyl-*N*-phenylnitrone. A solution of *C*-phenyl-*N*-phenylnitrone (0.0330 g, 0.167 mmol) and acenaphthylene[4,5]furoxan (0.030 g, 0.143 mmol) in 6 mL of cyclohexane and 2 mL of benzene was heated at reflux for 44 hours and monitored by TLC. The nitrone slowly started to break down after the second day. The furoxan's R_f never changed, no precipitate formed, and MS of the reaction showed no formation of product. The reaction did not occur.

Attempt at 2-phenylacenaphthylenimidazole 1-oxyl-3-oxide from acenaphthylene[4,5]furoxan and nitromethyl-benzene. A solution of acenaphthylene[4,5]furoxan (0.060 g, 0.286 mmol) in 2 mL of dry THF and 2 mL of dry DCM was sonicated and to this was added nitromethyl benzene (0.050 g, 0.34 mmol) and triethylamine (0.047 mL, 0.34 mmol). The reaction was stirred overnight at RT. The next day the red solution was evaporated under vacuum, and a new spot was isolated by column chromatography (DCM on silica). H-NMR of the reaction showed an acenaphthylene splitting pattern but no phenyl group. Coupling did not occur.

2-Acetamidenaphthalene (15). A solution of 2-aminonaphthalene (1.0 g, 0.0069 mol) in 20 mL of acetic acid was heated to 50 °C with stirring. To this was added acetic anhydride (4 mL, 0.030 mol). The solution was stirred overnight at RT.

The reaction was neutralized with saturated aqueous K_2CO_3 solution and filtered with suction to produce a light pink compound. The compound was washed with water and dried under vacuum to give a light pink solid (1.210 g, 94.7%). ^{1}H-NMR (200MHz, $DCCl_3$, δ): 8.22 (s, 1H, Ar-H), 7.81 (m, 3H, Ar-H), 7.47 (m, 3H, Ar-H), 2.28 (s, 3H, Ar-H).

Naphtha[1,2-c]furoxan (13c). A solution of 2-acetamidenaphthalene (1.12 g, 0.006 mol) was dissolved in 10 mL of acetic acid at RT, and 0.5 ml of conc. nitric acid was added over 2 minutes. The solution became yellow and, after 5 minutes, a precipitate had formed. After 10 minutes, the reaction was stopped and cooled in an ice bath for 2 hours. The precipitate was filtered under suction and then dissolved in 5 mL of ethanol and 2 mL of conc. HCl. The yellow orange solution was refluxed for 4 hours and poured into 30 mL of ice water. The solution was then cooled in a refrigerator overnight and filtered with suction. The 1-nitro-2-aminonaphthalene and isomers were dissolved in 10 mL of ethanol and 0.5 g of KOH. The yellow orange solution was stirred with the addition of 10 mL of bleach. The solution went from an orange/red to a pale yellow color and precipitate formed in 15 minutes. The reaction was diluted with 10 mL of water and placed in a refrigerator overnight. Next day the solution was filtered with suction and purified by column chromatography (silica, DCM). Evaporation of solvent under reduced pressure resulted in an off-white solid (0.159 g, 14.1%). mp = 122-125 °C (lit.[69] 126-7 °C). MS (direct probe) m/z: 186 $[M]^+$, 170 $[M-O]^+$, 154 $[M-O_2]^+$.

Attempt at 2-phenylnaphtho[1,2-*d*]imidazole 1-oxyl-3-oxide from naphtha[1,2-*c*]furoxan and *C*-phenyl-*N*-phenylnitrone. A solution of *C*-phenyl-*N*-phenylnitrone (0.160 g, 0.000805 mol) and naphtha[1,2-c]furoxan (0.150 g, 0.000805 mol) in 10 mL of benzene was heated at 75 °C for 60 hours. The nitrone slowly started to break down after the second day. A precipitate never formed and MS of the reaction after evaporation of the solution showed no formation of product. Reaction did not occur.

Naphtho-1-oxime-2-one (9c). A suspension of 1,2-naphthoquinone (1.58 g, 0.01 mol) and of $BaCO_3$ (1.97 g, 0.01 mol) in 80 mL EtOH was stirred at RT. The reaction was black but dissolved. To this suspension, NH_3OHCl (0.69 g, 0.01 mol) was added. The reaction was sonicated for 55 minutes. The solution turned a bright yellow color. The solution was then diluted with 50 mL of water. The brown solution was neutralized with 6M HCl and $NaHCO_3$. Once at pH = 7, the reaction was filtered to give a pale brown solid which was washed with water and ether to give a fluffy, light brown powder (1.5489 g, 94%). MS (direct probe) m/z: 173 $[M]^+$, 172 $[M-H]^+$, 157 $[M-O]^+$, 142 $[M-NOH]^+$.

Attempt at 2-phenylnaphtho[1,2-*d*]imidazole 1-oxyl-3-oxide from naphtho-1-oxime-2-one and benzaldoxime. A suspension of naphtho-1-oxime-2-one (0.2589 g, 0.00147 mol) in 5 mL of ethanol was stirred at RT. To this was added benzaldoxime (0.180 g, 0.00147 mol) in 5 mL of EtOH. Hydrogen chloride gas

was bubbled through the solution for 30 minutes. After addition, the solution was stirred for 48 hours at RT. The solution became purple-brown in color. The solution was filtered but the expected precipitate never formed. MS of the reaction showed no formation of the product.

Chapter 4. - Synthesis and Characterization of Annelated Nitronyl Nitroxides Based on Pyridyl and Quinoxaline

Section 4.1 - Introduction

In addition to purely organic magnetic materials, nitronyl nitroxides have been used in inorganic-organic hybrid materials. The idea focuses on using radical ligands with their own intrinsic spin giving rise to magnetic exchange between metal centers and radicals. Such materials are of interest since metal-ligand magnetic exchange can be extremely large, on the order of 200-300 cm^{-1}.[70] This magnetic exchange pathway allows for clever creation of ferrimagnetic materials, since antiferromagnetic exchange between the $s > 1/2$ metal center and $s = 1/2$ organic radical leads to an overall magnetic moment between the metal centers. The literature has focused on two major binding patterns between nitronyl nitroxides and transition metals: coordination though the oxygen on the N-O moiety of **TMNN**[70,71] and coordination through a Lewis base on the 2-position aromatic group(ex. pyridyl,[72] thiazole,[73] and phenanthroline[74]) (Figure 4.1).

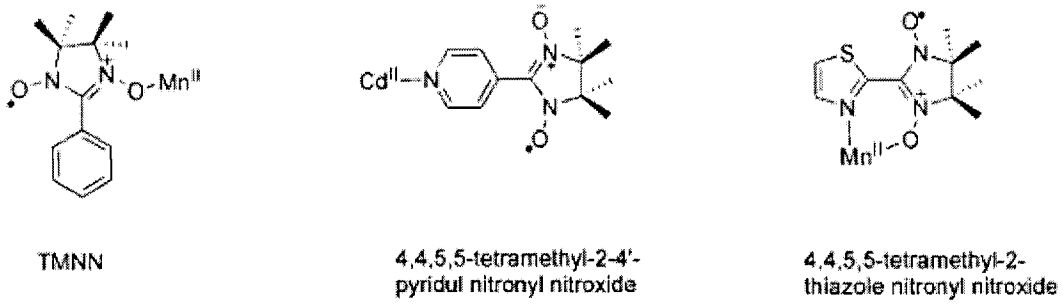

Figure 4.1 - Literature examples of radical-metal coordination

The effect of heteroaromatic substitution in the annelated portion of the BNN radicals was unknown. Our aim was to determine the effect of heteroatom incorporation on the electronic structure of the annelated radicals.

This chapter covers the synthesis, characteristics, and stability of this new class of pyridyl and quinoxaline based nitronyl nitroxides. The results of this research found that synthetic methodologies developed for the preparation of benzimidazole can be applied to make benzimidazole nitronyl nitroxides based of pyridine instead of benzene. Three new radicals incorporating heterocyclic moieties were successfully synthesized: 2-phenyl-5-azabenzimidazole nitronyl nitroxide (**P3PNN**), 2-phenyl-4-azabenzimidazole nitronyl nitroxide (**P2PNN**), and 2-phenylimidazo[4,5-b]quinoxaline nitronyl nitroxide (**PQNN**) (Figure 4.2).

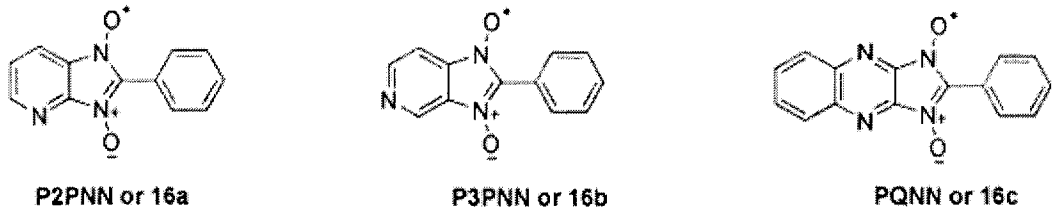

Figure 4.2 - Target Molecules for Potential Metal Binders

Unfortunately, the substitution of nitrogen in the benzimidazole ring decreased the chemical stability of these radicals in solution, precluding attempts to

characterize their crystalline state properties, such as magnetism and structure analysis in the solid state.

Section 4.2 - Results and Discussion

4.2.1 - Synthesis of 2-phenyl-5-azabenzimidazole nitronyl nitroxide.

The synthesis of 2-phenyl-5-azabenzimidazole nitronyl nitroxide (**P3PNN**) was accomplished by application of the furoxan/phenyl nitrone synthetic methodologies. The pyrido[3,4-*c*]furoxan was synthesized by reacting sodium azide with 4-chloro-3-nitro-pyridine to form 4-azo,3-nitropyridine. The 4-azo,3-nitropyridine was heated in toluene, causing the loss of nitrogen gas and ring closure, to produce pyrido[3,4-*c*]furoxan. The pyrido[3,4-*c*]furoxan was not stable in the solid state and decomposed quickly into a black, insoluble solid. The pyrido[3,4-*c*]furoxan was therefore immediately reacted with *C*-phenyl-*N*-phenylnitrone in toluene to yield the radical precursor, 2-phenyl-5-azabenzimidazole 1-oxyl-3-oxide. Oxidation of the precursor to the radical was done in benzene with lead (IV) oxide as the oxidizing agent (Scheme 4.1).

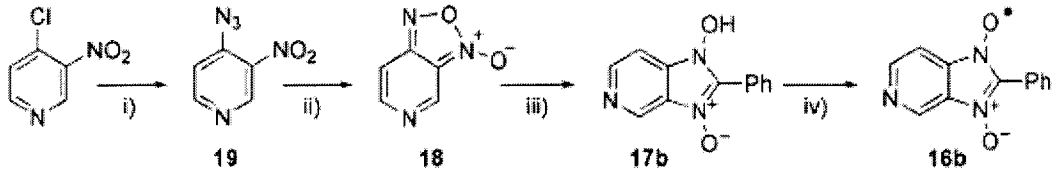

Scheme 4.1 - Synthesis of P3PNN

Reagents and conditions: i) NaN_3, DMSO, 84.6% ii) Δ, toluene iii) *C*-phenyl-*N*-phenylnitrone, toluene, Δ, 51.8% iv) PbO_2, benzene

The radical **P3PNN** was not as chemically stable as the **PBNN** derivative. The EPR signal was lost when the radical solution was evaporated under reduced pressure and re-dissolved with fresh solvent, suggesting that the chemical instability arose from intermolecular reactions such as radical dimerization and proton extraction. The radical was stable in solution in hydrocarbon solvents such as benzene for extended periods of time with a sample surviving at room temperature and exposed to air for 4 days.

4.2.2 - Synthesis of 2-phenyl-4-azabenzimidazole nitronyl nitroxide (P2PNN).

The synthesis of 2-phenyl-4-azabenzimidazole nitronyl nitroxide was accomplished by using the synthetic methodology developed in the synthesis of the benzimidazole nitronyl nitroxides. As with the **P3PNN**, the preferred method was synthesizing the corresponding pyrido[3,4-*c*]furoxan followed by reaction with a phenyl nitrone. The pyrido[3,4-*c*]furoxan was synthesized by reacting sodium azide with 2-chloro-3-nitro-pyridine to form 8-nitro-tetrazolo[1,5-a]pyridine[75]. The 8-nitro-tetrazolo[1,5-a]pyridine was heated in toluene, causing the loss of nitrogen gas and the ring closure of the resulting nitrene, to produce pyrido[2,3-*c*]furoxan[75]. The pyrido[3,4-*c*]furoxan was then reacted with *C*-phenyl-*N*-phenylnitrone to yield the radical precursor, 2-phenyl-4-azabenzimidazole 1-oxyl-3-oxide. Oxidation of the precursor to the radical was accomplished in benzene with lead (IV) oxide as the oxidant (Scheme 4.2).

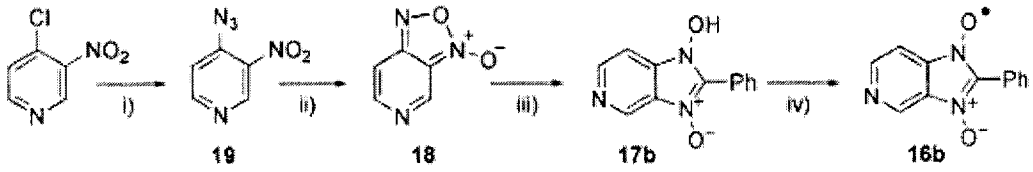

Scheme 4.2 - Synthesis of P2PNN

Reagents and conditions: i) HCl, NaN_3, 55.0% ii) Δ, toluene, 93.3% iii) *C*-phenyl-*N*-phenylnitrone, benzene, Δ, 79.9% iv) PbO_2, benzene

P2PNN was stable in solution for long periods of time in non-polar solvents, similar to the **PBNN** radical. Unfortunately, like the **P3PNN** derivative, the radical decomposed when the solvent was evaporated, and the resulting brown solid, when redissolved in solvent, was not green/yellow in color and was EPR-silent. The nature of the decomposition product was not determined.

4.2.3 - Synthesis of 2-phenylimidazo[4,5-b]quinoxaline nitronyl nitroxide (PQNN).

The synthesis of 2-phenylimidazo[4,5-b]quinoxaline nitronyl nitroxide started with 1,2-diaminobenzene and 1,2-dichloroglyoxime. 1,2-Dichloroglyoxime was generated by reacting glyoxal with hydroxylamine followed by the chlorination of glyoxime with N-chlorosuccinimide. The 1,2-dichlorogyloxime was then dehydrohaloginated with triethylamine to form dinitrile oxide and triethylamine chloride salt. The in-situ generated dinitrile oxide reacted with 1,2-diaminobenzene to form bishydroxyiminoquinoxaline. The bishydroxyiminoquinoxaline was then oxidized to furoxanoquinoxaline with nitric acid. The furoxanoquinoxaline was condensed with *C*-phenyl-*N*-phenylnitrone in benzene to give the radical precursor 2-phenylimidazo[4,5-

b]quinoxaline 1-oxide-3-oxyl. The radical was generated by oxidation of the precursor in benzene with lead (IV) oxide. (See Scheme 4.3.)

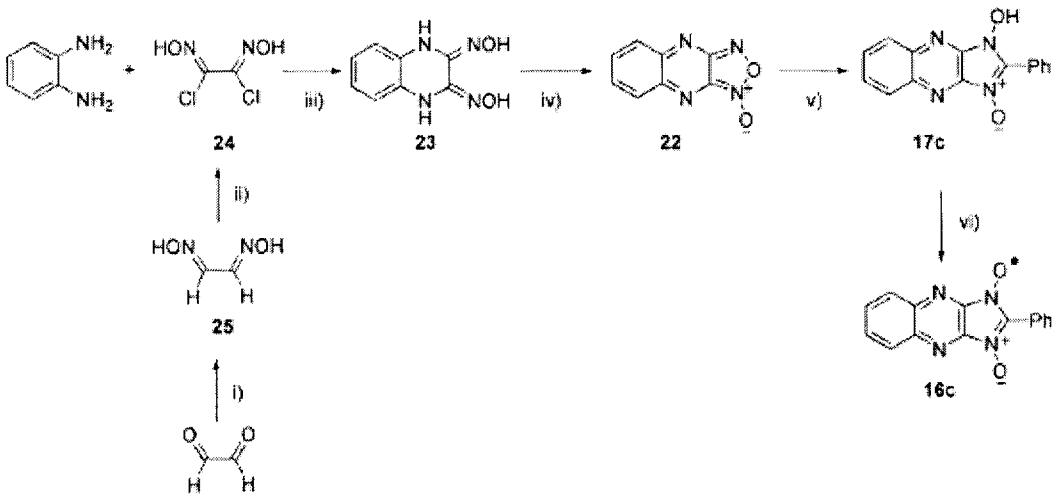

Scheme 4.3 - Synthesis of PQNN

Reagents and conditions: i) NH_3OHCl, KOH, H_2O, 78.4% ii) NCS, DMF, 84.8 % iii) Et_3N, MeOH, 60.4 % iv) HNO_3, DCM, 62.4% v) *C*-phenyl-*N*-phenylnitrone, benzene, Δ, 53.9% vi) PbO_2, benzene

The **PQNN** radical is the first example in the scientific literature of an extended aromatic nitronyl nitroxide with an annelated aromatic system larger than benzimidazole that is stable at RT and exposed to oxygen. The radical was a brilliant red color, strikingly different from the **PBNN** radical. The radical decayed slowly in solution over 12 hours in non-polar solvents. The radical was not stable in the solid state, and after the solvent is removed, the radical decomposed. EPR of the yellow decomposition product showed no signal. UV-Vis spectrum of the decomposition mixture showed a loss of all characteristic absorptions.

4.2.4 - UV-Vis Spectroscopy of P2PNN, P3PNN, and PQNN.

The UV/Vis absorption spectra for **P2PNN**, **P3PNN** and **PQNN** were measured in acetonitrile (Figure 4.3). None of the radicals were stable in the solid state, so measuring the molar extinction coefficients for this set of radicals was estimated roughly by assuming 50% oxidation of the imidazole 1-oxyl-3-oxide precursors to nitronyl nitroxide with corrections due to dilutions. The **P3PNN** and **P2PNN** shared the bright green/yellow color of the parent **PBNN**. However, the **PQNN** radical was bright red in color, and had a distinctly different absorption spectrum. They all shared a weak absorption in the near IR, which appeared to be a consequence of annelation since it was present in all BNN and **PQNN** radicals but not in the **TMNN** radicals (Table 4.1).

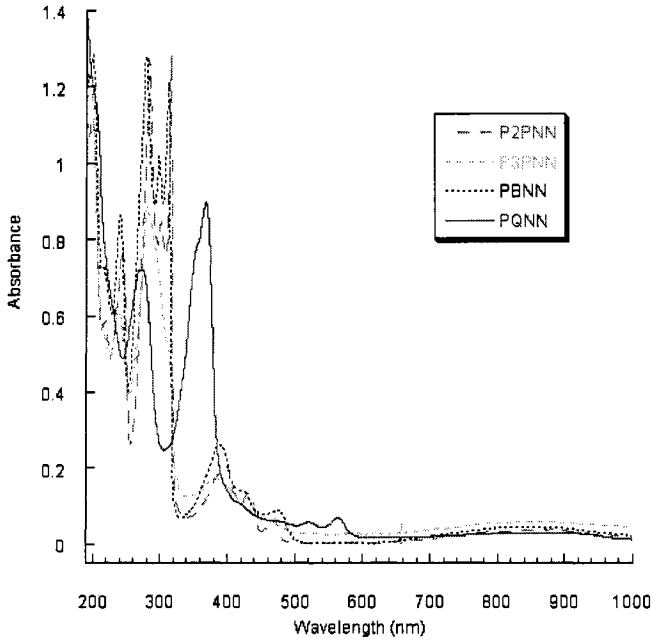

Figure 4.3 - UV-Vis of P2PNN, P3PNN and PQNN versus PBNN in acetonitrile

Table 4-1 - UV-Vis λ_{max}(nm) with estimate extinction coefficients (ε) for P2PNN, P3PNN and PQNN versus PBNN in acetonitrile.

	Short UV	Long UV	Visible	Near IR
PBNN	200 (21200)	279 (23000)	388 (6480)	825 (1280)
	241 (16500)	298 (18800)	421 (4320)	
		312 (22300)	475 (3220)	
P2PNN	243 (10000)	283 (20000)	400 (3000)	886 (600)
		301 (10000)	431 (2000)	
		315 (20000)	471 (1000)	
P3PNN	239 (10000)	281 (10000)	381 (3000)	861 (1000)
			430 (2000)	
PQNN	274 (10000)	368 (20000)	564 (1000)	

Since the change from benzimidazole to 4- and 5-azabenzimidazole represented a small change in overall structure, it was expected that the UV-Vis spectrum of both **P2PNN** and **P3PNN** would be similar to **PBNN**. This was the case for **P2PNN**, with the long-UV having the distinct three absorptions at 283, 301, and 315 nm, the visible having the same three absorptions at 400, 431, and 471 nm, and the near-IR having the similar broad weak absorption at 886 nm (Table 4.1).

P3PNN was distinctly different from the parent **PBNN**. The spectrum of **P3PNN** in acetonitrile missed the definition of the three near-UV λ_{max} absorption bands of **PBNN** at 279, 298, and 312 nm. Instead, there was an unresolved single absorption at 281 nm. The absorption in the visible range was also different from **PBNN**, with the **P3PNN** radical exhibiting two unresolved absorption bands at 381 and 430 nm, instead of three λ_{max} at 388, 421, and 475 nm for **PBNN**. The change may be due to nitrogen at this position in **P3PNN** affecting the vibrational energy levels of this electronic absorption, leading to more closely spaced

vibrational levels and lower resolution of each individual peak absorbance. The other possibility considered was that the transitions were closer in energy, resulting in an overlap of transitions.

The **PQNN** radical had a completely different absorption spectrum, showing that the annelation of the quinoxaline aromatic groups radically changed the electronic structure of the molecule. The absorption of **PQNN** in the visible region at λ_{max} = 564 nm was significantly weaker than the absorption band at 388, 421, and 475 nm of the **PBNN** radical and was red shifted compared to **PBNN**. The weak transition at 880 nm present in **PBNN** in the near IR was found to be extremely weak in the **PQNN** radical. The strength of this absorption does not increase with larger conjugation, like the change from **TMNN** to **PBNN**.

4.2.5 - EPR Spectroscopy of P2PNN, P3PNN, and PQNN.

The EPR of the radicals **P2PNN**, **P3PNN**, and **PQNN** were measured in degassed benzene by the same method as **PBNN**. Consistent with the benzimidazole nitronyl nitroxide radicals, the spectra showed the 5-line signal in a 1:2:3:2:1 pattern consistent with the coupling to two equivalent nitrogen atoms. Calculations using DFT B3LYP/6-31G* were used to help in the assignment of the hfccs to the corresponding nuclei on the radicals (Figures 4.4 through 4.6 and Table 4.2).

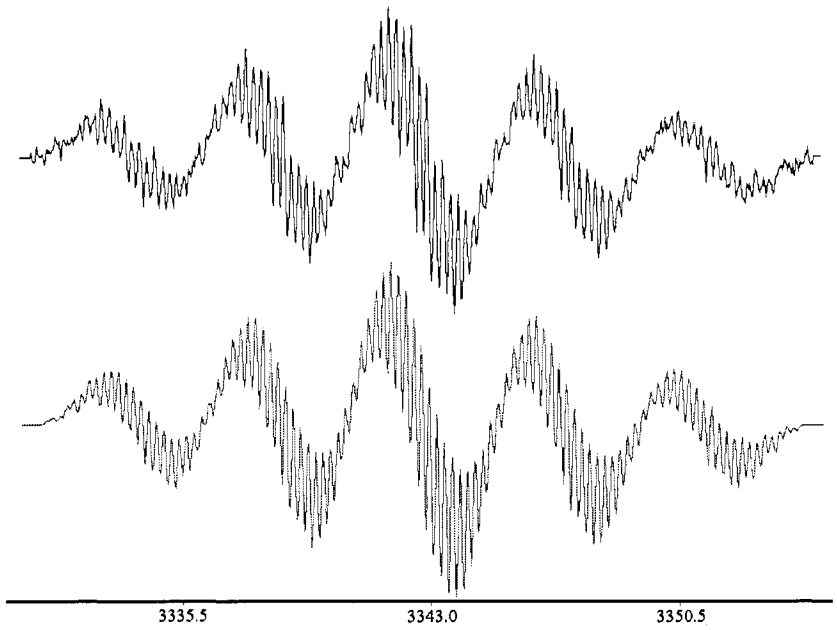

Figure 4.4 - EPR of P2PNN in degassed benzene (top = experimental: bottom = simulated) at RT and ~10-5 M.

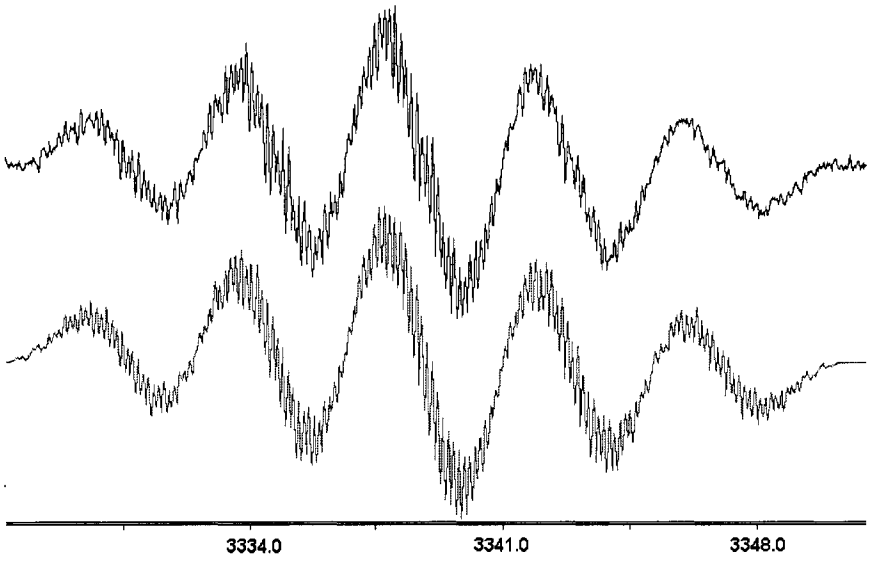

Figure 4.5 - EPR of P3PNN in degassed benzene (top = experimental: bottom = simulated) at RT and ~10^{-5} M.

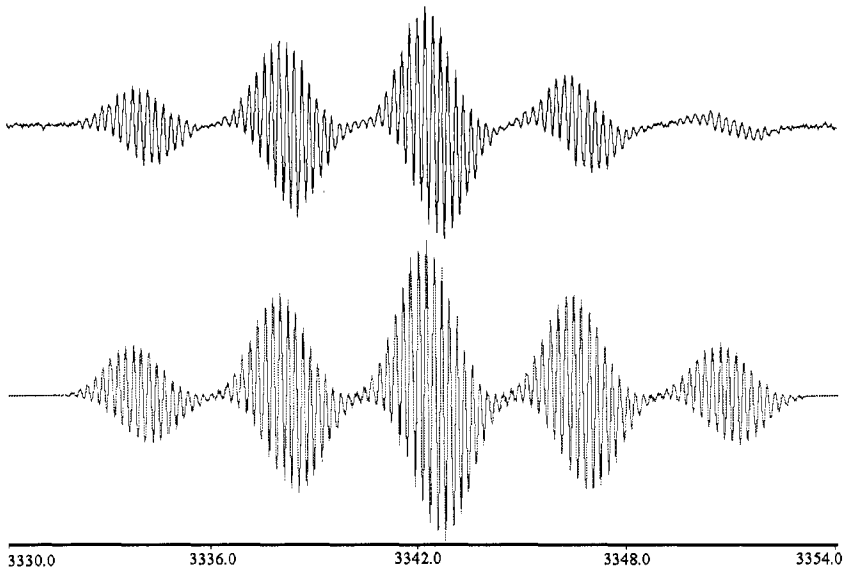

Figure 4.6 - EPR of PQNN in degassed benzene (top = experimental: bottom = simulated) at RT and ~10^{-5} M.

Table 4-2 - Hyperfine coupling constants for P2PNN, P3PNN, and PQNN versus PBNN

atom	PBNN	P2PNN	P3PNN	PQNN
N(1)	4.370	4.139	3.990	4.232
N(2)		4.367	4.150	
H_α	0.930	0.725	0.850	0.407
H_β	0.650	0.848	0.906	0.247
H'		0.694	0.703	
N'		0.792	0.725	0.440
H_o	0.490	0.440	0.419	0.471
H_m	0.220	0.201	0.145	0.190
H_p	0.410	0.392	0.447	0.468

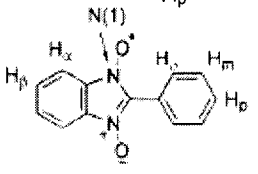

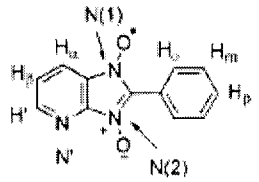

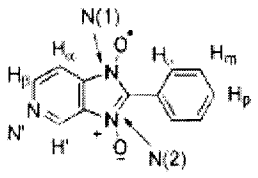

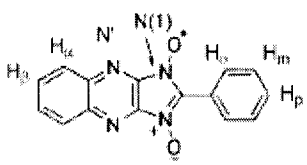

The hyperfine coupling constants on the C2-position phenyl ring did not change with the inclusion of nitrogen in the benzimidazole moiety for **P2PNN**, **P3PNN**, and **PQNN**. The spin density distributions were the same for the series, with average spin densities of 0.443, 0.179 and 0.436 for the ortho, meta and para positions. Extending the conjugated aromatic system attached to the nitronyl nitroxide from a benzimidazole/azabenzimidazole ring to a polycyclic imidazoquinoxaline moiety did not change the hfcc on the 2-position phenyl group. This was consistent with the SOMO being isolated on the benzimidazole and spin polarization being the primary pathway for spin density distribution on the 2-phenyl ring.

In the case of azabenzimidazole radicals **P2PNN** and **P3PNN**, the heteroatom substitution had a noticeable effect on the spin densities of the nitronyl nitroxide portion of the molecule. The substitution of a heteroatom into the benzene ring of BNN de-symmetrized the structure, which was revealed in the non-equivalent spin densities at the positions N(1) and N(2) of the nitronyl nitroxide. It was therefore necessary to include distinct coupling parameters for each nitrogen of the ONCNO moiety when fitting the spectrum.

The position of the nitrogen, whether in the alpha or beta position, had a great effect on the spin densities at N(1) and N(2). **P3PNN** had a distinctly lower hfcc for N(1) and N(2) at 3.990 G and 4.150 G. Since it was impossible to know which nitrogen corresponds to which hyperfine without using isotropic labeling, calculations were used to help assign the hyperfines. The low hfcc to N(1)/N(2) in **P2PNN** and **P3PNN** showed the consequence of the electronegativity difference

from carbon to nitrogen. The nitrogen inductive effects decreased the unpaired electron density on the nitrogen of the ONCNO moiety.

The heteroatom substitution had a much greater effect on the hyperfines on the benzimidazole annelated ring of the molecule for **P2PNN** and **P3PNN** than the hyperfines on the C2-position phenyl ring. The incorporated nitrogen N' changed the relative spin distribution on the carbons of the annelated ring. In **PBNN** there were two sets of two equivalent protons (H_α and H_β) with 0.930 G and 0.650 G coupling constants. The nitrogen addition in **P2PNN** and **P3PNN** disrupted this symmetry, and there were four individual hffcs for N', H', H_α, and H_β. The values for these hfccs were averaged over the entire ring. **P2PNN** had four distinct hyperfines associated with the protons on the ring, with N' = 0.792 G, H' = 0.694 G, H_α = 0.725 G, and H_β = 0.848 G. These four values were lower than the maximum hyperfine of 0.930 G for H_α but they were all higher than the minimum hyperfine of 0.650 G of H_β. The presence of the nitrogen perturbed the SOMO of the radical, causing an overall averaging of the radical density around the ring.

The extension of the extended aromatic system produced distinct changes for the hfcc for **PQNN** versus **PBNN**. As the only current example of an extended nitronyl nitroxide that was stable enough to determine superhyperfine coupling constants, **PQNN** demonstrated what happened when the aromatic system was extended to include polycyclic aromatic systems. Surprisingly, the hfcc associated with the nitrogen in the nitronyl nitroxide N(1) for **PQNN** (4.232 G) were lower than the **PBNN** (4.370 G) but not by a large amount, with a decrease of 0.138 G.

The hfcc of N'= 0.440 on the first 6-membered aromatic system were 0.4 G less than the corresponding position H_α = 0.930 G in **PBNN** (a decrease of 52.6%) or N'= 0.792 G in **P2PNN** (a decrease of 44.4%). This suggested that the spin distribution on the second ring in **PQNN** (ring with H_α and H_β) came at the expense of spin density on the diaza central ring and not the nitronyl nitroxide nitrogen. This also suggested that there was an inherent limit to the amount of unpaired spin density that could delocalize to the annelated polycyclic aromatic rings. The limit was most likely tied to the topology of the molecular orbital, which described the primary pathway for electron distribution.

In terms of chemical stability, having a more delocalized aromatic system withdrew unpaired electron density away from the electronegative atoms within the ONCNO moiety and served to destabilize the radical, such as was seen in the pyrene and phenanthrene hydrocarbon-based nitronyl nitroxide. The **PQNN** radical defied this trend by providing additional delocalization and including electronegative atoms that stabilized the unpaired electron density.

4.2.6 - Computational Spin Densities of P2PNN, P3PNN, and PQNN.

As with the 2-position aromatic benzimidazole nitronyl nitroxides, calculations using the UB3LYP/6-31G* were performed to help assign experimental EPR hfccs to atomic spin density on the molecule and to evaluate the effectiveness of computational analytical methods at predicting spin populations. Hfccs were converted to spin densities using McConnell equation[35] with Q_{CH}^{H} = 23.7 G and Q_N^N = 25 G, with the spin density (ρ_r) on the attached carbon related to the hfcc on the bonded hydrogen (a_H) by $Q * \rho_r = a_H$. Table 4.3

identifies how accurate the B3LYP/6-31G* level of theory was at estimating the spin populations for this class of compounds (Figures 4.7 through 4.9).

As stated in Chapter 2, the calculations overestimated the spin density on the phenyl ring, and the alternation of the sign of the spin showed that spin polarization was the primary pathway for spin density distribution in the phenyl ring substituent at C2. The calculations did an adequate job of predicting the spin density on the benzimidazole ring, but still underestimated the distribution into the benzimidazole by predicting overall low values on the annelated ring.

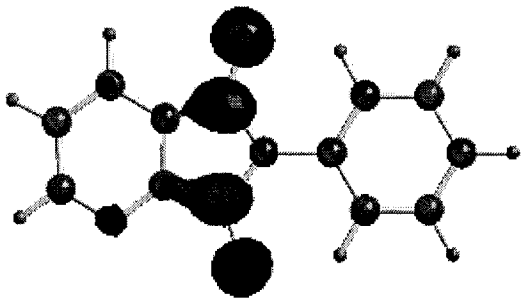

Figure 4.7 - Calculated SOMO of P2PNN generated at B3LYP/6-31G* with CubGen (isocontour = 40, scaling factor = 0.18) and visualized with Chem3D

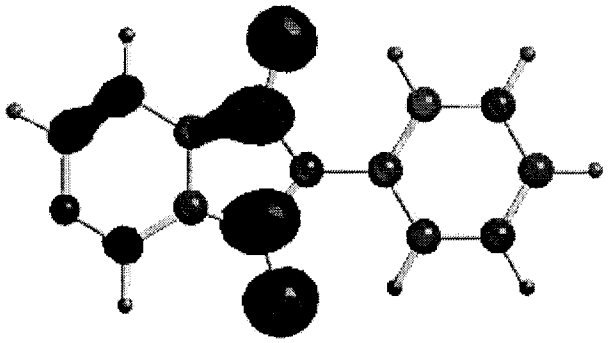

Figure 4.8 - Calculated SOMO of P3PNN generated at B3LYP/6-31G* with CubGen (isocontour = 40, scaling factor = 0.18) and visualized with Chem3D

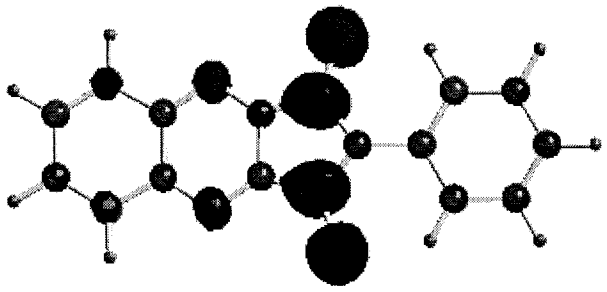

Figure 4.9 - Calculated SOMO of PQNN generated at B3LYP/6-31G* with CubGen (isocontour = 40, scaling factor = 0.18) and visualized with Chem3D

Table 4-3 - Comparison of calculated and simulated spin densities

	PBNN		**P2PNN**		**P3PNN**		**PQNN**	
	calc.	*EPR*	calc.	*EPR*	calc.	*EPR*	calc.	*EPR*
N (1)	0.1839	*0.175*	0.1742	*0.166*	0.1740	*0.160*	0.1784	*0.169*
N (2)			0.1752	*0.175*	0.1776	*0.166*		
C_α	0.0332	*0.039*	0.0202	*0.031*	0.0293	*0.036*	0.0101	*0.017*
C_β	0.0237	*0.027*	0.0269	*0.036*	0.0386	*0.038*	0.0078	*0.010*
C'			0.0149	*0.029*	0.0245	*0.030*		
N'			0.0245	*0.032*	0.0147	*0.029*	0.0394	*0.018*
C_o	-0.0456	*0.021*	-0.0470	*0.019*	-0.0462	*0.018*	-0.0510	*0.020*
C_m	0.0246	*0.009*	0.0255	*0.008*	0.0251	*0.006*	0.0277	*0.008*
C_p	-0.0448	*0.017*	-0.0462	*0.017*	-0.0456	*0.019*	-0.0513	*0.020*

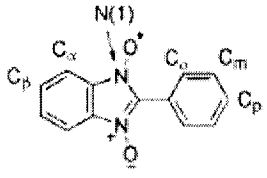

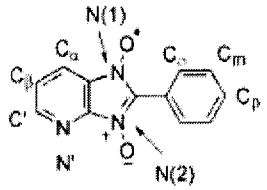

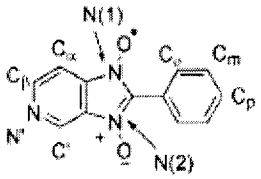

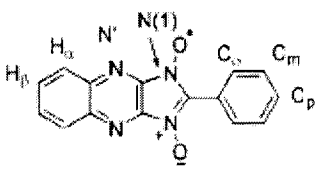

The calculated spin densities for the C2-position phenyl group were a factor of two larger than the experimental values for **PBNN**, **P2PNN**, **P3PNN**, and **PQNN**. For example, while theory predicted the C_o for **P2PNN**, **P3PNN**, and **PQNN** to be -0.0470, -0.0462, and -0.0510 respectively, those values were found experimentally to be 0.019, 0.018, and 0.020. The spin densities at N(1) for **P2PNN** and **P3PNN** were predicted to be 0.174 and 0.178 by theory, but were determined experimentally to be smaller at 0.166 and 0.160. Spin densities at N', C', C_α and C_β for **P2PNN** and **P3PNN** were calculated to be lower than those found experimentally. The calculations predicted the N' for **P2PNN** and **P3PNN** to be 0.0245, and 0.0147 respectively, while those values were found experimentally to be 0.032 and 0.029.

The calculations did poorly at predicting the asymmetry induced by the inclusion of nitrogen in **P2PNN** and **P3PNN** and the amount of spin density on the nitrogen of **PQNN**. As the calculations performed adequately, proving to be useful for helping interpret experimental results, clearly EPR (sign of the spin and SOMO estimations) cannot be relied upon solely to predict the electron spin distributions.

Section 4.3 - Conclusion.

The synthesis of 2-phenylimidazo[4,5-b]quinoxaline nitronyl nitroxide (**PQNN**), 2-phenyl-4-azabenzimidazole nitronyl nitroxide (**P2PNN**), and 2-phenyl-5-azabenzimidazole nitronyl nitroxide (**P3PNN**) presented the first reported case of heteroaromatic benzimidazole nitronyl nitroxide with nitrogen incorporated into the annelated moiety of the radical. Calculations with

B3LYP/6-31G* were found to estimate the spin distribution in the molecule and provided a useful way of assigning the hyperfine coupling constants. Spin distributions and electronic structure for **P2PNN** and **P3PNN** were similar to **PBNN**. **PQNN** was found to have a radically different electronic structure, and electron delocalization to the second polyaromatic ring was determined to be present but limited. The new radicals present a new potential structural motif for radical-transition metal complexes for developing inorganic-organic magnetic materials, if the problem of chemical stability could be solved.

Section 4.4 - Experimental.

4-azo,3-nitropyridine (19).[76] A solution of 4-chloro,3-nitropyridine (0.4744 g, 0.003 mol) in 1.5 mL of DMSO was prepared. To this solution was added NaN_3 (0.230 g, 0.0035 mol). The reaction was sonicated for 5 minutes. The yellow reaction solution was poured into 25 mL of ice water and the cream colored precipitate was collected by filtration with suction and washed with cold water to produce an off-white solid (0.418 g, 84.6%). ^{1}H-NMR (200MHz, $DCCl_3$, δ): 9.17 (s, 1H, Ar-H), 8.77 (d, 1H, J = 5.6 Hz, Ar-H), 7.30 (d, 1H, J = 5.6 Hz, Ar-H).

Pyrido[3,4-*c*]furoxan (18).[77] A solution of 4-azo,3-nitropyridine (0.4495 g, 0.00272mol) in 20 mL of toluene was refluxed for 4 hours. The toluene was evaporated under reduced pressure and the solid was purified by running a silica plug with chloroform. The product was not stable and had to be used immediately to prevent decomposition into a black insoluble solid. ^{1}H-NMR (200MHz, $DCCl_3$,

δ): 9.19 (s, 1H, Ar-H), 8.32 (d, 1H, J = 6.7 Hz, Ar-H), 7.44 (d, 1H, J = 6.7 Hz, Ar-H).

2-phenyl-5-azabenzimidazole 1-oxyl-3-oxide (17b). A solution of 4-azo,3-nitropyridine (0.4905 g, 0.003 mol) in 30 mL of toluene was heated for 4 hours at reflux. After the starting material spot had disappeared by TLC, *C*-phenyl-*N*-phenylnitrone (0.605 g, 0.00306 mol) was added and the solution was refluxed for 20 hours. The solution was filtered with suction, washed with benzene, ethyl acetate, and hexanes, and dried to obtain a brown solid (0.353g, 51.8%). $mp_{(explosive)}$ = 231 °C. ^{1}H-NMR (200MHz, 0.1 M KOH in D_2O, δ): 8.89 (s, 1H, Ar-H), 8.32 (d, 1H, Ar-H), 7.89 (m, 2H, Ar-H), 7.6 (m, 4H, Ar-H). MS (direct probe) m/z: 227 $[M]^+$, 211 $[M-O]^+$, 195 $[M-O_2]^+$. Anal. Calcd for $C_{12}H_9N_3O_2$: C, 63.43; H, 3.99; N, 18.49. Found: C, 63.18; H, 4.03; N, 18.15.

2-phenyl-5-azabenzimidazole nitronyl nitroxide (P3PNN, 16b). Before oxidation, 2-phenyl-5-azabenzimidazole 1-oxyl-3-oxide (0.012 g, ~0.1 mmol) was suspended in 20 mL of benzene. Lead (IV) oxide (~0.5 g) was added to the solution under nitrogen and the solution was stirred for 3 hours. The bright green solution was filtered through a Celite-545 plug, diluted, and degassed with N_2 to prepare EPR samples. UV-Vis (acetonitrile) λ_{max}, nm: 239, 281, 381, 430, 861.

8-Nitro-tetrazolo[1,5-a]pyridine (21).[75] A solution of 2-chloro-3-nitro-pyridine (1.50g, 0.00949 mol) and sodium azide (1.48 g, 0.023 mol) in 130 mL of 9:1

ethanol/water was stirred under nitrogen. To this was added 30 mL of 10% $HCl_{(aq)}$ and the reaction was heated for 24 hours under N_2. The ethanol was removed under reduced pressure and the solid was filtered with suction and washed with water. A crude brown solid was recrystalized with ethanol (~100 mL) to give a brown solid (0.83 g, 55%). mp 173-4 °C (lit.[75] 171-173 °C). ^{1}H-NMR (200MHz, d_6-DMSO, δ): 9.6 (d, 1H, J = 7.0 Hz, Ar-H), 8.9 (d, 1H, J = 7.2 Hz, Ar-H), 7.8 (t, 1H, J = 7.0, 7.2 Hz, Ar-H).

Pyrido[2,3-*c*]furoxan (20).[75] A solution of 8-Nitro-tetrazolo[1,5-a]pyridine (0.5 g, 0.0042 mol) in 50 mL of toluene was refluxed for 6 hours. The toluene was evaporated under reduced pressure and the solid was purified by column chromatography (silica, 97.5/2.5 % DCM/MeOH). A brown solid was obtained (0.423 g (98%). mp 51-2 °C (lit.[75] 52-3 °C). ^{1}H-NMR (200MHz, d_6-DMSO, δ): 8.8 (d, 1H, J= 3.4 Hz, Ar-H), 7.9 (d, 1H, J= 8.4 Hz, Ar-H), 7.3 (dd, 1H, J= 3.4, 8.4 Hz Ar-H). MS (electrospray, positive mode): 138.1 [M+1].

2-phenyl-4-azabenzimidazole 1-oxyl-3-oxide (17a). A solution of pyrido[2,3-*c*]furoxan (0.068 g, 0.49mol) and *C*-phenyl-*N*-phenylnitrone (0.108 g, 0.52mmol) in 3 mL of benzene was refluxed under N_2 for 16 hours. The solution was filtered with suction, washed with benzene and hexanes, and dried under vacuum to obtain a bright yellow solid (0.089 g, 79.9%). $mp_{(explosive)}$ = 183-4 °C. ^{1}H-NMR (200MHz, 0.1 M KOH in D_2O, δ): 8.4 (broad s, 1H, Ar-H), 8.1 (broad s, 1H, Ar-H), 7.9 (m, 2H, Ar-H), 7.6 (m, 3H, Ar-H), 7.4 (broad s, 1H, Ar-H). MS (direct

probe) m/z: 227 $[M]^+$, 211 $[M\text{-}O]^+$, 195 $[M\text{-}O_2]^+$. Anal. Calcd for $C_{12}H_9N_3O_2$: C, 63.43; H, 3.99; N, 18.49. Found: C, 63.02; H, 4.28; N, 18.44.

2-phenyl-4-azabenzimidazole nitronyl nitroxide (P2PNN, 16a). Before oxidation, 2-phenyl-4-azabenzimidazole 1-oxyl-3-oxide (0.010 g, ~0.1 mmol) was suspended in 20 mL of benzene. Lead (IV) oxide (~0.5 g) was added to the solution under nitrogen and the solution was stirred for 3 hours. The bright green solution was filtered through a Celite-545 plug, diluted, and degassed with N_2 to prepare EPR samples. UV-Vis (acetonitrile) λ_{max}, nm: 243, 283, 301, 315, 400, 431, 471, 886.

Glyoxime (25).[78] A solution of glyoxal (13.4 mL, 16.9 g, 0.117 mol) and hydroxylamine hydrochloride (16.24 g, 0.234 mol) in 15 mL of distilled H_2O was stirred at 5 °C while 12 M KOH_{aq} (20 mL, 0.234 mol) was added slowly over 20 minutes. After 10 minutes at 5 °C, the solution was heated to 90 °C. The heat source was removed, stirring was stopped, and the solution was cooled slowly to RT overnight. After 12 hours, white plate crystals had formed and were filtered with suction, washed with 20 mL of H_2O and 150 mL of hexanes, and dried under vacuum to give clear white crystals (8.08 g, 78.4%). mp 178-80 °C (lit. [78] 178 °C). ^{1}H-NMR (200MHz, D_2O, δ): 11.9 (broad s, 2H, NOH), 7.02 (s, 2H, C-H(oxime)). IR (KBr pellet, cm^{-1}): 3440 (s, OH(oxime)), 1586 (s, C=N(oxime)).

Dichloroglyoxime (24). Glyoxime (4.997 g, 0.056 mol) was dissolved in 80 mL of DMF and N-chlorosuccinimide (15.5 g, 0.155 mol) was added slowly over 2 hours so the temperature did not exceed 35 °C. The solution was then poured into 700 mL of ice water. A flaky solid precipitate was filtered with suction. The solid was washed with water and hexanes, dried under vacuum, and weighed (7.55 g, 84.8 %). ^{1}H-NMR (200MHz, d_6-DMSO, δ): 13.1 (s, =NOH). MS (direct probe) m/z: 156 $[M]^+$, 139 $[M\text{-}OH]^+$, 121 $[M\text{-}Cl]^+$.

Bishydroxyiminoquinoxaline (23). A suspension of 1,2-diaminobenzene (4.997 g, 0.0462 mol) and 1,2-dichloroglyoxime (7.55 g, 0.0481 mol) was dissolved in 12 mL of MeOH. The reaction was cooled to 0 °C. Triethylamine (16 mL, 0.111 mol) in 60 mL of MeOH was added dropwise over 40 minutes. The reaction went from cloudy white to clear green. The solvent was evaporated under reduced pressure and 50 mL of water was added. The solution was sonicated and a yellow/light green solid was filtered with suction, washed with water and DCM, and dried overnight under vacuum to give a yellow solid (5.36 g, 60.4 %). mp 240-2 °C (lit.[77] 238-240 °C). ^{1}H-NMR (200MHz, *d6*-DMSO, δ): 10.2 (s, 2H, N-H), 9.5 (s, 2H, NOH) 7.17 (dd, 2H, J = 3.4, 5.8 Hz, Ar-H), 6.75 (dd, 2H, J = 3.4, 5.8 Hz, Ar-H).

Furoxanoquinoxaline (22).[79] Bishydroxyiminoquinoxaline (1.996 g, 0.0104 mol) was suspended in 100 mL of DCM. To this was added 2.0 mL of concentrated nitric acid dropwise at RT. After 10 minutes of stirring, the solvent

was evaporated under reduced pressure and purified by column chromatography (silica, 100% $MeCl_2$) to give a bright red crystalline solid (1.24 g, 62.4%). mp 160 °C (lit.[79] 161-2 °C). ^{1}H-NMR (200MHz, $DCCl_3$, δ): 7.95 (dd, 2H, J = 2.4, 5.8 Hz, Ar-H), 7.77 (dd, 2H, J = 2.4, 5.8 Hz, Ar-H).

2-phenylimidazo[4,5-b]quinoxaline 1-oxide-3-oxyl (17c). A solution of furoxanoquinoxaline (0.094 g, 0.5 mmol) in 5 mL of benzene was stirred while *C*-phenyl-*N*-phenylnitrone (0.1057 g, 0.56 mmol) was added. The solution immediately turned orange. After 5 minutes, the precipitate was filtered with suction, washed with benzene and hexanes, and dried to give bright orange solid (0.075 g, 53.9%). $mp_{(explosive)}$ = 197 °C. ^{1}H-NMR (200MHz, d6-DMSO, δ): 12.7 (broad singlet, 1H, -NOH), 8.48 (dd, 2H, J = Hz, Ar-H), 8.19 (dd, 2H, J = Hz, Ar-H), 7.80(m, 5H, Ar-H). MS (direct probe) m/z: 278 $[M]^+$, 262 $[M-O]^+$, 246 $[M-O_2]^+$, 211$[M-C_6H_5]^+$. HRMS-ESI (m/z): $[M + H]^+$ calcd for $C_{15}H_{11}N_4O_2$, 279.0882; found, 279.0887.

2-phenylimidazo[4,5-b]quinoxaline nitronyl nitroxide (PQNN, 16c). Before oxidation, 2-phenylimidazo[4,5-b]quinoxaline 1-oxide-3-oxyl (0.020 g, ~0.1 mmol) was suspended in 20 mL of benzene. Lead (IV) oxide (~0.8 g) was added to the solution under nitrogen and the solution was stirred for 3 hours. The bright red solution was filtered through a Celite-545 plug, diluted, and degassed with N_2 to prepare EPR samples. UV-Vis (acetonitrile) λ_{max}, nm: 274, 368, 564.

Chapter 5. Investigations into Making Oligomers Based on the Benzimidazole Nitronyl Nitroxide.

Section 5.1 – Introduction

The synthesis of organic-based polyradicals has been a relatively new topic of interest for magnetochemists and polymer scientists. Many groups have tried to produce an organic polyradical with bulk ferromagnetic behavior in the last 20 years. One focus has been the synthesis of pendant polyradicals polymer systems with radicals not incorporated into the conjugated backbone (Figure 5.1).

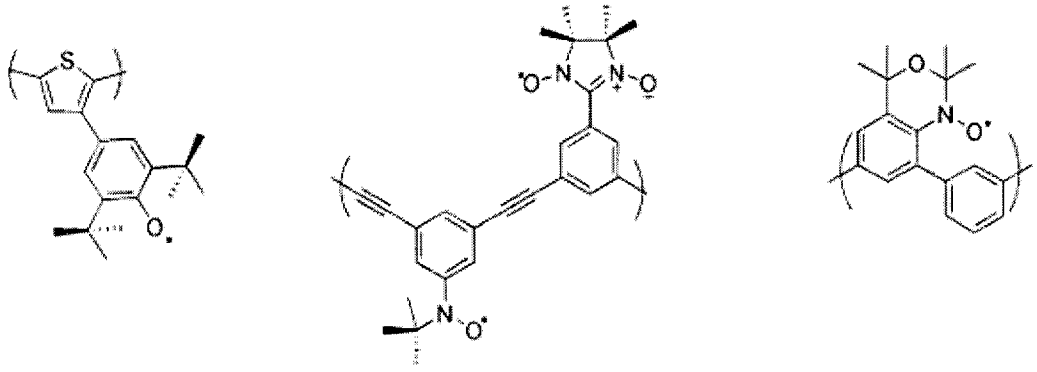

5.1 5.2 5.3

Figure 5.1 - Literature examples of pendant polyradicals

A perfect example of a pendant polyradical includes polythiophene with a phenoxyl pendant radical on the 3-position.[80] A polyradical (**5.1**) based on this structural motif produced a large ferromagnetic exchange of $2J = 73\ cm^{-1}$ using linear three-spin Heisenberg model. Another variation of the pendant polyradical was based on alternating aminoxyl and nitronyl nitroxide with poly(1,3-phenyleneethynylene) as the conjugated polymer. [27] Magnetic exchange in this

system (**5.2**) was extremely weak, with the magnetic susceptibility of the polyradical measured to be -1.5 K using a Curie-Weiss model, consistent with spin polarization between radicals with long (<10 carbons) intermolecular distances.

A polyradical based on pendant aminoxyl radicals on poly-para-phenylene conjugated backbone was synthesized (**5.3**) and found to have a magnetic interaction of -1.1 K using a Curie-Weiss model.[81] The common problem with the pendant polyradical approach was that the dominant pathway for magnetic exchange was superexchange and superexchange drops off exponentially with distance. In addition, all of the radicals had a dihedral angle between the radical and polymer backbone. Most pendant radicals therefore behaved as paramagnets or exhibited low magnetic exchange, but were stable to ambient and common polymerization conditions.

A different polyradical focus has been referred to as dendritic polyradicals, in which the radical is directly incorporated into the conjugated backbone (Figure 5.2).

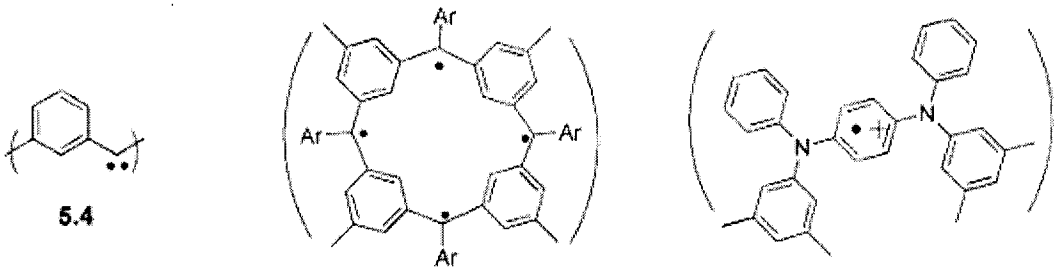

5.4 **5.5** **5.6**

Figure 5.2 - Literature example of dendritic polyradicals

Poly(m-phenylenecarbenes) (**5.4**) have been to shown to have high spin ferromagnetic ground states when studied by EPR at 77K, consistent with the prediction that radicals with meta-substitution patterns on aromatic rings will have ferromagnetic exchange.[82] Unfortunately, carbenes were extremely unstable and the poly(m-phenylenecarbenes) were not stable at ambient temperatures.

Another polyradical that used the same morphology but more stable carbon radicals was the poly(arylmethyl) system (**5.5**) developed by Rajca.[83] The poly(arylmethyl) radical was determined to have a high spin ground state, but only at extremely low temperatures ($T < 2$ K) without the presence of oxygen. In attempts to improve the chemical stability of these dendritic polyradicals, a polyradical composed of para-phenylenediamine (**5.6**) had been synthesized to produce a poly(aminium cation radical).[84]

Chemical oxidation of the amine to the radical cation with $NOPF_6$ yielded a polyradical with a room temperature half life of one week, in solution under nitrogen, that maintained a high spin ground state of $S = 7/2$. These polyradicals showed potential to create high spin ground state materials based on the topology of the radicals, but were extremely unstable and decomposed quickly when exposed to air and room temperature conditions.

A recent development has shown that the idea of organic polyradical with room temperature ferromagnet behavior is possible. A polyaniline doped with TCNQ and heated extensively at 150 °C produced a stable organic polymer with ferri or ferromagnetic exchange with a Curie temperature above 350 K.[85] The exact structure and mechanism of magnetic exchange are being investigated in

this system. However, the polyaniline/TCNQ material was a clear indication that incorporating organic radicals into a conjugated polymer has the potential to develop new ferromagnetic materials that have high magnetic interactions and are tolerance to ambient conditions.

Section 5.2 – Design

A conjugated polymer with 2-phenylbenzimidazole nitronyl nitroxide directly incorporated into the conjugated backbone of the polymer was designed, with the intent to combine the ambient condition stability of pendant polyradicals and the great exchange of dendritic polyradicals. The primary strategy was to create brominated derivatives on the 4-, 5-, 6-, or 7-position of the benzimidazole followed by coupling via trans-metalation polymerization techniques to produce a poly-radical (Scheme 5.1).

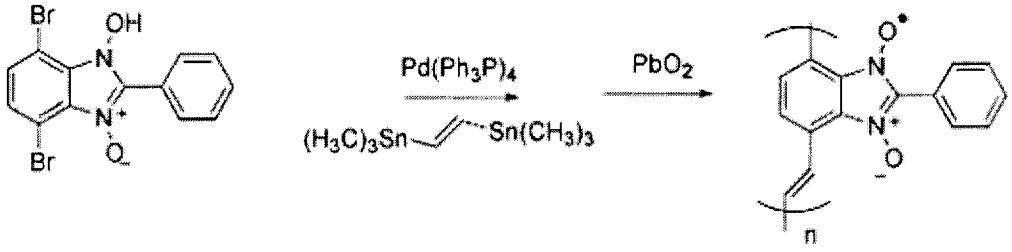

Scheme 5.1 - Example of synthetic strategy for creation of polyradicals based of BNN radicals

This synthetic strategy was chosen for several reasons. The polymer backbone could theoretically be synthesized at any of the intermediate steps before the formation of the benzimidazole 1-oxyl-3-oxide (Scheme 5.2).

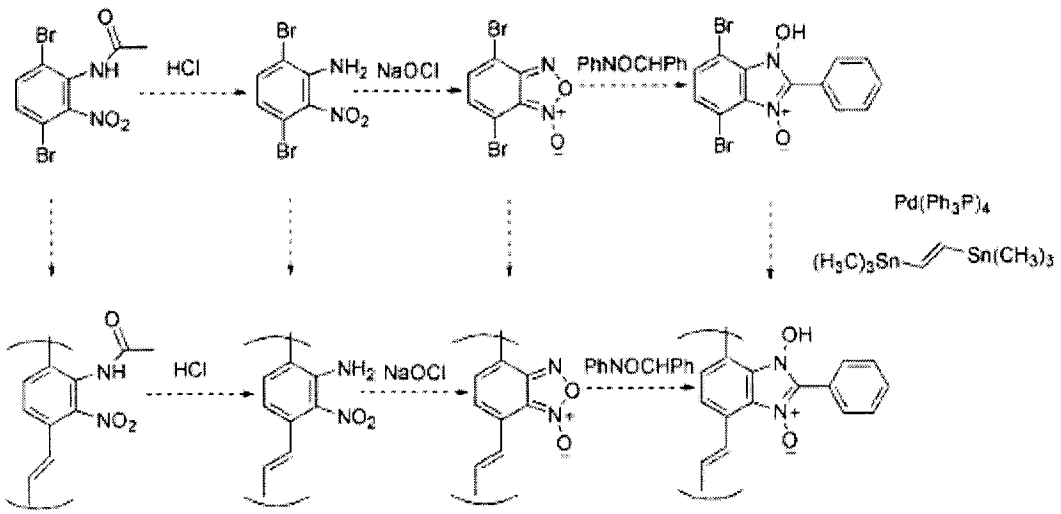

Scheme 5.2 - Possible synthetic pathways for making conjugated polyradicals

There is no precedence in the literature of most of these reactions, although several deoxygenated poly-benzimidazoles have been synthesized using various trans-metal coupling conditions. A poly(aryleneethynlene)(2-(3,5-di-t-butyl-4-hydroxylphenyl)benzimidazole) was prepared by a palladium-catalyzed condensation of 4,7-dibromo-2-(3,5-di-t-butyl-4-hydroxylphenyl)benzimidazole and H-C≡C-Ar- C≡C-H (Ar = p-phenylene, m-phenylene) in DMF with triethylamine and copper iodide.[86] Poly(2-phenylbenzimidazole) was synthesized from 4,7-dibromo-2-phenylbenzimidazole using Ni(0)-COD complex in DMF with 2,2'-dipyridyl and 1,5-cyclooctadiene.[87] Another example was the synthesis of poly[(2-phenylbenzimidazole)-*alt*-thiophene) in which 4,7-dibromo-2-phenylbenzimidazole and 2,5-bis(trimethylstannyl)thiophene were reacted with $Pd(PPh_3)_4$ in DMF.[88] However, it was unknown if the presence of the di-oxygen would change the reactivity of the benzimidazole, and it was known that the solubility of the deoxygenated would be much higher in organic solvents.

Polymerization of the dibromobenzofuroxan was not possible because the 4-bromobenzofuroxan was unstable towards transition metals, with the 4-bromobenzofuroxan being catalytically reduced back to the corresponding nitroaniline. Because more synthetic steps done on the polymer backbone introduce more potential for point defects, the reaction did not go to 100% completion or a side reaction disrupted the intended reaction. The reaction of just the benzofuroxan and nitrone was found to have <60% yield and this did not include the oxidation to the nitronyl nitroxide, which yielded <50%. Polymerization of the radical was also examined, since the **TMNN** was found to be tolerant to $(PPh_3)_2PdCl_2/CuI/Et_3N$ reaction conditions,[27] but determined not to be applicable to the BNN radicals due to the extremely low reduction potentials. Clearly, to make a regioregular polyradical with a low number of defects, the polymerization step should be as close to the oxidation of the benzimidazole as possible.

This chapter will focus on the synthesis and characterization of the brominated 2-phenylbenzimidazole 1-oxyl-3-oxide derivatives and the attempts to make a dimer of the 2-phenylbenzimidazole 1-oxyl-3-oxide. The dimer was never successfully made, primarily failing because of the low solubility of the phenylbenzimidazole 1-oxyl-3-oxide and unforeseen low reactivity of benzofuroxan when groups were in the 4- and 7- position. Several derivatives of the 5-bromo-benzimidazole 1-oxyl-3-oxide were successfully made, but their low solubility prevented any further polymerization reactions. The radicals successfully generated included: 2-4'-*t*-butylphenyl-5-bromobenzimidazole 1-

oxyl-3-oxide (**2q**), 2-4'-hexylphenyl-5-bromobenzimidazole 1-oxyl-3-oxide (**2r**), 2-phenyl-5-bromobenzimidazole 1-oxyl-3-oxide (**2p**), and 2-ethyl-5-bromobenzimidazole 1-oxyl-3-oxide (**2s**) (Figure 5.3).

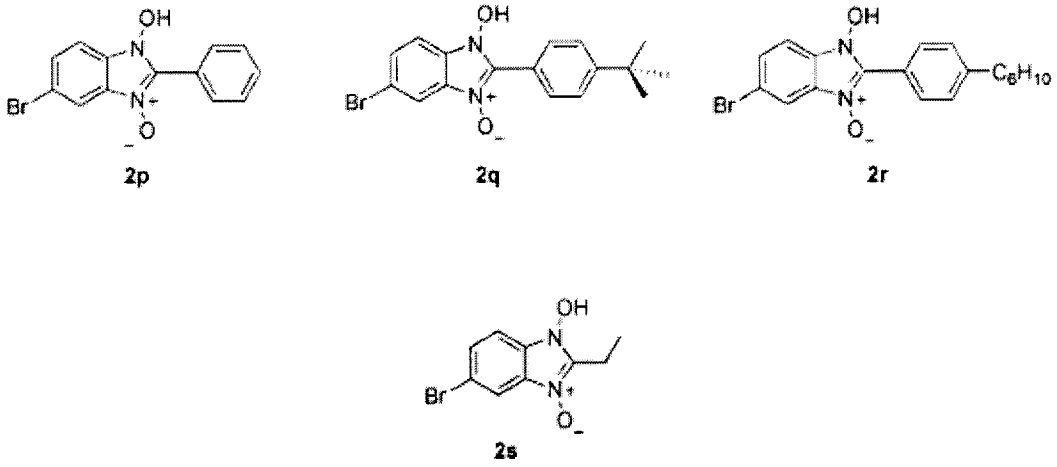

Figure 5.3 - Successfully synthesized brominated benzimidazole 1-oxyl-3-oxide

Section 5.3 - Results and Discussion.

5.3.1 - Attempted preparation of 4-bromo-2-phenylbenzimdazole 1-oxyl-3-oxide.

The synthetic procedures used to make the 2-phenylbenzimidazole 1-oxyl-3-oxide were applied to synthesizing the 2-phenyl-4-bromobenzimidazole 1-oxyl-3-oxide compound. The synthetic methodology used focused on making the 3-bromobenzofuroxan, followed by using the nitrone/furoxan reaction to produce the appropriate 4-bromobenzimdazole 1-oxyl-3-oxide (Scheme 5.3). The 3-bromofuroxan was synthesized from 2-bromoacetanilid, which was nitrated[89] and deprotected to give 2-nitro-6-bromoaniline. The 2-nitro-6-bromoaniline was converted to the 2-nitro-6-bromoazidobenzene with sulfuric acid and sodium

nitrite followed by nucleophilic aromatic substitution with sodium azide. The 2-nitro,6-bromoazidobenzene was heated in toluene, causing the loss of nitrogen gas and ring closure, to yield the ring closure product 6-bromobenzofuroxan (Scheme 5.3).

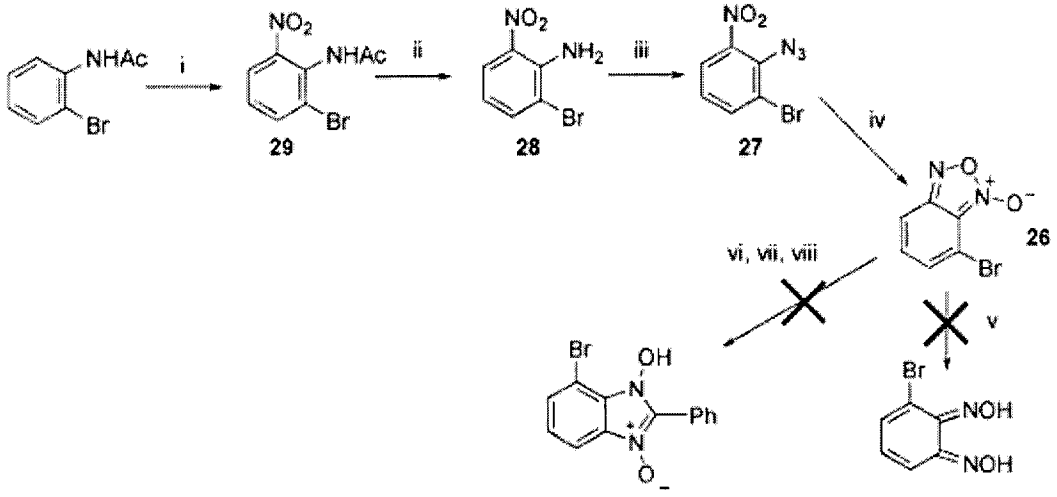

Scheme 5.3 - Attempted synthesis of 4-bromo-2-phenylbenzimidazole 1-oxyl-3-oxide

Reagents and conditions: i) HNO_3, F_3CCO_2H, 25 °C, 60% ii) 4M HCl in EtOH, 4h, 80 °C, 80% iii) $NaNO_2$, NaN_3, AcOH, 0 °C, 95% iv) toluene, Δ, 96.6% v) $CH_3(C_6H_4)SO_2N_2H_3$, NaS_2O_5 or N_2H_2, KOH, EtOH, vi) *C*-phenyl-*N*-phenylnitrone, benzene, 75 °C vii) $PhCH_2NO_2$, Et_3N, Δ viii) *C*-4-hexylphenyl-*N*-phenylnitrone, benzene, 75 °C

The bromo group dramatically changed the reactivity of the furoxan and prevented successful coupling. Attempts to couple the 4-bromobenzofuroxan with various nitrones were not successful. Furthermore, the furoxan was resistant to normal reduction conditions such as heating in the presence of N_2H_2 or NaS_2O_5. Benzofuroxan is normally quickly reduced to benzo-1,2-dioxime under these conditions but the 4-bromobenzofuroxan was resistant to these conditions

and did not reduce. This method of generating the 4-bromo-2-phenylbenzimidazole derivative was not successful.

5.3.2 - Attempted preparation of the radical precursor with bromine on the 4- and 7-position of 2-phenylbenzimdazole 1-oxyl-3-oxide.

In addition to the 4-position benzimidazole, attempts were made to synthesize a 4,7-position dibromobenzimidazole derivative that could be used in making extended polymer systems. The 4,7-dibromofuroxan was synthesized from benzofuroxan (Scheme 5.4). Benzofuroxan was fully brominated with Br_2 in carbon tetrachloride. This reaction was monitored by ^{1}H-NMR until the reaction had gone to completion. The reaction was columned on basic alumina to cause the double E_2 dehydrobromination to reform the correct 4,7-dibromofuroxan isomer.

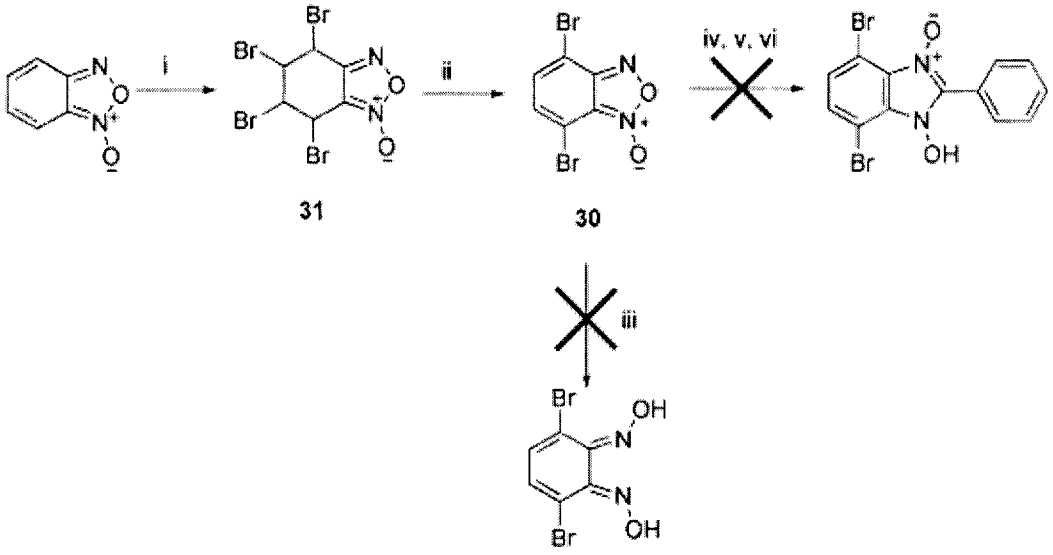

Scheme 5.4 - Attempted synthesis of 4,7-dibromo-2-phenylbenzimidazole 1-oxyl-3-oxide

Reagents and conditions: i) 4eq. Br_2, CCl_4, Δ ii) Alumina column, 67.1% iii) $Na_2S_2O_4$, EtOH, Δ, 0% iv) PhNOCHPh, diglyme, 140 °C v) PhNOCHPh, benzene, 80 °C vi) 1-nitropropane, diethylamine, THF, RT

Again, as with the 4-bromobenzofuroxan, the dibromo functionality dramatically changed the reactivity of the furoxan and prevented successful coupling. Attempts to couple the 4,7-dibromobenzofuroxan with various nitrones were not successful. The furoxan was even resistant to normal reduction conditions. This method of generating the 4,7-dibromo-2-phenylbenzimidazole 1-oxyl-3-oxide derivative was not successful.

The lack of reactivity of the 4-bromobenzofuroxan and 4,7-dibromofuroxan can be rationalized by looking at the isomerization of the furoxan in solution, depending on the substitution at the 4,7-position. The furoxan functional group was constantly going though a dynamic rearrangement in solution in which the furoxan ring opened to form a dinitroso and then reformed the furoxan (Figure 5.4).

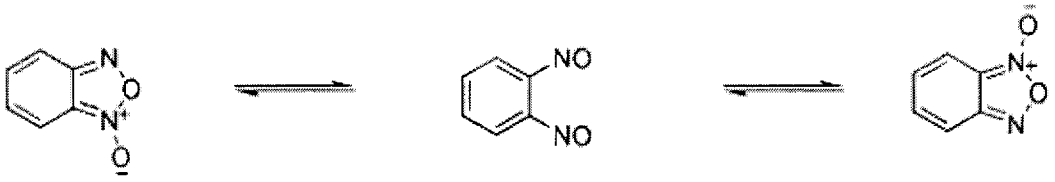

Figure 5.4 - Dynamic isomerization of benzofuroxan

This phenomenon has been studied extensively in the literature, and the rate of this rapid process can be measured using varied temperature ^{1}H-NMR. The rates of isomerization of 4,7-dibromobenzofuroxan (1.7×10^2 sec^{-1} at 30 °C) and 4,7-dichlorobenzofuroxan (2.2×10^2 sec^{-1} at 30 °C) were 20 to 30 times slower than

the isomerization rate of the 5,6-dichlorobenzofuroxan (5.3×10^3 sec^{-1} at 30 °C).[90] The size of the functional group directly impacted the rate, with the larger bromine atoms reducing the rate more than chlorine. Thus, reactions involving a ring opening mechanism of the furoxan would be greatly prohibited due to the steric contributions of the functional groups at the 4,7-position. The nucleophilic addition of nitrone to benzofuroxan involved a ring opening step, and experimentally, it was found not to work with the 4-bromobenzofuroxan and 4,7-dibromofuroxan. Not surprisingly, there was no literature precedence for a benzofuroxan with a functional group at the 4,7-position reacting with a nucleophile, while there was ample precedence for similar reactions with unsubstituted benzofuroxan.

5.3.3 - Preparation of 5-bromo-2-phenylbenzimidazole 1-oxyl-3-oxide.

After the attempts at functionalizing the radical precursors at the 4-position failed due to steric problems, the focus of making the dimer shifted to the 5- and 6- position. (Scheme 5.5) The steric problems found in the 4-position were not expected to be an issue since the 5- and 6- positions were further removed from the reactive furoxan.

The 4-bromobenzofuroxan was synthesized from 4-bromoaniline. 4-Bromoanline was protected with acetyl chloride to make 4-bromoacetanilide. 4-Bromoacetanilide was nitrated and then deprotected to give 2-nitro-4-bromoaniline[91]. 2-Nitro-4-bromoaniline was oxidized with aqueous sodium hypochlorite to yield 4-bromobenzofuroxan[92]. The 4-bromobenzofuroxan had similar reactivity of the benzofuroxan. 4-Bromobenzofuroxan was reduced to 4-

bromobenzodioxime and then reacted with 4-t-butylbenzaldehyde in the presence of acid to yield 2-4'-*t*-butylphenyl-5-bromobenzimidazole 1-oxyl-3-oxide. The 4-bromobenzofuroxan reacts predictably with nitrone derivatives to yield 2-4'-hexylphenyl-5-bromobenzimidazole 1-oxyl-3-oxide and 2-phenyl-5-bromobenzimidazole 1-oxyl-3-oxide, and it reacts with 1-nitropropane and diethylamine to produce the alkyl derivative, 2-ethyl-5-bromobenzimidazole 1-oxyl-3-oxide.

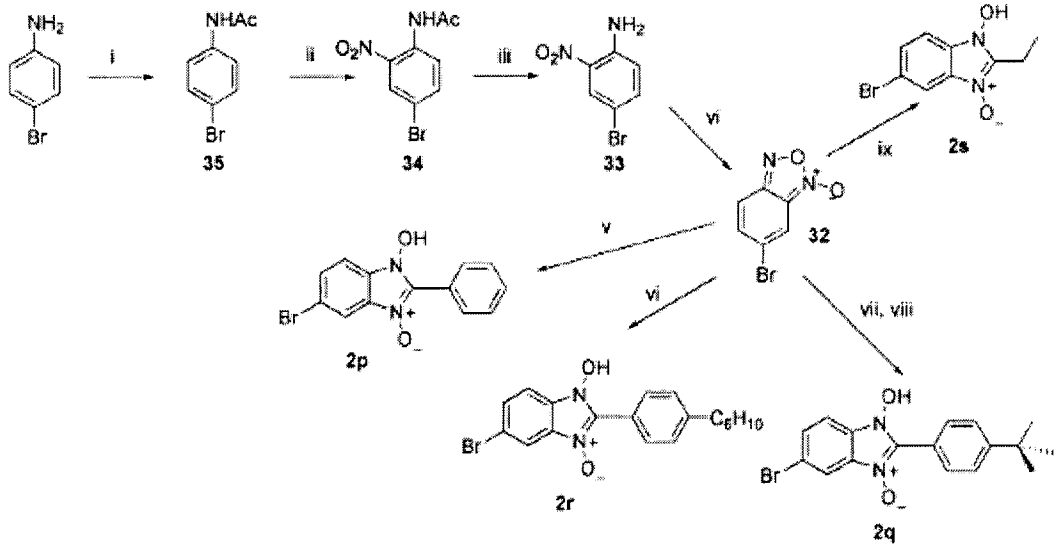

Scheme 5.5 - Synthesis of 5-bromobenzimidazoles 1-oxyl-3-oxide

Reagents and conditions: i) CH_3COCl, DCM, 70.5% ii) HNO_3, F_3CCO_2H, RT, 83% iii) 4M HCl in EtOH, 4h, 80 °C, 88% iv) 6% NaOCl, NaOH, EtOH, 94% v) *C*-Phenyl-*N*-phenylnitrone, cyclohexane, 75 °C, 54.8% vi) *C*-4-hexylphenyl-*N*-phenylnitrone, cyclohexane, 75 °C, 56% vii) hydrazine hydrochloride, KOH, EtOH, RT, 78.7% viii) 4-*t*-butylbenzaldehyde, 3.5M HCl in EtOH, Δ, 40% ix) 1-nitropropane, diethylamine, THF, RT, 44%

The synthetic methodologies developed for the 2-phenylbenzimidazole 1-oxyl-3-oxide led to a successful synthesis of several 2-phenyl-5-bromobenzimidazole nitronyl nitroxides, but the addition of the bromine to the

benzimidazole ring had an unintended side effect. The compounds were terribly insoluble in most organic solvents. Surprisingly, the compounds lost their solubility in basic water with the addition of the bromine. The addition of functional groups did not increase the solubility. Even the 2-ethyl-5-bromobenzimidazole 1-oxyl-3-oxide compound had lost all solubility in methanol, which was used to recrystallize the 2-ethylbenzimidazole 1-oxyl-3-oxide. Further polymerization reactions involving these compounds were not attempted.

5.3.4 - Attempt to synthesis a 2-phenylbenzimidazole 1-oxyl-3-oxide dimer from benzilidine.

Given the problems associated with generating the bromoderivatives of 2-phenylbenzimidazole 1-oxyl-3-oxide and the trans-metalation coupling, an alternate synthesis of the 2-phenylbenzimidazole 1-oxyl-3-oxide dimer was devised, based on creating the biphenyl moiety first and then creating the benzimidazole functional group afterwards. This idea focused on creating a bis-4,4'-benzofuroxan and then using a nitrone/furoxan coupling reaction to afford the desired benzimidazole dimer (see Scheme 5.7). The synthetic pathway started with benzilidine, which was protected with acetic anhydride, nitrated with fuming nitric acid in trifluoroacetic acid, and finally deprotected in sulfuric acid. Oxidation of the 3,3'-dinitrobenzilidine with sodium hypochlorite generated the bis-4,4'-benzofuroxan. Scheme 5.6 shows the attempted synthesis.

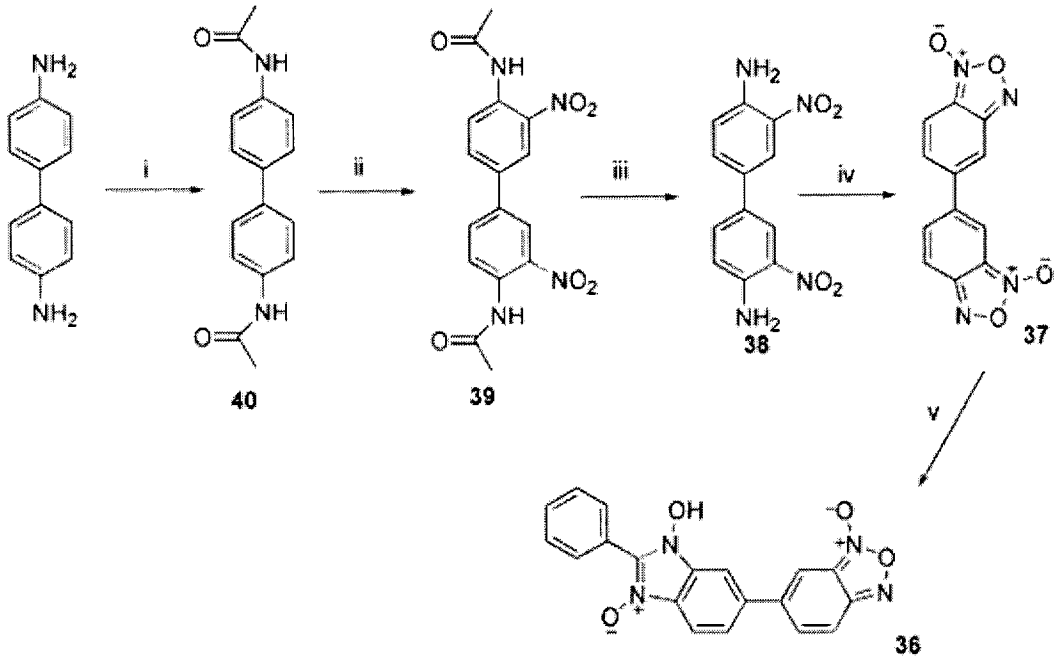

Scheme 5.6 - Attempted synthesis of a 2-phenylbenzimidazole 1-oxyl-3-oxide dimer by bis-4,4'-benzofuroxan.

Reagents and Conditions: i) Ac_2O, AcOH, 55 °C, 97% ii) TFA, fuming nitric acid, 95.6% iii) H_2SO_4, H_2O, Δ, 92.6% iv) 40% aqueous KOH, 6% NaOCl, Δ, 63.0% v) *C*-Phenyl-*N*-phenylnitrone, cyclohexane, 75 °C.

The reaction to couple the two molecules of *C*-phenyl-*N*-phenylnitrone to the bis-4,4'-benzofuroxan was not successful due to solubility problems. The single addition of one molecule of *C*-phenyl-*N*-phenylnitrone to one of the benzofuroxan leads to the premature precipitation of the mono adduct compound from solution, preventing the second nitrone from attacking the other benzofuroxan.

5.3.5 - Attempted synthesis of a new novel pyridazine polymer radical.

In an effort to create new novel nitronyl nitroxides, the attempted synthesis of a conjugated polymer with the nitronyl nitroxide incorporated into the polymer

backbone was performed. The idea was to use a pyridazine nitronyl nitroxide as the unpaired electron source in the polymer (see Scheme 5.7) in order to bypass the need to attach phenyl groups to the annelated ring, by starting with a radical with the phenyl groups already attached. This monomer was then polymerized with standard trans-metalation polymerization conditions after the benzimidazole had been formed.

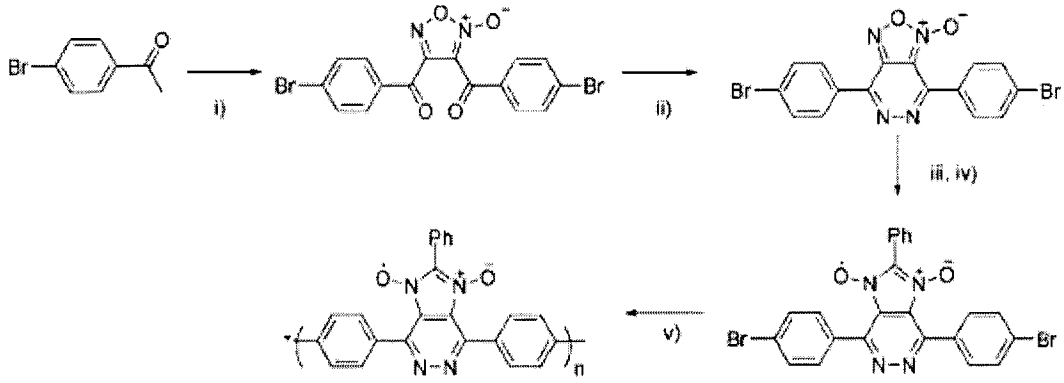

Scheme 5.7 - Proposed synthesis of pyridazine polymer radical with PBNN in the conjugated backbone

Reagents and conditions: i) $NaNO_2$, HNO_3, acetic acid, 60 °C ii) hydrazine dihydrochloride, MeOH, reflux, 1.5 hours, 65% iii) PhNOCHPh, benzene, Δ iv) Lead(IV) oxide, DCM v) $(Ph_3P)_2Ni(II)Cl_2$, PPh_3, Zn, DMF

To test this proposed oligomer system, the synthesis of the phenyl derivative was attempted, based on the idea that furoxan could be reacted with phenyl nitrone to afford the compound 2,4,7-triphenyl-imidazo[4,5-d]pyridazine 1-oxyl-3-oxide. (See Scheme 5.8.)

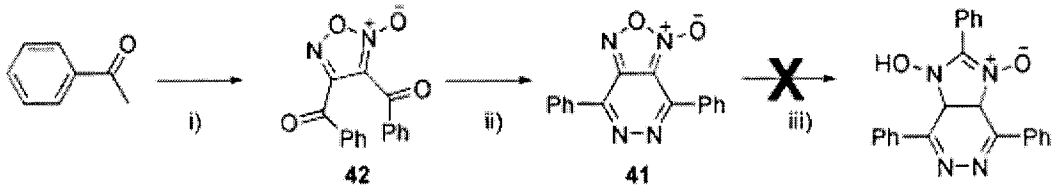

Scheme 5.8 - Synthetic results in the attempted making the pyridazine nitronyl nitroxide radical.

Reagents and conditions: i) $NaNO_2$, HNO_3, acetic acid, 60 °C, 6.4% ii) hydrazine dihydrochloride, MeOH, reflux, 1.5 hours, 65% iii) PhNOCHPh, benzene, Δ

The synthesis went according to Scheme 5.8 until the formation of the 3-oxy-2,4,7-triphenyl-imidazo[4,5-d]pyridazine 1-oxide. The 4,7-diphenylfuroxano[3,4-d]pyridazine 1-oxide was unreactive in the presence of *C*-phenyl-*N*-phenylnitrone. This followed the common trend with the benzofuroxan family of compounds with functional groups on the 4,7-position. As with the bromo derivatives, when functional groups are located on the ring next to the furoxan, the susceptibility of the furoxan to nucleophilic attack decreases because of steric hindrance. The phenyl rings blocked the reactive site on the benzofuroxan, just like in the bromo derivatives.

In the literature, the 4,7-diphenylfuroxano[3,4-d]pyridazine 1-oxide does not react with sodium borohydride like benzofuroxan.[93] Sodium borohydride reduces the C=N bond in the pyridazine ring when reacted with 4,7-diphenylfuroxano[3,4-d]pyridazine 1-oxide to form the 4,5-dihydro-4,7-diphenylfuroxano[3,4-d]pyridazine 1-oxide, leaving the furoxan group unaffected. Reaction of 4,7-diphenylfuroxano[3,4-d]pyridazine 1-oxide with Pd/C under H_2 yields the fully reduced 1,2-diamino-3,6-diphenylpyridine.[93] The nitrogen in the

pyridazine ring and the diphenyl group changed the reactivity of this compound sufficiently to prevent the application of nitrone-furoxan chemistry to this potentially interesting polyradical system.

Section 5.4 - Conclusion.

The generation of a series of brominated 2-phenylbenzimidazole 1-oxyl-3-oxides, 2-4'-hexylphenyl-5-bromobenzimidazole 1-oxyl-3-oxide, 2-phenyl-5-bromobenzimidazole 1-oxyl-3-oxide, 2-ethyl-5-bromobenzimidazole 1-oxyl-3-oxide, and 2-4'-*t*-butylphenyl-5-bromobenzimidazole 1-oxyl-3-oxide, was accomplished using synthetic methods developed and optimized in the synthesis of 2-phenylbenzimidazole 1-oxyl-3-oxides. The radicals for these compounds were all stable. Solubility was found to be a major problem with the 5-bromo-2-phenylbenzimidazole 1-oxyl-3-oxide class of molecules and prevented the further exploration of the polyradicals derived from this class of radicals. This problem must be addressed before the synthesis of polyradicals based on 2-phenylbenzimidazole nitronyl nitroxides can be achieved.

The reactivity of benzofuroxan with functional groups on the 3- and 6-positions was investigated, and it was found that their reactivity was drastically different, with the functional groups interfering with standard reaction conditions for the parent class. The attempted and failed syntheses of 4-bromo-2-phenylbenzimidazole 1-oxyl-3-oxide, 3-bromobenzo-1,2-dioxime, 3,6-dibromobenzo-1,2-dioxime, 4,7-dibromo-2-phenylbenzimidazole 1-oxyl-3-oxide, and 2,4,7-triphenyl-imidazo[4,5-d]pyridazine 1-oxyl-3-oxide demonstrated this

low reactivity, primarily due to steric hindrance from the groups at the carbon neighboring the furoxan function group. Using furoxan chemistry with this 4,7-substitution pattern was found to be incompatible with making polyradicals based on 2-phenylbenzimidazole nitronyl nitroxides.

Section 5.5 - Experimental.

2-nitro-6-bromoacetanilide (29).[89] A solution of 2-bromoacetanilide (4.0 g, 0.0186 mol) in 8 mL of trifluoroacetic acid was divided into eight test tubes and 1 mL of fuming nitric acid was added to each. The reaction was monitored by TLC (98:2 DCM/MeOH). After 10 minutes, the solutions were poured slowly, while being stirred, into 100 mL ice water. The resulting yellow solid precipitate was collected by filtration and washed with H_2O and hexanes. Separation of isomers was possible by recrystallization with EtOH, though it was easier to separate the o- and p-isomers by column chromatography after deprotection of the amine (see 2-nitro-6-bromoaniline (**28**) reaction for column conditions). Characterization of 2-nitro-6-bromoacetanilide was done on a 100 mg sample, and recrystallized from ethanol. mp = 193-4 °C (lit.[94] 193 °C). ^{1}H-NMR (500MHz, d_6-DMSO, δ): 10.2 (s, 1H, -Ar-NH-CO), 8.01 (d, 1H, J = 8.0 Hz, Ar-H), 7.96 (d, 1H, J = 8.0 Hz, Ar-H), 7.47 (t, 1H, J = 8.0 Hz, Ar-H), 2.08 (s, 3H, -$NCOCH_3$).

2-nitro-6-bromoaniline (28).[89] A mixture of crude o- and p-nitro-6-bromoacetanilide (~4.5g, 0.025 mol) was refluxed in 50 mL of 2:1 ethanol/6M HCl for 4 hours. The reaction was then poured into 60 mL of ice water and

neutralized with NaOH pellets. A yellow/brown solid precipitate formed and was collected by filtration, washed with H_2O, purified by column chromatography (silica, 8:2 hexanes/ethyl acetate), and dried to give the 2-nitro-6-bromoaniline isomer as a yellow solid (1.09 g, 28% yield from nitration step). mp= 73-4 °C (lit.[95] 73-4 °C). ^{1}H-NMR (500MHz, $DCCl_3$, δ): 8.10 (d, 1H, J = 9.0 Hz, Ar-H), 7.80 (d, 1H, J =7.5 Hz, Ar-H), 6.68 (t, 1H, J = 9.0, 7.5 Hz, Ar-H).

2-nitro-6-bromoazidobenzene (27).[96] A solution of sodium nitrite (0.032 g, 0.46 mmol) in 0.3 mL of conc. sulfuric acid was heated briefly to 70 °C and then cooled in an ice bath. To the sulfuric acid solution was added a solution of 2-nitro-6-bromoazidobenzene (0.100g, 0.46 mmol) in 2.5 mL acetic acid dropwise with stirring. The bright yellow solution turned clear almost immediately. The clear solution was diluted with 5 mL of ice water and a solution of sodium azide (0.0301g, 0.46 mmol) in 1 mL of H_2O was added dropwise. The solution bubbled slightly and a white precipitate formed immediately. After stirring for 30 minutes, the pale white precipitate was collected by filtration, washed with H_2O, and dried to give a white solid (0.089 g, 80%). mp= 52-5 °C. ^{1}H-NMR (500MHz, d_6-DMSO, δ): 7.91 (d, 1H, J = 8.0 Hz, Ar-H), 7.89 (d, 1H, J =8.5 Hz, Ar-H), 7.25 (t, 1H, J = 8.0, 8.5 Hz, Ar-H). MS (direct probe) m/z: 244/242$[M]^+$, 216/214 $[M-N_2]^+$, 170/168 $[M-N_2-NO_2]^+$.

6-bromobenzofuroxan (26). A solution of 2-nitro-6-bromoazidobenzene (1.30 g, 0.0053 mol) in 50 mL of toluene was refluxed for 20 hours. The reaction progress

was monitored by TLC using 1:2 ethyl acetate/hexanes. The solvent was evaporated under reduced pressure, yielding a brown solid (1.10 g, 96.6%). ^{1}H-NMR (500MHz, $DCCl_3$, δ): 7.64 (d, 1H, J = 7.5 Hz, Ar-H), 7.31 (d, 1H, J = 8.0 Hz, Ar-H), 7.10 (t, 1H, J = 7.5, 8.0 Hz, Ar-H). MS (direct probe) m/z: 214/216 $[M]^+$, 198/200 $[M-O]^+$.

Attempts to react 6-bromobenzofuroxan and *C*-phenyl-*N*-phenylnitrone. A solution of 6-bromobenzofuroxan (32.0 mg, 0.14 mmol) and *C*-phenyl-*N*-phenylnitrone (28.0 mg, 0.14 mmol) in 5 mL of benzene was stirred as the temperature was slowly increased to 65 °C over 24 hours. The solution was heated at 65 °C for an additional 6 days. No solid precipitate formed. After removal of the solvent by reduced pressure, the crude was extracted with 1M $NaOH_{aq}$. The basic extract was neutralized with 1M HCl_{aq} and no solid precipitated. Water was evaporated under reduced pressure and the crude yellow solid was separated from the salt with tweezers and less than 1 mg was collected. MS (direct probe) on the crude showed no peak corresponding to the product.

Attempts to react 6-bromobenzofuroxan and *C*-4-Hexylphenyl-*N*-phenylnitrone. A solution of 6-bromobenzofuroxan (53.7 mg, 0.25 mmol) and *C*-4'-hexylphenyl-*N*-phenylnitrone (73.6 mg, 0.25 mmol) in 1.5 mL of benzene was refluxed for 4 days. New spots appeared on TLC but the *C*-4'-hexylphenyl-*N*-phenylnitrone was not stable to refluxing conditions for extended periods of time (determined by refluxing addition flask with just *C*-4'-hexylphenyl-*N*-

phenylnitrone in benzene concurrently). No solid precipitate formed. The solvent was evaporated and the crude was extracted with 1M NaOH. When the basic extract was neutralized with 1M HCl_{aq}, no product precipitated. MS (direct probe) on the crude showed no signals for the successful coupling or any deoxygenated derivates.

3,4,5,6-tetrabromocyclohexanefuroxan (31). A solution of benzofuroxan (0.844 g , 6.3 mmol) and bromine (1.2 mL, 23.0 mol) in 20 mL of carbon tetrachloride was refluxed for 16 hours. A small aliquot was taken out of the reaction, diluted with $CDCl_3$, and examined by ^{1}H-NMR to check the progress of the reaction by comparing the intensity ratio of the broad starting material peaks at ~7.7 ppm versus the sharp resolved product peak at ~5.5 ppm. The reaction was continued at reflux for another 10 hours with more Br_2 (0.5 mL, 9.6 mmol). ^{1}H-NMR showed almost no starting material after 26 hours. The excess Br_2 was removed by aspiration and the reaction solution was immediately taken on to the next step. ^{1}H-NMR (200MHz, $DCCl_3$, δ): 5.77 (d, 1H, J = 2.8 Hz, -CHBr-), 5.53 (d, 1H, J =2.8 Hz, -CHBr-), 5.10 (t, 1H, J = 2.8, 4.0 Hz, -CHBr-), 5.07 (t, 1H, J = 2.8, 4.0 Hz, -CHBr-).

3,6-dibromobenzofuroxan (30). 3,4,5,6-tetrabromocyclohexanefuroxan in carbon tetrachloride was passed through a basic alumina column (alumina was dried in oven overnight before usage) with DCM as the eluent. A dull yellow spot was isolated (R_f = 0.75), the solvent was evaporated under reduced pressure, and

was recrystallized in EtOH. The recrystallization yielded a bright yellow solid (1.227 g, 67.1%). mp 130-131 °C (lit.[92] 132 °C). ^{1}H-NMR (200MHz, *d6*-acetone, δ): 7.68 (broad s, 1H, furoxan -H), 7.56 (broad s, 1H, furoxan -H). MS (direct probe) m/z: 292/294/296 $[M]^+$, 276/278/280 $[M-O]^+$, 216/214 $[M-Br]^+$, 156 $[M-Br_2]^+$.

Attempts at reducing 3,6-dibromobenzofuroxan with sodium hydrosulfite. A solution of 3,6-dibromobenzofuroxan (10.0 mg, 0.34 mmol) and $Na_2S_2O_4$ (0.015 mg, 0.8 mmol) in 1.0 mL of ethanol was refluxed for 3 days. There was no change observed by TLC and no color change. Reduction of benzofuroxan took 4 minutes under the same conditions, with a new spot by TLC and abrupt color change from yellow to bright red. Similar attempts at reducing 3,6-dibromobenzofuroxan with *p*-toluenesulfonhydrazide or 1,2-diphenylhydrazine failed to reduce the furoxan to the dioxime.

Attempts to react 3,6-dibromobenzofuroxan and *C*-phenyl-*N*-phenylnitrone. A solution of 3,6-dibromobenzofuroxan (39.2 mg, 0.2 mmol) and *C*-phenyl-*N*-phenylnitrone (58.7 mg, 0.2 mmol) in 12 mL of cyclohexane was refluxed for 2 days. No precipitate formed and MS showed all starting material.

Attempts to react 3,6-dibromobenzofuroxan and *C*-phenyl-*N*-phenylnitrone. A solution of 3,6-dibromobenzofuroxan (9.0 mg, 0.03 mmol) and *C*-phenyl-*N*-phenylnitrone (6.0 mg, 0.03 mmol) in 0.5 mL of diglyme was refluxed for 24

hours. Changes in TLC corresponded to decomposition of the starting material when heated separately in test tubes under the same conditions. No precipitate formed and MS was negative for product.

Attempts to react 3,6-dibromobenzofuroxan and 1-nitropropane. A solution of 3,6-dibromobenzofuroxan (25.4 mg, 0.0864 mmol) in 1 mL of THF was stirred at RT. 1-nitropropane (0.010 mL, 0.1 mmol) and diethylamine (0.010 mL, 0.1 mmol) was added to the solution. The reaction was heated at 50 °C overnight. No change in TLC, no precipitate, and MS all indicated the results were the starting material.

4-bromoacetanilide (35). A solution of 4-bromoaniline (5.75 g, 0.0334 mol) in 80 mL of dry methylene chloride was stirred while acetyl chloride (3.0 mL, 0.042 mol) was added slowly. The reaction was checked by TLC (95:5 DCM/methanol) and more acetyl chloride was added if necessary. The reaction was neutralized with aqueous saturated $NaHCO_3$ and then extracted with 3x100 mL of DCM. The organic layer was dried with $MgSO_4$ and the solvent was removed under reduced pressure. The solid was recrystallized in 95:5 ethanol/H_2O to produce a grey solid (7.0 g, 97%). mp = 164-7 °C (lit.[91] = 165-9 °C). ^{1}H-NMR (200MHz, d_6-DMSO, δ): 10.3 (s, 1H, -Ar-*NH*-CO), 7.58 (d, 2H, J = 10.0 Hz, Ar-H), 7.48 (d, 2H, J = 10.0 Hz, Ar-H), 2.08 (s, 3H, -$NCOCH_3$). MS (direct probe) m/z: 215/213 $[M]^+$, 171/173 $[M\text{-}C_2H_3O]^+$, 92 $[M\text{-}Br\text{-}C_2H_3O]^+$.

2-nitro-4-bromoacetanilide (34). A solution of 4-bromoacetanilide (4.71 g, 0.0220 mol) in 0.5 mL of trifluoroacetic acid was stirred while 0.5 mL of fuming nitric acid was added. The reaction was monitored by TLC (98:2 DCM/MeOH). After 10 minutes, the solution was poured into 20 mL of ice water. A yellow precipitate was collected by filtration and washed with H_2O to give a bright yellow solid (0.105 g, 75.1%). mp = 94-7 °C (lit[91]. 103-104 °C). ^{1}H-NMR (200MHz, d_6-DMSO, δ): 10.3 (s, 1H, -Ar-*NH*-CO), 8.1 (d, 1H, J = 2.2 Hz, Ar-H), 7.94(dd, 1H, J =2.2, 8.6 Hz, Ar-H), 7.6 (d, 1H, J = 8.6 Hz, Ar-H), 2.08 (s, 3H, -$NCOCH_3$). MS (direct probe) m/z: 260/258 $[M]^+$, 218/216 $[M\text{-}C_2H_3O]^+$, 172/170 $[M\text{-}NO_2\text{-}C_2H_3O]^+$.

2-nitro-4-bromoaniline (33).[91] A solution of 2-nitro-4-bromoacetanilide (0.240 g, 0.93 mmol) in 2 mL of EtOH and 2 mL of 20% $NaOH_{aq}$ was refluxed for 4 hours. The solution was cooled in an ice bath, filtered, washed with H_2O, and dried to give a yellow solid (0.174 g, 86.5%). mp= 106-8 °C (lit.[91] 104-109.0 °C). ^{1}H-NMR (500MHz, d_6-DMSO, δ): 8.09 (d, 1H, J = 2.4 Hz, Ar-H), 7.6 (s, 2H, -NH_2), 7.53 (dd, 1H, J =2.4, 9.0 Hz, Ar-H), 7.04 (d, 1H, J = 9.0 Hz, Ar-H). MS (direct probe) m/z: 218/216$[M]^+$, 202/200$[M\text{-}NH_2]^+$, 172/170 $[M\text{-}NO_2]^+$.

4-bromobenzofuroxan (32).[92] A solution of 2-nitro-4-bromoaniline (4.2 g, 0.0193 mol) in 80 mL of sat. ethanolic NaOH was cooled in an ice bath. To this solution, 30 mL of an ice cooled solution of 6% $NaOCl_{aq}$ was slowly added until the red color turned yellow. The ethanol was evaporated by reduced pressure and

the precipitate was filtered, washed with water, and dried to give a light yellow solid (3.90 g, 93.9%). mp= 65.0-69.0 °C (lit.[92] 69.0 °C). ^{1}H-NMR (500MHz, d_6-DMSO, δ): 8.20 (broad s, 1H, Ar-H), 7.65 (broad s, 1H, Ar-H), 7.53 (broad s, 1H, Ar-H). MS (direct probe) m/z: 216/214$[M]^+$, 200/198$[M\text{-}O]^+$.

4-bromobenzo-1,2-dioxime.[62] A solution of 4-bromobenzofuroxan (0.258 g, 0.0012 mol) and KOH (1.51 g, 0.027 mol) in 6 mL of ethanol was stirred at RT. To this was added hydrazine hydrochloride (0.246 g, 0.0013 mol) which then slowly changed from a bright red color to a dull brick red. After 30 minutes, 3 mL of H_2O was added and the ethanol was evaporated by reduced pressure. The solution was filtered, washed with 1M KOH, and the filtrate was acidified with acetic acid. A yellow precipitate was filtered, rinsed with water, and dried to give a yellow solid (0.205 g, 78.7%). ^{1}H-NMR (200MHz, d_6-DMSO, δ): 12.5 (broad s, 1H, NOH), 7.365 (d, 1H, J = 1.8, Ar-H), 7.07 (d, 1H, J = 10.4, Ar-H), 6.60 (dd, 1H, J = 10.4, 1.8, Ar-H). MS (direct probe) m/z: 218/216$[M]^+$.

2-phenyl-5-bromobenzimidazole 1-oxyl-3-oxide (2p). A solution of *C*-phenyl-*N*-phenylnitrone (0.025 g, 0.126 mmol) and 4-bromobenzofuroxan (0.028 g, 0.126 mmol) in 6 mL of cyclohexane was heated to 75 °C. The solution was heated for 24 hours and then filtered and washed with cyclohexane and benzene to produce a yellow solid (0.021g, 54.8%). The solid was not soluble in any organic solvent in the inventory or 1M $NaOH_{aq}$. mp 230-1 °C. MS (direct probe) m/z: 304/306 $[M]^+$, 288/290 $[M\text{-}O]^+$, 272/274 $[M\text{-}O_2]^+$, 224 $[M\text{-}Br]^-$. IR (KBr, pellet) cm^{-1}: 3062 (C-

H), 1245 (N-O), 759 (N-O--H-O), 594 (C-Br). HRMS-ESI (m/z): $[M - H]^-$ calcd for $C_{13}H_9{}^{79}BrN_2O_2$, 302.9769; found, 302.9772; $[M - H]^-$ calcd for $C_{13}H_9{}^{81}BrN_2O_2$, 304.9749; found, 304.9751. Oxidation of the solid with lead oxide gave a bright green solution with a five line EPR pattern characteristic of the two equivalent nitrogen in the known **PBNN** radical.

2-4'-hexylphenyl-5-bromobenzimidazole 1-oxyl-3-oxide (2r). A solution of *C*-4-hexylphenyl-*N*-phenylnitrone (0.025 g, 0.126 mmol) and 4-bromobenzofuroxan (0.028 g, 0.126 mmol) in 6 mL of cyclohexane was heated to just below reflux to prevent loss of solvent. The solution was heated for a total of 18 hours and then filtered and washed with cyclohexane and benzene. The solid was not soluble in any organic solvent in the inventory or 1M $NaOH_{aq}$. Brown solid (0.085 g, 56%) MS (direct probe) m/z: 390/388 $[M]^+$, 374/372 $[M-O]^+$, 358/356 $[M-O_2]^+$. IR (KBr, pellet) cm^{-1}: 2952 (C-H), 2851 (C-H), 1285 (N-O), 725 (N-O--H-O), 596 (C-Br). Anal. Calcd for $C_{19}H_{21}BrN_2O_2$: C, 58.62; H, 5.44; N, 7.20; Br, 19.53. Found: C, 59.17; H, 5.67; N, 7.05; Br, 18.62. Oxidation of the solid with lead oxide gave a bright green solution with a five line EPR pattern characteristic of the two equivalent nitrogen in the known **PBNN** radical.

2-4'-*t*-butylphenyl-5-bromobenzimidazole 1-oxyl-3-oxide (2q). A solution of 4-*t*-butylbenzaldehyde (0.150 mL, 0.9 mmol) and 4-bromobenzo-1,2-dioxime (0.196 g, 0.9 mmol) in 3.5 mL of 3.5M ethanolic HCl was refluxed until the red color disappeared (4 hours). The solution was cooled to RT. After addition of 8 mL of

H_2O the precipitate was filtered and washed with water and acetone to give a brown solid (0.130 g, 40%). The solid was not soluble in any organic solvent in the inventory or 1M $NaOH_{aq}$. MS (direct probe) m/z: 362/360 $[M]^+$, 346/344 $[M-O]^+$, 330/328 $[M-O_2]^+$. IR (KBr, pellet) cm^{-1}: 3061 (C-H), 2964 (C-H), 1268 (N-O), 656 (N-O--H-O), 572 (C-Br). HRMS-ESI (m/z): $[M + H]^+$ calcd for $C_{17}H_{18}{}^{79}BrN_2O_2$, 361.0552; found, 361.0552; $[M + H]^+$ calcd for $C_{17}H_{18}{}^{81}BrN_2O_2$, 363.0531; found, 363.0537. Oxidation of the solid with lead oxide gave a bright green solution with a five line EPR pattern characteristic of the two equivalent nitrogen in the known **PBNN** radical.

2-ethyl-5-bromobenzimidazole 1-oxyl-3-oxide (2s). A solution of 0.215 g (0.001 mol) 4-bromofuroxan in 5 mL of dry THF was stirred at RT. 1-nitropropane (0.165 mL, 0.0012 mol) and diethylamine (0.125 mL, 0.0012 mol) were added to the solution. The solution turned red almost immediately, and after stirring overnight, a yellow precipitate formed. The solid was filtered and washed with ethyl ether and hexanes to yield a yellow solid (0.135 g, 44%). The solid was not soluble in MeOH (like the parent 2-ethylbenzimidazole 1-oxyl-3-oxide), 1M $NaOH_{aq}$, or in any organic solvent in the inventory. MS (direct probe) m/z: 258/256 $[M-H]^-$, 242/240 $[M-O]^-$. IR (KBr, pellet) cm^{-1}: 2986 (C-H), 2943 (C-H), 1231 (N-O), 775 (N-O--H-O), 588 (C-Br). Anal. Calcd for $C_9H_9BrN_2O_2$: C, 42.05; H, 3.53; N, 10.90; Br, 31.08. Found: C, 42.16; H, 3.80; N, 10.88; Br, 31.21. Oxidation of the solid with lead oxide gave a bright green solution with a

broad five line EPR pattern characteristic of the two equivalent nitrogen in the known ethyl-BNN radical.

4,4'-diacetylbenzilidine (40).[98] A solution of benzilidine (0.866 g, 0.0046 mol) in 20 mL of acetic acid was heated to 55 °C (brown solution). Acetic anhydride (3.0 mL, 0.020 mol) was added to the solution. The reaction immediately produced a light brown precipitate which was filtered after stirring for 10 minutes, washed with water, and dried to constant weight to give a light brown solid (1.22 g, 97%). ^{1}H-NMR (200MHz, d_6-DMSO, δ): 9.86 (broad singlet, 2H, -Ar-*NH*-$COCH_3$), 7.75 (d, 2H, J = 8.8 Hz, Ar-H), 7.60 (d, 2H, J = 8.8 Hz, Ar-H), 2.05 (s, 6H, -$NCOCH_3$).

4,4'-diacetyl-3,3'-dinitrobenzilidine (39).[89] A solution of 4,4'-diacetyl benzilidine (0.0789 g, 0.3 mmol) in 0.3 mL TFA was stirred at RT. The solution was a bright purple color and 0.3 mL nitric acid (fuming) was added. The solution went from purple to yellow/orange in color with the addition of nitric acid. The solution was poured into 4 mL of ice water after 10 minutes and then cooled at 5 °C for 30 minutes, filtered with suction, washed with water and hexanes, and air dried to give a bright yellow/orange color solid (0.105g, 95.6%). ^{1}H-NMR (200MHz, d_6-DMSO, δ): 10.4 (broad singlet, 2H, -Ar-*NH*-$COCH_3$), 8.98 (d, 2H, J = 8.8 Hz, Ar-H), 8.50 (d, 2H, J = 7.0 Hz, Ar-H), 7.94 (dd, 2H, J = 8.8, 7.0 Hz, Ar-H), 2.12 (s, 6H, -$NCOCH_3$).

3,3'-dinitrobenzilidine (38).[89] A solution of 4,4'-diacetyl-3,3'-dinitrobenzilidine (0.720 g, 0.0020 mol) in 2.0 mL of concentrated H_2SO_4 and 0.5 mL of H_2O was refluxed for 4 hours, during which time the solution went from yellow to brown. The reaction was poured into 25 mL of ice water and cooled at 5 °C. The red precipitate was filtered, washed with water and dilute NH_4OH, and dried under vacuum to give a red brown solid (0.5225 g, 92.6%). ^{1}H-NMR (200MHz, d_6-DMSO, δ): 8.17 (d, 2H, J = 1.4 Hz, Ar-H), 7.8 (dd, 2H, J = 8.8, 1.4 Hz, Ar-H), 7.54 (broad single, 4H, NH_2), 7.15 (d, 2H, J = 8.8 Hz, Ar-H).

Bis-4,4'-benzofuroxan (37).[99] A solution of 3,3'-dinitrobenzilidine (0.54 g, 0.0019mol) in 8 mL of 40% aqueous KOH was heated to ~90 °C. To this was added 8 mL of 6% aqueous NaOCl. The solution was heated to reflux for 45 minutes during which time the reaction went from red to yellow in color. The solution was cooled, filtered with suction, washed with water and hexanes, and air dried. The crude solid was dissolved in DCM and passed through Celite-545. After evaporation of the solvent under vacuum, a bright yellow/orange color solid was isolated (0.320 g, 63.0%). ^{1}H-NMR (200MHz, d6-DMSO, δ): 8.22 (broad s, 1H), 7.99 (broad s, 2H). MS (direct probe) m/z: 270 $[M]^+$, 254$[M-O]^+$, 238$[M-O_2]^+$.

4-(4'-benzofuroxan)-2-phenylbenzimidazole 1-oxyl-3-oxide (36). A solution of *C*-phenyl-*N*-phenylnitrone (0.0237 g, 0.12 mmol) and bis-4,4'-benzofuroxan (0.0135 g, 0.05 mmol) in 25 mL of cyclohexane was heated to 75 °C. The

solution was heated for 4 days, filtered, and washed with cyclohexane and benzene to give a yellow-orange solid (0.010 g). The solid was not soluble in any organic solvents in the laboratory or 1M NaOH. Direct probe MS of product revealed bis,4-4'-benzofuroxan at low temperature. At high temperature, the parent peak and associated fragment pattern for the mono-coupled 4-(4'-benzofuroxan)-2-phenylbenzimidazole 1-oxyl-3-oxide were observed.

Dibenzoylfuroxan (42).[66] A solution of benzophenone (6.0 mL, 0.0489 mol) in 8 mL of acetic acid was stirred at RT while a second solution of sodium nitrite (0.6g, 0.0086mol) in 8 mL of concentrated nitric acid and 16 mL of acetic acid was added dropwise. The reaction was heated to 60 °C for 16 hours and then diluted with water, neutralized with $NaHCO_3$, and extracted with DCM. The organic layer was dried with $MgSO_4$ and evaporated under vacuum. The crude product was recrystallized twice with $EtOH/H_2O$ which gave a white solid (0.89 g, 6.4%). mp = 74-5 °C (lit.[66] 78 °C). ^{1}H-NMR (200MHz, $DCCl_3$, δ): 8.23 (m, 1H, Ar-H), 7.89 (m, 1H, Ar-H), 7.73 (m, 1H, Ar-H), 7.57 (m, 2H, Ar-H).

4,7-diphenylfuroxano[3,4-d]pyridazine 1-oxide (41). A solution of dibenzoylfuroxan (0.6868 g, 0.00216 mol) in 7.5 mL of MeOH was heated to reflux. A solution of hydrazine dihydrochloride (0.2729 g, 0.00260 mol) in 3 mL of MeOH was added. The reaction was refluxed for 90 minutes and then cooled to 3 °C until a precipitate formed. The precipitate was filtered, washed with water and MeOH, and dried to constant weight to produce a bright orange fine powder

(0.4041 g, 65%). mp = 205-7 °C (lit.[97] 209-11 °C). MS (direct probe) m/z: 290$[M]^+$, 274$[M\text{-}O]^+$, 244$[M\text{-}NO_2]^+$, 202$[M\text{-}N_3O_2]^+$. ^{1}H-NMR (500MHz, d_6-DMSO, δ): 8.52 (d, 2H, Ar-H), 7.94 (d, 2H, Ar-H), 7.60 (m, 6H, Ar-H).

Failed condensation of 4,7-diphenylfuroxano[3,4-d]pyridazine 1-oxide with *C*-phenyl-*N*-phenylnitrone. A solution of 4,7-diphenylfuroxano[3,4-d]pyridazine 1-oxide (0.0522 g, 0.25 mmol) and *C*-phenyl-*N*-phenylnitrone (0.0725 g, 0.25 mmol) in 3 mL of benzene was heated at 70 °C for 3 days. No precipitate formed and the *C*-phenyl-*N*-phenylnitrone started to break down.

List of References

(1) Van Vleck, J. H. *The theory of electric and magnetic susceptibilities*; Clarendon press: Oxford, 1932.

(2) Lahti, P. M. *Magnetic Properties of Organic Materials*; Marcel Dekker: New York, NY, 1999.

(3) Kahn, O. *Molecular magnetism*; VCH: New York, NY, 1993.

(4) Carlin, R. L. *Magnetochemistry*; Springer-Verlag: Berlin, 1986.

(5) Miller, J. S.; Dillon, M. *Magnetism: Molecules to Materials (Vol. I-IV)*; Wiley-VCH: Weinheim, 2001-2003.

(6) Ullman, E. F.; Osiecki, J. H.; Boocock, D. G. B.; Darcy, R. *JACS* **1972**, 7049-7059.

(7) Rajca, A. *Chem Reviews* **1994**, *94*, 871-893.

(8) Veciana, J.; Cirujeda, J.; Rovira, C.; Vidal-Gancedo, J. *Adv. Mater.* **1995**, *7(2)*, 221-225.

(9) Anderson, P. W. In *Magnetism I*; Rado, G. S., H., Ed.; Acedemic Press: New York, 1963.

(10) Watanabe, H. In *Ligand Field Theory*; Prentice-Hall: Englewood Cliffs, N.J., 1966; pp 256-274.

(11) Ogawa, M. Y.; Martinsen, J.; Palmer, S. M.; Stanton, J. L.; Tanaka, J.; Greene, R. L.; Hoffman, B. M.; Ibers, J. A. *JACS* **1987**, *109(4)*, 1115-1121.

(12) Bleaney, B.; Bowers, K. *Proc. Roy. Soc. (London)* **1952**, *A214*, 451-465.

(13) Feyerherm, R.; Loose, A.; Lawandy, M. A.; Li, J. *J. Phys. Chem. Solids* **2001**, *63(1)*, 71-77.

(14) Salem, L. *The Molecular Orbital Theory of Conjugated Systems*; W.A. Benjamin, Inc.: Reading, MA., 1974.

(15) Miller, J. S. *Adv. Mater.* **2002**, *14(16)*, 1105-1110.

(16) Borden, W. *Magnetic Properties of Org. Materials* **1999**, 61-102.

(17) Izuoka, A.; Murata, S.; Sugawara, T.; Iwamura, H. *JACS* **1987**, *109(9)*, 2631-2639.

(18) Rawson, J.; Palacio, F. *Structure and Bonding* **2001**, *100*, 94-126.

(19) Rawson, J.; Palacio, F.; A.;, A.; Less, R.; Pask, C. M.; Oliete, P.; Paulsen, C.; Yamaguchi, A.; Farley, R. D.; Murphy, D. M. *Angew. Chem. Int. Ed* **2003**, *42*, 4782-4785.

(20) Neugebauer, F. A. *Angew. Chem. Int. Ed* **1973**, *85(11)*, 485-493.

(21) Hicks, R. G.; Barr, C. L.; Chase, P. A.; Lemaire, M. T.; Stevens, C. L. *JOC* **1999**, *64(24)*, 8893-8897.

(22) Mukai, K.; Matsubara, M.; Hisatou, H.; Hosokoshi, Y.; Inoue, K.; Azuma, N. *J. Phys. Chem. B* **2002**, *106(34)*, 8632-8638.

(23) Hicks, R.; Barclay, T. M.; Lemaire, M. T.; Thompson, L. K. *Inorganic Chem* **2001**, *40(22)*, 5581-5584.

(24) Haddon, R. C.; Chi, X.; Itkis, M. E.; Reed, R. W.; Oakley, R. T.; Cordes, A. W. *J. Phys. Chem. B* **2002**, *106*, 8278-8287.

(25) Haddon, R. C.; Chi, X.; M.E.;, I.; Kirschbaum, K.; Pinkerton, A. A.; Oakley, R. T.; Cordes, A. W. *JACS* **2001**, *123*, 4041-4048.

(26) Rey, P.; Hirel, C.; Vostrikova, K.; Pecaut, J.; Ovchareko, V. *Chem. Eur. J* **2001**, *7*, 2007-2014.

(27) Miura, T.; Issiki, T.; Ushitani, Y.; Teki, Y.; Itoh, K. *J. Mater. Chem* **1996**, *6(11)*, 1745-1750.

(28) Nishide, H.; Miyasaka, M.; Yamazaki, Y.; Tsuchida, E. *Macromolecules* **2000**, *33*, 8211-8217.

(29) Gatteschi, D.; Caneschi, A.; Lalioti, N.; Sangregorio, C.; Sessoli, R.; Venturi, G.; Vindigni, A.; Rettori, A.; Pini, M. G.; Novak, M. A. *Angew. Chem. Int. Ed* **2001**, *40(9)*, 1760-1763.

(30) Veciana, J.; Cirujeda, J.; Deumal, Y.; Novoa, J. *Chem. Eur. J* **1999**, *5(5)*, 1631-1642.

(31) Zheludev, A.; Barone, V.; Bonnet, M.; Delley, B.; Grand, A.; Ressouche, E.; Rey, P.; Subra, R.; Schweizer, J. *JACS* **1994**, *116*, 2019-2027.

(32) Veciana, J.; Cirujeda, J.; Vidal-Gancedo, J.; Juergens, O.; Mota, F.; Novoa, J. J.; Rovira, C. *JACS* **2000**, *122(46)*, 11393-11405.

(33) Shultz, D.; Bodnar, S.; Vostrikova, K.; Kampf, J. *Inorg. Chem* **2000**, *39(26)*, 6091-6093.

(34) Balaban, A.; Halls, P. J.; Katritzky, A. R. *Chemistry and Industry* **1968**, *20*, 651.

(35) Gough, T. E.; Puzic, R. *J. of Magnetic Resonance* **1976**, *23*, 31-38.

(36) Kusaba, Y.; Tamura, M.; Hosokoshi, Y.; Kinoshita, M.; Sawa, H.; Kato, R.; Kobayashi, H. *J. Mater. Chem* **1997**, *7(8)*, 1377-1382.

(37) Kinoshita, M.; Hosokoshi, Y.; Tamura, M.; Shiomi, D.; Iswasawa, N.; Nozawa, K.; Katori, H. A.; Goto, T. *Mol. Cryst. Liq. Cryst. Sci. Tech. Sec. A* **1995**, *271*, 115-122.

(38) Zimmermann, H.; Volkamer, K.; Baumgartel, H. *Angew. Chem. Int. Ed* **1967**, *6(11)*, 947-948.

(39) Miller, J.; Zakrassov, A.; Shteiman, V.; Sheynin, Y.; Tumanskii, B.; Botoshansky, M.; Kapon, M.; Keren, A.; Kaftory, M.; Vos, T. E. *J. Mater. Chem* **2004**, *14*, 1827-1837.

(40) Minici, F.; Galli, R.; Quilico, A. *Tetrahedron Letters* **1963**, *12*, 785-790.

(41) Boulton, A.; Gripper Gray, A. C.; Katritzky, A. *J. Chem. Soc., (B)* **1967**, *9*, 911-914.

(42) Niclas, H.; Grundemann, E.; Patzold, F. *J. Prak. Chemie* **1990**, *332(3)*, 345-350.

(43) Uchida, S.; Yanada, K.; Yamaguchi, H.; Meguri, H. *J. Chem. Soc., Chem,. Commun.* **1986**, *22*, 1655-1656.

(44) Forth, M.; Oxley, P. W.; Adger, B. M.; Sasse, M. J. *Org. Synthesis* **1989**, *67*, 187-192.

(45) Panda, C. S.; Dora, E. K.; Dash, B. *J. Indian Chem. Soc.* **1979**, *56(6)*, 620-624.

(46) Abu El-Haj, M. J. *J. Org. Chem* **1972**, *37(15)*, 2519-2520.

(47) Graham, G.; Kronblum, N.; Larson, H. O.; Blackwood, R. K.; Mooberry, D. D.; Oliverto, E. P. *JACS* **1956**, *78*, 1497-1501.

(48) Anderson, L. *JACS* **1935**, *57*, 1673-1676.

(49) Nielsen, S. B.; Nielsen, M. B.; Qvortrup, K.; Jakobsen, M. T.; Gisselbrecht, J.; Boudon, C.; Jensen, F. *J. Mater. Chem* **2004**, *14(11)*, 1768-1773.

(50) Diederich, F.; Moonen, N. N. P.; Boudon, C.; Gisselbrecht, J.; Seiler, P.; Gross, M. *Angew. Chem. Int. Ed* **2002**, *41(16)*, 3044-3047.

(51) Catalan, J.; Mena, E.; Fabero, F.; Amat-Guerri, F. *Journal of Chemical Physics* **1992**, *96(3)*, 2005-2016.

(52) Shiomi, D.; Sato, K.; Takui, T.; Itoh, K.; Tamura, M.; Nishio, Y.; Kajita, K.; Nakagawa, M.; Ishida, T.; Nogami, T. *Mol. Cryst. Liq. Cryst.* **1999**, *335*, 1071-81.

(53) Coronado, E.; Giménez-Saiz, C.; Nicolas, M.; Romero, F. M.; Rusanov, E.; Stoeckli-Evans, H. *New J. Chem.* **2003**, *27(3)*, 490-497.

(54) Nozawa, K.; Hosokoshi, Y.; Shiomi, D.; Tamura, M.; Iwasawa, N.; Sawa, H.; Kato, R.; Kinoshita, M. *Syn. Metals* **1993**, *56(2-3)*, 3323-3326.

(55) Fischer, G.; Mann, C.; Pilawa, B.; Pongs, B. *Syn. Metals* **2003**, *137*, 1193-1194.

(56) Sato, M.; Tanaka, S.; Kaeriyama, K. *J. Chem. Soc., Chem. Commun.* **1986**, *11*, 873-874.

(57) Jen, K. Y.; Miller, G. G.; Elsenbaumer, R. L. *J. Chem. Soc., Chem. Commun.* **1986**, *17*, 1346-1347.

(58) Kimball, D. B.; Haley, M. M.; Mitchell, R. H.; Ward, T. R.; Bandyopadhyay, S.; Williams, R. V.; Armantrout, J. R. *JOC* **2002**, *67(25)*, 8798-8811.

(59) Mitchell, R. H.; Chen, Y. *Tetrahedron Letters.* **1996**, *37(30)*, 5239-5242.

(60) Kamm, O. *Organic Syntheses* **1925**, *Coll. Vol. 1*, 455.

(61) Haddadin, M. J. I., C.H.; Nazer, M.Z.; Alexanian, V. *Heterocycles* **1981**, *16*, 391-398.

(62) Nakai, H.; Konno, M.; Kosuge, S.; Sakuyama, S.; Toda, M.; Arai, Y.; Obata, T.; Katsube, N.; Miyamoto, T.; Okegawa, T. *J. Med. Chem* **1988**, *31(1)*, 84-91.

(63) Nelson, D. W.; Owens, J.; Hiraldo, D. *JOC* **2001**, *66(8)*, 2572-2582.

(64) Heaney, F.; Rooney, O.; Cunningham, D.; McArdle, P. *J. Chem. Soc., PT2* **2001**, *3*, 373-378.

(65) Sandhu, J.; Borah, H. N.; Boruah, R. C. *Heterocycles* **1985**, *23(7)*, 1625-1628.

(66) Funk, R. L.; Young, E. *JOC* **1998**, *63(26)*, 9995-9996.

(67) Black, D. S. C.; Horsham, M. A.; Rose, M. *Tetrahedron* **1990**, 4822.

(68) Boulton, A.; Tiddy, G. J. T.; Clifford, D. P.; Rahman, A. *J. Chem. Soc., (B)* **1968**, *12*, 1516-1523.

(69) Caneschi, A.; Gatteschi, D.; Paul Rey, P.; Sessoli, R. *Inorg. Chem* **1988**, *27(10)*, 1756-1761.

(70) Luneau, D.; Veciana, J.; Minguet, M.; Lhotel, E.; Villar, V.; Paulsen, C.; Amabilino, D. B. *Angew. Chem. Int. Ed* **2002**, *41(4)*, 586-589.

(71) Sutter, J. P.; Fettouhi, M.; El Ali, B.; El-Ghanam, A. M.; Golhen, S.; Ouahab, L.; Daro, N. *Inorganic Chem* **2002**, *41(14)*, 3705-3712.

(72) Mohanta, S.; Lin, H. H.; Lee, C. J.; Wie, H. H. *Inorganic Chem.* **2003**, *42(5)*, 1584-1589.

(73) Lowe-Ma, C. K.; Nissan, R. A.; Wilson, W. S. *J. Org. Chem* **1990**, *55(12)*, 3755-3761.

(74) Dyall, L.; Wah, W. M. *Aust. J. Chem.* **1985**, *38*, 1045-1059.

(75) Alexandrou, N. E.; Nicolaides, D. N. *J. Chem. Soc. C* **1969**, *17*, 2319-2321.

(76) Willer, R.; Park, D. J.; Stern, A. G. *Synth. Comm.* **1990**, *20(18)*, 2901-2906.

(77) Gallos, J.; Lianis, P. S.; Rodios, N. A. *J. Hetero. Chem.* **1994**, *31(2)*, 481-487.

(78) Nishide, H.; Miyasaka, M.; Yamazaki, T.; Tsuchida, E. *Polyhedron* **2001**, *20(11-14)*, 1157-1162.

(79) Miura, T.; Oka, H.; Tamura, T.; Teki, Y. *J. Mater. Chem* **2001**, *11(5)*, 1364-1369.

(80) Fujita, I.; Teki, Y.; Takui, T.; Kinoshita, T.; Itoh, K.; Miko, F.; Sawaki, Y.; Iwamura, H.; Izuoka, A.; Sugawara, T. *JACS* **1990**, *112(10)*, 4074-4075.

(81) Rajca, A.; Wongsriratanakul, J.; Rajca, S.; Cerny, R. *Angew. Chem. Int. Ed* **1998**, *37(9)*, 1229-1232.

(82) Nishide, H.; Inui, J.; Michinobu, T. *Org. Lett.* **2003**, *5*, 2165-2168.

(83) Zaidi, N. A.; Gilbin, S. R.; Terry, I.; Monkman, A. P. *Polymer* **2004**, *45*, 5683-5689.

(84) Yamamoto, T.; Hayashi, H. *Macromolecules* **1998**, *31(18)*, 6063-6070.

(85) Yamamoto, T.; Sugiyama, K.; Kanbara, T.; Hayashi, H.; Etori, H. *Macromol. Chem. Phys.* **1998**, *199(9)*, 1807-1813.

(86) Yamamoto, T.; Nurulla, I.; Morikita, T.; Fukumoto, H. *Macromol. Chem. Phys.* **2001**, *202(11)*, 2335-2340.

(87) Edlin, C. D.; Parker, D.; Perry, J. J. B.; Chartroux, C., .; ; Gloe, K. *New J. Chem.* **1999**, *23(8)*, 819-826.

(88) Mallory, F. B.; Manatt, S. L.; Wood, C. S. *JACS* **1965**, *87(23)*, 5433-5438.

(89) Britton, D.; Noland, W. E. *J. Org. Chem* **1962**, *27*, 3218-3223.

(90) Moje, W. *J. Org. Chem* **1964**, *29(12)*, 3722-3723.

(91) Lange, J.; Tondys, H.; Karolak-Wojciechowska, J. *Lienbigs. Ann. Chem.* **1992**, *6*, 547-551.

(92) Gibson, C. S.; Johnson, J. D. A. *J. Chem. Soc., Abstracts* **1928**, 3092-3093.

(93) Boulton, A.; Gripper Gray, A. C.; Katritzky, A. *J. Chem. Soc., (B)* **1967**, *9*, 909-911.

(94) Boyer, N. E.; Snyder, N. R. *JACS* **1955**, *77*, 4233-4238.

(95) Minato, M.; Lahti, P. M.; Van Willigen, H. *JACS* **1993**, *115(11)*, 4532-4539.

(96) In *Shaw, J. T. (American Cyanamid Co.)*; 5 pp. Division of U.S.: US, 1970.

(97) http://www.tf.uni-kiel.de/matwis/matv/pdf/met_26y.pdf

Appendix A: X-ray Crystal Structure

A1 : 2TBNN

A maroon crystal plate 0.48 x 0.12 x 0.02 mm was mounted on a glass capillary with oil. Data was collected at -143°C with one set of exposure as follows:

Scan	Type	Scanlength (deg.)	start (deg.)	ϑ	φ	Ω	κ
1	φ	183.0		3.70	-1.5	160	0

Crystal-to-detector distance was 30 mm and exposure time was 90 seconds per degree for all sets. The scan width was 1.3°. Data collection was 92.0% complete to 23.57° in ϑ. A total of 5877 partial and complete reflections were collected covering the indices, h = -8 to 8, k = -4 to 4, l = -16 to 16. 1218 reflections were symmetry independent and the R_{int} = 0.064 indicated that the data was of slightly better than average quality (0.07). Indexing and unit cell refinement indicated a monoclinic P lattice. The space group was found to be Pc (No.7). The data was integrated and scaled using hkl-SCALEPACK. This program applies a multiplicative correction factor (S) to the observed intensities (I) and has the following form:

$S = \exp(2B(\sin q/\lambda)^2)/ \text{scale}$

S is calculated from the scale and the B factor is determined for each frame and is then applied to I to give the corrected intensity (I_{corr}). Solution by direct methods (SIR97) produced a complete heavy atom phasing model consistent with the proposed structure. All hydrogen atoms were located using a riding model. Nearly all of the non-hydrogen atoms were refined anisotropically by full-matrix least-squares. Due to the disorder of the system constraints were placed upon the thermal parameters of several atoms to ensure positive definite matrix elements.

The model used to resolve the disorder of the system was the superposition of a two molecules on top of one another. The second molecule was symmetry related to the first molecule by a C2 rotation perpendicular to the plane of the molecules. Refinement of this model indicated the sample was comprised of approximately 28% of the disordered molecules.

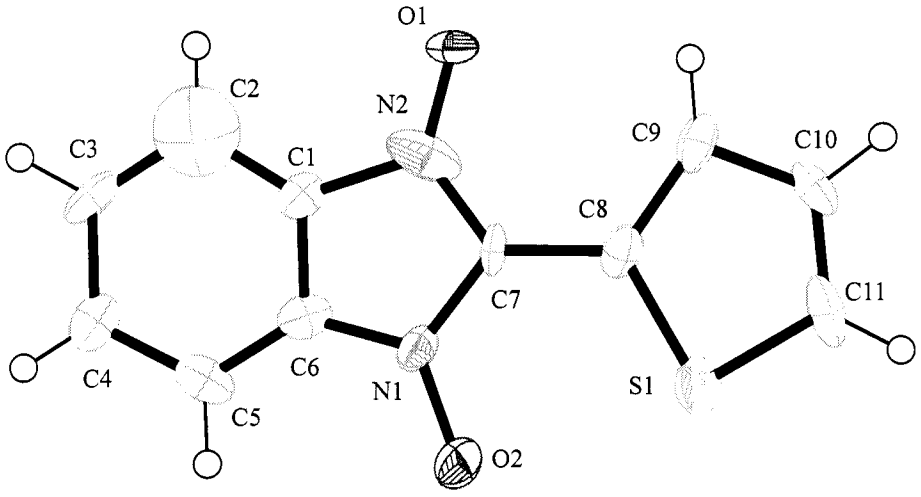

Table 1. Crystal data and structure refinement for **2TBNN.**

Empirical formula	C11 H7 N2 O2 S
Formula weight	231.25
Temperature	130(2) K
Wavelength	0.71073 A
Crystal description/color	plate / maroon
Crystal system, space group	Monoclinic, P c (No. 7)
Unit cell dimensions	a = 7.3310(10)A alpha = 90 deg. b = 4.6370(5)A beta = 104.331(5) deg. c = 14.750(3)A gamma = 90 deg.
Volume	485.81(13) A^3
Z, Calculated density	2, 1.581 Mg/m^3
Absorption coefficient	0.316 mm^-1
F(000)	238
Crystal size	0.48 x 0.12 x 0.02 mm
Reflections for indexing	85
Theta range for data collection	3.51 to 23.57 deg.
Index ranges	-8<=h<=8, -4<=k<=4, -16<=l<=16
Reflections collected / unique	1218 / 1218 [R(int) = 0.064]
Completeness to theta =	23.57 92.0%
Absorption correction	Denzo2000
Max. and min. transmission	0.9937 and 0.8632
Refinement method	Full-matrix least-squares on F^2
Data / restraints / parameters	1218 / 44 / 179
Goodness-of-fit on F^2	S = 1.001
S = root(sum(w*D*D)/(n-p)), where D = (Fo*Fo - Fc*Fc)	
Final R indices [I>2sigma(I)]	*R1 = 0.0630, wR2 = 0.1302
R indices (all data)	R1 = 0.1214, *wR2 = 0.1535

*Report these R factors.
R1 = sum||Fo|-|Fc||/sum|Fo|,

wR2=root(sum(w*D*D)/sum(w*Fo*Fo)),where D = (Fo*Fo - Fc*Fc)

Weighting scheme
calc w=1/[\s^2^(Fo^2^)+(0.0615P)^2^+0.0000P] where
P=(Fo^2^+2Fc^2^)/3

Absolute structure parameter	0.8(4)
Extinction coefficient	0.016(9)
Largest diff. peak and hole	0.313 and -0.262 e.A^-3

Table 3. Bond lengths [A] and angles [deg] for shelxl.

S(1)-C(11)	1.673(14)
S(1)-C(8)	1.76(2)
C(2)-C(1)	1.386(19)
C(2)-C(3)	1.393(19)
C(2)-H(2)	0.9500
O(1)-N(2)	1.255(16)
O(2)-N(1)	1.375(16)
C(10)-C(11)	1.356(12)
C(10)-C(9)	1.411(11)
C(10)-H(10)	0.9500
N(1)-C(6)	1.32(2)
N(1)-C(7)	1.392(18)
C(4)-C(3)	1.392(8)
C(4)-C(5)	1.403(8)
C(4)-H(4)	0.9500
C(1)-C(6)	1.33(2)
C(1)-N(2)	1.43(2)
C(5)-C(6)	1.319(14)
C(5)-H(5)	0.9500
C(9)-H(9)	0.9500
C(3)-H(3)	0.9500
N(2)-C(7)	1.320(17)
C(11)-H(11)	0.9500
C(7)-C(8)	1.461(18)
C(11)-S(1)-C(8)	89.9(8)
C(1)-C(2)-C(3)	116(2)
C(1)-C(2)-H(2)	122.1
C(3)-C(2)-H(2)	122.1
C(11)-C(10)-C(9)	118.2(12)
C(11)-C(10)-H(10)	120.9
C(9)-C(10)-H(10)	120.9
C(6)-N(1)-O(2)	125.3(14)
C(6)-N(1)-C(7)	111.8(16)
O(2)-N(1)-C(7)	122.9(12)
C(3)-C(4)-C(5)	117.5(10)
C(3)-C(4)-H(4)	121.3

N(2)-C(7)-C(8)-S(1)	-176.8(14)
N(1)-C(7)-C(8)-S(1)	0(2)

A2 : 3TBNN

A dark red plate 0.41 x 0.05 x 0.02 mm was mounted on a glass capillary with epoxy. Data was collected at -143°C with one set of exposure as follows:

Scan	Type	Scanlength (deg.)	start (deg.)	ϑ	φ	Ω	κ
1	φ	128.6		3.70	-9.27	160	0

Crystal-to-detector distance was 30 mm and exposure time was 120 seconds per degree for all sets. The scan width was 1.0°. Data collection was 59.2% complete to 23.77° in ϑ. A total of 13828 partial and complete reflections were collected covering the indices, h = -4 to 4, k = -14 to 19, l = -14 to 13. 865 reflections were symmetry independent and the R_{int} = 0.3254 indicated that the data was of less than average quality (0.07). Indexing and unit cell refinement indicated a monoclinic P lattice. The space group was found to be $P2_1/c$ (No.14). The data was integrated and scaled using hkl-SCALEPACK. This program applies a multiplicative correction factor (S) to the observed intensities (I) and has the following form:

$$S = \exp(2B(\sin q/\lambda)^2)/ \text{ scale}$$

S is calculated from the scale and the B factor is determined for each frame and is then applied to I to give the corrected intensity (I_{corr}). Solution by

direct methods (SIR97) produced a complete heavy atom phasing model consistent with the proposed structure. All hydrogen atoms were located using a riding model. All non-hydrogen atoms were refined anisotropically by full-matrix least-squares.

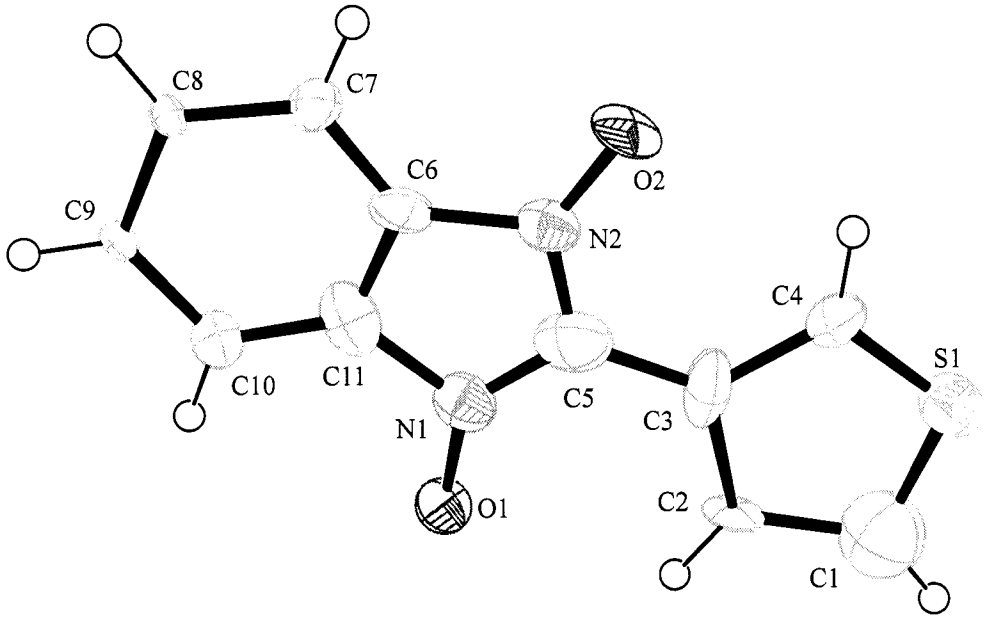

Additional notes: The structure was refined as a structure containing disorder in the C1 and S1 positions. The positions were refined as both atoms having a site occupancy of 50% in both sites, i.e. S1 occupies the S1 site 50% of the time and the C1 site, as S1a, the other 50% of the time.

Table 1. Crystal data and structure refinement for **3TBNN**.

Empirical formula	C11 H7 N2 O2 S
Formula weight	231.25
Temperature	130(2) K

Wavelength	0.71073 A
Crystal description/color	plate / dark red
Crystal system, space group	Monoclinic, P 21/c (No. 14)
Unit cell dimensions	a = 4.8000(10)A alpha = 90 deg. b = 17.022(4)A beta = 111.273(6) deg. c = 12.5200(15)A gamma = 90 deg.
Volume	953.3(3) A^3
Z, Calculated density	4, 1.611 Mg/m^3
Absorption coefficient	0.322 mm^-1
F(000)	476
Crystal size	0.41 x 0.05 x 0.02 mm
Reflections for indexing	121
Theta range for data collection	2.12 to 23.77 deg.
Index ranges	-4<=h<=4, -14<=k<=19, -14<=l<=13
Reflections collected / unique	1207 / 865 [R(int) = 0.3254]
Completeness to theta = 23.77	59.2%
Absorption correction	Denzo 2000
Max. and min. transmission	0.9936 and 0.8793
Refinement method	Full-matrix least-squares on F^2
Data / restraints / parameters	865 / 0 / 146
Goodness-of-fit on F^2 S = root(sum(w*D*D)/(n-p)), where D = (Fo*Fo - Fc*Fc)	S = 0.751
Final R indices [I>2sigma(I)]	*R1 = 0.0638, wR2 = 0.1025
R indices (all data) *Report these R factors. R1 = sum||Fo|-|Fc||/sum|Fo|, wR2= root(sum(w*D*D)/sum(w*Fo*Fo)), where D = (Fo*Fo - Fc*Fc)	R1 = 0.2491, *wR2 = 0.1786
Weighting scheme calc w=1/[\s^2^(Fo^2^)+(0.0000P)^2^+0.0000P] where P=(Fo^2^+2Fc^2^)/3	
Largest diff. peak and hole	0.174 and -0.216 e.A^-3

Table 3. Bond lengths [A] and angles [deg] for shelxl.

S(1)-C(4)	1.526(13)
S(1)-C(1)	1.633(5)
O(1)-N(1)	1.254(10)
O(2)-N(2)	1.287(10)
N(1)-C(5)	1.288(17)
N(1)-C(11)	1.459(15)
N(2)-C(5)	1.302(16)
N(2)-C(6)	1.440(15)
C(1)-C(2)	1.545(12)
C(1)-H(1)	0.9600
C(2)-C(3)	1.514(15)
C(2)-H(2)	0.9600
C(3)-C(5)	1.445(17)
C(3)-C(4)	1.458(14)
C(4)-H(4)	0.9598
C(6)-C(11)	1.297(12)
C(6)-C(7)	1.386(16)
C(7)-C(8)	1.429(13)
C(7)-H(7)	0.9500
C(8)-C(9)	1.432(11)
C(8)-H(8)	0.9500
C(9)-C(10)	1.429(14)
C(9)-H(9)	0.9500
C(10)-C(11)	1.379(16)
C(10)-H(10)	0.9500
C(4)-S(1)-C(1)	106.2(5)
O(1)-N(1)-C(5)	132.5(13)
O(1)-N(1)-C(11)	118.8(10)
C(5)-N(1)-C(11)	108.6(10)
O(2)-N(2)-C(5)	132.6(12)
O(2)-N(2)-C(6)	119.8(10)
C(5)-N(2)-C(6)	107.5(11)
C(2)-C(1)-S(1)	103.4(4)
C(2)-C(1)-H(1)	136.1
S(1)-C(1)-H(1)	120.5
C(1A)-C(1)-H(1)	120.1
C(3)-C(2)-C(1)	110.5(7)
C(3)-C(2)-H(2)	130.3
C(1)-C(2)-H(2)	119.1
C(5)-C(3)-C(4)	129.0(11)
C(5)-C(3)-C(2)	122.0(10)
C(4)-C(3)-C(2)	108.8(10)
C(3)-C(4)-S(1)	111.0(9)
C(3)-C(4)-H(4)	128.5
S(1)-C(4)-H(4)	120.5
N(1)-C(5)-N(2)	110.5(13)
N(1)-C(5)-C(3)	127.9(14)
N(2)-C(5)-C(3)	121.5(13)

C(11)-C(6)-C(7)	120.2(12)	
C(11)-C(6)-N(2)	108.0(11)	
C(7)-C(6)-N(2)	131.7(12)	
C(6)-C(7)-C(8)	120.2(10)	
C(6)-C(7)-H(7)	119.9	
C(8)-C(7)-H(7)	119.9	
C(7)-C(8)-C(9)	118.2(9)	
C(7)-C(8)-H(8)	120.9	
C(9)-C(8)-H(8)	120.9	
C(10)-C(9)-C(8)	118.0(9)	
C(10)-C(9)-H(9)	121.0	
C(8)-C(9)-H(9)	121.0	
C(11)-C(10)-C(9)	118.5(11)	
C(11)-C(10)-H(10)	120.8	
C(9)-C(10)-H(10)	120.8	
C(6)-C(11)-C(10)	124.7(13)	
C(6)-C(11)-N(1)	105.3(11)	
C(10)-C(11)-N(1)	130.0(13)	
C(4)-S(1)-C(1)-C(2)		-0.3(8)
S(1)-C(1)-C(2)-C(3)		-1.9(9)
C(1)-C(2)-C(3)-C(5)		178.6(10)
C(1)-C(2)-C(3)-C(4)		3.6(12)
C(5)-C(3)-C(4)-S(1)		-178.4(10)
C(2)-C(3)-C(4)-S(1)		-3.9(13)
C(1)-S(1)-C(4)-C(3)		2.6(11)
O(1)-N(1)-C(5)-N(2)		178.1(11)
C(11)-N(1)-C(5)-N(2)		2.3(13)
O(1)-N(1)-C(5)-C(3)		-6(2)
C(11)-N(1)-C(5)-C(3)		178.6(11)
O(2)-N(2)-C(5)-N(1)		174.3(11)
C(6)-N(2)-C(5)-N(1)		-2.5(13)
O(2)-N(2)-C(5)-C(3)		-2.2(19)
C(6)-N(2)-C(5)-C(3)		-179.0(11)
C(4)-C(3)-C(5)-N(1)		178.7(14)
C(2)-C(3)-C(5)-N(1)		4.8(19)
C(4)-C(3)-C(5)-N(2)		-5.4(19)
C(2)-C(3)-C(5)-N(2)		-179.3(11)
O(2)-N(2)-C(6)-C(11)		-175.6(8)
C(5)-N(2)-C(6)-C(11)		1.7(12)
O(2)-N(2)-C(6)-C(7)		0.2(17)
C(5)-N(2)-C(6)-C(7)		177.4(12)
C(11)-C(6)-C(7)-C(8)		-4.2(16)
N(2)-C(6)-C(7)-C(8)		-179.5(11)
C(6)-C(7)-C(8)-C(9)		3.7(15)
C(7)-C(8)-C(9)-C(10)		-2.9(15)
C(8)-C(9)-C(10)-C(11)		2.5(16)
C(7)-C(6)-C(11)-C(10)		4.0(18)
N(2)-C(6)-C(11)-C(10)		-179.7(11)
C(7)-C(6)-C(11)-N(1)		-176.6(10)
N(2)-C(6)-C(11)-N(1)		-0.3(11)
C(9)-C(10)-C(11)-C(6)		-3.1(17)
C(9)-C(10)-C(11)-N(1)		177.6(11)
O(1)-N(1)-C(11)-C(6)		-177.6(9)
C(5)-N(1)-C(11)-C(6)		-1.2(13)
O(1)-N(1)-C(11)-C(10)		1.8(16)

C(5)-N(1)-C(11)-C(10)	178.2(13)

References:

Instrument:	Nonius KappaCCD
	Nonius (1997). KappaCCD Operations Manual, Delft.
Data Collection Software:	Collect, (1998), Data Collection Software, Nonius.
Data Reduction:	HKL2000
	Otinowski, Z., Minor, W., (1996). Processing of X-ray Diffraction Data Collected in Oscillation Mode, Methods in Enzymology, 276, 307-326., C. W. Carter, Jr., R. M. Sweet, Eds., Academic Press.
Cell Refinement:	HKL Scalepack (Otwinowski & Minor 1997) ibid.
Structure Solution:	SIR97
	Altomare, A., Cascarano, G., Giacovazzo, C., Burla, M.C., Polidori, G., Camalli, M.,(1994)., SIR. J. Appl. Cryst. 27, 435-442.
Structure Refinement:	SHELXL-97 (Sheldrick, 1997)
	Sheldrick, G.M. (1997). SHELXL97, Program for the Refinement of Crystal Structures. Univ. of Gottingen, Germany.
Molecular Graphics:	maXus, Zortep
maXus:	MacKay, S., Gilmore, C.J., Edwards, C., Tremayne M., Stewart, N., Shankland, K.,(1998), "maXus: a computer program for the solution and refinement of crystal structures from diffraction data"
	University of Glasgow, Scotland, UK, Nonius BV, Delft, The Netherlands and MacScience Co. Ltd., Yokohama, Japan.

Zortep: L. Zsolnai, G. Huttner, (1994), University of Heidelberg.

Vita

Steven Edward Bowles was born in San Diego, California on August 23, 1978. He grew up primarily in Los Altos, California. After graduating from high school in 1996, he moved across the country to Pittsburgh, Pennsylvania where he attended Carnegie Mellon University. In 2000, he earned a B.S. in Chemistry with departmental and research honors and a Minor in Biology from Carnegie Mellon University. In 2005, he earned a Doctor in Philosophy in Chemistry from the Organic Division at the University of Washington.